Republic of Iraq
Ministry of Higher Education and Scientific Research
University of Babylon/College of Engineering
Department of Civil Engineering

Shear Repairing and Strengthening of Fire Damaged Normal and High Strength Reinforced Lightweight Concrete Beams Using Slurry Infiltrated Fibre Concrete

A Thesis

Submitted to the College of Engineering at the University of Babylon in Partial Fulfillment of the Requirements for the Master Degree in Engineering /Civil Engineering /Construction Materials

By
Ahmed Habeeb Abdulhussein Youssef

Supervised by
Prof. Dr. Mohammed Mansour Kadhum

2022 A.D. 1443 A.H.

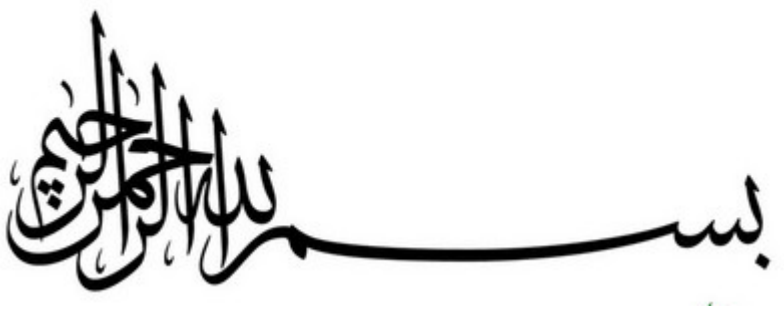

هُوَ ٱلَّذِى بَعَثَ فِى ٱلْأُمِّيِّـۧنَ رَسُولًا مِّنْهُمْ يَتْلُواْ عَلَيْهِمْ ءَايَٰتِهِۦ وَيُزَكِّيهِمْ وَيُعَلِّمُهُمُ ٱلْكِتَٰبَ وَٱلْحِكْمَةَ وَإِن كَانُواْ مِن قَبْلُ لَفِى ضَلَٰلٍ مُّبِينٍ ۙ

(سورة الجمعة : الآية 2)

Abstract

This study discusses the using of Slurry Infiltrated Fiber Concrete (SIFCON) as shear strengthening materials for normal and high strength lightweight reinforced concrete beams through using lightweight expanded aggregate (LECA) as a coarse aggregate in the reference mixture. The aim of the study is to provide an effective high-performance construction material utilized in strengthening process of fire damaged lightweight concrete beams.

The experimental section in this study passed into main three stages. The first stage included an investigation the behavior of normal and high strength (LWA) concrete beams after exposed to high temperature (600°C). For this purpose, a total of twenty-eight specimen with dimension of (150mm ×200mm ×2000mm). The second stage involved a post-development procedure for jacketing fire-damaged beams with SIFCON material layer was also examined. Aside from the reference samples, several parameters of concrete beams and conditioning were investigated, including duration of fire exposure, cover of concrete, and thickness of SIFCON jacket. The primary factors in this investigation were two concrete cover 20mm and 30mm, half and one-hour fire duration exposure, and two SIFCON layer thicknesses 20mm and 30mm. The heat gradient through the beam cross section was measured by embedding thermocouples sensors in various locations inside the beam. The physical and chemical properties were tested for all used materials in this study. Overall, twenty-eight concrete beam samples were tested for all the three phases (high and normal references, fire damaged samples, and post enhancement with SIFCON jacket). The level of comparison for the test specimens was concentrated on various parameters, including ultimate load capacity and corresponding displacement, ductility index, cracking load, stiffness (initial and secant), and energy absorption. The experimental test findings obtained as

part of this study revealed a significant enhancement for the strengthened beams when compared to the damaged samples. Furthermore, the results demonstrated that, excluding the absorption energy, the strengthened beams were recovered as well as similar and more than the undamaged (reference beam) in terms of the parameters indicated. According to the test findings, all of the strengthened beams with SIFCON jackets had a good load carrying capacity. After burning the load-carrying values of damaged beams were reduced. The decay rate for the NSC and HSC beams of (20 and 30) mm concrete cover were (24.4 and 20.5) % and (41.56 and 35.6) % respectively. While for the strengthening beams the carrying capacity were increased significantly, for the NSC the increment was between (159 and 207) %, and for HSC was between (180 and 220) %. Furthermore, the SIFCON jackets used as external strengthening avoided brittle shear failure and raised the ultimate shear strength of strengthened specimens. Finally, a simulation theoretical expression was conducted through constructing of finite element model (FEM), modelling and simulation the concrete beams that experimentally tested in the lab and ensure the accuracy of the results. Such approach, which is called numerical validation by using ABAQUS program with an acceptable absolute error of less than 15%.

Supervisor Certification

I certify that this thesis, titled " ***Shear Repairing and Strengthening of Fire Damaged Normal and High Strength Reinforced Lightweight Concrete Beams Using Slurry Infiltrated Fibre Concrete*** *", has been prepared by "* ***Ahmed Habeeb Abdul Hussein Youssef*** *" under my supervision at the Department of Civil Engineering, the University of Babylon, in partial fulfillment of the requirements for the degree of Master of Science in Civil Engineering.*

Supervisor

Signature:

Name: Prof. Dr. Mohammed Mansour Kadhum

Date: / /2022.

Acknowledgements

In the Name of Allah, the Most Gracious, the Most Merciful

The path towards this thesis was challenging. The credit for its completion is largely due to the special people who have supported me and stayed with me along the way.

Above all, I would like to offer this quest to our Almighty **Allah** who has helped and enabled me to complete this thesis I have been blessed with.

I would like to express my thanks, appreciation, and deep gratitude to my thesis advisor, **Dr. Muhammad Mansour Kazem**. For his continuous support and guidance throughout the research stages, he dedicated his time and knowledge to me whenever I encountered a problem or had a question about my research or writing. He gave me the freedom to research, analyse, and extrapolate the results, but he was guiding me in the right direction whenever he thought I needed it. It is an honour to work under his supervision, for his constant encouragement and invaluable guidance throughout this thesis.

Thanks are due to the head of the Civil Engineering Department, the department's staff and the construction materials laboratory staff, for their assistance and support during the laboratory research.

Special thanks and gratitude to my family, friends and colleagues for their care, patience and encouragement throughout the research period.

Ahmed Habeeb Abdul Hussein Youssef (2022)

Dedication

I dedicate this research

To the spirit of the greatest man in my life, the ideal that I wished to be present at this moment, who planted in me the sanctity of knowledge, **my father** (**Allah** have mercy on his soul).

To the great human being, the paradise of **Allah** who I grew up in her kindergarten.... tender, warm.... **my beloved mother**.

To the woman who gave me her love and support and was a wonderful example of affection and mercy.... **my beloved wife**.

To my wonderful family.... my brothers, sisters and sons for their continuous support.... (may **Allah** protect them all).

To my wonderful friends and colleagues...

To every person who had a beautiful imprint and a wonderful position in the pages of my life.

Ahmed Habeeb Abdul Hussein Youssef

(2022)

List of Contents

List of Tables

List of Figures

List of Plates

List of Abbreviations

CDP	concrete damaged plasticity
C–S–H	calcium silicate hydrate
E_c	modulus of elasticity
f_{cu}	cube compressive strength
fr	modulus of rapture
FRP	fiber-reinforced polymers
FRC	fiber-reinforced concrete
f_{sp}	splitting tensile strength
HPFRCC	high-performance fiber-reinforced cementitious composite
HRWRA	High Range Water Reducing Admixture
HSC	high strength concrete
ISO	International Standard organization
LECA	lightweight Expanded clay aggregate
LWC	Lightweight Concrete Members
LWRC	lightweight reinforced concrete
NSC	normal strength concrete
NWC	normal weight concrete
ODB	object data base
RC	reinforced concrete
SAI	strength activity index
SDC	specified density concrete
SF	Silica fume
SFRC	steel Fiber Reinforced Concrete
SIFCON	Slurry Infiltrated Fiber Concrete
SIMCON	Slurry Infiltrated Mat Concrete
SLC	structural lightweight concrete
SP	superplasticizer

CHAPTER ONE

Chapter 1. Introduction

1.1 Overview

In many new structures, the need for lightweight concrete is on a rise because of the advantages of the low density of load-carrying parts and small cross-sections which resulted in a decrease in the size of the construction foundation **(Babu&Babu,2003).** The lightweight aggregates are obtained naturally from volcanic cinders, diatomite, etc., or artificially from clay, sintered, etc. The mentioned lightweight aggregate is normally used to produce lightweight concrete **(Kiliç et al., 2003).** This concrete has several advantages such as an improved strength/weight ratio, higher tensile capacity, and reduced thermal expansion owing to the higher air voids content in the concrete. Lightweight concrete production growth has accelerated. Nowadays, this concrete is produced in different varieties ranging from low-density concrete such as block manufacturing with densities up to 1200 kg/m^3 to high-density concrete with densities of up to 2000 kg/m^3 that have a compressive strength of up to 100 MPa **(Topçu & Uygunoğlu, 2007).**

During fire incidents, the concrete is exposed to a significantly elevated temperature which leads to a significant loss in the properties of the concrete like compressive strength and ductility. Besides, a significant increase happens in the internal stress due to the vapor pressure in the pores which generates cracks of various sizes and lengths, particularly at high temperatures of more than 550^{o}C. At high temperatures like 550^{o}C, Dehydration of calcium hydroxide takes place and aggregates start to weaken. At higher temperatures (700^{o}C or above), the binding materials like hydrated cement (C–S–H) start to disintegrate which results in a significant loss in the mechanical properties (stiffness and compressive strength) of reinforced concrete (RC). Besides, the concrete suffers from losses in the bonds between the aggregate and the cement

paste which leads to the development of cracking and the concrete starts to dramatic lay deteriorate. As a consequence, the capacities of the structural components cannot handle dead and living loads unless they are reinforced Which is broadly agrees with the opinions of the following researchers, **(Alarcon-Ruiz et al., 2005; Haddad&Shannis, 2004)**

The only viable approach for regenerating structural capacity would often be to replace heat damaged components. Many aspects should be addressed carefully for carrying out repairs for fire-damaged components, including damage size, component shape, repair materials, cost, time, and the functions of the component. Although many research studies have already been carried out on RC's structural restoration **(Khalif& Nanni, 2002;Ashour, El-Refaie & Garrity, 2004;Adhikary & Mutsuyoshi, 2006)**. The work on the restoration of heat-damaged structures is scarce. For example, examined the performance of RC columns that are repaired after exposure to high temperatures. The authors exposed eleven columns to high temperatures and used fresh cast-in-place concrete to repair the damaged columns. The performance of the reference and strengthened columns in terms of ultimate strength and stiffness were tested using eccentric axial loads. The researchers reported that most strengthened columns have either recovered their original preference or even achieve improved performance in terms of stiffness than reference columns. **(De Lange, 1980)**, on the other hand, studied the efficiency of special repair techniques that were employed in St. Elizabeth Hospital in Holland after an intense fire incident. The authors reported that the consultant team found that if suitable repair approaches were followed there is no need for taking down the hospital. Three approaches were applied, which included epoxy injection, shotcrete repairs, and stiffening, to restore the performance of the structural members of the hospital structure.

The repairs of damaged concrete members normally take place either by building exterior RC support or shotcrete jackets or by attaching steel plates

using epoxy to the damaged component etc. **(Ng &Tan,2006).** A new method includes replacing the steel plates with fiber-reinforced polymers (FRP) or composite materials as a laminate like carbon and glass fiber reinforced polymer. The use of high-performance fiber-reinforced cement composites in structural repairs and restoration of RC components has recently become increasingly important **(Krstulovic-Opara & Al-Shannag, 1999; Shannag & Al-Rousan, 2004).** The high strength-to-weight, enhanced toughness, superior durability, and cost-effectiveness of composite materials offer exceptional properties to replace conventional repair materials.

Using composites in structure restoration projects may significantly reduce maintenance needs, improve safety and extend the service life of the structure.

1.2 Slurry Infiltrated Fiber Concrete (SIFCON)

SIFCON matrix is a flowing cement mortar or slurry of high cementitious content with no coarse aggregates. It may have fine/coarse sand, which is very different from the concrete in fiber-reinforced concrete (FRC). So, the preparing technique of SIFCON is different from FRC. The FRC is made by mixing the fiber with the fresh concrete. While the SIFCON is produced by replacing the fibers in the molds until it's filled and the cement slurry is then added to the fiber in the mold. If required, vibration is applied throughout to make sure the slurry infiltrates the fiber network **(Deepesh & Jayant, 2016; Ali, 2018).**

SIFCON is also known as a high-performance fiber-reinforced cementitious composite (HPFRCC). The HPFRCC normally contains a fraction of fibers. From **Figure (1-1),** it can be seen that higher fibers content (**Figure 1-1, b)** leads to multiple cracks in all directions in structural members under tension. On the other hand, low fibers content in a structural member under tension **(Figure1-1, a)** leads to the generation of a single crack only. Therefore,

A strengthening in the concrete is achieved by a greater fiber volume and this is done in a similar way to strain hardening in parallel with the cracking process. Lastly, failure is located in one crack process and the concrete is weakened **(Elnono et al., 2009)**.

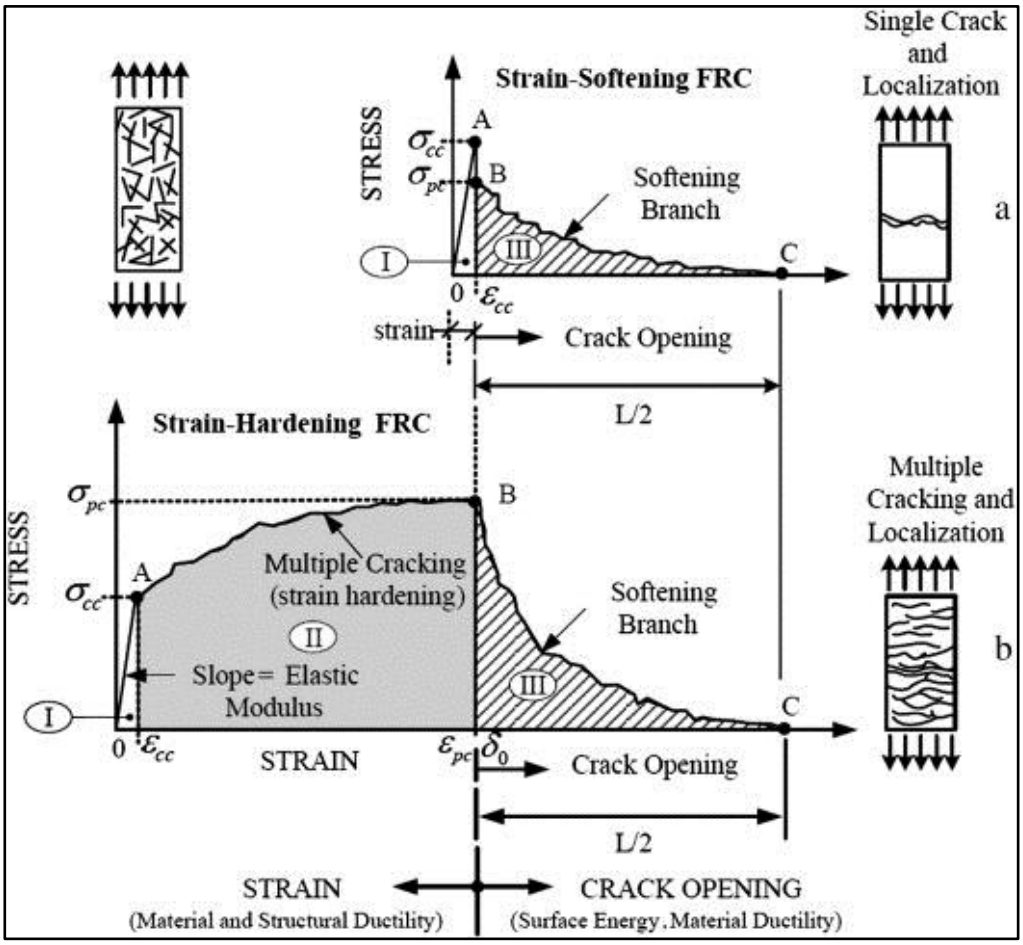

Figure 1-1: Behavior of HPFRCC against FRC **(Naaman, 2003)**.

To improve the performance of the SIFCON, the slurry can be produced using mineral and chemical admixtures like superplasticizer (SP), fly ash, and silica fume **(Sonebi et al., 2004)**. To ensure proper slurry infiltration of the fiber bed, vibration is often necessary **(Wang & Maji, 1994)**.

Based on scientific research, it can be deduced that the SIFCON has very good mechanical properties, where its enhanced tension, compression and shear strengths, and optimized ductility and energy absorption capabilities **(Sonebi et al., 2005)**. These properties are affected by several factors including **(Vijayakumar & Kumar, 2017)**:

i. The strength characteristics of the cement slurry.

ii. The volume of fiber in the SIFCON.

iii. The installation of the fiber and its alignment.

iv. The type and properties of the fiber.

1.3 Historical Background

In order to assure a ductile flexing failure mode under severe load, a reinforced concrete beam must be constructed to acquire its full flexural strength. Accordingly, a structural member has to have a safety factor for potential failures due to other reasons which are more severe and less anticipated than flexing failures. Shear failure is one kind of failure mechanism that should be avoided as it has a catastrophic consequence. Unlike flexural failure, shear failure could suddenly happen without any signs of deterioration. While the flexural failure happens progressively which has several signs like clear deflection and cracking. Thus, in order to ensure ductile flexural failure, concrete members must be adequately protected and strengthened against shear failure in the shear zone **(Sharif et al.1994)**.

The strengthening of the structural components against shear is nowadays one of the key issues faced by the construction sector. First, models have been built to determine RC beams' shear capacity taking into consideration the shear force transferred inside the beams and failure mechanisms. Second, The shear strength of reinforced concrete components was enhanced by using new methods and techniques **(Oluokun &Haghayeghi , 1998)**. Recently, the repair and enhancement of existing buildings are considered major civil engineering problems. The main causes for structural repairing and strengthening are:

- To endure underestimated loads,
- Improve the load-carrying capacity,
- Reduce early failure,

- Recover reduced mechanical properties owing to various damages such as an earthquake.

The improvement strategy of damaged structures can result in considerably enhanced properties (durability, ductility, and strength) and cheaper than conventional building procedures. The most common types of HPFRCC in the market as SIFCON **(Abdollahi et al., 2012)**, steel Fiber Reinforced Concrete (SFRC) and Slurry Infiltrated Mat Concrete (SIMCON) **(Naaman , 1992).** Since the early eighties, the SIFCON has been employed in the construction sector effectively even though it is still a rather new material **(Gilani, 2007)**. Common SIFCON applications include:

1- Earthquake resistant: scholars examined the implementation of precast SIFCON hinges to increase the seismic resistance of concrete. The SIFCON hinges are used to show the deformation in a beam section where plastic bending happens. Engineers also used plastic hinges in earthquake engineering as a kind of energy restraining apparatus permitting plastic deformation. For instance, these hinges are used as development in seismically resistant constructions of the ductile concept design. Energy will disperse without collapsing the remainder of the structure through plastic deformations of certain areas near the end of the member.

The reinforced SIFCON hinges are undoubtedly verified to be performing better than reinforced concrete hinges. Studies have also demonstrated that SIFCON is substantially stronger than standard fiber concrete when used in cast-in-place systems in framing systems **(Naaman et al., 1987; Long & Bergad, 2004)**. **Figure (1-2)** shows how SIFCON joints are applied to seismic-resistant frames.

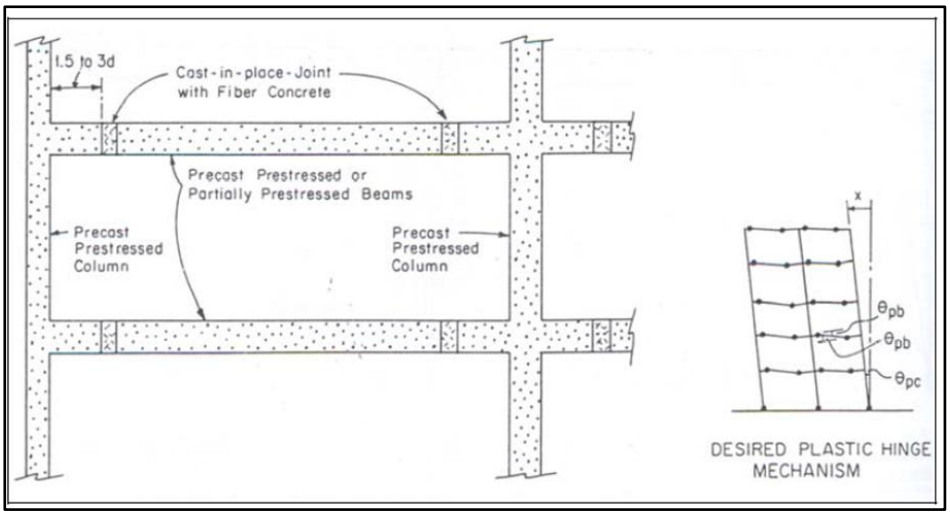

Figure 1-2: SIFCON joints in the structural system **(Naaman et al., 1987)**.

2- Restoration and retrofit: SIFCON serves as the ideal repair material as it is compatible with reinforced concrete in terms of stiffness and dimensional changes due to temperature. Accordingly, SIFCON is largely implemented to mending prestressed concrete members such as beams **(Gilani, 2007)**.

3- Bridge deck and pavement overlay: The New Mexico Engineering Research Institute has recently employed the SIFCON to rebuild decking on three interstate road bridges in Albuquerque, New Mexico Plate (1-1). The gravity flow alone achieved the slurry infiltration step (no vibration) **(Lankard, 1984)**. Rehabilitation of the pavement is comparable to the rehabilitation of the bridge deck, although repair areas are usually vast of primarily compressive loading pattern. The installation procedure is identical to repairs to bridge decks Plate (1-2) **(Gilani, 2007)**.

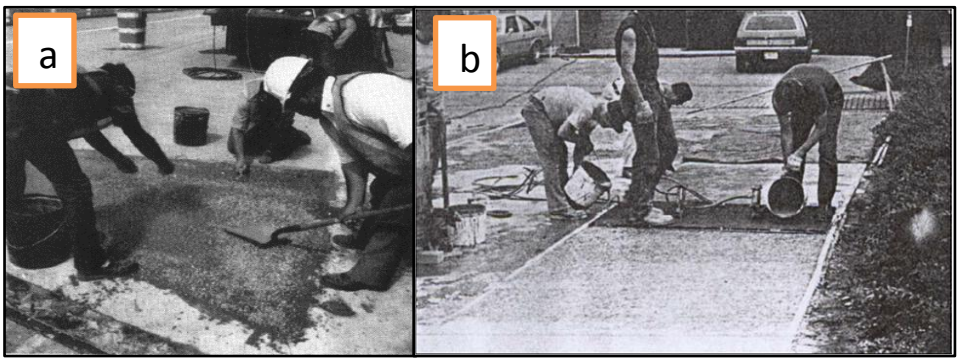

Plate (1-1): (a) SIFCON repairs for a bridge deck **(Lankard, 1984)**, (b) SIFCON application pavement overlay **(Gilani, 2007)**.

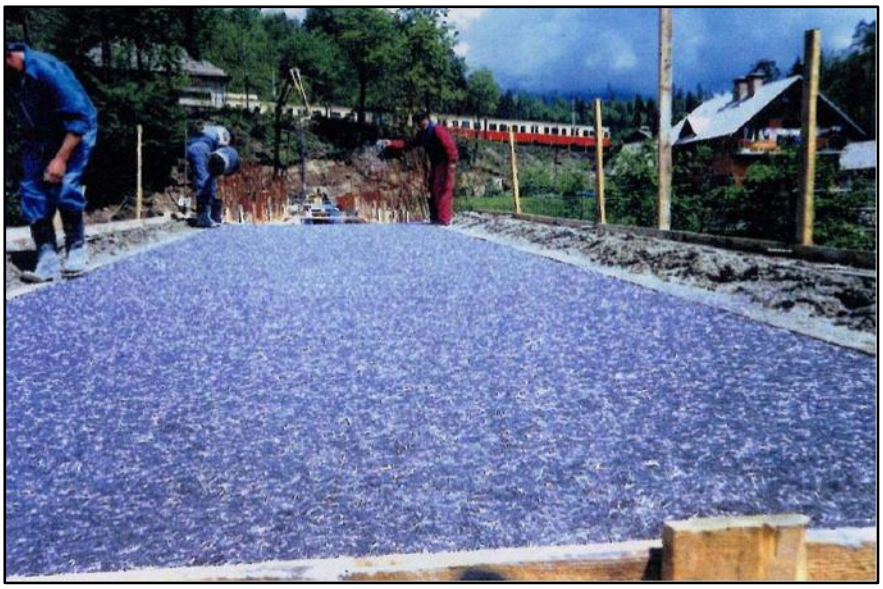

Plate (1-2): SIFCON was used for the construction of a deck overlay of a bridge over the River Sava at Globoko, Slovenia **(Šušteršič & Zajc, 2012)**.

4- Precast products: Many precast concrete products have been produced using SIFCON like slabs, vaults, and pipe sections **(Ali, 2018)**.

5- Explosive-resistant: SIFCON is also applied to buildings designed to resist explosive impact. The SIFCON has considerably high ductility, flexural and compressive strengths. SIFCON also has demonstrated great resistance to missile impact on structures **(Ali, 2018)**.

6- Refractory resistance: SIFCON has high refractory resistance. Therefore. It was successfully applied in construction exposed to high temperatures seal plates and furnace lintels **(Lankard, 1984)**.

1.4 Lightweight Concrete Members (LWC)

In modern construction, LWC has been introduced as a significant and useful material. Many technological and economic motivations have led to the current progress in terms of LWC usage in construction. There are several advantages to the usage of lightweight concrete. It has a low density compared to other concrete types which means that the size of the foundation can be reduced due to the reduction in the dead weight of the building. Besides,

without the need to adjust production techniques, the dimensions of any components may be enlarged. In addition, an element's geometric shape might be simplified considerably without increasing its weight (**Lytag UK, 2011**).

Conversely, lightweight aggregates have weaker mechanical properties compared to traditional aggregates. The cracks developed in LWC can easily pass through lightweight aggregate with minor resistance. The tensile failure is normally initiated within the aggregate particles as well as the concrete paste surrounding the aggregates. The LWC is considered weaker when compared to normal weight concrete (NWC) as the intensity and the width of the crack are higher in LWC. Besides, LWC's cracking load or tensile strength is much lower than that of the NWC of the same concrete grade. Thus, cracking propagation in LWC also affects the LWC characteristics such as shear capacity, bonding between steel and concrete, and anchoring strength **(Clarke, 2002).** Over recent decades, LWC has been widely employed **(Aljaafreh,2016).** The main structures built using LWC in the past 30 years are summarized in **Table (1.1)**. This type of concrete usage is expected to expand significantly over the coming few decades as the decline the characteristics of the structures developed using LWC can be retrofitted.

Table 1-1: Major projects implemented LWC over the last three decades **(Zareef, 2010)**.

Major Project	Year	Density Kg/m^3	Concrete Grade (MPa)
Auditorium Maximum, Germany	1994	1600	25
Amts- and Landgericht, Frankfurt/Oder, Germany	2006	1200	15
Gartmann Family House, Switzerland	2004	1100	8
German Technical Museum, Berlin, Germany	2001	1400	25
House of Youth Center, Berlin, Germany	2001	1200	15
MPU Heavy Offshore Lifter, Rotterdam, Netherland	2009	1250	35

1.5 Standard Fire Curve (ISO 834)

Standard, heating conditions, test steps, and criteria for the measurement of the fire endurance of building construction elements in different categories

are specified by International Standard ISO 834. This testing technique allows the fire resistance of construction elements (walls, columns, beams, floors, and roofs) to be determined based on the time length for which the test samples satisfy the specified criteria. The ISO 834 standard indicates that the rise in furnace temperature of the test sample is subject to the equation shown below:

$$T = 345 * \log_{10}(8*t + 1) + T_0 \quad (1\text{-}1)$$

Where:

t = time, in (minutes),

T = temperature of furnace at time (t), in (^oC), and

T_o = initial furnace temperature, in (^oC).

Values obtained from the above relationship are presented in Table (1-2). The curve representing this relationship between the time and temperature which is called the standard time-temperature curve is presented in Figure (1-3).

Table 1-2: Time-temperature data for the ISO 834 standard fire curve.

Time (t) (min.)	Temp. (T) (^oC)	Time (t) (min.)	Temp. (T) (^oC)	Time (t) (min.)	Temp. (T) (^oC)
5	576	45	902	85	997
10	678	50	918	90	1006
15	739	55	932	95	1014
20	781	60	945	100	1022
25	815	65	957	105	1029
30	842	70	968	110	1036
35	865	75	978	115	1043
40	884	80	988	120	1049

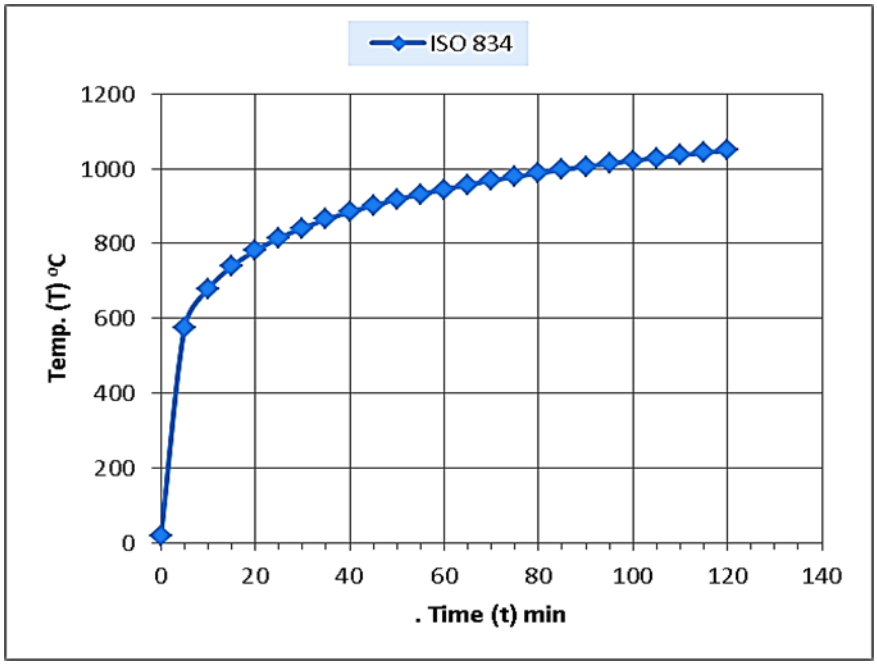

Figure 1-3: Standard fire curve for the ISO 834.

The specimen's fire resistance represents the time (in minutes) of heating until failure occurs, and is defined by one of the following specifications:

- **Load-bearing capacity:** failure occurs when the test sample collapses in such a manner that it no longer performs the load-bearing function which it was intended.
- **Insulation**: the failure happens in construction elements that separate two building parts (e.g., floors and walls) in three cases. One, the temperature on the unexposed face rises by more than (140°C) over the initial temperature. Two, the maximum temperature rises more than the initial value by over 180°C at any point on the unexposed surface. Three, the unexposed surface temperature exceeds 220°C.
- **Integrity:** construction elements like floors and walls collapse occurs when the element shows holes, cracks, or other openings that hot gasses or flames may pass. This can be tested by using standard cotton pads or observation. The element loses its integrity if cotton pads with 100 mm^2 in area of 20 mm thickness are ignited when held at a distance up to 30 mm from any opening on the unexposed side. Similarly, the element loses its integrity when sustained flaming of at least 10-sec duration appears on the unexposed side.

1.6 Fire Damaged Assessment of Lightweight Concrete

Concrete is an excellent structural material that can be utilized to display strong strength and reaction when a fire occurs for construction. It does not add to the fire load as a building material. It offers important properties (fire prevention as thermal insulation) which are essential to minimize fire spreading across compartments without the need for extra protective materials. Therefore, concrete is suitable to maintain escape routes and fire structural integrity when compared with other construction materials. Thus, the use of concrete in fire protection construction is dependable and cost-effective.

Concrete buildings have excellent fire resistance and can have a very high residual strength. In most circumstances, concrete could be re-used based on the condition of a building after a fire, the remaining load capacity, acceptable remaining displacements, and the load usage level. The function of a structural element is a major step in assessing the damage. The damage and implications on the load-bearing capability of a structure must be properly assessed. A small percentage of the overall repair expense of a building was estimated to be related to the cost of the structural repair.

Visual examination is the main mode for on-site investigations that are implemented to categorize the degree of damage for each member. Visual damage related to heat includes breakdown, bending, cracking of surfaces, color alteration, and smoke. The **(Concrete Society,1990; Smart,1999)** developed a surveying scheme to be used to inspect concrete structures as shown in Table (1-3). Each structural component is assigned to a damage class from 0 to 4 using visual inspection and each class has a suitable repair category from decorating to severe repair.

Table 1-3: Classification of fire damage classification**(Concrete Society,1990; Smart,1999).**

Observed Member							
Class of damage	Finishes	Color	Crazing	Spalling	Reinforcement bars	Cracks	Deflection
0 Decoration required	Unaffected	Normal	None	None	None exposed	None	None
1 Superficial repair required	Some peeling	Normal	Slight	Minor	None exposed	None	None
2 General repair required	Substantial loss	Pink	Moderate	Localized	Up to 25% exposed	None	None
3 Principal repair required	Total loss	Whitish grey	Extensive	Consider -able	Up to 50% exposed	Minor	None
4 Major repair required	Destroyed	Buff	Surface lost	Almost total	Up to 50% exposed	Major	Distorted

1.7 Significance of The Research

Reparation of concrete structures is crucial as it is not only extending their life but also rehabilitates their function after they have been damaged in exceptional cases like earthquakes and fires.

SIFCON has been used all over the world in the construction and reparation of structures exposed to explosives and other effects despite its high cost. The SIFCON has improved durability and mechanical properties compared to conventional FRC. SIFCON steel fibers are the same as conventional fiber concrete having several lengths and diameters. The SIFCON fibers can also deform to a certain level to enhance the mechanical bonding between structural members. Researchers and developers from around the world have increasing interest in using LWC for a long time. They showed that LWC can be manufactured in a wide variety of strengths and densities which offers a wider area of application in civil development and infrastructure.

The influence of fire on ordinary and reinforced concrete elements was investigated by many scholars through subjecting those elements to elevated temperatures in specialized burners or through direct contact with fire. The scholars examined the change in concrete properties like strength and deformation due to the effect of increased temperatures. But little research investigated the impact of direct fire on the behavior of lightweight normal strength (LWNSC) and high strength (LWHSC) reinforced concrete beams which are strengthened or repaired using U-shaped SIFCON thin jackets as external shear reinforcement. Accordingly, this research was conducted to examine the effects of using externally applied U-shaped thin jackets of SIFCON on the shear behavior of (LWRC) beams with and without burning. The LWRC manufactured using NSC and HSC grades. Research validity is assessed experimentally by assessing the efficacy of the repaired beams using two-point loading.

The importance of the research is summarized by preparing and studying the behavior of several models of beams with different characteristics and scenarios, which leads to covering the impact of most variables on beams behavior before and after exposure to burning. The models were as closest to practical conditions as possible to cover the limited researches on using SIFCON to repair the fire-damaged LWRC. To simulate real fire, a set of methane burners were used to subject normal and high LWRC beams to a real fire flame.

1.8 Objectives of This Study

Depending on reviewing of the previous researches and studies, no research investigated the effects of applying a U-shaped thin jacket made from SIFCON on the behavior of fire-damaged LWRC beams. As a result, the necessity for extensive research on the development and usage of SIFCON thin jackets to repair and strengthening of damaged regions after burning prompted

this study. This includes investigating (experimentally and theoretically) the contribution of several parameters like the grade of concrete, concrete cover, the thickness of the SIFCON jacket, and fire duration on the performance of the repaired LWRC beams. This study also focuses on evaluating the behavior of NSC and high-strength LWC concrete beams with and without burning. The following objectives are defined to fulfill the aims of this research:

1- Investigating the impact of fire on the mechanical properties of lightweight concrete specimens like compressive, tensile, and flexural strength as well as elasticity modulus.

2- Offering a comprehensive review of literature about the impact of fire on the load-carrying capacity of lightweight reinforced NSC and HSC beams (P_u) as well as comparing the results with the bearing capacity of strengthened beams using U-shaped SIFCON jackets.

3- Examining the effect of the concrete cover and compressive strength of the LWRC beams as well as the fire duration on cracking properties like width, length, and location. This also includes investigating the deformation properties as well as the impact of loading on the deflection of the beams.

4- Investigating the stiffness, ductility, and energy absorption performance of the LWRC beams which as strengthened and repaired using U-shaped SIFCON thin jackets after fire exposure.

5- Exploring the impact of concrete cover on the enhancement of fire resistance performance of the LWRC beams.

6- Using non-destructive tests (Schmidt rebound hammer and ultrasonic pulse velocity) to examine the degree of damage that occurs in the beams as a consequence of fire exposure.

7-Evaluating the maximum temperature distribution along the concrete cross-section.

8- Simulating the interface behavior and shear capacity of NSC, HSC, and LWRC beams using finite element (ABAQUS software) to estimate the failure modes and shear strength of LWRC beams after burning. The experimental and theoretical results of this research were compared with the prediction model findings.

1.9 Thesis Layout

Six chapters are included in this dissertation to achieve the goal of this research:

- **Chapter One (Introduction)**

  This chapter offers background about the subject of this research. it also presents the goal and objectives of this research study.

- **Chapter Two (Literature Review)**

  This chapter investigates the findings of previous scientific research into the properties of LWC and SIFCON, as well as the performance of structural parts after burning.

- **Chapter Three (Experimental Program)**

  In this chapter, the materials and the methods adopted in this research are presented and discussed. This includes mixes proportions, casting methods, testing setup, and the instrumentation used to develop and test LWRC and SIFCON. The variables that influence the behavior of the LWRC beams are presented.

- **Chapter Four (Results and Discussion)**

  The outcomes of this research about the performance of LWRC beams that were strengthened and repaired using U-shaped thin jackets of SIFCON after burning are presented and discussed in this chapter.

- **Chapter Five (Numerical Simulation)**

  The present chapter addresses the construction, via ABAQUS/Standard 2016, of a non-linear finite element model that simulates the behavior of

normal and high strength LWC beams both with and without fire exposure. In addition, a comparison of experimental and theoretical outcomes is presented in this chapter.

- **Chapter Six (Conclusions and Recommendations)**

  This chapter offers a comprehensive conclusion about the results of the research as well as recommendations.

CHAPTER TWO

Chapter 2. Literature Review

2.1 Introduction

This chapter discusses the literature relating to this study. The background and definition of lightweight concrete (LWC), mechanical properties of lightweight concrete, the influence of fire flame on concrete members, the characteristics of lightweight concrete and steel reinforcement at high temperatures, the performance of concrete beams before and after fire exposure, past experimental and theoretical research into concrete beam fire performance, SIFCON concrete definition, SIFCON concrete preparation, ingredients and mix proportion, and the effect of using SIFCON as a strengthening material on the structural behavior of lightweight concrete beam are all covered in this literature review.

2.2 Development of Modern Lightweight Structural Concrete

Lightweight concretes are not a new development in construction materials. They have already been known since ancient times and are the forerunners of today's concrete. As during early Roman Empire, the oldest lightweight concrete references in Europe were erected two thousand years ago. The use of lightweight concrete was limited following the fall of the Empire due to the paucity and irregularity of natural, volcanic materials. The developing and producing of artificially created lightweight aggregate was a major turning point in material technology in the nineteenth and twentieth centuries **(Lamprecht, 1996)**.

(Chandra&Berntsson,2002) stated that in 1920, the first commercial facility for the production of expanded aggregates was created in Kansas, USA. The uniform quality and composition of industrially produced aggregates has been shown to be superior than natural aggregates. At that time, Larger slate was used as aggregate in lightweight concrete in the construction of numerous

bridges. More than 200 lightweight concrete bridges have already been built in the United States of America during the last fifty years (**Holm& Ries,2007)**. The usage of lightweight concrete in construction applications increased in the mid-twentieth century. As a result, multi-story large structures like Chicago's Prudential Plaza and the Marina City Towers were constructed. Lightweight concrete, on the other hand, was increasingly used for structural purposes, while purposeful adaption of lightweight concrete by architecture remained mostly isolated according to **(Raithby& Lydon, 1981).**

In Germany, technical standards for concrete construction have been updated since the 1990s. Because of these new regulations, as well as continuous technological and scientific advancements, the usage of lightweight concretes has increased. However, the number of cases performed remained rather modest. Recent advancements attempt to further reduce concrete density while retaining adequate and as high as possible strength. In recent years, monolithic structures made with fair faced lightweight concretes in the lowest strength and density classes have gained popularity in Europe. These designs enable the construction of a finished wall in a single process, eliminating the need for multi-layer wall systems **(EC2, 1995)**. The decision to use a large lightweight concrete wall is typically prompted by a desire to make a one-of-a-kind building that can be easily shaped while utilizing the creative potential of exposed concrete. Moreover, the physical properties of lightweight concrete, such as low density, superior building physics, and high fire resistance, are significant qualities of a potential material, as is its outstanding longevity. **(Fares et al., 2015)**.

Light weight concrete has gained popularity in recent years owing to the several benefits it provides versus normal concrete. A greater knowledge and development of new technology has also contributed to the marketing and usage of light weight concrete.

2.3 Properties of Light Weight Concrete

Lightweight concrete has an oven dry density of 300 to 2000 kg/m3, a cube compressive strength of 1 to 60 MPa, and thermal conductivities of 0.2 to 1.0 W/mK. These values are comparable to those for normal weight concrete, which range between 2100 and 2500 kg/m3, have a compressive strength of 15 to 100 MPa, and have a specific gravity of (1.6–1.9). There are three varieties of light weight concrete: no-fines concrete, aerated concrete, and light weight aggregate (**Newman & Choo, 2003)**.

2.4 Classification of Lightweight Concrete

Light weight concrete can be classified into the following types based on its manufacturing method:

1. Light Weight Aggregate Concrete: It is produced of porous light weight aggregate with a specific gravity below 2.6.
2. Cellular, Aerated, Gas or Foamed concrete: This type of concrete is created by adding larger spaces into the mortar or concrete. Fine voids created by air entrainment must be segregated from these gaps.
3. Concrete of No fines: This concrete type is made by removing the fine aggregate in the mix, resulting in a significant number of interstitial spaces. Coarse aggregate of normal weight is utilized in this concrete. In essence, the existence of voids in the mortar, aggregate, or the interstices between coarse aggregate particles causes the density of the concrete to drop in each process. When compared to standard weight concrete, the existence of voids diminishes the strength of light weight concrete. Figure (2-1) depicts a schematic of the main procedures used to produce lightweight concrete.

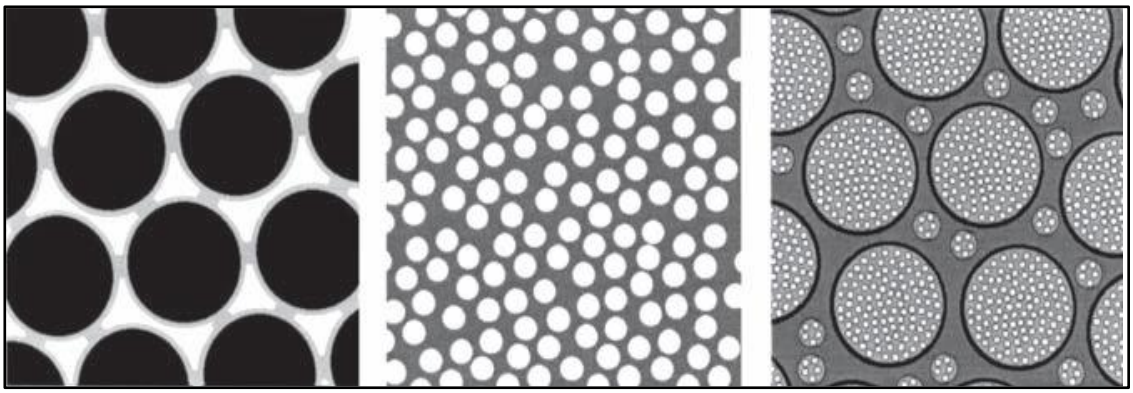

No fine Aggregate Cellular or aerated Lightweight aggregate

Figure 2-1: Basic types of Lightweight concrete **(Newman & Choo, 2003)**.

Lightweight concrete can even be classified according to its usage and strength, as described in the following:

1. structural concrete: The 28-day cylinder compressive strength of this concrete should not be less than 17 MPa. Its density should not exceed 1840 kg/m3. It should be in the range of 1400 to 1800 kg/m3.

2. masonry concrete or non-load carrying concrete: The 28-day cylinder compressive strength of this concrete must be between 7 and 14 MPa. Its density ought to be between 500 and 800 kg/m3.

3. Thermal insulation concrete must have a thermal conductivity coefficient with less than 0.3 J/m2S°C/m. It must have a strength of 0.7 to 7 MPa and a density with less than 800 kg/m3.

Lightweight structural concrete is less dense than standard concrete yet strong enough to be used for structural purposes. It combines the advantages of standard weight concrete and avoiding the disadvantages of normal weight concrete. This low weight concrete has a bright future ahead of it. Among the primary classifications of light weight concrete, light weight aggregate concrete and aerated concrete are more widely used than no fines concrete. Aerated concrete was formerly primarily utilized for insulation. It is being used in construction purposes with reinforcing steel.

In Scandinavian regions, aerated concrete is more extensively made and utilized. Light weight aggregate concrete is commonly created and utilized in United Kingdom, France, Germany, and the United States as a result of large-scale artificial manufacturing light weight aggregate. Nowadays, a wide range of industrial light weight aggregates with differing qualities are accessible under several market names. Examples of them are: (a) LECA (Expanded clay), (b) Hadite and Aglite (Expanded shale), (c) Lytag (Sintered pulverized fuel ash), and so on.

2.5 Lightweight Aggregates

International standards such as **(EN 13055,2016, ASTM C330,2006; ASTM C331,2010; ASTM C332,2017)** specify lightweight aggregates. LWA for structural concrete, LWA for masonry concrete, and LWA for thermal insulating concrete respectively, are all defined by ASTM standards. The European standard **(EN 13055,2016)** requires, among other things, that LWA be used for any form of lightweight concrete. However, the given requirements only take into account LWA of mineral origin. EN 13055 does not list LWA by common name, but rather describes their origins. LWA can be of natural origin, made from natural resources, or artificial manufactured from industrial byproducts or recycled source materials. This specification covers two general types of lightweight aggregates: aggregates prepared by expanding, pelletizing, or sintering products such as blast-furnace slag, clay, diatomite, fly ash, shale, or slate; and aggregates prepared by processing natural materials such as pumice, scoria, or tuff.

Aside from their origin, the specification of aggregate qualities, particularly density, is essential in distinguishing between normal weight and lightweight aggregate. (**ASTM C330,2006; ASTM C331,2010)** set upper limits for the loose bulk density of fine LWA at 1120 kg/m^3, coarse LWA at 880 kg/m^3, and the combination of fine and coarse LWA at 1040 kg/m^3.

Furthermore, structural lightweight concrete adhering to (**ASTM C330,2006)** should be attainable, where compressive strength is evaluated on cylindrical specimens (**ASTM C39 ,2016)**.

2.6 Properties of Lightweight Concrete

There are different definitions of lightweight concrete, which sometimes leads to ambiguity when discussing lightweight concrete. There are variations in terms of strength, density, and the type of lightweight concrete. **(ACI 213R,2014)** specifies a minimum cylinder strength of 17 MPa and an equilibrium density between 1120 and 1920 kg/m^3 for structural lightweight concrete (SLC) and an equilibrium density between 800 and 2240 kg/m^3 for specified density concrete without any strength requirement (SDC). High strength lightweight concrete is defined as SLC with a compressive strength of 40 MPa after 28 days.

2.6.1 Compressive Strength of Lightweight Concrete

The researchers investigated the characteristics of LWC composed of cinder and light expanded clay aggregates (LECA) in 2015 (**Kumar& Prakash, 2015)**. There was a reduction in weight and, respectively, a reduction in compressive strength by trying to replace coarse aggregate with mixed lightweight aggregates such as cinder and LECA, but they were able to use cinder and LECA as a replacement for normal coarse aggregate to reduce cost, while the compressive strengths were close to the strengths of NWC. The average compressive strength for samples containing the previously indicated LWA was 39.2 N/mm^2, whereas the average compressive strength for NWC was 43.4 N/mm^2. The LWC density ranged from 1800 to 1950 kg/mm^3, whereas the NWC density was 2637 kg/m^3.

In the case of standard weight concrete, a wide variety of particles results in a large range of cube strengths. When compare lightweight aggregate

concrete to normal weight concrete, the sorts of component materials in both situations must be considered Figure (2- 2) **(Cook,1983)**.

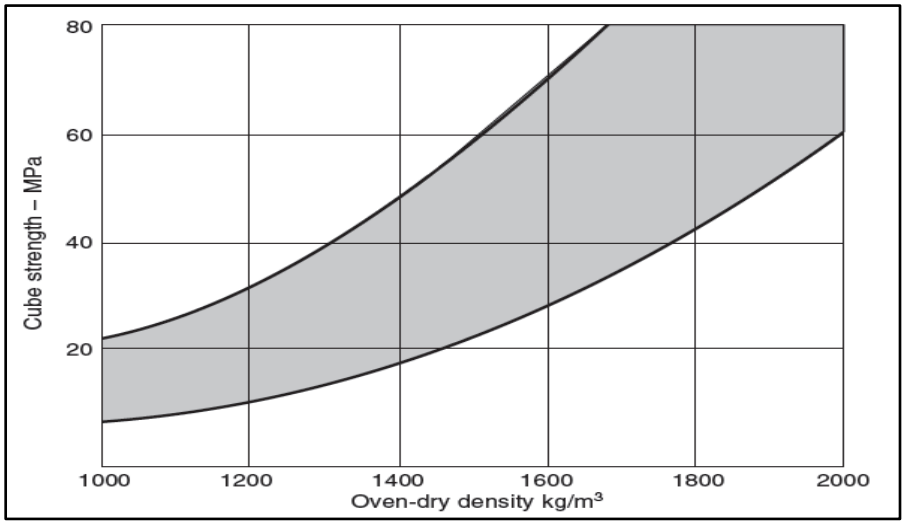

Figure 2-2: Cube strength versus oven-dry density of lightweight aggregate concretes **(Cook,1983)**

2.6.1.1 Factors Affecting Strength Include:

- **Strength and Stiffness of Aggregate Particles**

Weaker particles necessitate stronger mortars and consequently larger cement content. The strength of concrete is determined by the type of aggregate. The excellent particle-matrix bonding and similarity of particle and matrix moduli guarantee that the matrix is employed efficiently (**Newman, 1993)** Figure (2-3).

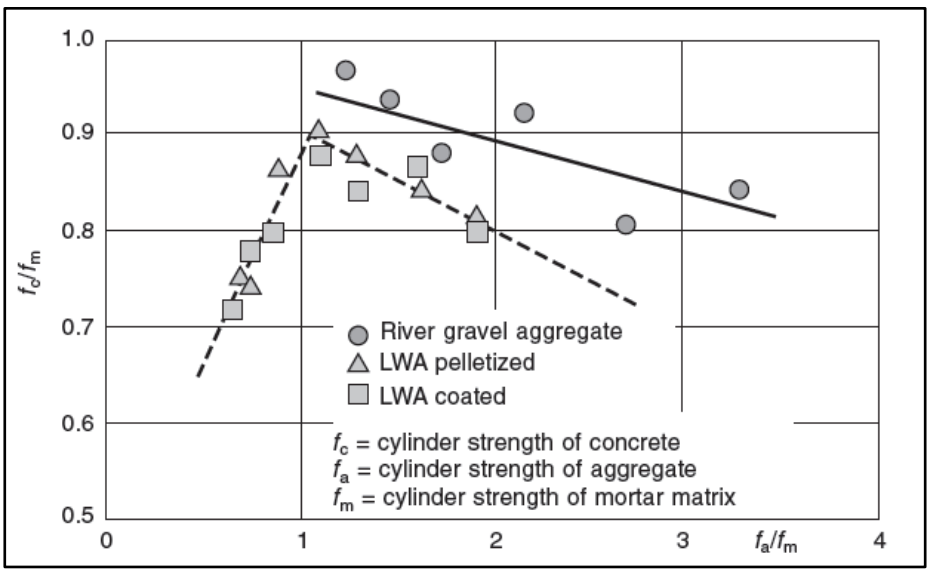

Figure 2-3: Concrete strength versus aggregate strength **(Newman, 1993)**.

- **Water/Cement Ratio**

It has the same effect on strength like normal weight concrete, and the same water/cement ratio range is used (**Newman& Owens, 2003)**. However, the free water/cement ratio reduction owing to water absorption of lightweight aggregate is difficult to estimate, making the specification of effective water/cement ratio for mixtures impractical because it is difficult to test and verify. The free water content is the same as for normal weight concrete (around 180–200 $1/m^3$), but aggregate absorption demands a greater total water content (around 250–300 $1/m^3$). In the case of lightweight aggregate concrete, it is more important for mix design purposes to connect strength to cement content**.**

• Cement Content

(**Lydon,1982**) stated that the strength increases with cement content for a certain workability, with the increase depending on the type of aggregates employed. In general, higher cement content are required than for regular weight concrete (about 10% more below 35–40 MPa and 20–25% higher beyond). Although the increase in strength for a given increase in cement content varies depending on the kind of aggregate used and the cement content itself, for lightweight aggregate, a 10% increase in cement content results in a 5% increase in strength.

• Age

The strength–age relation is similar in many aspects in normal weight concrete. When concrete dries, hydration stops, however the situation is better for lightweight aggregate concrete than for normal concrete due to the store of water in aggregate pores. As a result, lightweight aggregate concrete is more resistant to poor curing than normal concrete.

• Density

The aggregate particle density, which is related to particle porosity and hence particle strength, has the greatest influence on the density of compacted

concrete. As a result, particles of varying densities will produce concrete with varying strengths and densities.

2.6.2 Modulus of Elasticity and Poisson's Ratio

The stiffness of any concrete is influenced by the stiffness's of its components and their relative proportions in the mix. Simplifying concrete as a two-phase material which consists of coarse aggregate particles embedded in a mortar matrix, the E-value of the matrix will decrease with (a) a decrease in the stiffness of the mortar, which is determined by the volume proportions of cement, water, and sand, as well as the type sand, and (b) a decrease in the stiffness of the coarse aggregate. Because the moduli of lightweight aggregate particles are often smaller than those of natural dense aggregates, and because most lightweight aggregate concretes contain more cement, the total moduli of lightweight aggregate concretes will be lower than those of normal weight concretes. As a result, concretes created with lightweight coarse and fine aggregate will have a lower density than those formed with lightweight coarse aggregate and natural dense fines.

Lower E-values for lightweight concretes cause larger deformations for structural elements under a given load, while this impact is mitigated by the lower dead loads of lightweight concrete members themselves. Reduced stiffness, on the other hand, might be advantageous under dynamic scenarios such as impact or load variation.

2.6.3 Tensile Strength of Lightweight Concrete

When it comes to cracking in concrete members, tensile strength is significant. Compressive strength is influenced by the same factors that influence tensile strength. The main differences between lightweight and normal weight concrete are as follows:

- Fracture path

This generally goes through lightweight aggregate particles rather than around them. In that the flexural/compressive strength ratio is larger, the behavior is similarly to that of normal weight concrete produced with crushed aggregate (2-4).

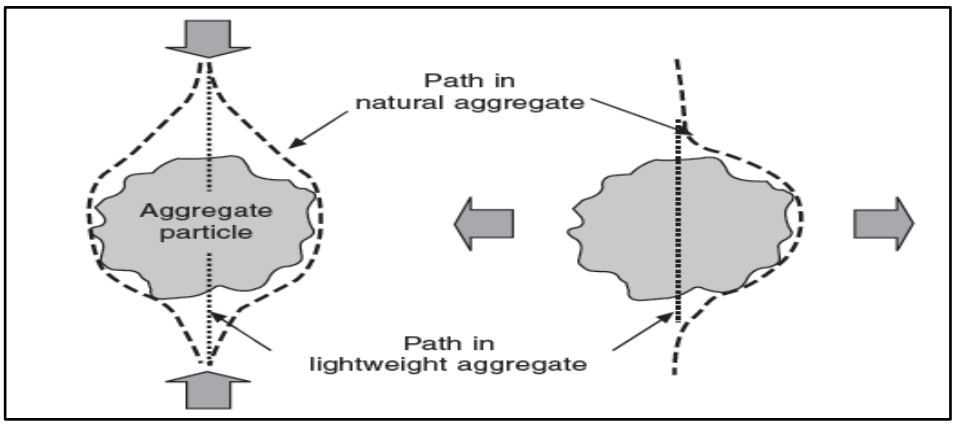

Figure 2-4: Fracture patterns in lightweight and normal weight concretes **(Newman& Owens, 2003)**

- Total water content

Because of the absorption of the lightweight aggregate, this is higher in lightweight aggregate concrete. Thus, under drying settings, larger moisture gradients can cause a considerable drop in tensile strength, however the benefits of increasing hydration mitigate this impact slightly Figure (2-5).

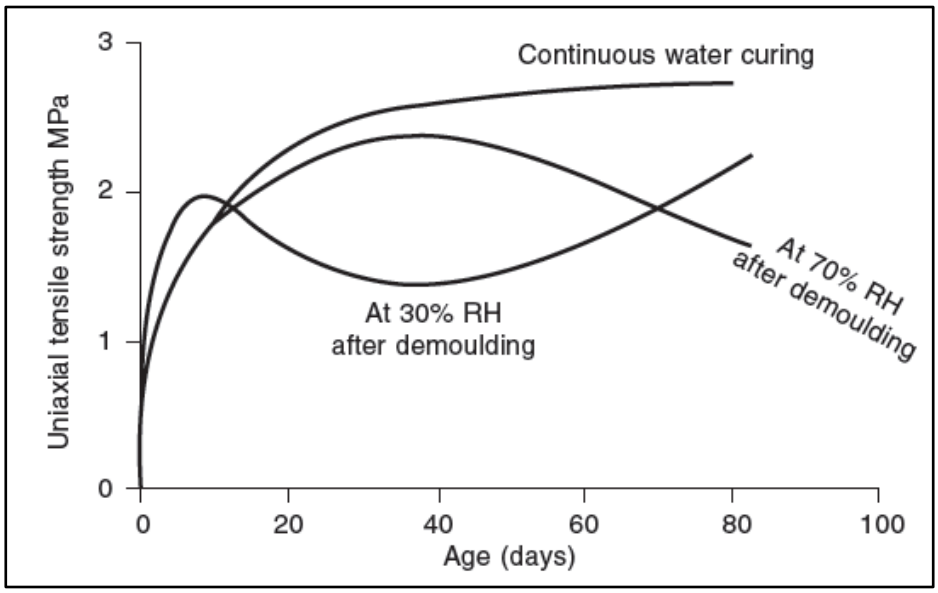

Figure 2-5: Drying effect on tensile strength **(Newman& Owens, 2003)**.

When testing, these influences should be taken into account. Flexural strength suffers more than cylinder splitting strength. The observed tensile strength as a proportion of the compressive strength is identical for both lightweight concrete and normal weight concrete in continually moist-cured concretes. Therefore, the tensile strength of lightweight aggregate concrete is lower than that of normal weight concrete with the same compressive strength when dry. This decrease has an effect on other parameters like as shear, anchoring, bond and so on. **(Lydon,1982)** showed that deformations are bigger when the stiffness of lightweight aggregate particles is low and the cement content is high. However, because lower concrete density mitigates these effects, small-scale laboratory testing can yield pessimistic findings when contrasted to on-site behavior. The stress–strain relationship in lightweight aggregate concrete seem to be more linear and brittle than those in normal weight concrete as shown in Figure (2-6)

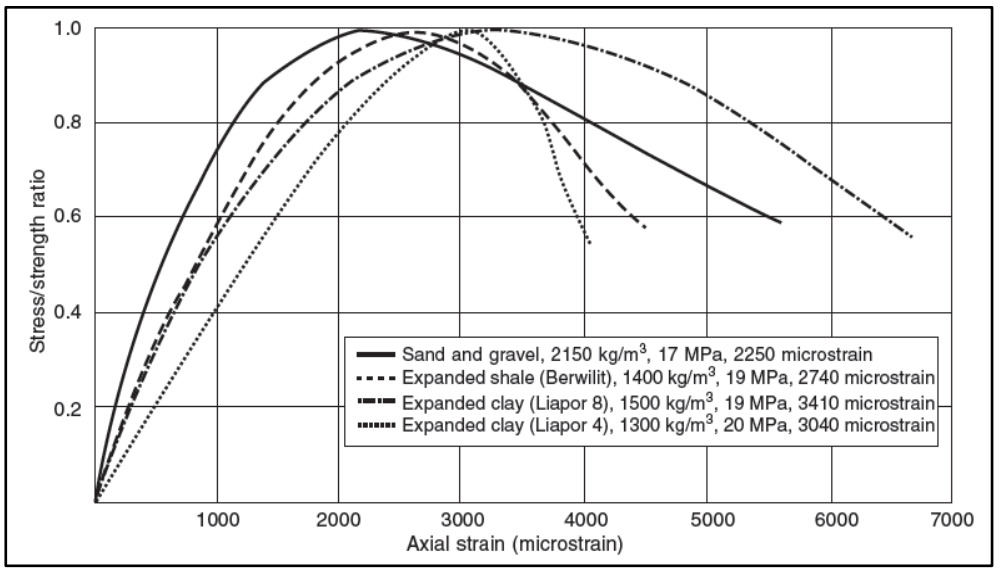

Figure 2-6: Stress–strain relationships of lightweight and normal weight concretes **(Lydon, 1982)**.

2.7 Beam Behavior under Fire Exposure

High temperatures are well known to cause severe damage to both the macroscopic and microscopic structures of concrete, resulted in massive mechanical degradation and even bad effects at the structural level as a result

of concrete spalling. Damage to the binder or aggregates is the primary cause of concrete degradation at high temperatures; their effects on the mechanical properties of the concrete at high temperatures have already been **(Choi et al., 2017; Gao et al., 2017).** Lightweight aggregates are often produced by volcanic eruptions or cremation. As a result, they have low heat conductivity and a high heat resistance. As a consequence, concrete made with such aggregates should have better mechanical properties at high temperatures than concrete made with ordinary aggregates **(Jiang et al., 2013; Sancak et al., 2008; Tanyildizi & Coskun, 2008; Turkmen & Findik, 2013; Yoon et al., 2015)**.

(Kodur,2014) stated that the behavior of a fire-exposed concrete structural member is based, in part, on the mechanical, thermal, and deformation properties of the concrete of which the member is constructed. Concrete's mechanical, thermo-physical, and deformation properties, like those of other materials, alter significantly within the temperature range associated with building fires. The properties change with temperature and are determined by the composition and features of the concrete. Concrete's strength has a considerable effect on its characteristics at both room and high temperatures.

2.8 Effect of Fire on Concrete

Concrete, according to **(Kodur& Raut,2010)**, has the best fire-resistant capabilities of any construction material. This high fire resistance is due to the basic ingredients of concrete (cement and aggregates), which when chemically mixed make a material that is virtually inert, has poor thermal conductivity, a large heat capacity, and a slow strength deterioration with temperature. Because of the slow rate of heat movement and strength loss, concrete may behave as an efficient fire shield not just between adjacent areas, but also to protect itself from fire damage.

Concrete is a composite material composed mostly of mineral aggregates bound together by a matrix of hydrated cement paste. Unless artificially dried,

the matrix is very porous and includes a high volume of free water. Concrete's chemical composition, physical properties, and content of water all change when exposed to high temperatures. In unsealed settings, these changes occur mostly in the hardened cement paste. Changes in the physical and mechanical properties of the concrete related with temperature increase reflect such changes.

(Tai et al.,2011; Bashandy,2013; Al-Jabiri ,2015; Kadhum ,2015) investigated the influence of fire flame burning on the mechanical characteristics of reactive powder concrete. These tests concluded that at fire temperatures less than 300ºC, a little increase in compressive strength was observed when compared to data at ambient temperature. At this temperature, the splitting tensile, flexural strength, and modulus of elasticity all increase. While exceeding 300ºC fire temperature, the mechanical properties of the RPC have rapidly deteriorated.

As illustrated in Figure (2-7), **(Ozawa et al., 2012)** described the behavior of reinforced concrete during the fire and the degree of influence. After one hour of exposure, for each degree of heating, where the elevation in temperature degree rises the degradation of concrete member damages produced by a combination of the impacts of gases generated by burning materials, as well as the effects of flames and high air temperatures.

The characteristics of high strength concrete (HSC) differ from those of normal strength concrete (NSC) with temperature. (**Jiang et al., 2013)**, have reported that high temperature-induced spalling does not occur when the moisture content (calculated by dividing the evaporative water content in a concrete specimen at a certain moment by the moisture content in the specimen just taken out of the standard curing room) in normal concrete is less than 75%, whereas this value for lightweight concrete is 25%. This suggests that spalling

of lightweight concrete at high temperatures is substantially more sensitive to moisture content than normal concrete.

Temperature (°C)	What happens
1000	
900	Air temperatures in fires rarely exceed this level, but flame temperature can rise to 1200°C.
800	
700	
600	Above this temperature, concrete is not functioning at its full structural capacity.
550-600	Cement-based materials experience considerable creep and lose their load bearing capacity.
400	
300	Strength loss starts, but in reality only the first few centimeters of concrete exposed to a fire will get any hotter than this, and internally the temperature is well below this.
250-420	Some spalling may take place, with pieces of concrete breaking away from the surface.

Figure 2-7: The microstructure process of concrete in the fire for a one-hour time **(Ozawa et al., 2012)**.

The porosity of lightweight aggregates, and hence their water absorption, is well known to be substantially greater than that of normal aggregates. In practice, lightweight aggregates are frequently pre-saturated before mixing to reduce water absorption and its influence on the workability and subsequent setting and hardening of the concrete produced. However, such treatment will add additional water into the concrete, increasing its moisture content and, as a result, increasing the potential of spalling at high temperatures.

2.9 Spalling of Concrete under Fire Exposure

(Dwaikat& Kodur,2009) pointed out that Spalling is a property that, in addition to thermal, mechanical, and deformation qualities, has a major effect on the fire performance of a concrete structural part. This characteristic is specific to concrete and may be used to determine the fire resistance of a reinforced concrete structural part **(Kodur& Phan,2007)**. Spalling is described as the separation of layers (pieces) of concrete from the surface of a concrete

part when subjected to high and quickly rising temperatures, such as those found in fires. Spalling can occur shortly after rapid heating and be followed by strong explosions, or it can occur later in the fire when the concrete has become so weak after heating that when cracks form, chunks of concrete fall off the surface of the concrete structure. As long as the damage is mild, the risks are limited, but excessive spalling may result in early loss of strength and integrity. Furthermore, spalling exposes deeper layers of concrete to fire temperatures, increasing the rate of heat transfer to the member's interior layers, including the reinforcement. When the reinforcement is expose directly to fire, the temperatures in the reinforcement rise at a rapid rate, resulting in a rapid reduction in structural member strength (capacity). The loss of reinforcing strength, along with concrete loss due to spalling, severely reduces a structural member's fire resistance (**Kodur& Dwaikat,2008; Yu et al.,2011)**. While spalling can occur in any concrete type, HSC is more prone to fire-induced spalling than NSC because to its lower permeability and water-cement ratio. The permeability of concrete, the type of fire exposure, and the tensile strength of concrete are all factors that influence fire-induced spalling (**Kodur& Phan,2007).** As a result, information on concrete permeability and tensile strength, which change with temperature, is critical for forecasting fire-induced spalling in concrete members. Whereas the moisture in lightweight aggregates may evaporate into the atmosphere during concrete service, due to their highly porous nature, lightweight aggregates would also highly absorb moisture again to cause spalling of the concrete in a fire caused by gas or other fuel **(Lindgard& Hammer, 1998)**.

This severely limits the heat resistance of lightweight aggregate. Many researches **(Sancak et al., 2008; Tanyildizi &Coskun, 2008; Turkmen &Findik, 2013; Yoon et al., 2015)** did not adhere to the actual technique of pre-saturating lightweight aggregates prior to concrete mixing. (**Jiang et al.,2013)** dried lightweight concrete sample at 100°C before exposing them to

high temperatures, which greatly reduced spalling. In practice, however, such pre-drying operation is impossible.

2.10 Introduction to Slurry Infiltrated Fiber Concrete (SIFCON)

Slurry-infiltrated fibrous concrete (SIFCON) (**Ibrahim & Jannoulakis ,1994)** is a form of fiber concrete with a high fiber concentration. The matrix is often made of cement slurry or flowing mortar. SIFCON is consider as pioneering building material that combines great strength and ductility. **(Thirugnanam et al. 2001)** studied the flexural behavior of SIFCON beams and found that SIFCON specimens had better ductility and energy absorption capacity than FRC specimens. According to **(Elnono et al. 2009),** using SIFCON in the joints enhanced the efficiency and ductility of the joints. The use of SIFCON jackets as external shear reinforcements has been shown to avoid brittle shear failure and enhance the ultimate shear strength of repaired beams from 25% to 50%, according to researchers (**Shannag et al. 2001**). **(Sashidhar et al. 2011)** have studied the flexural behavior of SIFCON and found that the deflection of SIFCON specimens was lower than that of control specimens, and that the load bearing capacity and energy absorption capacity of SIFCON specimens had risen substantially. Infer that perforated SIFCON block is an innovative structural material with compressibility. **(Abdollahi et al. 2012)** indicated that SIFCON can be used as a container for reinforcing concrete pillars. SIFCON has a high potential for use in applications requiring high ductility and impact resistance. SIFCON is not the same as normal FRC. The fiber content of FRC ranges from 1 to 3 percent by volume, whereas the fiber content of SIFCON ranges from 5 to 20%. **(Ibrahim & Jannoulakis ,1994)**, have reported that SIFCON producing differs greatly from FRC production (Fiber Reinforced Concrete). Unlike FRC, which is made by adding fibers to a wet or dry concrete mix, SIFCON is made by infiltrating cement slurry into a bed of fibers that has been preplaced and packed firmly in the molds. SIFCON has been utilized effectively in refractory applications,

pavement overlays, and blast and dynamic stress constructions. Because of its extremely ductile reactivity and significantly larger impact resistance, the composite has great potential for structural applications involving accidental or abnormal loads such as explosions (**Ibrahim & Jannoulakis ,1994)**.

2.10.1Preparation of SIFCON

SIFCON is a one-of-a-kind construction material with great strength, ductility, and considerably superior potential for structural applications when accidental (or) abnormal loads are encountered during services. SIFCON also exhibits a unique behavioral phenomenon known as "Fiber lock," which is thought to be responsible for its exceptional stress-strain performance. SIFCON's matrix has no coarse aggregates but a high cementitious percentage. It may, however, consist fine (or coarse) sand as well as additives such as micro silica, fly ash, and latex emulsions. A high strength SIFCON mix can be easily designed and procured with nearly any type of steel fibers available at the time, if the slurry is also of high strength, as slurry strength is a function of water-cement ratio, because the slurry mixes used in SIFCON generally contain significant percentages of fly ash (or) silica fume (or) both. When producing a slurry mix, the phrase "water-cement with admixtures" is employed. Furthermore, the "admixtures to cement" ratio is an important factor in SIFCON design. Higher percentages of fibers required a lower viscosity slurry to fully penetrate the fibers. In general, the greater the slurry strength, the higher the SIFCON strength. SIFCON preparations involve the following procedures **(Vijayakumar& Kumar, 2017)**:

- Place the fibers into the mold.
- Mixing of SIFCON dry ingredients.
- Slurry Preparation
- Infiltration of slurry
- The surface finishing.

SIFCON cannot be produced using normal mixing processes due to the interlocking effect of the large quantity of steel fibers. SIFCON is made by preplacing short different fibers within the moulds to its full capacity or to the necessary volume percentage, so forming the network. A fine liquid cement-based slurry or mortar is subsequently used to permeate the fiber network. For large sections, the fibers can be distributed by hand or by fiber-dispensing apparatus. Infiltration is often performed by gravity flow combined with mild vibration or through pressure grouting **(Farnam et al., 2010; Thomas & Mathews, 2014)**. **(Parameswaran et al., 1993)** prepared slurry-infiltrated fibrous concrete (SIFCON) by adding steel fibers into the matrix through three ways. The steel fiber is preplaced in the mold in the first (single layer approach), and the slurry is allowed to flow through the fiber with the assistance of appropriate compaction by a vibration table, see Plate (2-1). The second procedure involved initially inserting and packed the fibers into the mold just approximately to one-third depth, following by slurry penetration up to the present level. The mold's contents were then vibrated. The operation was repeated until the entire mold was filled and compressed, and it was known as (three-layer technique).

The third approach, known as the (immersion technique), involved filling the mold approximately to one-third depth with slurry, instantly embedding the fibers into it, shaking the contents, and repeating the process until the mold was filled. During the deposition of the SIFCON samples, the researchers discovered that these three approaches were efficient. Nevertheless, in practice, the three-layer and immersion procedures were proven to be easier than the single-layer technique **(Yazc et al., 2006; Ail, 2018)**.

Plate (2-1): SIFCON casting technique **(Yazc et al., 2006)**.

2.10.2 Materials and Mix Proportions

In general, proportions of cement and sand generally used for making SIFCON are 1:1, Fly ash or silica fume equal to 50%by weight of cement is used in mix. w/c is 0.45 and super plasticizers varies from 2% to 5% of weight of cement used. The percentage of fibers by volume can be where from 6% to12% used. Sand is taken in to passing through 600 μ and retains 300 μ. The proportions of SIFCON slurry from various researches are shown in Table (2-1). The proportion of fibers by volume can vary from (4 – 20%), despite the fact that the present practical limit is just (4 – 12%) **(Dagar, 2012; Ail, 2018)**.

It was discovered that using a high cement content in the SIFCON influences cost of production, as well as having adverse effects on the heat of hydration and might causing shrinkage problem. To address these issues, it appears that substituting the cement with alternative cementitious materials is a viable option. These materials alter the microstructure of concrete and decrease its permeability, limiting water and salt-borne salt entry into concrete **(Kani, 2016)**.

Table 2-1: Mix proportions of SIFCON slurry (by weight of cement) from different references.

Cement	Sand	Silica Fume %	Fly ash	W/B	HRWR%	References
1	1	5,10,15, 20, and25**	---	0.40	2	**(Elavarasi &Mohan, 2016)**
1	1	---	---	0.5	---	**(Parthiban et al., 2013)**
1	1	---	---	0.45	1.5	**(Rao & Ramana, 2005)**
1	1	15*	---	0.28	1.5	**(Yan et al., 1999)**
1	---	---	0.3	0.3	1.9	**(Wang & Maji, 1994)**
1	1	---	---	0.38 0.38 0.35 0.32	2 1 2 1	**(Parameswaran et al., 1993)**

*Silica fume was used as additives not replacement by weight of cement

** Silica fume was used as replacement by weight of cement

To improve slurry flow ability and ensure effective infiltration, high-range water-reducing admixtures (superplasticizer) are added. The amount of superplasticizer used has the largest effect on the cohesion, fluidity, and penetrability of cement slurry **(Gilani, 2007)**. **(Wang & Maji, 1994)** reported that an inadequate dose of superplasticizer limits appropriate flow and infiltration, while an overdose causes 'bleeding' and 'segregation' of the cement and fly ash to the bottom.

2.10.3 Physical and Mechanical Properties of SIFCON

Many researches are investigating the mechanical properties of SIFCON produced with fly ash or crushed coarse furnace slag as a replacement. Furthermore, there is relatively little data on SIFCON properties produced silica fume with steel fiber as an additive to cement paste or slurry.

(Balaguru, & Kendzulak,1987) investigated the behavior of SIFCON under monotonic and high amplitude cyclic loads in compression, tension, flexure, and shear. SIFCON's direct tensile strength was determined using dog bone specimens, while its shear strength was determined using double L specimens. The author found that fiber length has little or no influence on strength, that the inclusion of silica fume enhanced compressive and flexural strength, and that a cement-sand ratio of up to 1:1.5 may be utilized for cement slurry not impacting the strength of SIFCON.

The modulus of elasticity of the SIFCON under compressive and tensile loads was investigated experimentally by **(Naaman et al.,1992)**. Two types of steel fibers (deformed and hooked steel fibers), two aspect ratios (60 and 100), seven volume fraction ratios, and four matrix formulations were tested. The cement slurry was supplemented with fly ash, fine aggregate, and super plasticizer. Compression cylinders and dog-bone tension specimens were utilized to measure the stress-strain curve and modulus of elasticity, respectively. The findings show that the modulus of elasticity of the SIFCON is affected by multiple parameters, including fiber orientation, volume fraction-fiber ratio, alignment, and fiber aspect ratio.

The ultimate strength and elastic modulus of SIFCON in tension do not appear to be highly responsive to the water-cement ratio over the value range investigated. The modulus of elasticity of SIFCON in tension is related to the volume percentage of fiber at unchanged fiber length. Everything else being equal, the longer the fiber, the greater the elastic modulus of SIFCON.

(Elavarasi,2016) studied the behavior of SIFCON in the presence of silica fume. The work program was carried out to investigate the compressive and splitting tensile strength of SIFCON, which had 10% fiber content and a variable ratio of silica fume of around (5, 10, 15, 20, and 25%) partially replaced by cement. The test results revealed that (15%) of the silica fume

produced the best compression and tension values when comparing to the other replacement rate and FRC mixes.

According to **(Vijayakumar & Kumar,2017)**, the compressive strength of SIFCON mixes grows as the percentage volume of fiber increased. The test findings are compared to those of conventional concrete under similar loading conditions. According to the findings of this study, increasing the volume of steel fibers fraction leads to an increase in compression, tension, and flexural strength. When compared to standard concrete, a 12% addition of steel fibers boosts strength by around 36.2 percent. The cement slurry (without fibres) used to produce SIFCON normally has a one-day strength of 25 to 35 MPa and a 28-day strength of 50 to 70 MPa, whereas the values obtained for SIFCON composites are 40 to 80 MPa and 90 to 160 MPa, depends on the proportion of steel fibres incorporated in the matrix. The greatest compressive strength recorded for SIFCON is 210 MPa. Under compression, SIFCON is highly ductile **(Gilani, 2007; Dagar, 2012)**.

(Kim & Choi, 2006) investigated SIFCON's compressive and tensile properties. Researchers used hooked end steel fibers in the mix, with a fiber volume percentage ranging from 4% to 10%. The water/cement ratio is fixed at 0.4. They used 10% silica fume by weight of cement, as well as 0.5 percent water reducing agent, to increase the slurry's flow ability. The results of the tests revealed that the compressive strength of SIFCON is approximately (1.59 to 2.68) times that of cement paste. Tensile strength increased by around 2.51 to 8.77 times. With increasing fiber volume fraction, there is also a considerable rise in SIFCON toughness and ductility.

2.10.4 Ductility, Toughness and Stiffness of SIFCON

The key specifications that are demanded from concrete are strength and toughness. These requirements can be met with high-strength concrete. Furthermore, ductility has emerged as one of the most significant hardened

properties in recent times. Brittleness is a problem of concrete use, and attempts have been made to solve it by increasing ductility. Figure (2-8) presents the difference between brittle and ductile materials. The incorporation of fiber in concrete is one of the better solutions to the brittleness challenge. However, incorporating fibers into the concrete decreases its workability, limiting the fiber ratio that may be added to the concrete **(Ipek et al., 2014)**.

SIFCON is applied in the construction of a variety of structures that require high strength specifications as well as high performance and durability. SIFCON has a number of excellent properties, including high strength and ductility. It also has a high level of ductility, which gives it greater stability under dynamic, fatigue, and cyclic loads **(Elavarasi, 2016)**.

According to studies, the use of SIFCON in normal RC beams improved cracking behavior by significantly increasing the initial crack load and forming a greater number of finer cracks. When compared to normal RC beams, composite beams have better ultimate load bearing capacity, stiffness, ductility, and energy absorption capacity.

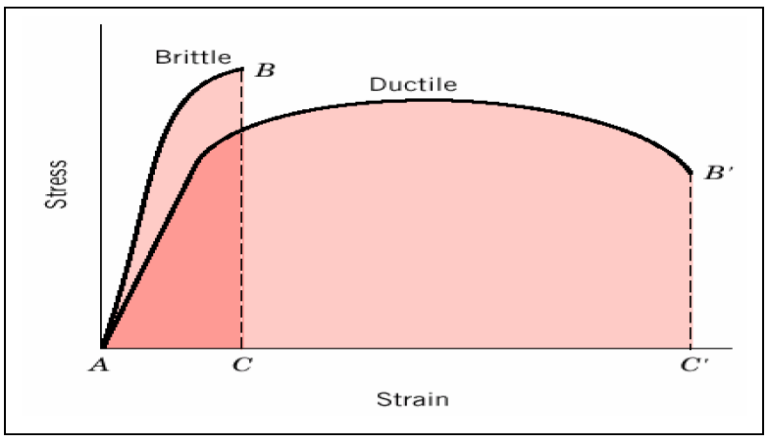

Figure 2-8: Stress-strain curves for ductile and brittle materials **(Amin, 2014)**.

2.11 Shear Strength of RC Beams

Concrete is considering as a brittle material that has a limited ability to withstand tensile stresses/strains without cracking. As a result, it requires

reinforcing before it can be utilized as a material for construction. Previously, this reinforcement comes in the form of longitudinal reinforcing bars that could be installed in the structure at appropriate places to resist the applied tensile and shear forces. As research improves, fibers that are short, discontinuous, and randomly dispersed throughout the concrete are employed to produce fiber reinforced concrete, an advanced composite material (FRC). Steel fiber (SF) seems to be the most commonly used fiber in reinforced concrete. Fibers are used in concrete to prevent/control plastic and drying shrinkage, as well as to considerably increase its flexural toughness, energy absorption capacity, ductile behavior prior to ultimate failure, decrease cracking, and improve durability **(Behbahani et al., 2012)**.

Designers often refer to conventional strengthening solutions based on externally bonded steel plates or reinforced concrete jacket, but a new method that has recently gained popularity involves the use of externally bonded Fiber Reinforced Polymer (FRP) **(Du Béton, 2001)**. All of these solutions can be used successfully, but they have significant limitations. Due to the presence of reinforcement bars, which need a minimum concrete cover, the use of reinforced concrete jacket is particularly possible by adding layers of concrete with thicknesses more than 60–70 mm **(Fib bulletin, 2010)**.

The usage of externally bonded steel plates as well as Fiber Reinforced Polymer may present fire resistance problems. Furthermore, the application of these solutions may fail to meet the minimal requirements for serviceability limit states. Because of its improved qualities following cracking of the cementitious matrix, the application of fiber-reinforced concrete has grown during the last ten years **(Rossi&Chanvillard,2000)**.Fiber Reinforced Concrete (FRC) is currently widely employed in sectors whose fiber reinforcing is not required for structural safety (for example, industrial pavements or shotcrete for initial stage tunnel linings). Aside from this, there are two

applications in which fiber reinforcement is employed as a whole or partial replacement for conventional (rebars or welded mesh) reinforcement **(Falkner et al., 1997)**.

Several investigations, in particular, indicated that fibers may be employed to replace a part of the shear reinforcement in beams, or transverse reinforcement in thin-web sections **(Minelli et al., 2006)**. Due to the obvious ability of stress redistribution, an FRC with a post-peak softening behavior in tension can be used in all of these applications. Recently, FRC materials with a hardening characteristic under tension, often referred to as High Performance Fiber Reinforced Concrete (HPFRC), have been widely available, allowing for additional applications **(Li, 1993; Van Mier, 2004)**.

Indeed, by utilizing these materials, it is possible to form structures with new geometry and shape that are no longer restricted by reinforcing details limitations. Both FRC and HPFRC will be included in the upcoming New fib Model Code and treated as construction materials for existing and future structures **(Fib Bulletin, 2010)**. Figure (2-9) shows a comparison of the findings of the three tested beams. When focusing on the two RC beams (with and without strengthening jacket), it can be seen that the HPFRC jacket increases the structural capacity of the beam (2.15 times), even if the post-peak behavior shows significant softening. Because of the jacket, the load stabilized with a horizontal branch greater than that achieved in the RC beam without jacket at the end of the softening branch. It should be noted that the maximum load of the beam with the HPFRC jacket and also no conventional reinforcement is greater than that of the RC beam without the HPFRC jacket.

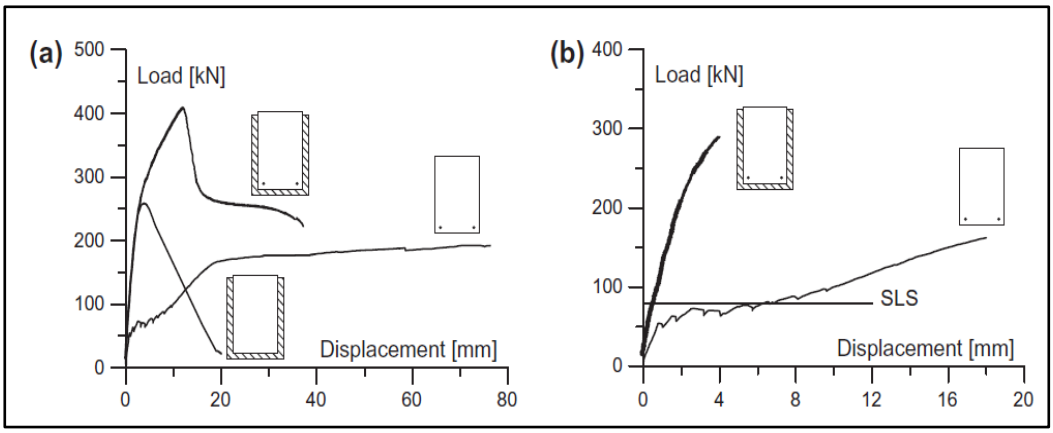

Figure 2-9: Comparison of the load–displacement curves obtained from strengthened beams: (a) complete curves; (b) and initial part of the curves (for serviceability limit state SLS) **(Giovanni et al., 2010)**.

In terms of ductility, it is important to note a reduction in ultimate displacement in the reinforced beams, even if the seeming extremely high ductility of the unstrengthen element is owing, at partially, to bond loss. If the reinforced beam also has to be more ductile, an appropriate steel reinforcing in meshes or tiny diameter rebars might be placed in the jacket **(Marini& Meda, 2009)**.

Another important aspect of the proposed method is the service conditions. Design codes, in fact, demand that the reinforced structure be verified at both the ultimate limit state (i.e. increased bearing capacity) and (SLS) the serviceability limit state (i.e. deflection and crack initiation control). In this regard, the proposed approach results in a significant increase in beam stiffness, with behavior similar to the un-cracked stage in an unreinforced beam (Figure 2-9b). Indeed, the HPFRC jacket minimizes the formation of macro-cracks, which has evident benefits in terms both durability and stiffness, especially when considering the high-performance matrix's very low w/c ratio.

2.12 Failure Modes of Concrete Beams in Shear

Reinforced concrete beams must have a sufficient safety margin against bending and shear stresses in order to function efficiently during their service life. The combinations of bending and shear may surpass the resistance capacity

of the beam in the maximum stress, resulting in tensile cracking. Despite extensive experimental investigation, shear failure is hard to predict effectively. It is not considered a possibility to retrofit reinforced concrete beams with many shear cracks **(Al-Nasra& Wang,1994)**. Diagonal cracks are the most common kind of shear failure in RC beams that are located close the supports and are produced by excessively applied shear stresses.

Beams collapse rapidly when significant cracks form in the high-shear zone near the beam supports. Shear reinforcement must be added if the value of actual shear forces exceeds the allowable shear stress of the concrete used. The goal of shear reinforcement is to avoid shear failure and enhance beam ductility, which reduces the chance of unexpected failure. The causes of shear failure are likely to be associated with the stress conditions in the region of the path along which the compressive force is transmitted to the supports after the occurrence of diagonal cracking; an analytical description of these conditions could lead to the formulation of a lower bound criterion for failure.

On the basis of this argument, the shear modes of failure exhibited by the beams under two-point loading may be broadly classified into two types:

- **Type 1**

This includes types of failure that occur in beams with (av/d) less than or equal to a value between 2 and 2.5. Such beams have a compressive force path consisting of linear parts inside both the shear and middle spans crossing each other in the zone of the load point Figure (2-10a).

It has been claimed that, despite the high compressive stresses at the load point zone, diagonal cracking is unlikely to result in a crushing mode of failure because the multi - axial compressive state of stress that occurs there will produce an enhancement in local strength. Alternatively, the diagonal crack should spread near-horizontally towards the compressive region of the beam's flexure span to avoid this high strength zone. The tensile stress consequent at

the crack branch's tip, along with the compressive stress resultant from the bending action, will decrease the strength capacity of the compressive zone of the beam's flexure span. As a result, the failure of this part would eventually lead to the beam collapsing.

- **Type 2**

This comprises shear modes of failure that occur in beams with (av/d) values greater than around (2 to 2.5). Such beams have a compressive force path included of two linear parts throughout the shear span joined in the region of the diagonal crack tips Figure (2-10b).

This difference in compressive force direction creates a tensile stress as a result of intersecting the obtuse angle of the linear parts, which is overlaid on the tensile force present near the tip of the diagonal crack for balancing reasons. When the region's ability to withstand the combined compression-tension stress field is surpassed, failure happens **(Kotsovos, 1983)**.

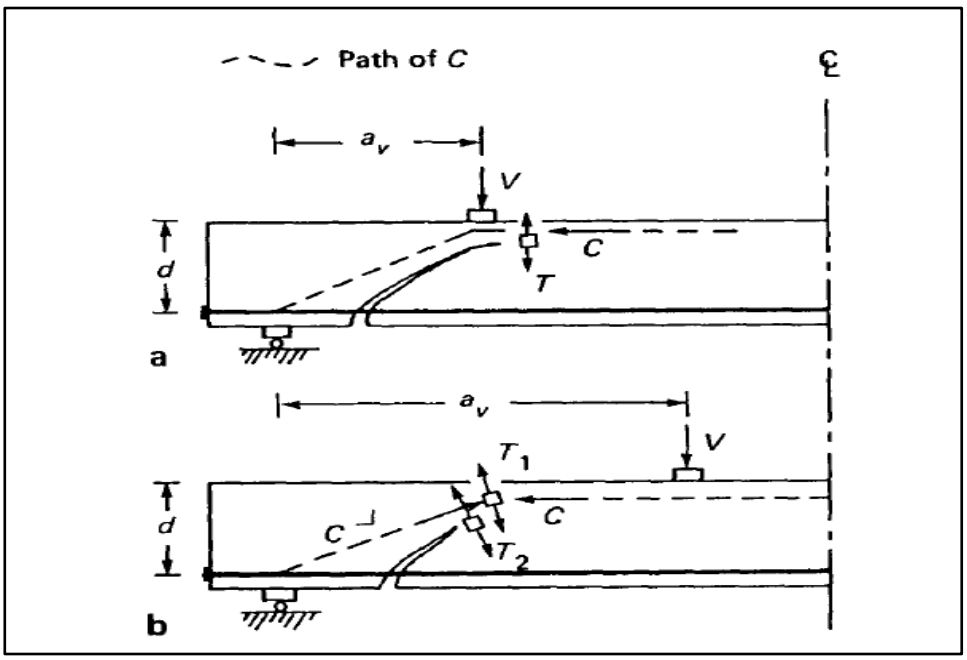

Figure 2-10: Path of compressive force (C), and combinations of compressive and tensile forces (T), resulting in: (a) type 1, av/d< 2-2.5; (b) type 2, av/d> 2-2.5 **(Kotsovos,1982)**

It should be observed, however, that the presence of shear forces invariably results in an inclined tensile force inside the near-horizontal region of the compressive force path proximal to the load point for equilibrium purposes. There is no experimental evidence that the abovementioned tensile force may produce failure, and this appears to be due to the tri - axial stress conditions that have always been observed to occur within the compressive zone **(Kotsovos,1982)**.

The compressive region in the zone of cross-sections with deep web cracks is subject to a tri - axial compressive stress state, as explained for the case of RC beams in flexure. Because a part of the vertical component of this compressive stress state counteracts the tensile stresses that form in the presence of shear forces, the combined stress conditions remaining compressive. Transverse reinforcement put inside the shear span of the beams has the result of delaying or even preventing a shear mode of failure within this span. Furthermore, when $av/d > 2$, an additional influence may be that the angle between the longitudinal axis of the beam and the part of the compressive path within the shear span at the load point decreases from a near-zero value Figure (2-10b) to a much higher value Figure (2-11).

Such behavior may create a wedge-like action in the load point zone, resulting in failure of the compressive region of the flexure span, where state of stress is basically uniaxial, instead of the load point zone, where a triaxial compressive state of stress occurs **(Kotsovos, 1983)**. It should be noticed that such failures are similarly to those classed as type 1 shear failures above and may be brittle since they occur before the beam's maximum flexural capacity is reached. As a result, it appears that, while existing shear design approaches may protect against diagonal failure of the shear span, they may not always result in ductile behavior that provides advance warning of potential structural collapse **(Bobrowski, 1982).**

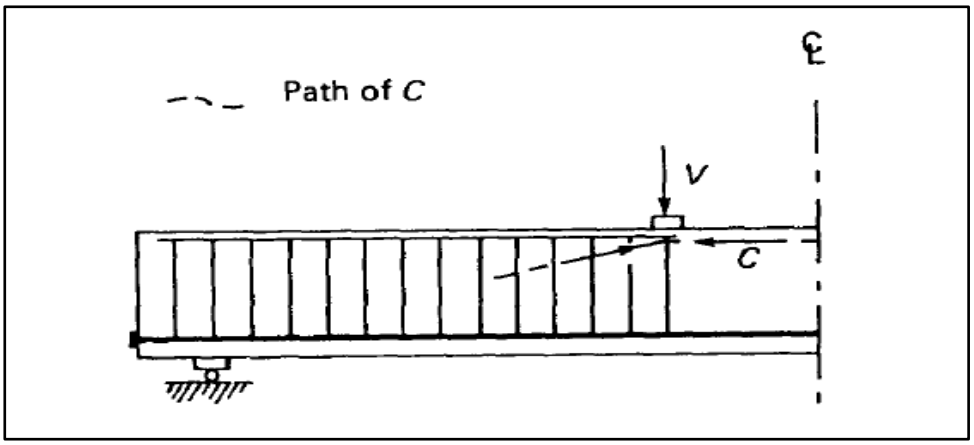

Figure 2-11: The transverse reinforcement effect on the path of compressive force, C, in a beam shear span with an av/d> 2.

2.13 Previous Studies on Beams Exposed to Fire Flame

Despite the fact that there are several articles on the behaviour of normal weight concrete, exposed to flame, thermal characteristics, stiffness and strength, and the capacity of the structure to redistribute internal stresses during the fire's evolution. Only a few articles studied the structural behaviour of lightweight concrete beams following a fire.

(Bernhart,2004) demonstrated that if a simply supported beams is exposed to burning at the sides and bottom, it gradually deflects downwards. The displacement is caused by non-linear heat transfer that develop over the beam's cross-section and cause the beam to thermally deflect downwards. The increased temperatures at the sides and bottom of the structural member reduce the strength and elastic modulus of the steel reinforcement and concrete. Furthermore, create a decrease in the flexural strength of the beam, resulting in increased deflection. Whenever the bending moment exceeded the residual flexural strength of beam, the failure occurs preceded by a plastic hinge forming. The use of steel fibres results in multiple tiny cracks instead of one large crack on the tension face.

(Prasad et al.,2010) tested twelve reinforced concrete beams using two-point load test. The studied variables were concrete grades, period of fire exposure, and spacing of stirrups. In a full-scale fire oven, the concrete

beams were initially exposed to standard fire. Following that, after cooling, it was tested with two-point loading. According to the findings, the concrete grade, spacing of stirrups, and period of fire exposure all have a significant impact on the moment bearing capacity and curvature of the section. With increasing fire exposure, the yield and ultimate moment capacity of all fire-damaged samples dropped. Whereas the yield and ultimate curvatures grew as the fire time increased, the total curvature ductility decreased. The ductility of reinforced concrete members is mostly determined by the moment-curvature curve shape, since ductility is defined as the ability to absorb deformation without significantly reducing the member's flexural capacity.

The effects of compressive strength and concrete cover thickness on exposed simply supported beams were studied by (**Choi& Shin, 2011)**. Four high- and normal-strength concrete beams were tested for this purpose in accordance with ISO 834. The test findings revealed that, except for the upper section of the beam, the relations of time and temperature distributions in the beam sections are quite comparable and independent to the concrete strength. They also demonstrated that before spalling, the rates of deflection increase for both high-strength and normal-strength concrete are relatively similar, but become surprisingly high in case of high-strength concrete beams.

(Kadhum,2011) investigated the impact of fire on the behaviour of reinforced concrete rigid beams as well as its load bearing capacity. 5 end-restrained specimen beams were tested in fire flame temperatures ranging from 25 C° to 750 C°. The beams measured 375 mm wide, 375 mm in depth, and 2250 mm in length. The mid-span displacement of reinforced concrete specimen beams exposed to fire flame at the bottom side of the beam by using burner is caused by loading to 25% of the ultimate load before applying fire, loading 25% and burning for 90 minutes, then cooling by air or water, and the rest of the loading was applied until defeat. The researcher indicated that

ultrasonic pulse velocity was reduced by 28 per cent and 33 per cent for beams cooled in air at 400 C° and 750 C°, respectively, and by 52 per cent and 54 per cent for beams cooled using water at about the same temperatures. Fire degree has a considerable influence on the flexural behaviour of reinforced concrete rigid specimen beams; as fire temperature rises, the ultimate and serviceable structural capability of reinforced concrete beams decreases. The load-displacement relationship of beams subjected to fire at temperatures about 750 degree Centigrade indicates softer behaviour than that of the control beam, which can be attributed to earlier cracks and a decreased modulus of elasticity.

(Ryu et al.,2015) used analytical and experimental approaches to study the rehabilitating benefits for high strength fire-damaged concrete beams. Beams subjected to high temperatures depending of the ISO 834 standard time. The findings of the two-point loading test demonstrate that the ultimate loads of the rehabilitated beams are comparable to or greater than those of the non-exposed RC beam.

(Arafa&Ali,2017) evaluated the influence of fire on structural behaviour of normal and high strength concrete beams and determined that the displacement of a beam exposed to fire is directly proportional to fire exposure duration and inversely to thickness of concrete cover. Furthermore, for beams with a prolonged fire exposure duration, concrete compressive strength has no influence on the percentage decrease of ultimate loading capacity.

According to (**Abeles&Bardhan-Roy,2014)**, the residual strength of LWAC (light weight aggregate concrete) linearly decreasing from 100 per cent to 40 per cent from about 500ºC to 800ºC, and the residual strength of normal concrete is about 20 per cent at 800ºC, while the strength reduction for normal reinforcement is about 50 per cent at 500ºC. However, this does not indicate if the steel reinforcement is in contact directly with fire or is protected by a concrete cover.

2.14 Concluding Remarks

Based on the previous studies' results, the following conclusions can be drawn:

- Installing a 40 mm thick HPFRC jacket on an RC beam improves the ultimate load by 2.15 times, as in case of a pre-damaged beam, the increase is roughly 1.90 times. The experimental and numerical results show that the suggested approach is effective in developing load carrying capacity in both strengthening and repair scenarios.
- The proposed method provides a significant structural improvement at the serviceability limit state; due to the significantly increased beam stiffness under service load, the mid-span displacement can be significantly reduced. In practice, the jacked works as a type of external pre-stressing by maintaining the material's initial uncracked stiffness.
- The use of SIFCON (cement-based composite including steel fibers) to strengthen reinforced concrete beams in shear seems to be a highly successful technology. Brittle shear failure was eliminated in beams repaired with SIFCON jacket, and ultimate shear strength improved from 48 to 60% in those beams examined. This might be related to the crack stopping mechanism, the energy absorbed in debonding, and the stretching of the fibers.
- The HPFRC application technology is relatively simple: curing at ambient temperature and humidity is sufficient to allow the development of the HPFRC's strength characteristics; due to the self-leveling property, the material can be cast in a thin layer; and normal sand blaster of the beam surface ensures good jacket adhesion without the need for any primer.
- Depending on previous studies, the thickness of the concrete cover seems to have effect in short fire exposing time (less or equal to 1 hr.), and not very high temperature (not exceed 600ºC), but it has no influence on the

decrease in strength properties when exposed to a 2 hour fire, meaning that cover thickness has no major effect on the strength of the embedded steel reinforcement. This is due to the fact that the thermal conductivity of normal concrete is relatively low up to 400ºC and increases insignificantly as the temperature rises to around 1000ºC. This supports the findings of (**Hu et al.,1993).**

- According to (**Kigha et al.,2015)**, after a two-hour fire with a maximum temperature of 700ºC, the flexural capacity owing to tensile reinforcement of the beam remains unchanged, contrary to the (**EC2**,**1995)** prediction model.

CHAPTER THREE

Chapter 3. Experimental Program

3.1 Introduction

The specifics of the experimental program are described in this chapter. It elaborates on the research methods utilized to achieve the objectives stated in Chapter One, as well as the materials used. (cement, lightweight aggregate, sand, steel fiber, mineral and chemical admixtures), mix proportions, preparation, mixing, casting procedures, curing, and testing program of high strength and normal strength lightweight concrete beams.

The experimental research is undertaken in order to studies the structural behavior of post-fire LWRC beams that repaired and strengthened by using U-shaped SIFCON jackets. The following experimental variables were studied for LWC beam specimens:

1) Grade of lightweight concrete (normal and high strength concrete).
2) Concrete cover of reinforcement thickness [20 and 30mm];
3) Period of exposure to fire flame [30 and 60 minutes]; and
4) Thickness of SIFCON jacket [20 and 30 mm].

Details of the tests on Lightweight concrete and SIFCON specimens used throughout this study are explained such as: -

1) Tests of fresh SIFCON (mini slump flow and V- funnel test);
2) Compressive strength;
3) Modulus of elasticity;
4) Load deflection relationship
5) Ultimate load carrying capacity of the beam specimens.

It is imperative to know the properties and characteristics of constituent materials of concrete, as it is aware, SIFCON and lightweight (NSC and HSC). SIFCON is a composite material consisting from several components such as

cement, sand, fiber, water, and admixtures. These materials have different properties and characteristics, like as (specific gravity, unit weight, gradation and water content). Lightweight concrete (LWC) that contains lightweight expanded clay aggregate (LECA).

To achieve appropriate concrete production, stringent measures in material selection, control, and proportion of the overall material have been used. The sources of materials, chemical compositions, and physical properties of the materials used are explained in detail in this experimental study; the required testing was carried out at Babylon University, Faculty of Engineering, Civil Engineering Dept. laboratories.

3.2 Flow Chart of the Research

This thesis's experimental program is divided into two sections. The first stage involves the selection, preparation, and testing of the physical and chemical properties of raw materials applied in this research. As part of the overall structural LWAC program, different grades of LWAC with two compressive strengths of concrete have been produced. The target compressive strength was (30 and 67 MPa) designated as a normal and high strength lightweight concrete respectively.

The manufactured lightweight aggregate, 'LECA' was used for lightweight concretes of normal and high strengths. To date, appropriate guidelines for LWAC mix proportioning are limited, and those that are available are not specified. As a result, in order to reach the necessary strength and workability, using any lightweight aggregate, trial mixes are needed and so were done in this study.

Superplasticizer was generally used to attain the required workability, as well as mineral admixtures were used for all mixes. Subsequently, this stage also performs trail mixes of SIFCON to select the optimum mix proportions and to select the proper type and dosage of mineral and chemical additives.

Then, the selected materials are mixed with the selected optimum mix proportions and with a suitable mixing procedure. Finally, the casted samples and beam specimens cured for the required ages (7, 28 and 90 days). The second stage consists of the burning of the LWC beam specimens and samples with different durations of fire exposure (30 and 60 min.) after reaching the required age (56 days).

While the third stage, after the burning process is finished, this stage deals with the repaired and strengthened post-fired beams by using U-shaped SIFCON jacket, then preparing and testing of the exposed (with and without repaired) and unexposed concrete samples and LWC beams.

The overall experimental investigation is shown in the flowchart given in Figure (3-1). This chapter describes the testing procedure only, while the obtained results from the mentioned tests will be discussed in Chapter Four.

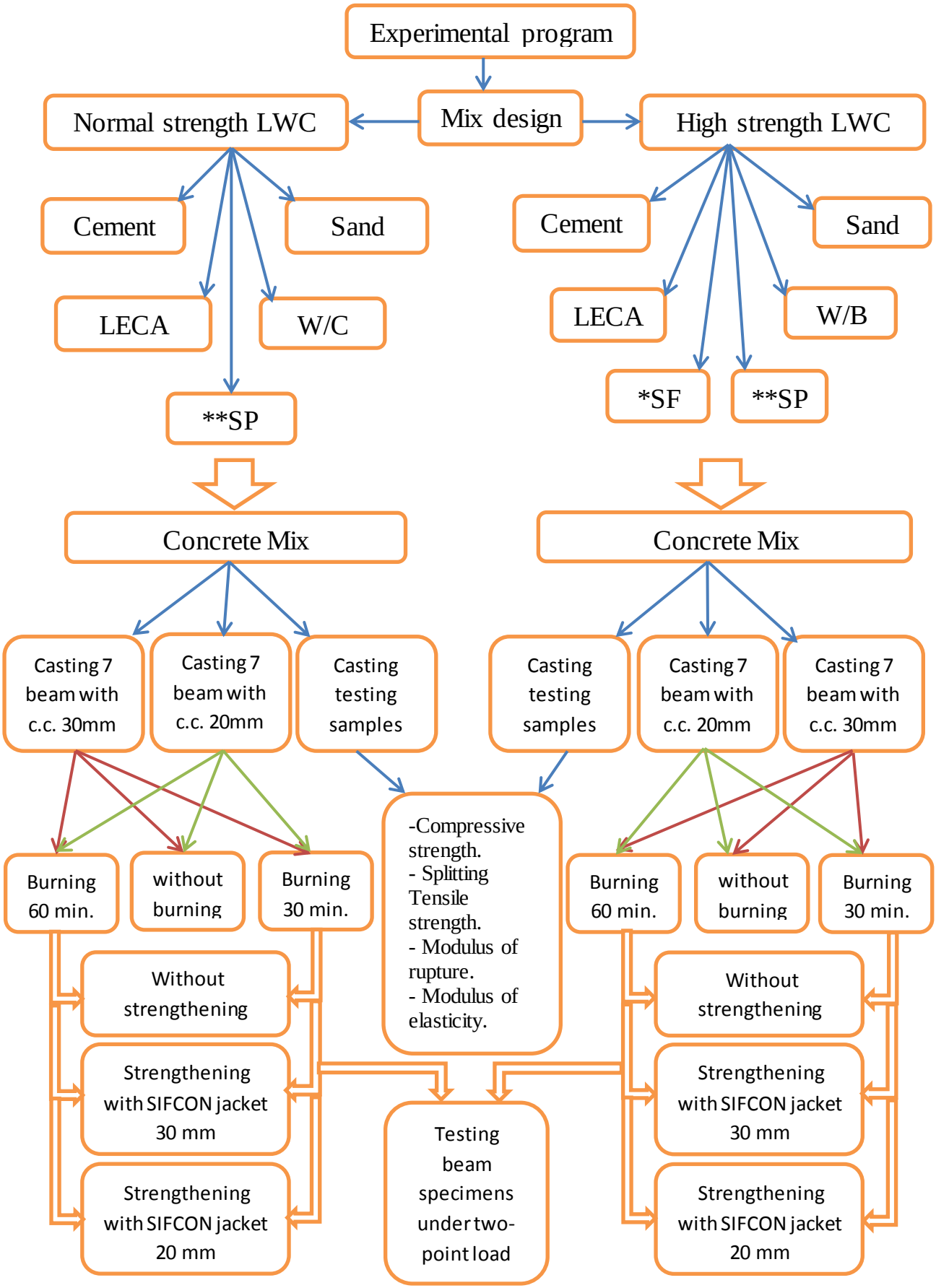

Figure 3-1: Flow chart of the research plan (where*mean silica fume and **mean super plasticizer).

3.3 Selection of Materials and Basic Characteristics

It is imperative to know the properties and characteristics of constituent materials of concrete, as it is aware, concrete is a composite material made up of several different materials such as gravel, sand, water, cement and admixtures. These materials have properties and different characteristics such as (Unit weight, Specific gravity, gradation and water content). In order to ensure adequate concrete production, rigorous process adopted in the chosen of the materials, controlling and proportioning of the entire mixture's ingredient. The supplies of ingredients, physical characteristics and chemical compositions of the materials which were utilized are represented in full details under this experimental study. The principal characteristics of these materials are as follows:

3.3.1 Portland Cement

In this investigation, Portland Limestone Cement (PLC) of the CEM II/A-L 42.5R brand name (Karasta) was utilized. The Lafarge company manufactures it in Iraq. It was kept in a dry place to avoid exposure to different atmospheric conditions. The chemical analysis and physical test results of the used cement are given in Table (3-1) and (3-2) respectively. This cement complied with the **(BS EN 197-1,2011)**.

Table 3-1: Main components and chemical composition of Karasta Portland limestone cement (PLC).

Chemical composition	**Percentage by weight**	**Limit of (EN 197-1:2011)**
Lime (CaO)	61.9	---
Silica (SiO_2)	20.1	---
Alumina (Al_2O_3)	4.8	---
Iron oxide (Fe_2O_3)	2.7	--
Magnesia (MgO)	2.5	---
Sulfate (SO_3)	2.6	$\leq$ 4.0 %

Chloride content	0.02	≤ 0.1 %
Loss of ignition (L.O.I.)	1.94	---
Insoluble residue (I.R.)	1.00	---
Lime saturation factor (L.S.F.)	0.9	---
Main compounds (Bogue's equation)		
Tricalcium silicate (C_3S)	55.65	---
Dicalcium silicate (C_2S)	15.73	---
Tricalcium aluminate (C_3A)	8.16	---
Tetracalcium aluminoferrite (C_4AF)	8.21	---

Table 3-2: Physical properties of Karasta cement.

Physical properties	**Test result**	**Limit of (EN 197-1:2011)**
Specific surface area (Blaine method) m^2/kg	314	-
Setting time (Vicat's apparatus)		
Initial setting, (min)	122	≥ 60 min
Final setting, (min)	188	
Soundness using autoclave method	0.61 %	≤ 10 mm
Compressive strength (MPa) at:		
2 Days	21.0	≥20
7 Days	45.8	≥ 42.5, ≤62.5

3.3.2 Fine Aggregate

Fine aggregate from local natural resource (AL-Akhaider) has been utilized as sand. The sand was suitable to use in lightweight concrete mixes, but for SIFCON the important requirement of sand used in slurry is its size, it has to be small enough to ensure complete infiltration through the dense steel fiber without clogging. AL-Akhaider natural sand was too coarse to be used successfully in making SIFCON slurry. Therefore, only fine sand, which was sieved through (1.18 mm sieve) to segregate the coarser particles, was used in preparing SIFCON slurry. Using this size of sand proved to be successful for

all SIFCON mixes during the experimental work. Table (3-3) shows the sieve analysis of the sand used. It conforms to the limits of Iraq specification No. 45/1984 Zone (2). Figure (3-2) shows the grading curve of the natural sand in accordance with **(IQS No. 45,1984)**, and the chemical and physical properties of natural sand are illustrated in Table (3-4).

Table 3-3: The original fine sand grading compared with the requirements of **(IQS No. 45,1984)**.

Size of sieve (mm)	Cumulative passing	Limits of IQS No. 45/1984 as in (Zone 2)
10	100	100
4.75	92	90-100
2.36	81	75-100
1.18	73	55-90
0.60	55	35-59
0.30	24	8-30
0.15	7	0-10

Table 3-4: The physical and chemical properties of fine aggregate.

Physical Properties		
Properties	**Test results**	**Iraqi specification No. 45/1984**
Specific gravity	2.65	---
Absorption	0.92%	---
Fine material passing from sieve (75 μm)	2.5%	Max ≤ 5.0%
Fineness modulus	2.6	---
Chemical properties		
Sulfate content	0.352%	Max ≤ 0.5%

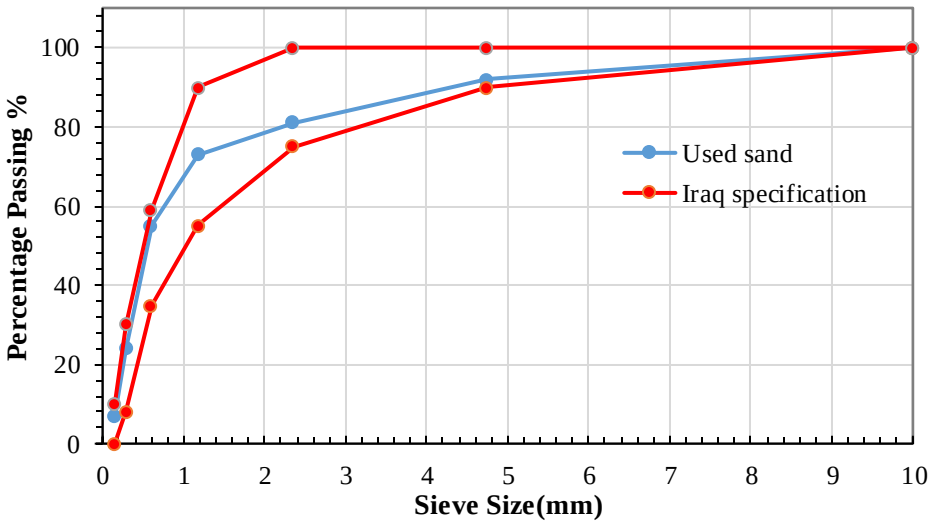

Figure 3-2: Grading curves for fine aggregate compared with requirements of **(IQS NO.45,1984, Zone 2)**.

3.3.3 Lightweight Coarse Aggregate

Lightweight Expanded Clay Aggregate (LECA) was used with regular sizes of between 0.475 cm and 1 cm, which was brought from north of Tehran, Iran. This type of lightweight aggregate is characterized by porous ceramic materials with uniform, small, closed-cell pores, as well as tightly sintered and strong exterior surfaces. LECA made from raw materials of clay minerals which are burned in rotary kilns at a temperature ranging between 1100 and 1200° C thus leading to increase the volume of particles significantly as a result of swelling. Table (3-5) provides requirements for (**ASTM C330,2017)** for gradation of lightweight aggregate along with the test results of LECA used herein while Table (3-6) describes its chemical and physical characteristics.

Table 3-5: Grading of LECA coarse aggregate.

Sieve Size (mm)	Cumulative passing %	Limits of ASTM C330, 2017
12.5	100	100
10	100	80-100
8	79	-
6	46	-
4.75	5	5-40
2.36	2	0-20
`1.18	0	0-10

Table 3-6: Physical and chemical properties of LECA*.

Physical Properties	
Properties	**Test Results**
Specific Gravity	1.2
Absorption	12%
Bulk density Kg/m^3	700
Chemical Properties	
Chemical Composition	**Percentage by Weight%**
CaO	3.78
SiO_2	61.58
Al_2O_3	16.99
Fe_2O_3	7.62
MgO	2.56
SO_3	0.19
TiO_2	0.80
MnO_2	0.10
Na_2o	1.03
K_2 o	2.34
Loss on Ignition (L.O.I.)	0.2

*Chemical tests were conducted from LECA factory, IRAN.

As shown in Plate (3-1a) LECA was immersed in water for at least 48 hours, in order to prevent absorbing water by LECA during mixing because of its high-water absorption capacity. As in Plate (3-1b), the LECA spread in laboratory condition until the surface became dry so that the aggregate had the saturated and surface dry condition (SSD), as suggested by (**ACI 211.2,1998).**

Plate (3-1): (a) LECA was soaked in water, (b) LECA was drained in the laboratory air.

3.3.4 Silica Fume (SF)

Silica fume (SF) is a very fine non-crystalline silica produced in electric arc furnaces as a by-product of the production of elemental silicon or alloys. The silica fume, which condenses from the gases escaping from the furnaces, has a very high content of amorphous silicon dioxide and consists of very fine spherical particles typically ranging from 0.1 to 0.2 μm diameter. Silica fume was initially viewed as a cement replacement material, but currently the most important reason for its use is the production of high-performance concrete, where adding silica fume provides enhancements in concrete properties. In this role, silica fume has been used to produce concrete with enhanced compressive strength and with very high levels of durability **(ACI 234R, 2006)**.

Plate (3-2) shows the silica fume used in this research; which is commercially known as Mega Add MS (D) from chemical company (CONMIX), and it was utilized in this investigation as a partial replacement (10%) by weight of cement. Silica fume improves the micro structure of the cement paste and makes it of more resistance to any type of external influence. The chemical analysis of the silica fume used is tabulated in Table (3-7), whereas the physical requirement is listed in Table (3-8). The results showed that the (SF) used in this study conforms to the requirement of (**ASTM C1240,2015)**.

Plate (3-2): Micro silica employed in this investigation.

Table 3-7: Silica Fume chemical analysis*.

Oxide composition	Oxide content %	ASTM C1240-15 limitations
SiO_2	89.41	Min. 85%
Al_2O_3	0.63	-
Fe_2O_3	0.45	-
CaO	0.82	< 1
SO_3	0.87	< 2
K2O+Na2O	1.35	-
L.O.I.	4.10	Max. 6%
CI	0.18	-
CaO (free)	2.15	-

* Manufacturer properties.

The sustainability movement has encouraged renewed interest in reducing the cement content of concrete mixtures by replacing an ever - growing portion of Portland cement with additional cementitious materials such as silica fume **(Mehta, 1999)**.

In this study, Strength Activity Index (SAI) was used. In principle, SAI is determined by molding two sets of test specimens according to a standard recipe: one with 100 percent Portland cement (reference), and another in which a standardized part of the Portland cement is replaced by a corresponding pozzolana mass to be tested.

Table 3-8: Physical properties of silica fume used*.

Physical properties	Result	ASTM C1240- 15
Strength activity index at 7 days	135%	≥ 105
Percent retained on 45 µm (No.325) sieve, max, %	1.4	≤ 10
Specific surface, min, (m^2/g)	23	≥ 15

* Manufacturer properties.

The strength activity index of the used micro silica fume utilized in this research was tested according to **(ASTM C1240, 2015)**, in which the specimens were prepared for strength activity index (Pozzolanic activity) consisted of one part of cement and 2.75 part of standard graded sand by weight. Six cubes (50×50 mm) were used in this test, three for the mixture of reference and three for the mixture of tests. The cubes were demolded after 24 hours of initial healing in the wet room at a temperature of (23 ± 2 ° C) and relative humidity of not less than 95 %. Samples tested in accordance with the test method **(ASTM C109,2009)** to determine the compressive strength at 7 days after molding. The results of the tested samples were used according to **(ASTM C1240, 2015)** in an equation to calculate the pozzolanic activity index (P.A.I).

$$\mathbf{P.A.I.} = \frac{\mathbf{A}}{\mathbf{B}} * \mathbf{100} \quad \text{..... (3-1)}$$

A: Average compressive strength of standard mortar of cement, sand and pozzolanic material at given age, (MPa).

B: The average compressive strength of control mortar at the same age as that of age **A**, (MPa).

3.3.5 High Range Water Reducing Admixture (HRWRA)

The high - performance water reducing admixture used in this study is a third-generation super plasticizer for concrete and mortar, known commercially as (Hyperplast PC200), a high - performance super plasticizer for concrete admixture imported from the company (DCP), aqueous solution of modified polycarboxylic polymers with long chains, free of chlorides, and comply with the requirements of **(ASTM C494, 2017)** type **F**, specifically designed to enable a more efficient performance of the concrete water content by significantly improving the dispersion of cement, the polymer chains increase the negative charge on the cement particle surface at the start of the mixing process and the electrostatic repulsion of the cement. In this study, the

percentage of 3.7% was used to produce appropriate slurry for SIFCON. The technical description (Hyperplast PC200) is presented in Table (3-9).

Table 3-9: Technical description of (Hyperplast PC200) *.

Chemical basis	Aqueous Solution of Modified Polycarboxylate
Freezing point	≈ -3 °C
Color	Light yellow liquid
Specific gravity	1.05 ± 0.02
Air entrainment	Typically, less than 2% additional air is entrained above control mix at regular dosages.
Chloride content	None
Toxicity	Not classified as hazardous material.
Storage	Stored at temperatures between 2 °C and 50 °C.
Fire	Nonflammable

*Manufacturer Properties.

3.3.6 Water

Drinking water from the university campus has been utilized in all concrete mixes and in the samples curing which was free of salts, turbidity and, organic matter content.

3.3.7 Steel Fibers

Previous studies have shown that bundles glued fibers dose not preferred for using in SIFCON, where it preferred to be loose (single or discreet) to infiltrate the fiber bed without clogging or honeycombing. Therefore, before placing them in the molds, glued fibers had to be dissolved and separated. **(Gilani, 2007)**.

In the present work the type of steel fiber, hooked end was used. The type of fiber was hooked end steel fibers with length of (30 mm) and diameter of (0.5) mm, the hooked fiber was supplied from DURAFLEX company in

India. The steel fiber was imported in 25 Kg bags. Plate (3-3) displays the hooked end steel fiber used in this research. Table (3-10) indicates technical properties of hooked end used according to the manufacturer company.

Table 3-10: Properties of hooked end steel fiber*.

Property	Results of hooked end steel fiber
Description	Deformed shape hooked end
Appearance	Bright and clean wire
Length (l), mm	30
Diameter (d), mm	0.5
Aspect ratio(l/d)	60
Density (kg/m3)	7800
Tensile strength (MPa)	>1100
Description	Of shape hooked ends
Appearance	Bright and clean wire

*Manufacturer Properties.

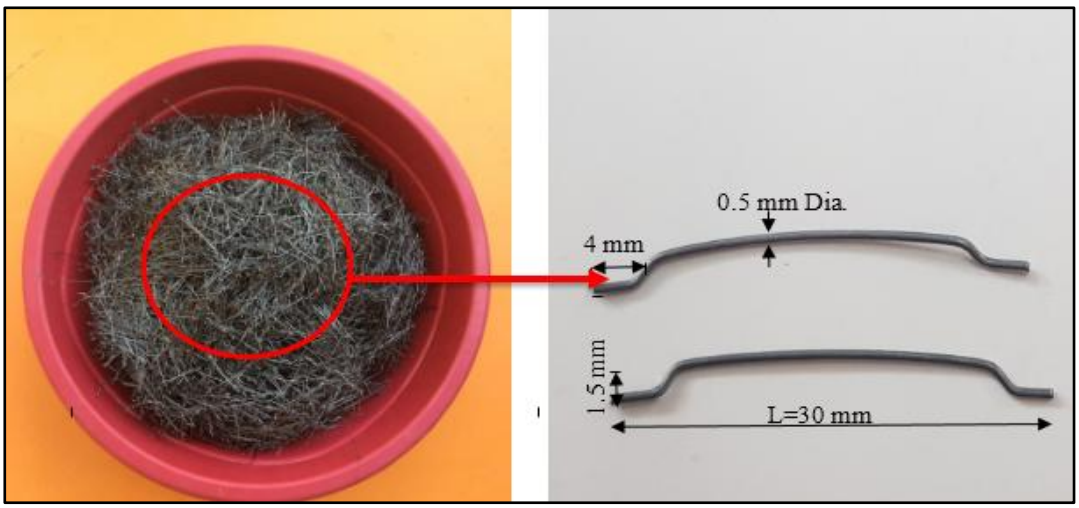

Plate (3-3): Geometrical configuration of hook end steel fiber steel fiber used before and after magnification.

3.3.8 Steel Reinforcement

In lightweight reinforced concrete beams, two deformed steel bars with (Ø10 mm) diameter in the top, three deformed steel bars with (Ø12 mm) diameter in the bottom were used as longitudinal reinforcement and (Ø8 mm)

bars were used for stirrups reinforcement as shown in plate (3-4). Thus, the model used can be considered to represent the beam situation. The mechanical properties of the reinforcement bars were obtained by a digital computer complementary with the testing machine as presented in Table (3-11). Test results referred that the adopted steel bars conformed to **(ASTM A615-05)**.

Table 3-11: Specifications and test results of steel reinforcing bars*.

Nominal Bar Diameter (mm)	Actual bar Diameter (mm)	Yield Stress Fy (MPa)	Ultimate strength Fu (MPa)
8	7.95	550	678
10	10	581	724
12	11.96	663	828

*Testing of steel bars was carried out in Strength of Materials laboratory at Al-Musayib Technical Institute.

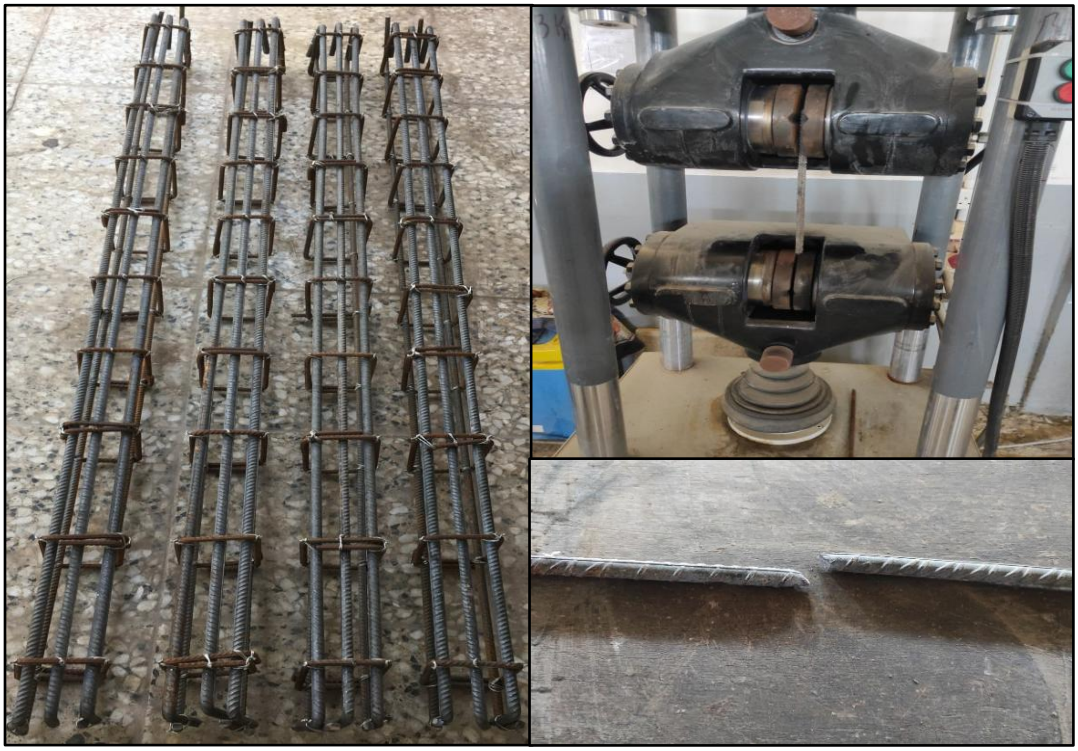

Plate (3-4): Steel reinforcement used in NSC and HSC beam specimens.

3.4 Test Methods for Fresh (LWC and SIFCON)

3.4.1 Tests for Fresh LWC

The following tests were used to measure fresh properties of LWC:

3.4.1.1 Slump Test

The slump test of LWC was performed in accordance with (**ASTM C143,2008)** as shown in Plate (3-5).

Plate (3-5): Slump test for LWC.

3.4.1.2 Fresh Density Test

Fresh density which is also called unit mass or unit weight in air, is the summation of the mass of all the fresh constituents of concrete divided by the bulk size occupied by the concrete. Fresh unit weight was measured directly after pouring.

3.4.2 Tests for Fresh SIFCON Mortars

For the production of SIFCON, testing SIFCON mortar in its fresh state is of serious importance. Its matrix must be sufficiently liquid and fine enough to flow through the dense fiber bed. EFNARC has only proposed two tests for SIFCON mortar, which are mini slump flow and V-funnel tests. These tests were used to determine SIFCON mortar flowability, filling capacity, resistance to segregation and viscosity. The mini-flow test represents the slurry's flowability, segregation resistance and uniformity, while the V- funnel test were used to measure the slurry's viscosity (flow rate measurement). The two tests conducted on SIFCON mortar are briefly described below.

3.4.2.1 Mini Slump Flow Test

The mini slump flow test is the simplest and the fastest test procedure, used to assess the horizontal flow and the filling ability of SIFCON mortar, also can indicate segregation resistance and uniformity of the slurry through the visual observation during the test **(Ali, 2018)**. The apparatus used for the mini slump flow test was a mold in the shape of a cone with internal dimensions of 100 mm base diameter, 70 mm top diameter, and a height of 60 mm, as shown in Plate (3-6). Also, this test required base plate of a stiff nonabsorbent material, trowel and scoop.

Approximately (0.5) liter of mortar is required for the test. It is necessary to moisten the base plate and inside the slump cone, ensuring that there is no free water, followed by placing the base plate on a stable ground level and the slump cone was placed centrally on the base plate and firmly held down. The cone was filled with scoop mortar; with the trowel, the mortar leveled off with the top of the cone. Around the base of the cone, excess mortar was removed. The cone rose vertically and gave free flow to the mortar. The table is then immediately dropped 25 times in 15 seconds.

Plate (3-6): Process of the flow table test.

The final diameter of the mortar was then measured in two perpendicular directions and the average of the two measured diameters, which is the slump

flow in mm, was calculated. The higher the slump flow value, the greater its ability to fill formwork under its own weight. A value between (240-260) mm spread diameters is required for SIFCON Slurry.

3.4.2.2 V-funnel Test

The slurry's viscosity can be assessed by the flow time of the V-Funnel. The time value obtained does not measure the slurry's viscosity, but is related to the flow rate. The slurries showing the higher flow time from the V - funnel test can therefore be considered to have a relatively high viscosity. The device used for the test is: V-Funnel, bucket, scoop, trowel and stopwatch, as Plate (3-7).

Plate (3-7): V-Funnel test apparatus.

The amount of mortar required for the test was approximately (10) liter. On firm ground, the V-funnel was placed. Then wet the inner surfaces of the funnel and the lower gate while the trap door opened to allow the excess water to drain. The trap door was closed afterwards and the bucket was placed underneath. The apparatus was completely filled with the mix without compacting, and the trowel hit the mortar level with the funnel top.

The trap door was opened within 10 seconds of filling and allowed the mortar to flow out. When the trap door was opened, the stopwatch was started and the time to complete the discharge (the flow time) was recorded. This was taken when light was seen through the funnel from above. A flow time between

7 - 11 seconds is considered appropriate for SIFCON mortars **(EFNARC, 2005)**.

3.5 SIFCON Trial Mixes

The high - range water reduction admixture (HRWR) can be regarded as the most important component for the achievement of a homogeneous mixture with the required properties of SIFCON mortars with a low w/c ratio. It is therefore important to check the optimal dosage, which complies with the other component materials of the mortar used, the HRWR selected for this research is (Hyperplast PC200) from (DCP) company.

Many trial slurries mixes have been prepared to achieve optimum fresh properties for SIFCON mortars with mini slump flow range between (240 - 260) mm and V - funnel time between (7 - 11) seconds, while at the same time achieving easy and complete penetration of prepared mortars through the steel fiber network.

Table 3-12: Fresh properties of SIFCON mixes

Mix	Mini slump flow (mm)	V-funnel (s)	SP. % by wt. of cement
M1	245	9.5	2.4
M2	251	8.9	3.0
M3	259	7	3.7

The method used to determine the amount of HRWR required for SIFCON mortars is to first check the slump flow with a different amount of HRWR until the target value of (240 - 260) mm is reached, and then to check the time of the V - funnel. This is because the mini slump flow test is the simplest and fastest, and the steel fiber is then checked for infiltration. Details of the test mixes are shown in the Table (3-13). In that table some words were used to express the success of the slurry, where (Bad) indicate that the slurry failed to penetrate into all shapes of fiber, (Good) means that the slurry is successful in penetrating through the hooked end fiber only, (Very good)

successfully penetration through hook end fiber only. (Excellent) denotes that the slurry is ideal for the shape of fiber used in this study.

Table 3-13: Trial mixes of SIFCON slurry.

Dosage of HRWR (%) by weight of cement	w/b ratio that satisfied EFNARC requirement*	The infiltration of mortar through the dense steel fiber
2	0.3	Bad
2.3	0.32	Bad
2.4	0.3	Bad
2.8	0.35	Bad
3	0.33	Bad
3	0.38	Good
3.5	0.33	Very good
3.7	0.33	Excellent

* The EFNARC requirements are: a value between (240-260) mm spread diameters is required for mini slump flow test and a flow time between (7-11) seconds for V-funnel test.

3.6 Mix proportion

3.6.1 SIFCON Mix design

In the experimental work, a trail slurry mixtures were carried out to find a suitable mix that has the optimum properties in the fresh state with respect to fluidity, viscosity and filling ability without bleeding and segregation or pore pockets in the fiber network that cause dramatic reduction in the mechanical properties of SIFCON, as listed in Table (3-14).

Table 3-14: Experimental Trial mixes of SIFCON slurry.

Mix	Cement kg/m^3	Sand kg/m^3	SF (10% rep.) kg/m^3	W/Cm* ratio	Water L/m^3	SP % by wt. of cement
M1	872.4	969	96.9	0.30	290.7	2.4
M2	872.4	969	96.9	0.33	319.8	3.0
M3	872.4	969	96.9	0.33	319.8	3.7

*W/Cm = water / (cement + silica fume)

Since there is not any standard specification for SIFCON mix design yet. The literature review findings, as given in Table (2-1) in chapter two, helped in the design of SIFCON mixes. It can be seen from this Table that the proportion of (sand: cementitious materials) by weight in most cases is equal to (1:1), so this value was adopted in this investigation.

Many investigators **(Giridhar et al.,2015; Yan et al., 1999; Yazıcıet al.,2006)** used cement content range from (800-1000) kg/m^3 and recommended to use W/C ratio less than 0.4 (by weight) for the production of SIFCON matrix. Therefor after many trails, ordinary Portland cement of (872.4) kg/m^3 content was used in this work, while the water/binder ratio was kept constant as 0.33 (by weight).

The type of SIFCON prepared in this investigation is (hooked end fiber SIFCON) which was produced by using mortar with the hooked end steel fiber and micro steel fiber with volume fraction of 6%. These fiber contents were selected from the experimental work and from different studies dealt with SIFCON **(Yazıcı et al.,2006;Gilani,2007)**, it was found that 6% volume fraction was improved as a minimum practical limit that could fill the mold and produce SIFCON with different types of mortar without using vibration.

Table (3-15) and Figure (3-3) reveal the optimum mixes used in this study with weight proportions.

Table 3-15:SIFCON Materials mix proportion.

Mix Proportions					
Cement Kg/m^3	**Sand Kg/m^3**	**Silica Fume Kg/m^3 10% rep.**	**Hooked-end Steel Fiber Kg/m^3**	**W/Cm**	**Super Plasticizer by wt. of Cementitous (%)**
872.4	969	96.9	468	0.33	3.7

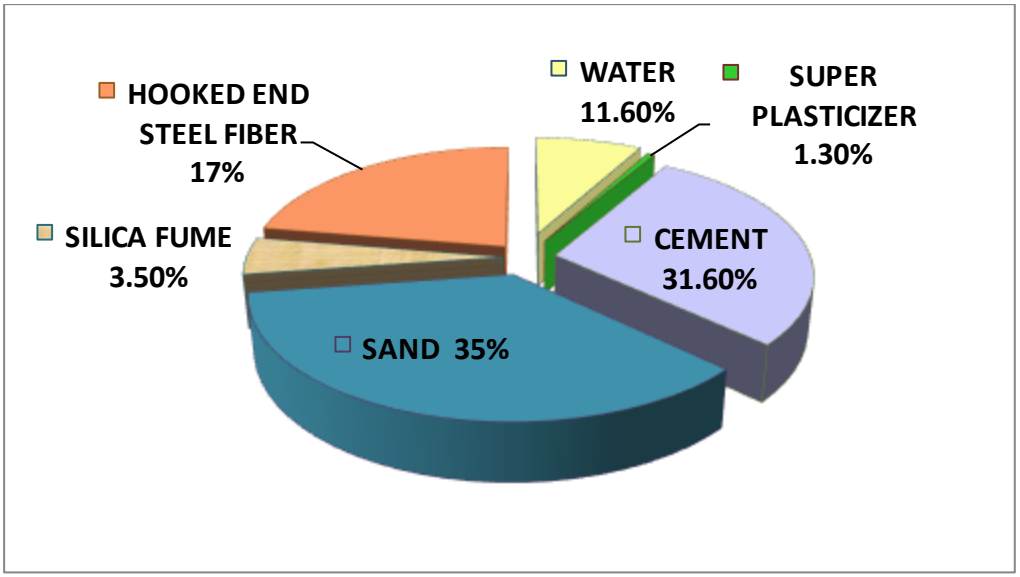

Figure 3-3: Materials proportion used in SIFCON mixture (% of total mix weight).

3.6.2 Lightweight Concrete Mix Design

Lightweight concrete (LWC) is typically dependent on its mass, as described earlier. In several codes, lightweight structural concrete (LWC) is described as a concrete with a hardened density of lower than 2000 kg / m^3 and a compressive strength at 28 days exceeding 17 MPa, whereas normal concrete weight with a density range from 2200 to 2600 kg/m^3 **(SikaViscocrete-5930L)**. Lightweight aggregates used in this experiment is LECA made of expanded clay made heating clay in a rotary kiln to around 1200 °C and is produced in Iran. LWC mixtures of this work contained LECA as a coarse lightweight aggregate in addition to cement, natural sand, and chemical admixture**.** (**ACI 211.2,1998** and **ACI 211.4R,2008)** were used as a guideline to prepare concrete mixes that satisfied the requirements for density and compressive strength of normal and high strength concrete respectively. For the purpose of comparison, two grades of LWC (NSC and HSC) mixtures were designed in this research. The objective of the concrete mix design was to have a slump of 75 mm, and a 28-days cube compressive strength were 33 MPa and 67 MPa of NSC and HSC respectively. Various trial mixes were used to achieve the required strength; the mix details of high strength lightweight concrete are

given in Table (3-16). Flexural reinforcement used in these concrete beams was the same bars used in the normal concrete beams.

Table 3-16:Details of LWC trial mixes (kg/m3)

Mix Code	Cement Kg/m^3	Sand Kg/m^3	LECA Kg/m^3	Silica Fume Kg/m^3	Water Kg/m^3	SP by wt. of cm (%)	W/Cm	Slump mm	28-day Compressive Strength MPa	Target compressive strength
HSC1	450	661	355	50	200	1.8	0.4	100	43.7	Less
HSC2	495	639	274	55	176	1.8	0.32	95	45.68	Less
HSC3	540	678	424	93	164	1.7	0.26	85	51.6	Less
HSC4	560	782	210	110	154	1.7	0.23	85	67.33	Satisfied

Table (3-17) also represents the ratio of the mixtures, compressive strength, fresh density and slump while Figure (3-4) and (3-5) shows the proportion of ingredients of LWC mix as a percentage by weight.

Table 3-17: Details of LWC mixes (kg/m3)

Grade of LWC	Cement Kg/m^3	Sand Kg/m^3	LECA Kg/m^3	Silica Fume Kg/m^3	Water Kg/m^3	SP by wt. of cm (%)	W/Cm	Slump mm	Fresh Density kg/m^3	28-day Compressive Strength MPa
NSC	478	667	420	-	153	1.5	0.32	90	1725	38.26
HSC	560	782	210	110	154	1.7	0.23	85	1828	67.33

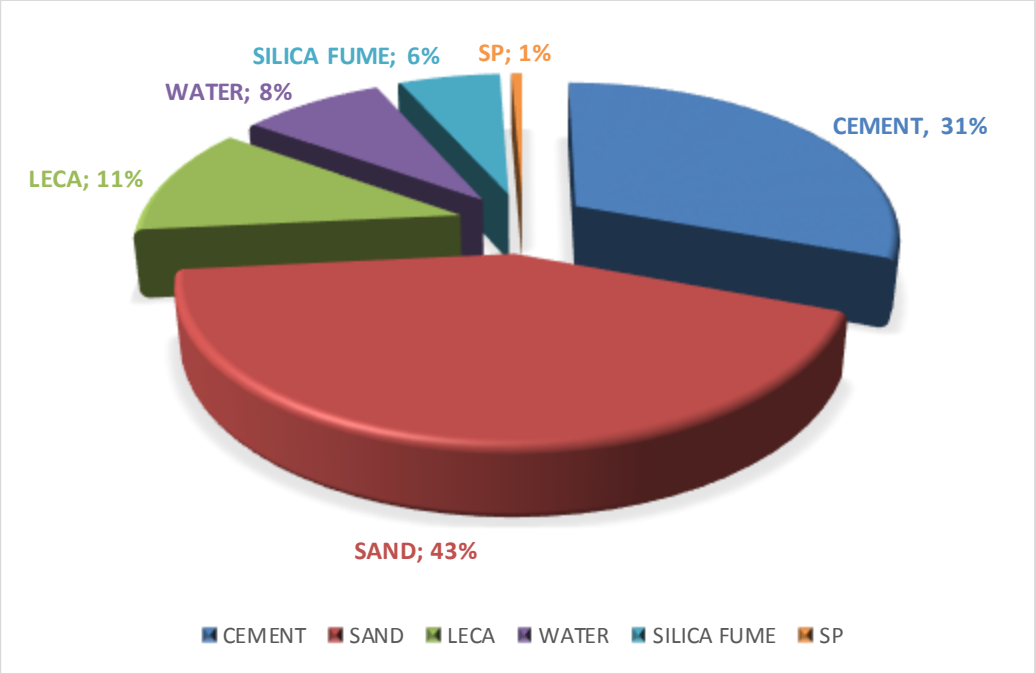

Figure 3-4: Materials proportion used in HSLWC mixture (% of total mix weight).

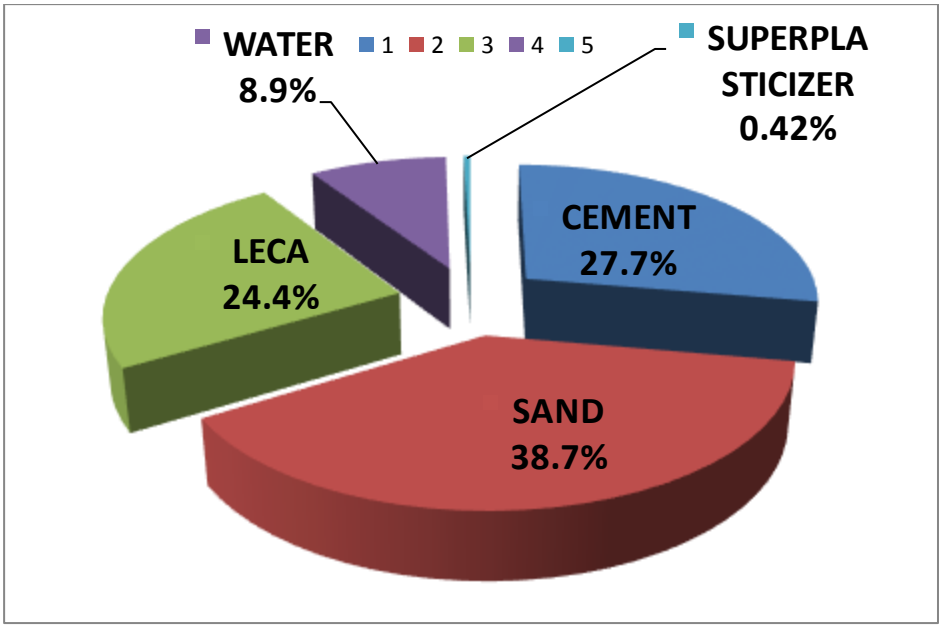

Figure 3-5: Materials proportion used in NSLWC mixture (% of total mix weight).

3.7 Description of the Tested Lightweight Beam Specimens

The test program consisted of testing twenty-eight beam specimens of NSC and HSC lightweight concrete. Each LWC beam was reinforced with deformed steel bars with (Ø12 and 10 mm) diameter were used as longitudinal reinforcement and (Ø8 mm) bars were used for stirrups reinforcement and kept constant in all beams. The provided stirrups were such as to prevent shear failure in any of the beams. The longitudinal and transverse steel reinforcement in the LWC beams is shown in Figure (3-6). The selected dimensions were constant for all beam specimens; therefore, beams were manufactured with a rectangular cross-section of 150mm × 200mm, and a total length of 2000mm also as shown in Figure (3-6).

Due to a large number of beam specimens investigated in this research and in order to facilitate the comparison between these beams, each LWC beam is identified by four symbols. The first symbol is letter that refer to the grade of concrete (NSC or HSC). The second letter concrete cover of beam (25mm or 35mm). The first number is denoted the thickness of U-shaped SIFCON jacket (0, 20 or 30 mm).

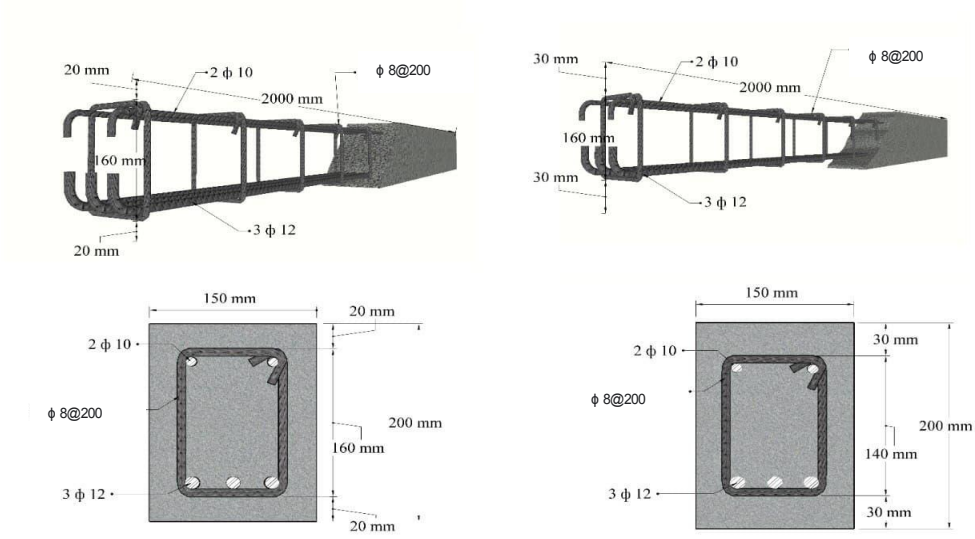

Figure 3-6:Main section geometry and typical LWC beam cross-section (dimensions are in mm).

Finally, the second number symbolized the fire duration exposure of beams (with or without burning). In Figure (3-7), the procedure in which samples were identified was explained.

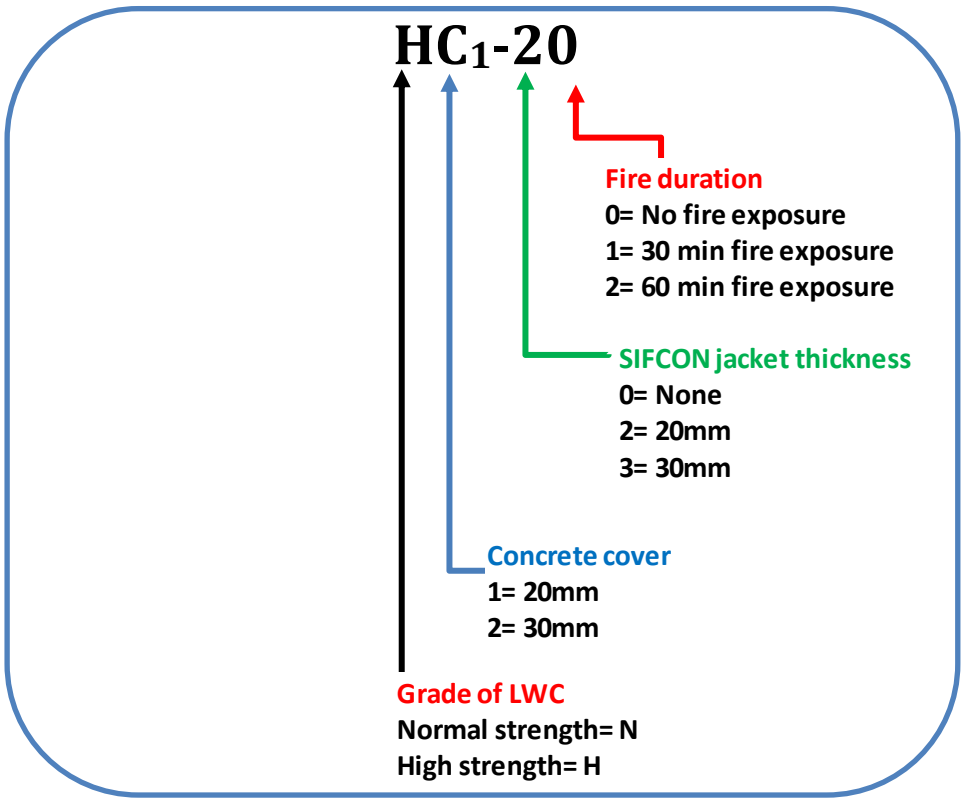

Figure 3-7: An instance for the method used to identify the beam specimens.

The entire experimental program comprises testing 28 of normal and high strength reinforced lightweight concrete beam specimens cast in the laboratory and tested under two-point loading. Twenty-eight LWC beams of which were exposed to fire flame and compared with the reference four beam specimens, which were not exposed to fire flame.

Table (3-18) lists the details of LWC beam specimens. The beams were all cast in the same period to prevent or minimize the variation in the exposure conditions. Thus, the model used can be considered to represent the beam situation. Eight plywood molds were designed and fabricated for casting of LWC beam specimens in each batch as shown in Plate (3-9). Molds were used to cast 28 LWC beams with inner dimensions of (150×200×2000mm) (width × depth × length) respectively. After greasing the molds of beam specimens, reinforcement bars were held carefully in their position inside these molds. In order to get a cover, small pieces of steel were placed at sides of the beam reinforcement.

To prevent the LWC beam from developing significant axial forces, which could create artificial strut action, the LWC beams were supported by a roller on one end and a hinge at the other as shown in Fig. (3-8). At both of these locations, the contact area between the concrete and the supports includes loading plate with dimension of 75 mm x 150 mm (the width of the beam).

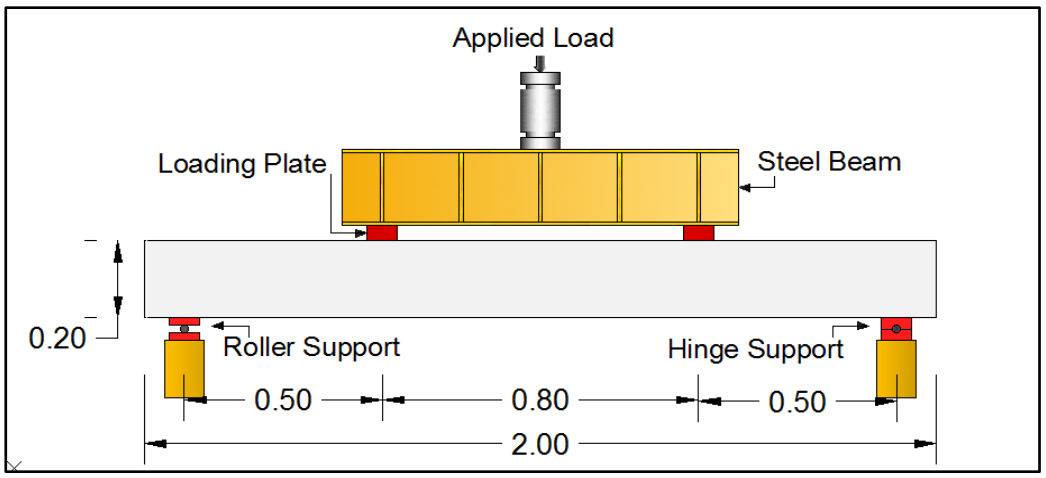

Figure 3-8: The mechanical loading configurations.

Table 3-18: Summary of NSC and HSC LWC beam test specimens.

Grade of concrete beam	Concrete cover (mm)	SIFCON jacket thickness (mm)	Beams designation	Fire duration (Min)
NSC LWC Beams	**20**	None	NC_1-00	0
			NC_1-01	30
			NC_1-02	60
		20	NC_1-21	30
			NC_1-22	60
		30	NC_1-31	30
			NC_1-32	60
	30	None	NC_2-00	0
			NC_2-01	30
			NC_2-02	60
		20	NC_2-21	30
			NC_2-22	60
		30	NC_2-31	30
			NC_2-32	60
HSC LWC Beams	**20**	None	HC_1-00	0
			HC_1-01	30
			HC_1-02	60
		20	HC_1-21	30
			HC_1-22	60
		30	HC_1-31	30
			HC_1-32	60
	30	None	HC_2-00	0
			HC_2-01	30
			HC_2-02	60
		20	HC_2-21	30
			HC_2-22	60
		30	HC_2-31	30
			HC_2-32	60

3.8 Mixing Procedure

Sufficient mixing is necessary to achieve the required performance and homogeneity of SIFCON slurry, also, the extending mixing time is important both to allow the HRWR to develop its full potential and to obtain fully dispose of silica fume by breaking up any agglomerated particles. All trial mixes were performed in a small rotary mixer of 0.01 m^3 capacity, while the specimens' mixes were performed in a horizontal rotary mixer with a capacity of 0.125 m^3 as shown in Plate (3-8). Any residual particles of concrete from prior batch must be cleaned off before using the concrete mixer. A moist cloth is used to clean the blades and pan of the concrete mixer.

a) Mixer used for trial mixes. b) Mixer used for specimen's mixes.

Plate (3-8): Mixers used in this study.

The adopted method in this research, is presented in Figure (3-9), based on previous researches and trail mixes to produce satisfactory workability. The steps of mixing can be summarized as follows:

1) The mixer was cleaned from any remaining fresh or hardened materials (from the older mixtures) before the mixing operation.

2) The entire amount of HRWR was mixed separately with mixing water (1/3) for almost 0.5 minutes.

3) For SIFCON slurry, the binder material [cement and silica fume (SF)] was mixed in a mixer for (1) minute to disperse the particles of silica fume through the cement particles, then the sand was added and mixed for (2) minutes.

4) (2/3) of mixing water was then added to the rotating drum and mixed for 1 minute. HRWR was then fed to the mixer with (1/3) mixing water and mixed for 3 minutes.

5) The mixer is then stopped and the mixing for the portion not reached by the mixer blades is continued manually.

6) Finally, to obtain the required fluidity, mortar ingredients are mixed for an additional (1) minute.

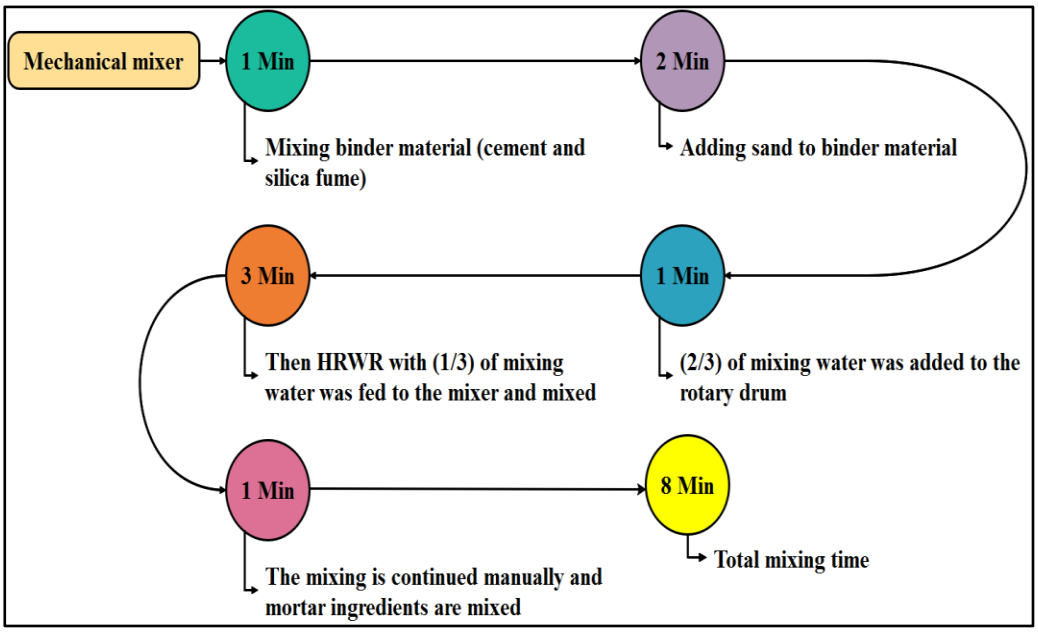

Figure 3-9: SIFCON mixing time process.

LWC were mixed according to (**Lotfy, 2012**) with some modification. As a result of high lightweight aggregates capacity for absorption water, the aggregates were before-soaked for at least two days, then the extra water has been drained and the materials mass have been measured see Plate (3-1).The

process of producing LWAC was adopted based on information provided by the aggregate manufacturers as summarized below, see Figure (3-10):

1. The LECA and sand were blended with 50 percent of the mixing water for two minutes.
2. The mixer left standing for four minutes to allow aggregate water absorption. During that period, the mixer was kept covered to minimize evaporation.
3. The powder materials namely cement was supplied to the mixer and blended for an extra 60 seconds.
4. Finally, the remaining water and SP were added to the mixture and mixed for another seven minutes.
5. Break time of two minutes was taken before pouring the fresh mixes. The entire mixing cycle takes approximately 16 minutes.

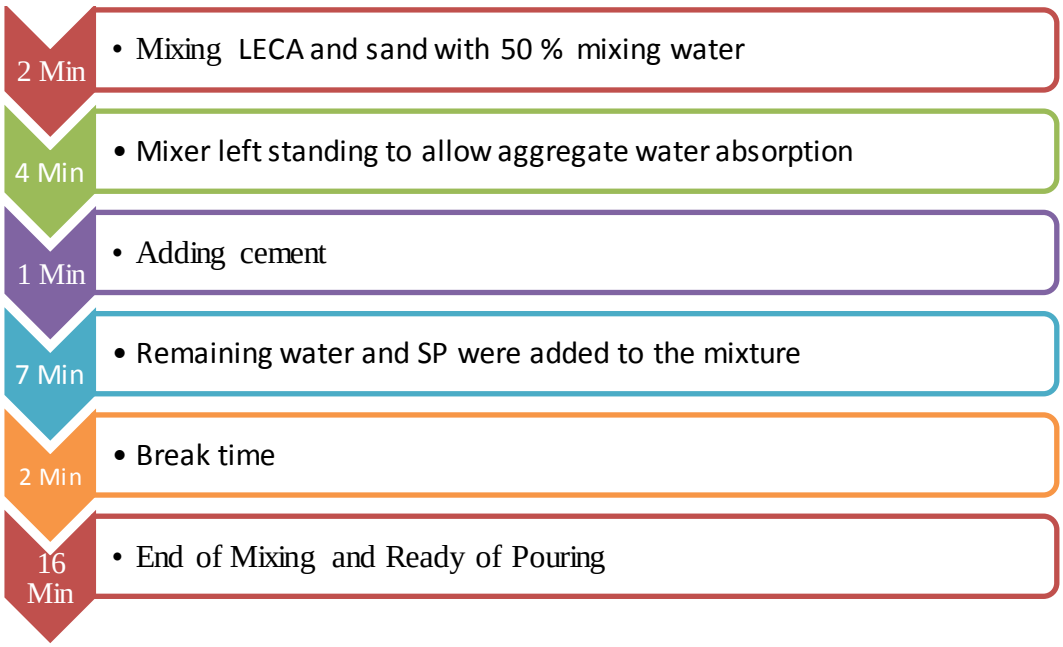

Figure 3-10: LWC mixing time process.

Beyond mixing, the flow test was performed for LWC mix. Compaction was achieved using a plunger mechanical vibrator (3000 vibration per minute) having a metal rod with a diameter of 50mm vibrating for 5 seconds for each insertion until no air bubbles, samples of (prisms, cylinders, and cubes) was

utilized to stabilize the LWC. Since levelling was done utilizing hand trowel, the upper concrete surface has been finished smoothly. The samples were kept for one day in the moulds before placing in the water tank to start the curing process which continued up to the age of testing.

3.9 Casting and Curing Procedures of LWC Beam Specimens

Before casting, the materials were selected and weighted according to the volume of the mixture. All beam specimens tested in this study were cast in plywood molds. Each batch from the mixer was sufficient to cast two beams. Plate (3-9) presents the procedure of casting reinforced LWC beams, and Plate (3-10) shows the method of casting LWC samples (cubes and cylinders).

The casting process is described in the following steps:

1) The plywood molds were prepared by proper cleaning and lightly lubricating of the inner faces with oil in order to prevent the adhesion of hard concrete before each casting and then, each mold was placed on a horizontal ground, and adjust the horizontal and vertical of the wood molds, Plate (3-9 A).

2) The reinforcement was positioned carefully inside the plywood molds with the required bottom cover being accurately maintained as shown in Plate (3-9B).

3) After the mixing was finished, the fresh LWC mixture poured into the molds by placing the specific concrete directly from the mixer and vibrated by using a plunger vibrating and full compaction was made sure by observing the air bubbles on the surface as presented in Plate (3-9C).

4) Shortly after the casting and finishing of the top surface of all specimens, the molded specimens were covered (to prevent the loss of moisture) and left for 24 hours until they were removed.

5) Conventional curing method was used to simulate the practical site conditions.

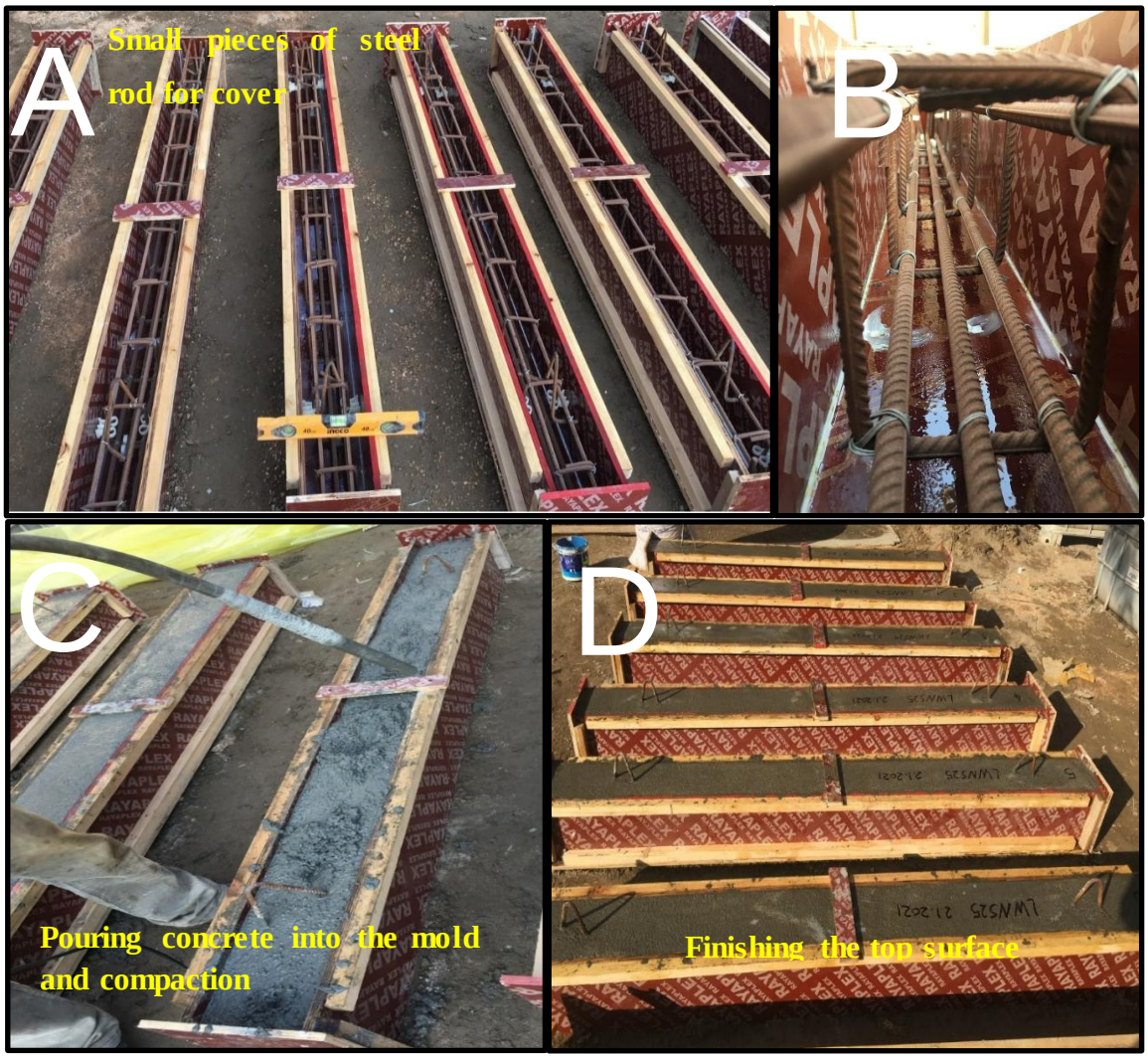

Plate (3-9): Garmenting processes of casting LWC beam specimen.

Plate (3-10): The procedure of casting, Compaction and curing of LWC samples.

Thereafter, beam specimens were cured from its first casting day with saturated wet coverings by using burlap for 56 days and spray daily with portable water until the treatment period is complete as visible in Plate (3-11A). While, control samples cubes and cylinders of each batch cured in a water tank with a temperature of (23±2 °C), also are kept in the laboratory under ambient conditions after ensuring a complete molds disposal see Plate (3-11B).

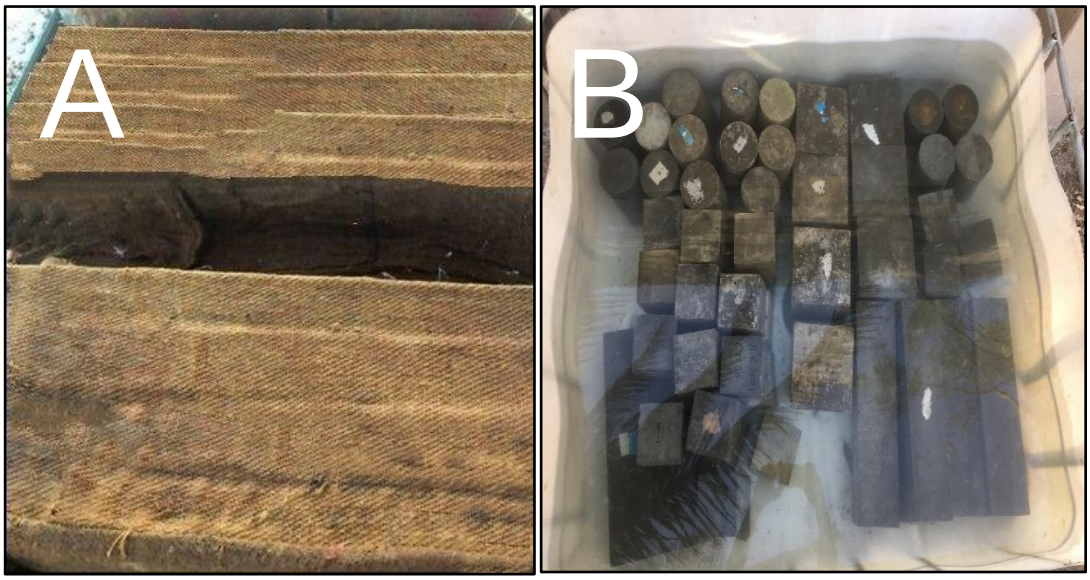

A) Covering of beam specimens with burlap and plastic sheet.

B). Samples curing.

Plate (3-11): Curing procedures for beam specimens and samples.

3.10 Fire Test Furnace Description

The fire test furnace consists of a furnace or a burner combustion chamber including a gas evacuation system, and a steel frame with a hydraulic linear actuator to applied loads on the elements see Figure (3-11). It was designed to follow either a custom designed fire development profile or a time-temperature curve specified in fire resistance standards such as ISO 834. To provide a uniformly distributed temperature inside the furnace a Proportional-Integral-Derivative (PID) controller was used. The PID controls the process of the structural test under fire conditions satisfying the requirements of the European directives on safety and electromagnetic compatibility.

The furnace can test vertical and horizontal elements such as beam, wall, slab and column elements, and subject them to specific heating. Summarizing, the following tests can be carried out on the designed equipment:

- Fire resistance tests on horizontal separation elements, such as beams on one, two or three faces.
- Fire resistance tests on vertical elements, such as columns on one, two and three sides.

Key aspects of the design and operation of this equipment are burner adjustment and refractory properties of all industrial furnace components. The burners manage flame to control the temperature inside the furnace. This furnace has twenty-seven burners placed on the bottom and side walls that heat the interior of the furnace uniformly. The refractory materials reduce heat loss and ensure that the standard time temperature curve is followed, maintaining the heat in the furnace. Finally, heat flux and gases are extracted during the fire resistance test by means of a gas evacuation system. PID controller is added to control temperature and pressure in real-time and follow Standard time-temperature curves. PID controller includes an emergency power off system to ensure the furnace operates under fire conditions. The control of the system is crucial to minimize existing hazards.

A furnace is used to follow the standard time-temperature curves. To record temperature, thermocouples are placed inside the furnace and near the specimen. The fuel, the burners and the refractory lining are the key aspects of furnace designs. Furnace designs vary as to their function and type of fuel **(del Coz-Díaz et al., 2020).** The main purpose of the fire flame furnace is to raise the temperature levels of LWC beam models to the target temperature and holds the temperature constant for a required duration. In order to control the burning procedure, consists of the following equipment:

1. Brick furnace.
2. Network methane burners.
3. Thermocouple.
4. Electrical gas regulator control.
5. Digital gage.
6. Electrical network.
7. Methane gas bottle.
8. Oxygen gas bottle.
9. Gas connections and pipelines.
10. Furnace steel cover.
11. Ignition tool.

The full details of the furnace and equipment are shown in Figure (3-11).

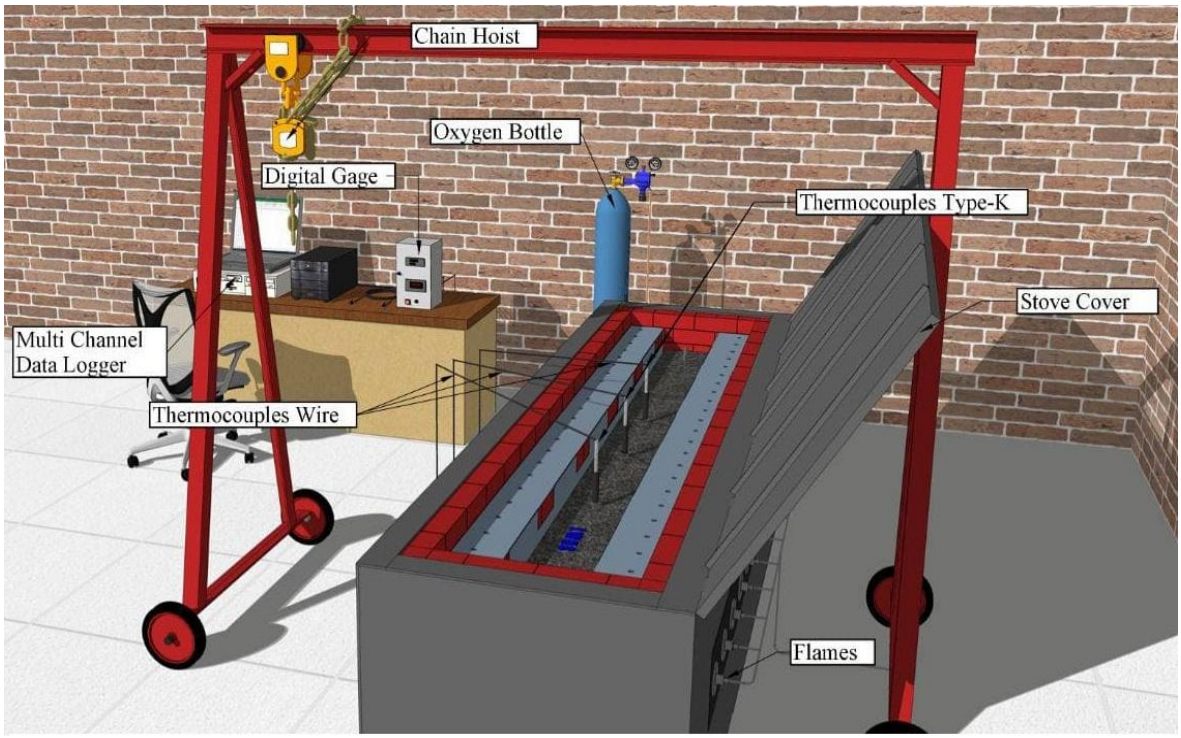

Figure 3-11: Details of the furnace and equipment**.**

3.10.1 Brick Furnace: Dimensions and Description

This furnace is designed to generate typical conditions, such as temperature and heat transfer, to which a structural member might be exposed

during an actual fire incident. The internal dimensions of the furnace are 2200 mm length, 450 mm width, and 650 mm height. Furnace floor and wall insulation are made up of three layers with different refractory materials are illustrated in Figure (3-12). This ensures correct thermal insulation and uniform conditions inside the furnace. The floor of the furnace has an opening used to fix a vertical element or structure inside the furnace to test it under fire conditions.

The wall thickness in all sides are fixed at 136 mm, the main structure is made of thermal bricks and mortar with small opening to provide the necessary fresh oxygen for the burners, the furnace cover is made of insulator plate with thickness of 8 mm to keep the temperature constant as described in Table (3-19) and Figure (3-12). The burners network consists of twenty-seven arranged in three lines, one in the bottom and one in each lateral side, each line consist of nine burners. All methane burners connected together to electrical regulator which connected to two valves controlling the discharge of gas coming from Oxygen and methane bottles. Two networks are equipped for the purpose of burning three scenarios to simulate the heating condition in a realistic fire. The aim of the fire-flame bars was to simulate the heating condition in a realistic fire.

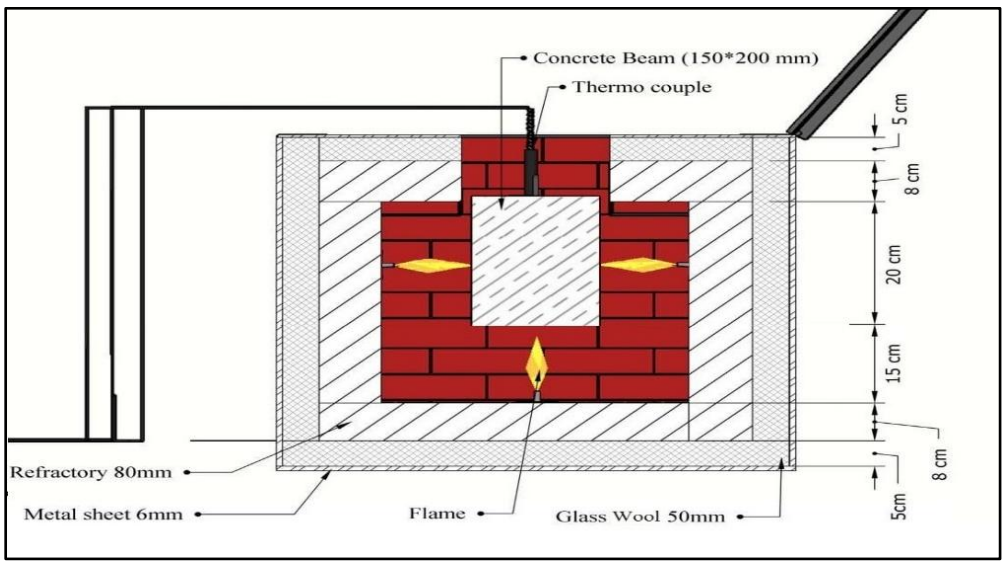

Figure 3-12: Furnace floor and wall insulation.

Table 3-19: Furnace floor and walls composition and main properties.

Layers	Thickness (mm)	Density (kg/m3)	Thermal conductivity (W/mK)
Steel plate	6	7800	54.37
Ceramic fibre blanket	50	128	0.324
Dense refractory bricks	80	2600	2.398

3.10.2 Thermocouple

Thermocouple is a temperature sensing element consists of two wire legs made from different metals inside a metal tube (thermocouple cover). The wires legs are welded together at one end, creating a junction. This junction is where the temperature is measured. When the junction experiences a change in temperature, a voltage is created, and this voltage can be interpreted to measure temperature. Thermocouple usually connected to a thermometer or any other thermocouple-capable device (digital gage used in this investigation) by a thermal-insulated electric wire to resist high temperatures during burning. Plate (3-12) show the specifics of thermocouple and the digital gage.

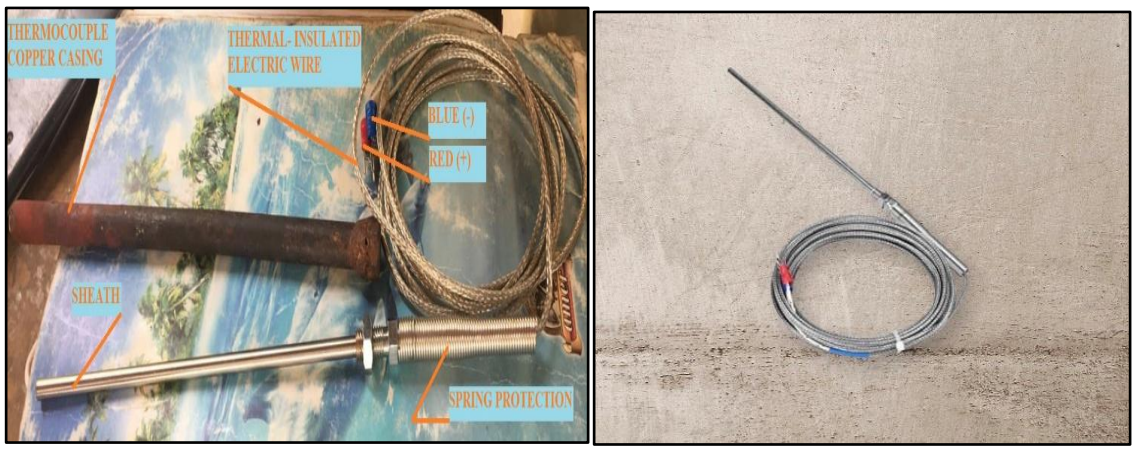

Plate (3-12): The specifics of type- K thermocouple.

One of the instrumentations mounted used in the test beams included thermocouples, data transducers and MATLAB data logger. The location and numbering of the thermocouples in cross section are shown in Figure (3-13).

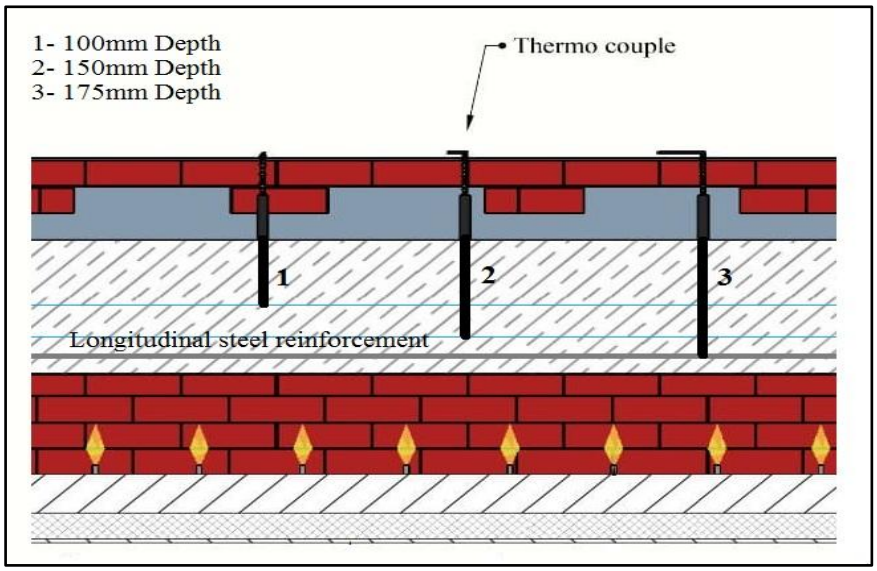

Figure 3-13: The location of the thermocouples in the cross section

A total of four Type-K chrome Lumel thermocouples, 0.91 mm thick, were installed at three different cross sections (mid-depth, quarter-depth and reinforcement concrete cover). The fourth one used to measure the temperature of the furnace atmosphere in each NSC and HSC LWC beam for measuring concrete and reinforcement temperatures at different depths.

3.10.3 Electrical Gas Regulator and Ignition-Burning System

Gas regulator device is an electronic valve designed to provide very fast and accurate gas flow for the furnace burners. The electronic circuit compares the gas injection pressure to its set point of temperature and regulates the gas flow in order to maintain the temperature at its set point by closing or opening the gate. The electrical gas regulator is connected to digital gage to provide gas flow according to the set temperature require, these connections permit to remain fire flame in burners as an ignition system during the firing process. Ignition equipment usually remains ignited during gas locking intervals to be ready for reigniting process again when temperature degree reduces below the level required. Plate (3-13) shows the electrical gas regulator and ignition-burning system.

Plate (3-13): The electrical gas regulator

3.10.4 Burning Procedure of the Specimens

After curing was finished the burning procedure was applied. The specimens were burnt with direct fire flame by a net of Oxy-methane burners inside a brick furnace to the target temperature. The burning procedure was done by the following steps:

1. After preparing the furnace with all connections, the lightweight concrete samples and beam specimens were held carefully by chain hoist and placed inside the furnace.
2. The LWC specimens were positioned fair-faced toward the Oxy-methane burners with the same distance from each line of burners.
3. The gas valve was opened and the burners were ignited, and the measured temperature was increased gradually every (2 min.) according to the designer curve of ISO834 mentioned in chapter one. standard values which were listed in chapter one to obtain an approaching fire temperature to that of the standard fire test method.
4. As shown in Figure (3-12), only three sides (bottom and two sides) of the LWC beams section were exposed to fire, while the fourth side (top surface) of the beam was to be in adiabatic conditions. This is similar to the conditions encountered in practice where a concrete slab is present

on the top side of the beam.

5. Three networks of Oxy-methane burners were developed for the purpose of burning LWC beam specimens. One at the bottom of the furnace, and the other at the two sides and placed directly under and besides the beam specimen with the distance of 15 cm between the exposed surface of the beam specimen and the nozzles of the methane burners.
6. When the target temperature reached, the electrical gas regulator started to work by regulating the gas flow so the target temperature stayed constant. The target temperature was measured by two digital thermometers continuously measured the temperature one of them was positioned in fire flame contact area, while the other was at the face of the specimen. Also, three thermocouples were used to measure the temperature, two of them were positioned at 150mm and mid depth 100mm of the cross-section of reinforced LWC beams, another one was positioned at the longitudinal steel reinforcement layer of the beam, the holes made during the concrete cast of specimens. The Plate (3-14) depicts thermocouples location inside LWC beam.

Plate (3-14): Fixing the thermocouples sheath with rebar inside LWC beam.

7. After the duration of burning was finished (0.5 and 1 hrs. of fire exposure) the gas valve was closed and the reinforced lightweight

concrete specimens were cooled immediately. Recording the specimen's weight before and after the burning. The full details of the burning process and burning furnace with all connections are shown in Plate (3-15).

Plate (3-15): Burning furnace with all connections.

3.10.5 Fire Loading

In experiments performed at high fire temperature, the fire history and the testing time are very important. To provide fire temperature load a brick furnace was used. After specified age of the LWC beam specimens they were exposed to fire in the furnace. The LWC beam specimens were burning in the furnace according to the standard fire curve recommended of ISO-834 as shown in Figure (3-14). The furnace was designed to attain a maximum temperature of 1200 ºC. The temperature in the furnace was regulated so as to follow ISO curve. However, it should be noted that the rate of heating used is considerably lower than ISO-834 regulation, which is presented in Figure (3-14). The durations of the fire loading were 0.5 and 1 hours in every case because it was enough to warm up the reinforced LWC beams to a uniform temperature.

Observations were made every 5 min through the view ports in the furnace to record any major changes in the specimen including occurrence of fire induced spalling. Following the completion of fire resistance test and after

complete cool down of each beam to ambient temperature (around 35 °C), detailed observations on cracking and extent of spalling were made.

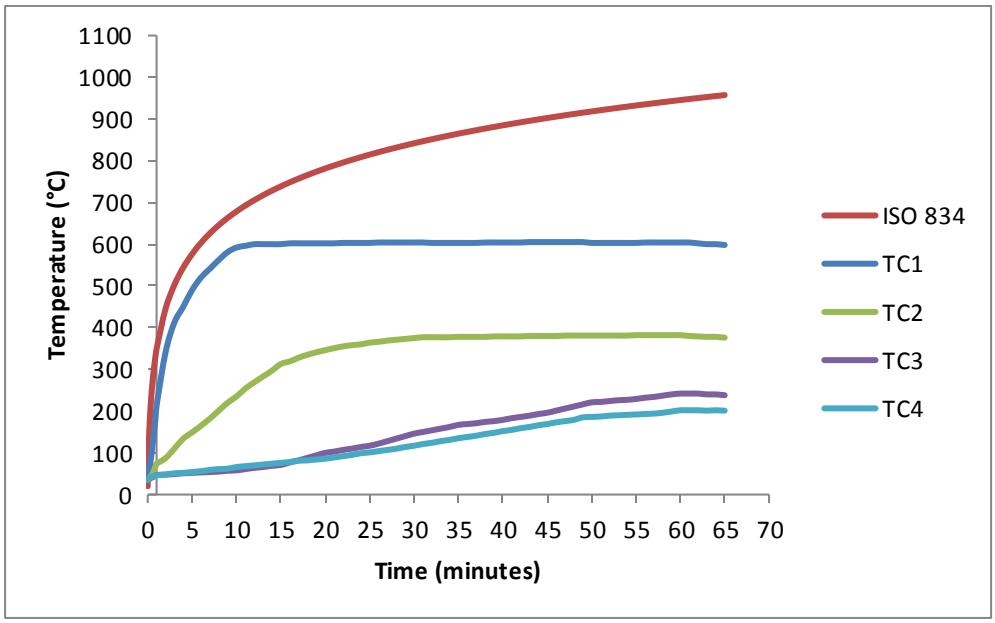

Figure 3-14: Experimental and ISO-834 Standard recommended temperature-time curves.

The real time-temperature curve was programmed by MATLAB program so that the heat thermocouple inside the furnace was connected to the computer in order to record the temperature values directly with the time. Then at the end of the burning process the data of temperatures and times are stored with the final shape of the time-temperature curve on the computer. Figure (3-15) illustrates an example of the time-temperature curve drawing by MATLAB program.

The flame length was 200 ~ 350 mm. The temperature was controlled by a computer. The bottom surface and two vertical side surfaces were exposed to fire. The starting temperature of the test was 35 °C. Three sides of the LWC beams were exposed to fire after 30 min of fire loading. The temperatures at different locations of the LWC beams were recorded at an interval of 10s. After the fire test, the beams were left in the furnace for cooling and then lifted from the furnace the next day.

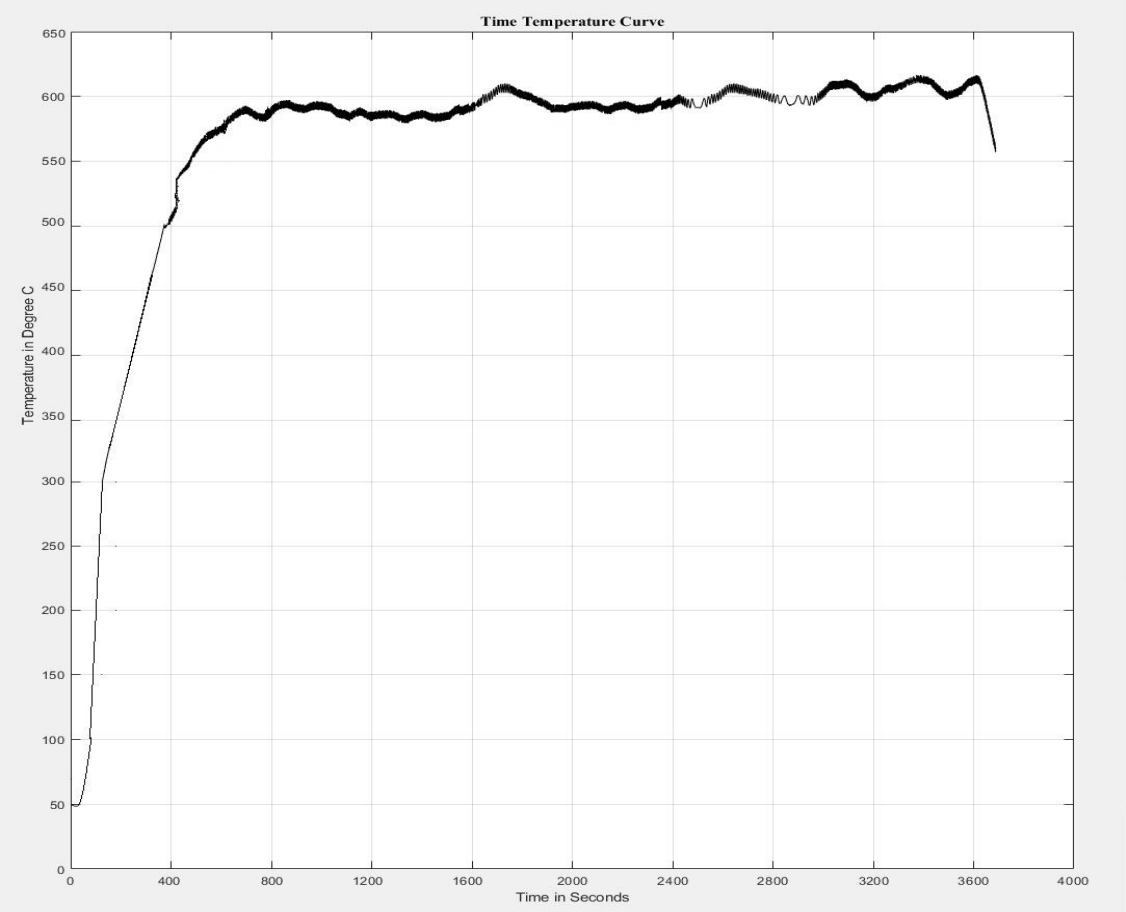

Figure 3-15: the time-temperature curve drawing by MATLAB program.

3.11 Cooling Procedure

After the duration of burning was finished, the gas valve was switched off, the lightweight concrete specimens were immediately extinguished by foam spray fire extinguisher and then lifted from stove by using thermal gloves. This process of cooling adopted in this investigation in order to simulate this problem to practical site conditions.

3.12 Preparing the SIFCON Thin Jackets

A new technique has been recently proposed for strengthening reinforced concrete structures via thin jackets made of high-performance fibre-reinforced cementitious composites (HPFRCC). These materials are characterized by a high compressive strength, which is accompanied by a rather high tensile strength, as well as by a hardening behavior in tension. As the traditional reinforcement is no longer necessary, the usual limits specified for the

minimum cover do not apply to the jacket (no rebars and stirrups), and the thickness of the jacket can be as small as 30–40 mm. In this work, the SIFCON thin jacket (20- and 30-mm thickness) was prepared by infiltrating randomly discrete fibers with specially designed cement-based slurry. Six percent volume fraction of hooked fibers was enough to fill the mold, so it was used in this investigation. The proportion of the materials used and the mechanical behavior of the matrix and SIFCON was described in this chapter. Hooked end fiber type is used with aspect ratio (L_f/D_f) of 60. The slurry mix was specially designed to have a high compressive strength and a very high workability. The slurry mix proportion was 1: 1.11: 0.11: 0.37: 0.041 by weight of cement, silica sand, silica fume, water and superplasticizer respectively. The slurry mix designed yielded a compressive strength of 60 MPa at 28 days. These jackets were prepared using fibers; namely hooked end steel.

3.13 Repair and Strengthening Technique of Fire Damaged LWC Beam Specimens

Specimens control LWC beams were without repair, the former is under room temperature, while the latter beams were fire-damaged strengthened with SIFCON thin jacket. As well as, the specimens which experienced fewer burning times compared to other beam specimens, received no severe damage and only small cracks were observed on their surface, there is no need to take action to repair concrete surface before shape modification and performing three-faces SIFCON jacket (U-shaped jackets). The jacket was prepared using especially designed wooden mold**.** Wooden molds with the same shape cross section as the LWC beam specimens. The mold was filled with fibers to achieve the required volume fraction, in multi layers. Each layer was infiltrated with the slurry mix. Careful attention was paid to ensure homogeneous distribution of fibers, and to ensure that no leakage happens during the infiltration process. This was made by using special rubber strip as a sealant material at the interface between wooden pieces.

The molds having larger dimensions were used to cast the three-faces SIFCON jacket as shown in Figure (3-16). These molds allowed casting (20 and 30) mm cover jackets and applying at the bottom and two sides (U-shaped jackets). After fire exposure, the fire damaged beams which got cracked and crumbled, were repaired before further strengthening. The cracked section was removed and restored using slurry infiltrated fiber reinforced concrete.

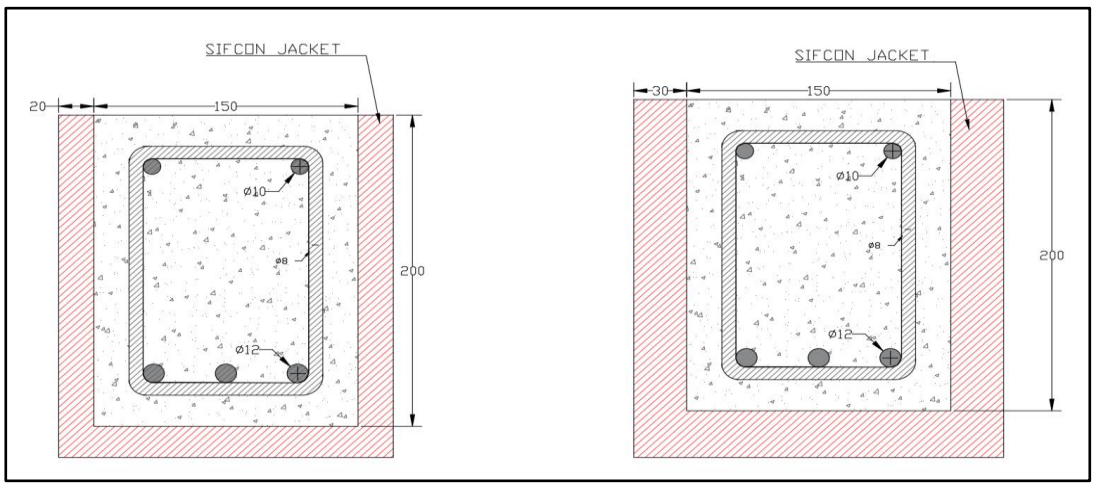

Figure 3-16: Strengthened section using three-faces SIFCON jacket.

The beams strengthening process using SIFCON thin jacket in this study includes four important stages that we will discuss briefly in the following, as shown in Figure (3-17):

- **First Stage: Removing Damaged Parts Resulting of Fire Exposure.**

At this stage, damaged, disassembled and burnt parts and places containing cracks, usually fragile and weak, are removed through the use of special machines with a precise and focused effect to avoid damage to the healthy parts adjacent to them from the body of the concrete member, a small grinding machine was used to obtain on a focused effect, taking into account the accuracy in removing the damaged parts and not others, the grinding process included the three sides that were burned from the concrete beams, which are the lower area and both sides, taking into account the continuous cleaning of the area that was grinded by water and then by compressed air to ensure no dust as shown in Plate (3-16A).

- **Second Stage: Notching of the LWC Beams**

After the final removal of the damaged parts was completed, the grooving process was carried out to obtain a rough surface that ensures a relatively perfect bond between the concrete beam body and the reinforcing jacket, which is what we need to ensure the reinforcing jacket's contribution to bearing part of the stresses on the beam, so high accuracy was taken into account in the implementation this stage, As the presence of a small defect in the bonding area may lead to a leak in the bonding in the neighboring regions and thus lead to the separation of the reinforcement layer and the loss of its role in resisting stresses. For this purpose, special discs for cutting hard stones were used to make grooves inclined in opposite directions at an angle of approximately 45 degrees to ensure a good interlock between the concrete surface and the reinforcing layer. After the roughing process was completed, a final cleaning process was performed using a water extrusion and then by compressed air to ensure no dust. Then the specimens were left to dry before the binder was applied see Plate (3-16B).

- **Third Stage: Application of the Binder**

After making sure that the surfaces were dry and clean, the binder according to the instructions of the manufacturer was applied to the surfaces to be strengthened with a soft brush to ensure that the binder penetrated well into the grooves and external surfaces see Plate (3-16C).

- **Fourth Stage: Pouring SIFCON**

Before each casting, the molds internal faces were properly cleaned, the spacers fixed at the bottom and both sides of the mold to ensure that the required reinforcement jacket thickness is obtained and lubricated with oil to avoid adhesion with hardened concrete. They were then positioned on a horizontal ground and as shown in Plate (3-16D).

Step1: steel fibers are divided into three parts before preplaced in the mold. The amount of fibers allocated to the strengthening of each beam is divided into three parts, depending on the volume of the slurry in each part (the bottom and both sides) to ensure an equal density of the fibers in the reinforcing layer. The first part belongs to bottom of the mold see Plate (3-16E).

Step2: Cement, sand, silica fume for each part is weighted and mixed with water, superplasticizer for making slurry. Slurry is poured into the mold.

Step3: After completing the bottom layer of the jacket, the beam to be strengthened was lowered into the mold so that it rests on top of the spacers that were previously installed inside the mold see Plate (3-16F).

Finally, the fibers are distributed in multi-layers and each layer is followed by the addition of the slurry to ensure that the slurry penetrates well through the fibers and that there are no voids.

Casting of the multi-layer technique for incorporating fiber in the slurry was utilized in this study, which proved efficient during the casting of SIFCON thin jacket and was found to be easier in practice than the single layer technique, especially in cases with high steel fiber content. The technique was repeated until the mold was completely filled with the specified fiber content.

The specimens, which did not undergo any damage or some damage some of these steps of repairing will deleted which conform with situation of beam, were directly strengthened. Then the specimens were cured using wet burlap for another 28 days. This was accomplished by keeping the LWC beams in upside-down position; preventing water from reaching the original (lightweight concrete).

Plate (3-16): Garmenting processes of strengthening LWC beam specimen.

At the end, the preparation of the three-faces SIFCON thin jackets was performed in the following sequence.

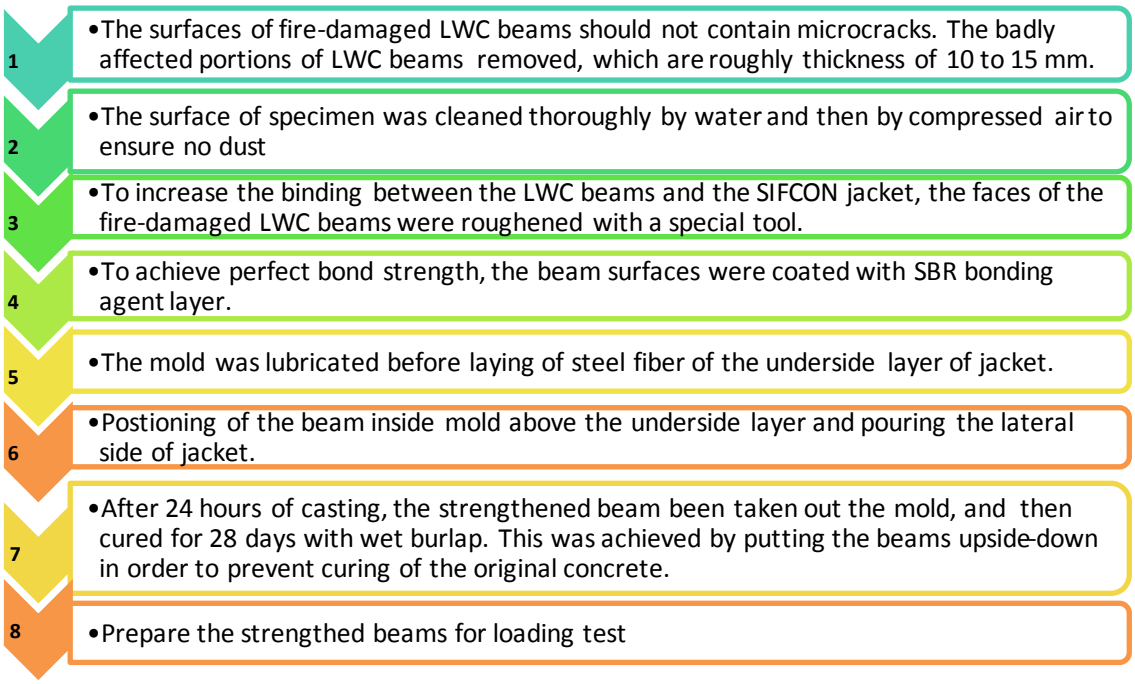

Figure 3-17: Repair and strengthening technique process of LWC beams by using three-faces SIFCON jacket.

3.14 Test Condition and Procedure of Reinforced LWC Beams

One day before testing, all reinforced LWC beams surface was cleaned then coated with white emulation before testing to clarify cracks propagation and make cracks observation easier. The beam specimen was placed in its position for testing, and making sure that it is in a horizontal position. For each beam the horizontally was checked accurately at both sides using a spirit level, before applying the load.

The beams are tested under two-point loading system. The two-point load system is believed to be creating a portion of pure bending along span of the beams which allows smooth transfer of load, application of constant moment and occurrence of their failure in the side zone. Hence, the two-point loading pattern is preferred as compared to that of single-point load system in the present investigation. Each beam of which was placed at 1.8 m from the end supports. The load was applied and spread by a steel beam at two points, which divided the tested LWC beam into three parts to simulate a nearly equal load applied on the LWC beam. The distance between two-point loads was 800 mm.

Special supports were made from hardened steel plates with a thickness of 20 mm to sustain the applied load without any deformation and avoiding crushing in the contact point of specimen body that may affect the test results, The supports was design to work as a hinge from one end and a roller from the other end. The two-point loads were applied on all beams by using a hydraulic testing machine of 600kN capacity under stroke control at a rate of 0.02 kN/s. All beams were tested under monotonic increasing load up to their failure. The following measurements were taken and stored in a data acquisition system, as shown in Figure (3-18). Loads as obtained from the load cell of the machine, displacement of the machine actuator, a linear variable differential transducer (LVDT), placed at the middle point of the bottom of the beam and under the location of the two point loading as obtained from three LVDTs placed at these locations, and mid-span curvature as obtained from two LVDTs placed along the top and bottom fibers and measuring changes in displacements over a distance of 20 cm, as shown in Figure (3-19).

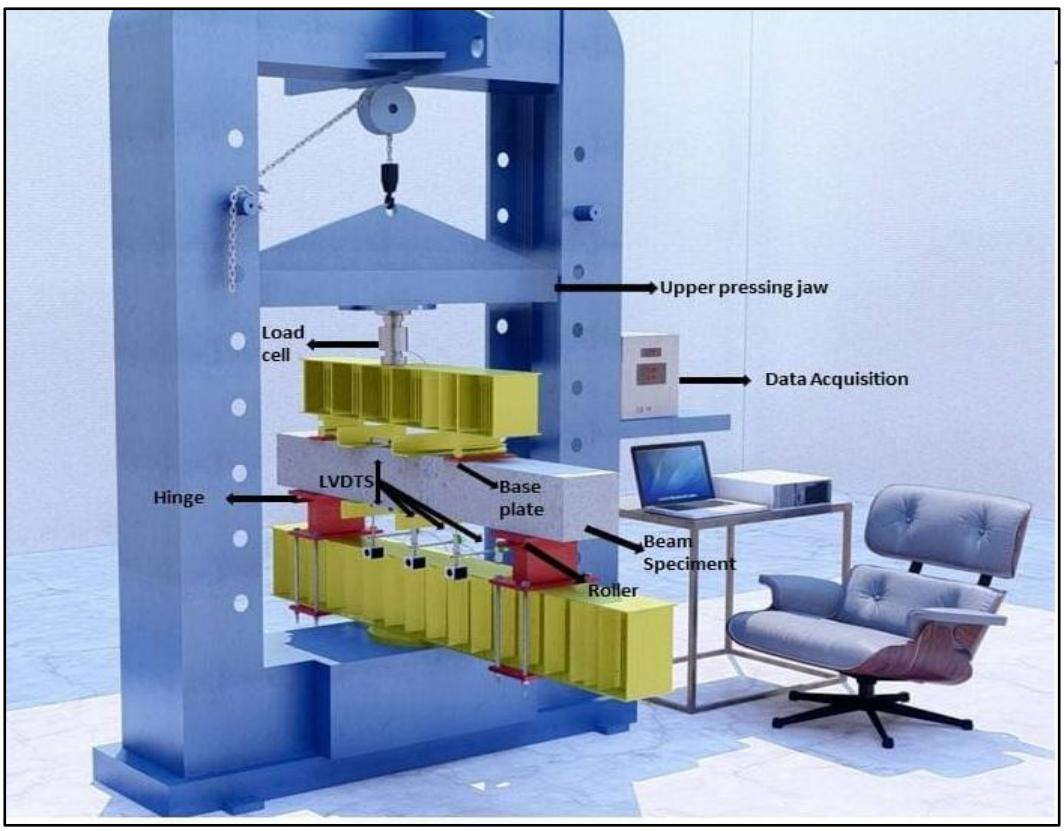

Figure 3-18: The loading setup of two-point load system

During testing, the main characteristics of the structural behavior of the specimens were detected at every stage of loading. These LVDTs were connected to a data acquisition system to measure mid-span and points loading deflection as shown in Plate (3-17).

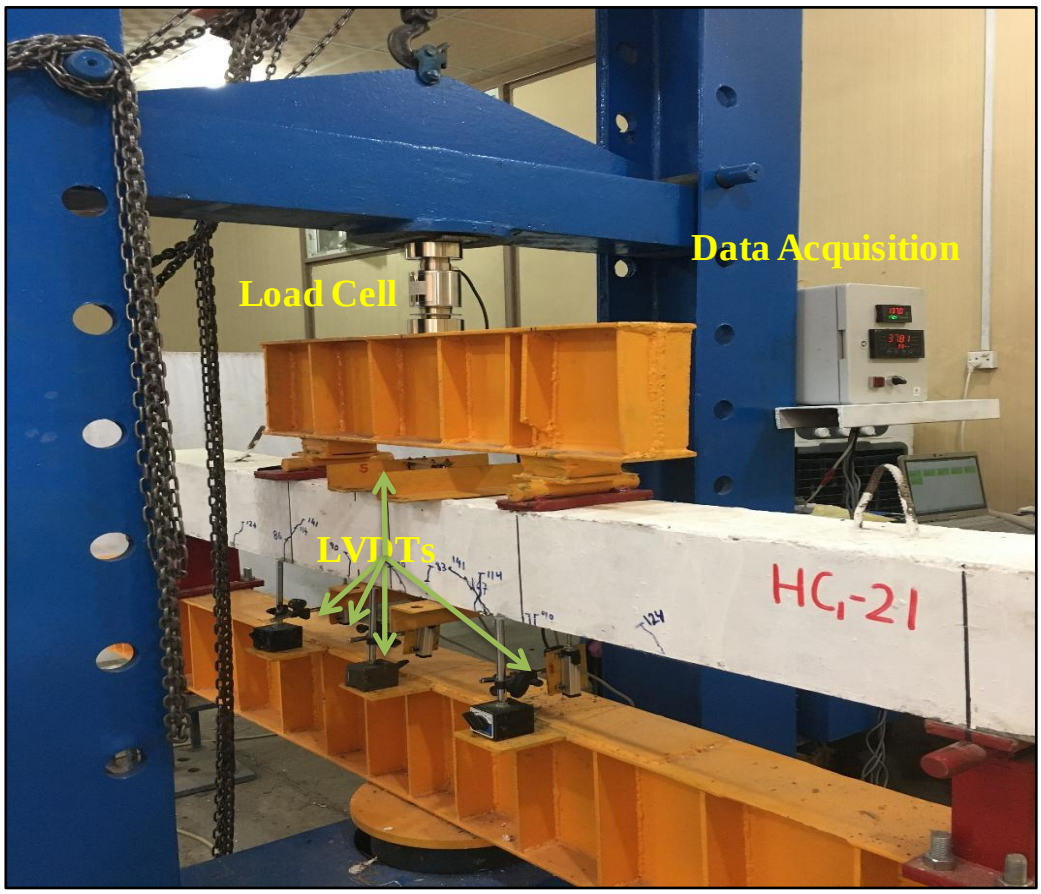

Plate (3-17): Arrangement of LVDTs and Load Cell within the test device.

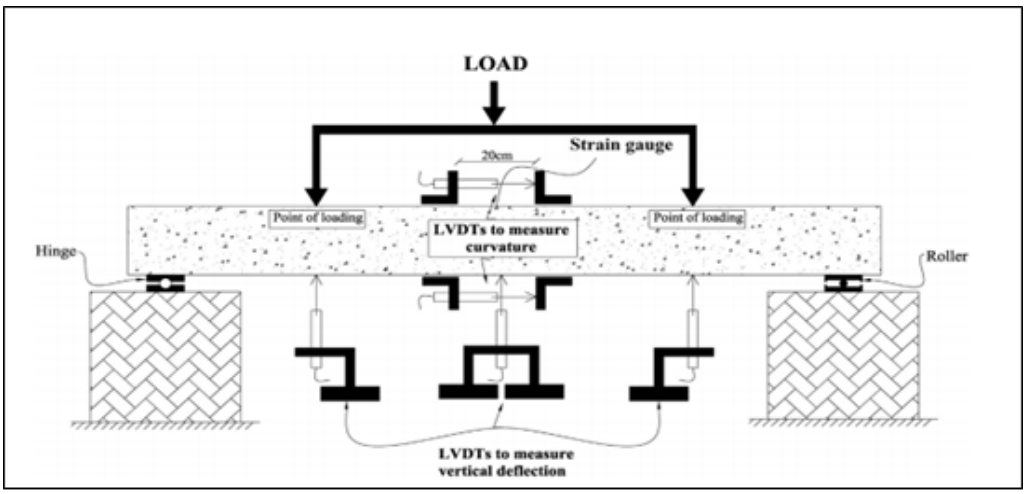

Figure 3-19: Loading setup and measurements.

The test was performed in the laboratory of the College of Engineering at University of Babylon. All of the LWC beam specimens were tested at the age of 28 days under increasing load up to failure by using a calibrated electro-hydraulic testing machine.

The first crack and crack development were observed through using crack meter device Plates (3-18), the corresponding load values were recorded and the crack pattern is marked on the beam specimens to determine the cause of failure and identify the failure mode. The failure modes were reported based on visual observation.

Plates (3-18) A: Crack meter device; **B:** crack development observation.

3.15 Testing of Control Samples (Destructive Tests)

After selecting the mixes for two types of concrete (LWC and SIFCON), in addition for various grades of LWC (NSC and HSC) produced as part of the overall program of LWC beam specimens and U-shaped SIFCON thin jacket, cubes, cylinders and prisms were casted in order to test it at ages of (7,28 and 56 days) at room temperature and after exposure to fire flame of (600)°C and with the same procedures and conditions of burning of LWC beam specimens, while for SIFON at room temperature only. These testing consisted of cube compressive strength (f_{cu}), modulus of elasticity (E_c), splitting tensile strength (f_{sp}) and modulus of rapture (fr). All the tests were carried out at Babylon

University, College of Engineering, Civil Department, Construction Materials laboratory.

3.15.1 Compressive Strength Test

The compressive strength was an established measure that represents one of the important concrete engineering properties that could provide an overall picture of the concrete quality. In order to determine the compressive strength, three cubes (100×100×100 mm) were cast in the same manner as for each grade of LWC (NSC and HSC) and three cubes for SIFCON, and the average value of these cubes was obtained according to (**BS. 1881: part 116)**. The Plate (3-19) shows the testing machine for compressive strength.

The compressive strength test was determined by crushing three cubes at the age of 7, 28 and 56 days using a digital testing machine with a capacity of (1900 kN), the loading rate was applied at (0.3 MPa/sec).

Plate (3-19): Compressive strength testing machine.

3.15.2 Static Modulus of Elasticity (Es)

The static modulus of elasticity of concrete was performed on (100×200 mm) cylindrical specimens and according to **(ASTM C469, 2014)**. The top surface of cylinder was well finished and smoothed by using electric grinding machine to prevent any loss of strength. The specimens were tested in a

hydraulic machine with a capacity of (1900 kN). In order to carry out the elastic module test, as shown in Plate (3-20), 40 percent of the ultimate compressive strength of the concrete sample was applied to the concrete cylinders. Three samples were tested at ages 7, 28 and 56 days and the average of each 3 samples was considered for each grade of LWC (NSC and HSC) and three cubes for SIFCON. Static modulus of elasticity was computed by the following equation:

$$\mathbf{Es} = \frac{\mathbf{S_2 - S_1}}{\mathbf{e2 - 0.0005}} \quad \text{(3-2)}$$

Es: static modulus of elasticity, (GPa).

S_2: stress corresponding to 40% of ultimate load, (MPa).

S_1: stress corresponding to a longitudinal strain (0.00005), (MPa).

e_2: longitudinal strain produced by stress S_2.

Plate (3-20): Modulus of elasticity test device.

3.15.3 Splitting Tensile Strength

Splitting tensile strength test was carried out using cylindrical specimens of 100×200 mm. The average result of three specimens was taken at 7, 28 and 56 days for each grade of LWC (NSC and HSC) and three cubes for SIFCON. The bearing strips were made from (3.2 mm) thick luaun plywood cut into (25.4 mm) broad strips. The cylinder's length and diameter were measured along the predicted failure plane. The cylinders were loaded at the prescribed rate until the ultimate load was reached. The test was done according to **(ASTM C496,**

2017) by using a digital testing machine with a capacity of (1900 kN) and loading rate of (0.3 MPa / sec), as shown in Plate (3-21).

The splitting tensile strength (f_{sp}) of specimen is calculated by the following Equation:

$$f_{sp} = \frac{2P}{\pi DL} \quad \text{(3-3)}$$

f_{sp} : Splitting tensile strength (MPa).
P : Maximum applied load in splitting test (N).
D : Diameter of cylinder (mm).
L : Length of cylinder (mm).

Plate (3-21): Splitting tensile strength test.

3.15.4 Flexural Strength (Modulus of Rupture)

The modulus of rupture (MOR) was tested using concrete prisms with dimensions of (100x100x400) mm in accordance with (ASTM C78/2016). Prisms were cast and cured in the same way that beam specimens were. For each age (3, 7, 28, and 56) days, each value reflected the average of three prisms. Third-point loading (MOR) tests were carried out with a hydraulic machine CONTROLS digital with a capacity of 150 KN, as illustrated in Plate

(3-22). Using the following Equation, the ultimate modulus of rupture (fr) was computed.

$$\boldsymbol{fr} = \frac{\boldsymbol{PL}}{\boldsymbol{bh^2}} \quad \text{(3-4)}$$

Where:

fr: Modulus of rupture, (MPa).

P: Failure load, (N).

L: distance between the supports, (mm).

b: Prisms width, (mm).

h: Depth of prisms, (mm).

This equation is only applicable if the failure line is inside the mid third of the span length; otherwise, the MOR is computed using equation (3-5):

$$\boldsymbol{fr} = \frac{\boldsymbol{3Pa}}{\boldsymbol{bh^2}} \quad \text{(3-5)}$$

Where:

a: The average distance measured on the tension surface of the beam between the point of fracture and the nearest support (mm).

Plate (3-22): Flexural strength test.

3.16 Testing Non-Destructive Tests

In order to determine the effect of fire on the lightweight concrete the compressive strength of the beams was measured one day after exposure to fire

using nondestructive tests. First, an ultrasonic pulse velocity test was used but the readings were unreliable, which was attributed to the random cracks which occurred during fire. So, the Schmidt hammer was used for estimation of concrete compressive strength. Each LWC beam was divided into 36 squares (10 X 10 cm) on the side and 18 rectangles (12 x 10 cm) on the bottom. An average of ten readings was determined for each square or rectangle.

3.16.1 Ultrasonic Pulse Velocity Test (U.P.V)

Ultrasonic Pulse transit times were measured by direct transmission method. This test was carried out according to (**ASTM C597, 2002).** The velocity of ultrasonic pulses transmitted through the control lightweight concrete specimens was determined before and after burning. Portable ultrasonic concrete tester known as (PUNDIT) 54 KHz was used for this purpose which is shown with its accessories in Plate (3-23). Calibration of the PUNDIT was done before testing to check the accuracy of the transit time measurements. This was achieved by the calibration with the reference bar.

A thin layer of grease was applied on the surface of the tested points to act as a compliant and to prevent dissipation of transmitted energy. The pulse transit path length was measured accurately and the time of its travelling was recorded to the order of 0.1 µsec. The test was accomplished in concrete laboratory of College of Engineering in Babylon University. The pulse velocity was calculated as follows:

$$\boldsymbol{V} = \frac{\boldsymbol{L}}{\boldsymbol{T}} \qquad (3\text{-}6)$$

Where: V: Ultrasonic pulse velocity (km/sec).

L: The path length (mm) and

T: The transit time (µsec).

Plate (3-23): Ultrasonic pulse velocity test for beams and cube samples.

3.16.2 Rebound Number Test

Schmidt hammer was used to estimate the surface hardness of lightweight concrete specimens by recording the rebound number, which could be considered as a measure of the LWC strength and percentage of voids.

The Schmidt hammer rebound number was recorded at 16 distributed points on the face of the LWC specimens which is shown in Plate (3-24).

Plate (3-24): Schmidt hammer test for lightweight concrete specimens.

The mean rebound number was calculated for each area of LWC specimens (exposed to realties fire flame). Schmidt hammer type (MC) was used. The test method is prescribed by **(BS 1881: part 202, 1986)** specifications. The test was accomplished in concrete laboratory of College of Engineering in Babylon University.

3.17 Summary

The development various grades of strength of lightweight concrete NSC and HSC, in addition SIFCON are presented in this chapter. As mentioned, this partly belongs to the overall research program on LWC being carried out at Babylon University - college of engineering. Materials used for these types of concretes and their properties are discussed. Mechanical properties of these concretes related to the structural response of reinforced concrete members are presented and discussed taking into account the available studies and code provisions. The procedure of burning LWC beam specimens, then repairing and strengthening technique using U-shaped SIFCON jacket are presented in this chapter.

CHAPTER FOUR

Chapter 4. Results and Discussion

4.1 Introduction

The main objective of this study is to investigate experimentally the structural behavior of lightweight concrete beams exposed to fire flame and reinforced with slurry infiltration fiber reinforced concrete SIFCON U-shape jacket, covering the bottom and both lateral sides of beam with different parameters, like concrete cover, compressive strength of concrete (normal and high), exposure duration, and thickness of reinforcing jacket. The goal of the experiment was to investigate the shear performance and mechanism of failure of simply supported beams that had been externally reinforced with SIFCON jackets. A total of twenty-eight with high and normal strength reinforced concrete beam specimens were casted. The research methodology based on the studying and comparing the behavior, mode of cracking, and failure of reinforced concrete beams before and after strengthening with SIFCON jacket, with respect to the resistance to applied shear stresses. In addition to comparing the results obtained from the experimental test with those obtained from the simulation program to verify the conformity of the behavior in both cases.

4.2 Mechanical Properties of Hardened Concrete

Understanding the behavior of concrete beam specimens requires a thorough understanding of the material's mechanical properties. Compressive strength, splitting tensile strength, modulus of rupture, and modulus of elasticity are among the most important mechanical characteristics of hardened concrete investigated in this study. The average of three control samples taken at various ages, including the age of beam testing, was used to calculate each of these properties value. These characteristics are studied in order to determine lightweight concrete fire resistance and capabilities.

4.2.1 Compressive Strength

The most common test on hardened concrete is the compressive strength test. It is used to evaluate the concrete's potential strength. Concrete compressive strength is a criterion used in national and international regulations to categorize concrete. The compressive strength ($f$cu) test was conducted on (100×100×100) mm NSC and HSC LWC cubes, which were casted using expanded clay lightweight aggregate (LECA). The compressive strength of the cubes was determined by testing it at ages of 7, 28, 56 and 90 days, the cubes were examined at laboratory temperature (25°C). The compressive strength of normal and high lightweight concrete and SIFCON jacket is shown in Table (4-1). In order to minimize the probable error in each measured result, the result in this table reflects the average value of (3) cubes.

Table 4-1: Results of experimental test of cube compressive strength of NSC, HSC LWC and SIFCON samples at room temperature.

Symbol	Age (days)	Compressive strength f_{cu} (MPa)	% f_{cu} development with respect to 90 days age
LWHSC	7	46.60	66.37
LWHSC	28	67.33	95.89
LWHSC	56	68.12	97.02
LWHSC	90	70.21	100
LWNSC	7	20.34	60.37
LWNSC	28	28.26	83.88
LWNSC	56	32.00	94.98
LWNSC	90	33.69	100
SIFCON	7	97.46	76.87
SIFCON	28	111.13	87.65
SIFCON	56	123.41	97.33
SIFCON	90	126.79	100

Concrete compressive strength development with time of various mixtures types are illustrated in Figure (4-1). With reference to the 28 day's strength, both of HSC and NSC showed the same value of development, which were

about 70% at early age. While SIFCON mixture had reflected strength development of about 87%. For 56 days, both NSC and SIFCON compressive strength development were the same, were about 112%, while a slight strength development (101%) was observed for HSC. At age of 90 days, the highest strength development was observed for NSC mixture, which was about 119%, followed by SIFCON mixture (114%), while the HSC reflected lowest development value (104%). On the other hand, when compared, considering that the resistance at the age of 90 days represents the semi-final outcome of the concrete element, then SIFCON acquires strength quickly during the early stages of development (at 25 °C, about 80 percent of compressive strength was reached in 7 days and continued until roughly 91 percent of compressive strength was achieved at 28 days). While for HSC and NSC LWC the strength gain was (66 and 69.7 percent of compressive strength at 7 days age) and (96 and 87.5 percent of compressive strength at 28 days age) for HSC and NSC LWC respectively. However, strength gains proceeded until the completion of the curing period, but at a lower rate.

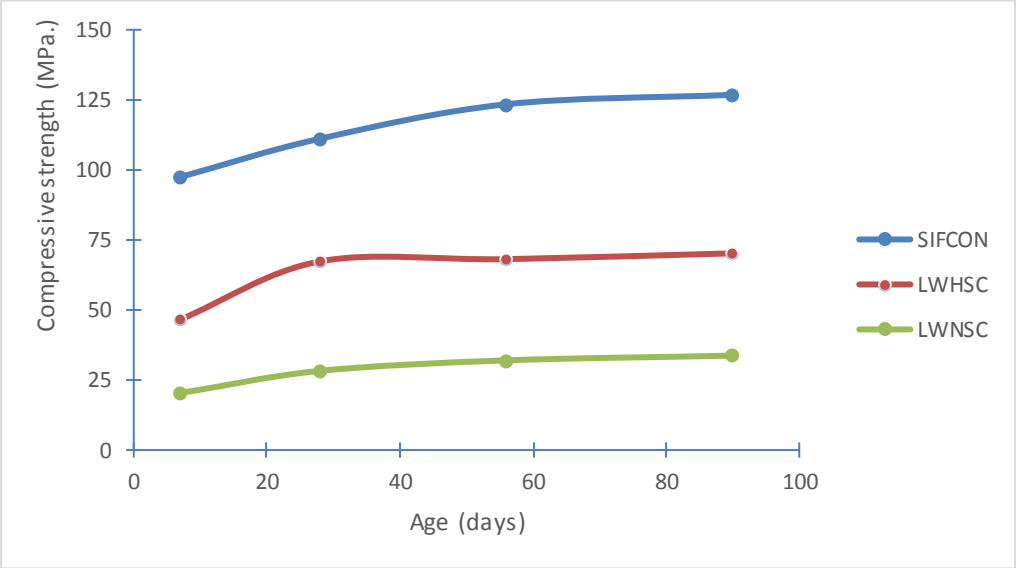

Figure 4-1: Development of compressive strength.

Generally speaking, the reduction in compressive strength for NSC and HSC at various ages ranged from 31%-38% and 38%-46%, respectively, as can be seen in Table (4-2).

Table 4-2: Results of experimental test of cube compressive strength of NSC, and HSC LWC samples after burning at 600ºC temperature.

Symbol	Age (days)	Compressive strength f_{cu} (MPa)		% Residual of compressive strength
		At 25ºC	At 600ºC	
LWHSC	7	46.60	25.02	53.7
LWHSC	28	67.33	37.13	55.2
LWHSC	56	68.12	41.69	61.2
LWHSC	90	70.21	43.74	62.3
LWNSC	7	30.44	18.84	61.9
LWNSC	28	38.26	25.29	66.1
LWNSC	56	42.00	28.77	68.5
LWNSC	90	43.69	30.23	69.2

$$\%\ Residual\ of\ compressive\ strength = \frac{fcu\ (T = 600°C)}{fcu\ (T = 25°C)}\ X\ 100 \quad (4\text{-}1)$$

Figure (4-2) illustrates the residual strength of concrete cube specimens for both NSC and HSC mixtures. Overall, the NSC mixture have sustained higher residual strength when compared with the HSC mixture. A slight residual strength difference has noticed between these mixtures at various ages, ranged between 7%-10%. Moreover, at early ages, the effect of fire on the residual strength was higher than its effect at lately ages.

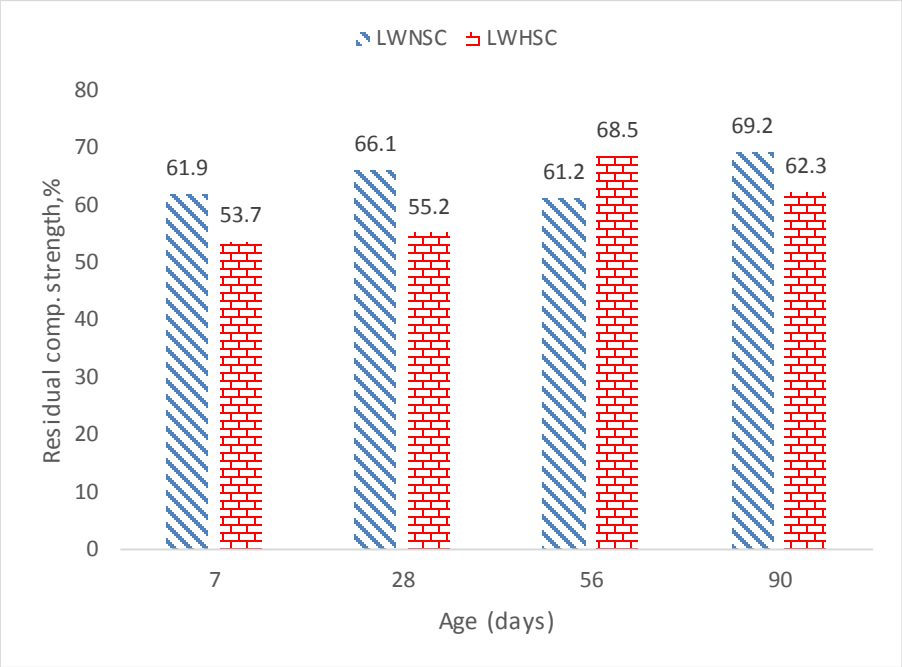

Figure 4-2: Concrete residual strength at various ages.

This may be attributed to the presence of water trapped inside LECA aggregate was utilized in building cement microstructure at hydration process, while large amount of water that existed at early age was activated by the fire and converted to expandable gas. The trapped gas tends to produce internal pressure which leads to weaken the internal microstructure and hence reduces the overall concrete strength.

4.2.2 Splitting Tensile Strength

The minimum 28-day splitting tensile strength necessary for structural LWAC, according to **(ASTM C330,2006)**, is 2.0 MPa. As shown in Table (4-3), both mixes of LWC had considerably greater splitting tensile strength than the **(ASTM C330,2006)** minimum requirement (49 percent for HSC and 45 percent for NSC). The results show that the LWC's splitting tensile strength frequently improves with aging. However, under tensile strain, the crack rapidly propagates, resulting in a substantially lower tensile strength than compressive strength. Increasing the strength over time is the result of the matrix's hydration mechanism progressing by completing its internal

microstructure, which results in increased strength contributed to the composite material. In general, the compressive strength of concrete is related to its splitting tensile strength; the higher the compressive strength, the higher the splitting tensile strength. The results show that SIFCON reflecting higher splitting strength than both mixes of high and normal at age of 28 days by (4.3 and 5.44 times) for HSLWC and NSLWC respectively. This represents the hypothesis adopted by this study to take advantage of the SIFCON strength acquired in the early ages to employ it in the repairing process.

Table 4-3: Results of experimental test of cylinder splitting tensile strength of NSC, HSC LWC and SIFCON samples.

Identification	**Age (days)**	**Splitting tensile strength *fsp* (MPa)**
LWHSC	28	4.617
LWHSC	56	5.416
LWNSC	28	3.657
LWNSC	56	3.997
SIFCON	28	13.93
SIFCON	56	18.37

4.2.3 Flexural Strength (Modulus of Rupture)

The flexural strength fr test was performed using (100×100×400) mm prism specimens for LWC and SIFCON, where each prism was tested as simply supported and subjected to two-point loading, and applying the same procedure. It is evident from the results provided in the Table (4-4) that the flexural strength values are close to both mixes of LWC, with little progress for the high strength, while there is a great superiority for SIFCON in acquiring the strength of all ages, where it were more than (4.5 and 7 times) at 28 days age for (HSLWC and NSLWC) respectively. Also Figure (4-3) shows that HSLWC have a higher flexural strength development than NSLWC by a range of (33% to 62%). While SIFCON shows much higher strength development, that its strength in 7 days age higher than the maximum strength obtained in the final

age of 90 days for both LWC mixes by (2.76 and 3.98 times) for HSC and NSC respectively.

Table 4-4: Results of experimental test of prism flexural strength of NSC, HSC LWC and SIFCON samples.

Identification	Age (days)	Flexural strength f_r (MPa)
LWHSC	7	4.62
LWHSC	28	6.27
LWHSC	56	6.85
LWHSC	90	7.17
LWNSC	7	3.47
LWNSC	28	3.89
LWNSC	56	4.59
LWNSC	90	4.98
SIFCON	7	19.83
SIFCON	28	28.56
SIFCON	56	32.88

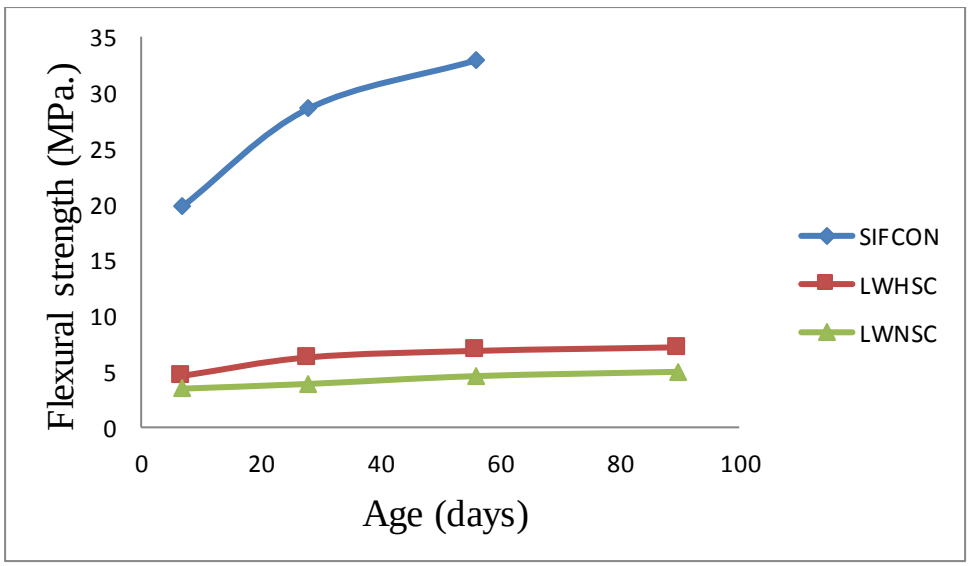

Figure 4-3: Development of Flexural strength.

4.2.4 Static Modulus of Elasticity

The modulus of elasticity is simply a measurement of a material's stiffness. The modulus of elasticity is an important component in calculating the

deformation of members, as well as a significant factor in determining the modular ratio, m, which is employed in the design of flexure-prone sections of members. The modulus of elasticity is commonly used in sizing reinforced and unreinforced structural elements, determining reinforcement amount, and estimating stress given observed strain values. As a result, the modulus of elasticity of concrete is an important parameter that reflects the capacity of concrete to deform elastically. The static modulus of elasticity (E_c) is a material measure that indicates the stiffness of a material and are therefore one of the most essential characteristics of solid materials. The concrete components and their proportions have a significant effect on the modulus of elasticity. Because the slope of the ascending branch of the stress-strain diagram becomes steeper as compressive strength increases, a rise in modulus of elasticity is expected **(Ramezanianpour et al., 2009)**.

Table 4-5: Results of experimental test of cylinder modulus of elasticity of NSC, HSC LWC and SIFCON samples.

Symbol	Age (days)	Modulus of Elasticity E_c (GPa)
LWHSC	28	37.03
LWHSC	56	37.47
LWNSC	28	21.04
LWNSC	56	23.1
SIFCON	28	61.12
SIFCON	56	67.89

The findings clearly demonstrated that the use of light aggregates in the production of lightweight concrete resulted in a drop in the modulus of elasticity of all samples, whether in normal or high strength lightweight concrete. At 28 days, the modulus of elasticity of the lightweight concrete was 37.03 MPa and 21.04 MPa, for HSC and NSC respectively. Because coarse

aggregate accounts for roughly 40%–45% of the overall volume of lightweight concrete, every variation in the type of coarse aggregate used has a major impact on the mechanical properties of the concrete. Previous research has found that normal-weight concrete is more resistant than lightweight concrete. This is due to LECA aggregates having lower mechanical performance than other type of aggregate.

4.2.5 Ultrasonic Pulse Velocity (U.P.V)

Each sample was tested as direct transmission in this study. Through the results of the tests are shown in Tables (4-6), the pulse velocity decreased after burning for all samples where the reduction rates were between (28-37%) and (24-30%) for HSLWC and NSLWC respectively.

Table 4-6: Results of experimental test of cube Ultrasonic Pulse Velocity of NSC, and HSC LWC samples before and after burning.

Symbol	Age (days)	(U.P.V) (m/sec)		% Residual of (U.P.V)
		At 25°C	At 600°C	
LWHSC	7	3788	2375	62.7
LWHSC	28	4717	3250	68.9
LWHSC	56	4785	3311	69.2
LWHSC	90	4876	3501	71.8
LWNSC	7	3460	2401	69.4
LWNSC	28	3876	2837	73.2
LWNSC	56	4049	3025	74.7
LWNSC	90	4184	3176	75.9
SIFCON	28	4829	---	---
SIFCON	56	5162	---	---

The main explanation for the reduction of ultrasonic pulse velocity after fire exposure was as the temperature rises, LECA aggregate contains large amounts of water as a result of the high absorption rate compared to normal types of aggregate, and therefore the evaporation of water leaves air spaces

through which the pulse wave travels at a lower speed, which affects the decrease in results. In addition to that, the chemical components disintegrate, and the number of micro-cracks and holes increases. A component of the sound wave was reflected as it came into contact with the air, according to the sound wave's propagation characteristic. Another component of the sound wave straight traveled the air, while the remainder detoured concretes and continued to spread.

4.2.6 Rebound Hammer Results

the Schmidt rebound hammer is still the surface hardness testing device of the most widespread use for concrete. Rebound hammer can be used very easily and the measure of hardness (i.e. the rebound index) can be read directly on the display of the testing device. According to **(Malhotra&Carino,2003)**, the accuracy of assessing the strength of specimens cast, maintained in cure, and tested in labs to compression using correctly calibrated hammers is between 15% and 20%. However, the accuracy of the hammer's estimation of the compressive strength of the concrete structure is 25%.

It can be seen from the results shown in Table (4-7) that the rebound number values reduction clearly when concrete exposed to fire, that the reduction was (45 and 33%) for high and normal strength lightweight concrete respectively.

Table 4-7: Results of Rebound Number of NSLWC, and HSLWC samples.

Symbol	Age (days)	Average Rebound Number	Quality of concrete
HC1-00	56	55	Very good hard layer
HC1-02		38	Good layer
HC2-00		55	Very good hard layer
HC2-02		39	Good layer
NC1-00	56	40	Good layer
NC1-02		30	Fair
NC2-00		41	Very good hard layer
NC2-02		31	Good layer

4.3 Description of Experimental Program of LWC Beam Specimens

The test program consisted of testing twenty-eight beam specimens of NSC and HSC lightweight concrete, these beam specimens divided into two main groups, first group included the beams that were made of normal strength concrete mixture, while the second group including these with high strength mixture. Each group dividing into two branches, first branch including the beams with concrete cover of 20mm and the second branch including these where made with 30mm concrete cover. Each one of these branches dividing into four subcategories, the first included beams that were exposed to fire and were not strengthened, the second included the beams that were exposed to fire and were strengthened using SIFCON jacket with thickness of 20mm., the third including the beams that were exposed to fire and were strengthened using jacket with thickness of 30mm., the forth included the beams that were not exposed to fire and were not strengthened with SIFCON, which considered as a control for tested beams, each one of the four subcategories was divided depending on its duration of exposure.

For each tested beam first crack load, ultimate load carrying capacity, modes of failure, load-deflection behavior and longitudinal strain distribution were recorded. The main objective is to choose the optimum cover and SIFCON jacket thickness which reduce deterioration and spalling effects of the original lightweight concrete beam subjected to fire flame and then to meet the practical, load carrying capacity, energy absorption requirement and to eliminate the brittle shear failure and increased the ultimate shear strength of the repaired beams through using the SIFCON jackets as external shear reinforcements. A two-point flexural loading system is adopted. At each stage of loading, three LVDTs instrument were used to measure the displacement of the beam at the mid-span of the specimen and under the location of the two-point loading. The mid-span curvature of the beam is also measured using two LVDTs placed along the top and bottom face of the beam, where the LVDTs

measure the changes in displacements over a distance of 20 cm. The load was applied in small increments until the failure. The beams test results including, the first crack load, ultimate load, residual ultimate load and load-deflection are shown in Table (4-8) as follows:

Table 4-8: Results of experimental test of first crack load, ultimate load and maximum deflection for NSC and HSC LWA beam specimens exposed to fire.

Group No.	Grade	Specimen Identification	Frist Crack Load (kN)	Ultimate Load (kN)	Percentage residual Ultimate Load %	Serviceable load corresponding to (L/360) mid-span deflection (kN).	Max Deflection(mm)		
							At Mid-span	Under loading point on hinge side.	Under loading point on roller side.
Group One	NSC	**NC1-00**	**15.4**	**117.00**	**100**	**36.5**	**22.85**	**20.54**	**19.20**
		NC1-01	10.6	91.63	78.3	28.32	24.32	22.04	19.03
		NC1-02	8.5	88.5	75.64	25.06	16.94	18.59	18.35
		NC1-21	45	157.60	134.7	75.9	14.94	13.89	13.02
		NC1-22	73.4	147.90	126.4	73.4	13.46	12.08	10.68
		NC1-31	89.5	188.10	160.8	88.85	13.55	14.11	12.16
		NC1-32	70.9	166.10	142	90.9	12.32	11.00	11.37
		NC2-00	**13.5**	**102.70**	**100**	**38.7**	**24.41**	**21.21**	**19.32**
		NC2-01	10	86.28	84	33.28	22.47	19.20	17.75
		NC2-02	7.69	81.60	79.5	23.6	18.32	15.77	14.67
		NC2-21	63.7	141.70	138	77	12.15	10.82	9.76
		NC2-22	56.7	129.60	126.2	68	13.24	13.40	11.02
		NC2-31	60	172.20	167.7	94.6	13.25	15.74	11.87
		NC2-32	77.9	168.90	164.4	47.4	15.91	12.49	9.18
Group Two	HSC	**HC1-00**	**25.4**	**139**	**100**	**47.3**	**24.87**	**22.41**	**21.05**
		HC1-01	11.2	95.44	68.7	31.4	19.09	16.89	16.25
		HC1-02	8.8	81.23	58.44	30.3	20.31	18.65	15.39
		HC1-21	63.7	159.70	114.89	77.6	13.69	13.00	11.91
		HC1-22	83.1	146.40	105.3	77.5	12.19	10.79	10.59
		HC1-31	85.3	190.60	137.1	96.5	12.93	11.84	9.57
		HC1-32	80.3	178.40	128.4	86.8	13.84	12.21	12.62
		HC2-00	**17.2**	**124.08**	**100**	**56.7**	**24.73**	**22.09**	**21.68**
		HC2-01	11.68	89.70	72.3	29.0	28.04	25.48	20.39
		HC2-02	7.5	79.88	64.4	23.8	21.04	19.25	17.21
		HC2-21	72.3	159.90	128.9	75.4	14.63	13.09	11.13
		HC2-22	50.2	146.50	118.1	77	12.83	10.88	10.38
		HC2-31	98	197.20	159	92.4	14.67	12.44	12.04
		HC2-32	89.6	186.00	149.9	91.7	13.59	12.23	11.96

4.4 Load Carrying Capacity of NSC and HSC LWA Beam Specimens

Load carrying capacity reflects the ultimate applied load that may be subjected to the beam specimens under test, after which a drop in machine reading occurs accompanied by rapid deformation on the beam, known as failure. To study the effect of fire exposure on the load-carrying capacity of beam specimens, the characteristics of NSC and HSC LWA beams before and after burning should be investigated and summarized as follows:

4.4.1 Behavior of NSC LWA Beams Before and After Burning (Group One)

The behavior of beam specimens was analyzed in this study through studying some of an important indication strongly relating with the load carrying capacity. The first indication is the cracks pattern, which is formed by the crack's development in synchronism with applied load. For NSC LWA, the reference beam and fire damage without repairing specimens, a very tiny with short extent flexural cracks formed first within the pure bending region (near mid span). With increasing load, the both the reference and damaged specimens displayed a same crack pattern. As that the loading was raised, flexural cracks occurred in both the reference and damaged specimens, and the before existing cracks (in the damaged specimen) expanded. The first crack formed near the mid-span region, with a cracking loads value of (13.5-15) and (7.7-8.5) kN for the reference and damaged specimens, respectively. The lower cracking load of the heat-damaged specimens might be attributed to affected of reinforcing steel. This happened because of residual tensions of steel after cooling burned specimens were substantially higher than those of lightweight concrete, then in line with increased loading cracks began to appear within the regions of shear span. Owing to the presence of shear stresses, cracks in the shear span would bend towards the loading point and diagonal cracks thus formed, the cracks that ordinarily started in the vertical direction began to migrate in inclined orientations (shear-flexure cracks).The development of the diagonal crack

suddenly propagated through nearly the total depth of the beam. The redistribution of stresses formed secondary cracks which also appeared within the lower 100 mm of beam depth, see Plate (4-1). The beam would sustain higher load and then failed when the concrete in the compression zone crushed.

For reference beams, when the steel yielded, cracks spread in the compression region towards the location of the loading points, resulting concrete crushing beneath the point of loads. The failure process of NC1-00 was almost similar to that of NC2-00, although it has different (C.C) concrete cover, except the number of cracks and its extensions was slightly lower in NC1-00. The control beams failed, as expected, in shear with yielding of stirrups.

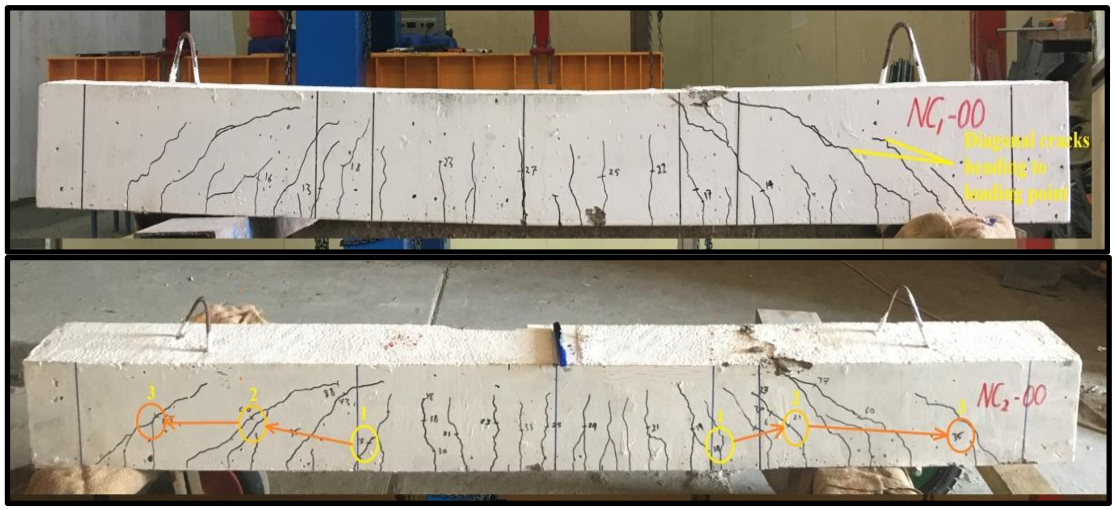

Plate (4-1): Cracks pattern of NSC LWA beams before burning.

Heat-damaged beams, on the other hand, revealed a quick shear failure, most likely due to the lead to losing in shear strength of concrete caused by heating, see Plate (4-2). After burning the angle of diagonal cracks inclination was slightly larger, also the extension was little shorter and almost similar on both sides, while hinge side seemed longer before burning. The secondary cracks formed more after burning and appeared so close to each other. The failure process of the NC1-02 is similar to that of the NC1-00, except that the concrete falls into the shear zone due to fire damage.

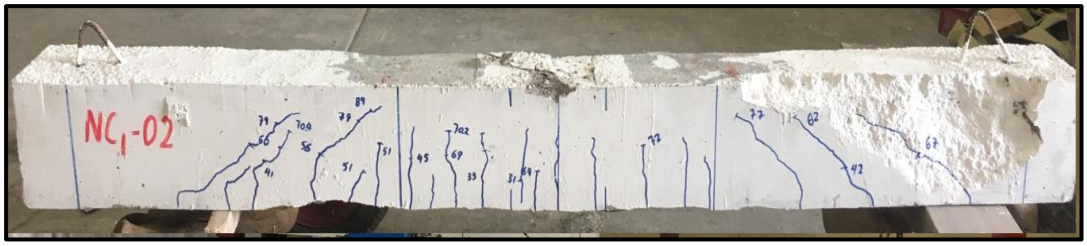

Plate (4-2): Cracks pattern of NSC LWA beams after burning.

The second criterion by which the structural behavior of the beam specimen can be studied is the relation between the load carrying capacity and concrete cover with different SIFCON jacket thicknesses, relationships of each pair of the reference beams having the same reinforcement amount and different concrete cover (C.C) presented in Figure (4-4).

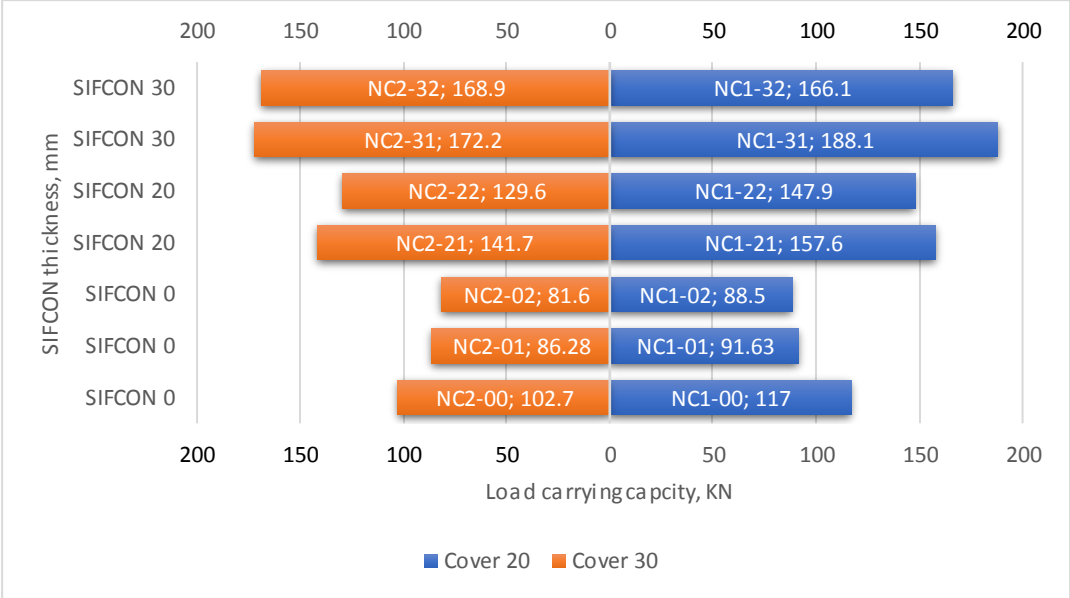

Figure 4-4: Effect of concrete cover on load carrying capacity of NSC beams with different SIFCON jacket thickness.

The results showed a decrease in the load carrying capacity values as a result of the change in the thickness of the concrete cover for the reference models by 14% for the models with a concrete cover 20 mm before burning. Where the values were (117 and 102.7) for the concrete cover 20 mm and 30 mm, respectively. After exposure to burning, the results remained advanced for the 20 mm concrete cover, but at a lower rate, where the exposure period (30 and 60 minutes) was about (6% and 8.5%) respectively. It is clear that the

effective depth remains as a control factor for the resistance of the specimen. On the other hand, as for the damaged beams that were strengthened, the results showed that the 20 mm concrete cover remained advanced by about (11% and 14%) for a burning period (30 and 60 minutes) sequentially when strengthening with a SIFCON jacket thickness of 20 mm, but it decreased by 1.6% for a burning period of 60 minutes and strengthen with 30 mm jacket thickness. See Figure (4-5). This can be attributed to the loss of the effective depth of its role as a controller as a result of increasing the thickness of the SIFCON layer as a compensation for the damaged concrete cover.

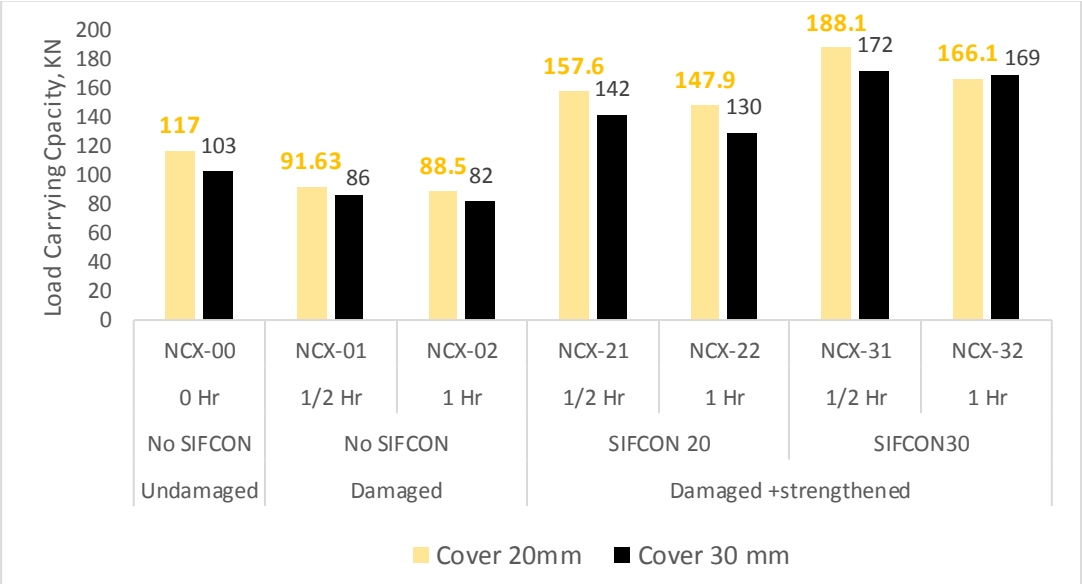

Figure 4-5: Effect of fire exposure duration on load carrying capacity of NSC beams with different SIFCON jacket thickness.

Regarding the change in ultimate load of the cases studied in this research, the results showed that increasing the concrete cover from 20mm to 30mm Contribute to reducing the rate of decline in the ultimate load as a result of burning by 19%, while after strengthening there was no role for the change in the thickness of the concrete cover when using reinforcement with a thickness of 20 mm, where the improvement values for the SIFCON were equal at this level, then the improvement values of 30mm concrete cover increased when using SIFCON with a thickness of 30 mm by 53% as shown in Figure (4-6).

Which indicates that the concrete cover has a role in maintaining the concrete's resistance to burning, especially in the short periods of exposure, even if it is slight, and its effect recedes after strengthening.

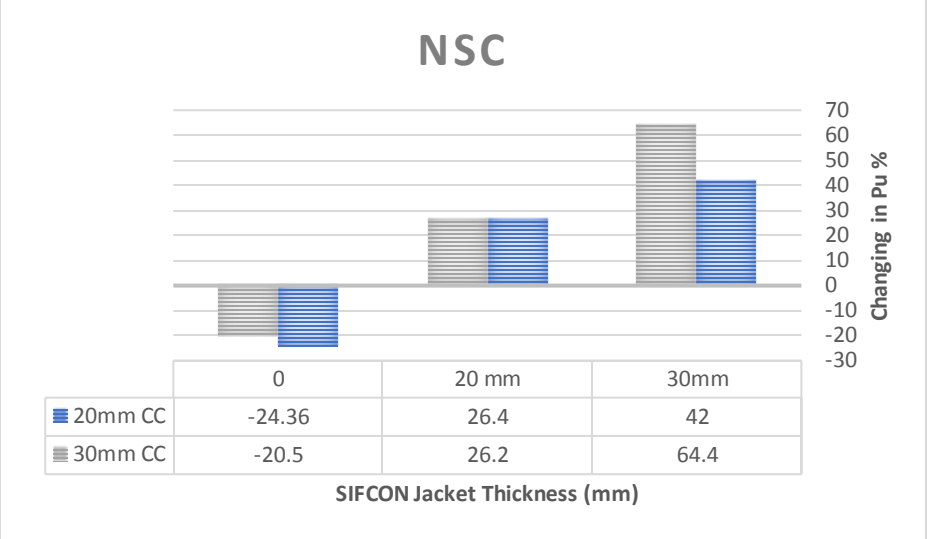

Figure 4-6: The percentage of change in load carrying capacity of the exposed NSC beam specimens at 600°C fire temperature.

4.4.2 Behavior of HSC LWA Beams Before and After Burning (Group Two)

The behavior of HSC beams was approximately similar to that in NSC, where the first crack appear in the bending zone about 10 cm. from the left of load applying point, then gradually a number of cracks appeared in the left of first crack heading vertically, later diagonal cracks formed and propagated along the distance between the supporting and load applying points. Plate (4-3) shows that the inclination angle of diagonal cracks becomes bigger after burning, the cracks extension shorter, and number of cracks was less after burning.

Prior to the formation of the diagonal cracks, several small cracks appeared in the shear zone and at less rate in bending zone as well. HSC behaved with a much higher sensitivity than NSC to burning, where after (600°C) of burning spalling noticed to be occur.

The vapor in the HSC particles found it difficult to exit through the surface, resulting in concrete spalling. Spalling removed rapidly the surface layers of concrete and exposes the core to direct fire flame, thereby increasing the rate of heat transfer to the core and reinforcement.

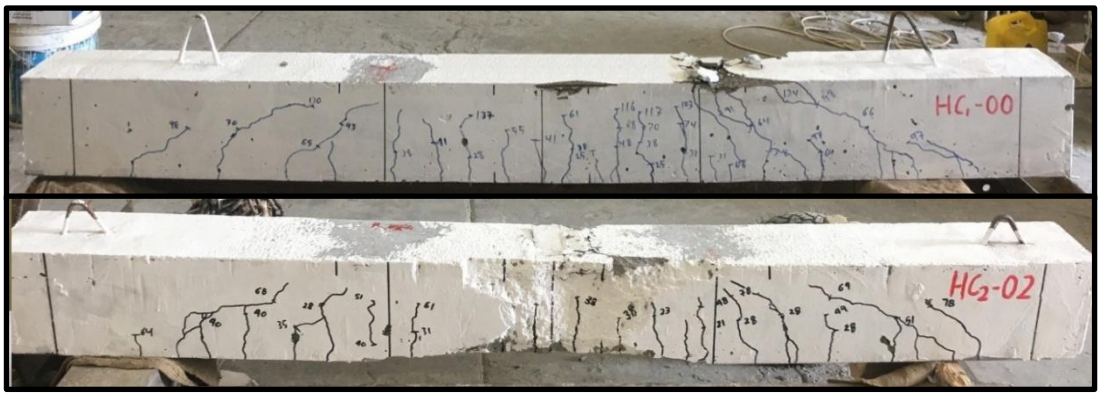

Plate (4-3): Cracks pattern of HSC LWC beams before and after burning.

Furthermore, no spalling was observed during the burning process of the NSC beams, which occurred significantly in the HSC beams. If the concrete cover remains in place during firing (the cover does not come off), the heat flow to the concrete core is slow**.** So that increasing the concrete cover will delay the transferring of heat to the reinforcement and prevent spalling. Figure (4-7) highlights that the contribution of increasing concrete cover (C.C) in improving the fire resistance of HSC beams after burning at 600°C is small.

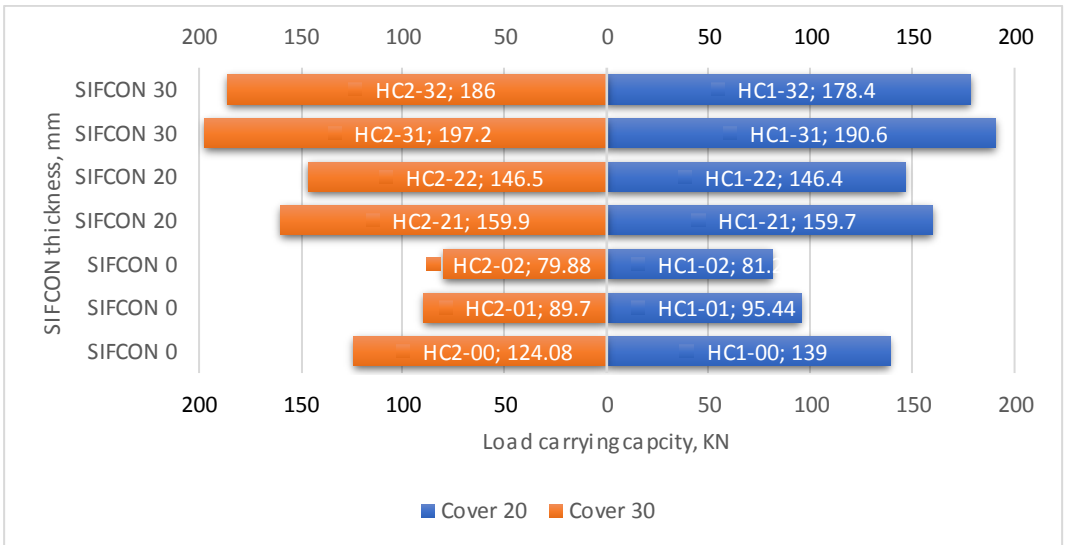

Figure 4-7: Effect of concrete cover on load carrying capacity of HSC beams with different SIFCON jacket thickness.

For the reference models, the results showed a progress for the model with a concrete cover of 20 mm by 12% higher than that of the model with a cover of 30 mm, which is normal because the effective depth in the first is greater, so it is expected to give a higher resistance. After burning, the results showed a great convergence of the resistance values for both models and the disappearance of the effect of changing the thickness of the concrete cover, which can be attributed to the influence of the steel reinforcement by a slight amount that allowed to reduce the difference that was caused by increasing the effective depth of one of them over the other, as shown in Figure (4-8). What reinforces this hypothesis is that the difference in resistance has decreased from about 6% after burning for half an hour to about 1.5% after burning, which indicates that the longer the burning period, the effect of the concrete cover as a protection factor for the rebar, and thus its effect is greater, which changes the amount of its sustainability to the resistance loads.

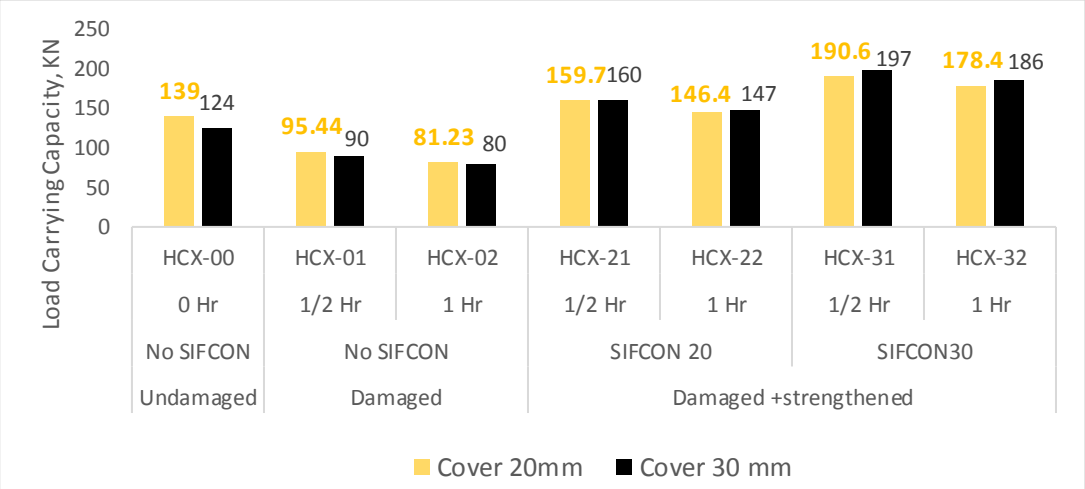

Figure 4-8: Effect of fire exposure duration on load carrying capacity of HSC beams with different SIFCON jacket thickness.

On the contrary, it is observed from the results that the models presented with a concrete cover of 30 mm after strengthening, which indicates the effect of the thickness of the SIFCON as a controlling factor that replaces the effective depth, and eliminates the decline in the sustainability of the resistance of the rebar. The results in Figure (4-9) showed that increasing the concrete cover

from 20mm to 30mm Contribute to reducing the rate of decline in the ultimate load as a result of burning by 16%. More over after strengthening there was an important role for the change in the thickness of the concrete cover when using strengthening with a thickness of 20 mm, where the improvement value for the SIFCON of the models with 30 mm concrete cover was 3.4 times these with 20 mm concrete cover at this level, then the improvement values of 30mm concrete cover increased when using SIFCON with a thickness of 30 mm by 75%. Which indicates that the concrete cover has an important role in maintaining the concrete's resistance to burning, especially in the short periods of exposure, although the increase in the concrete cover was affected by compensating the resistance difference resulting from the effective depth.

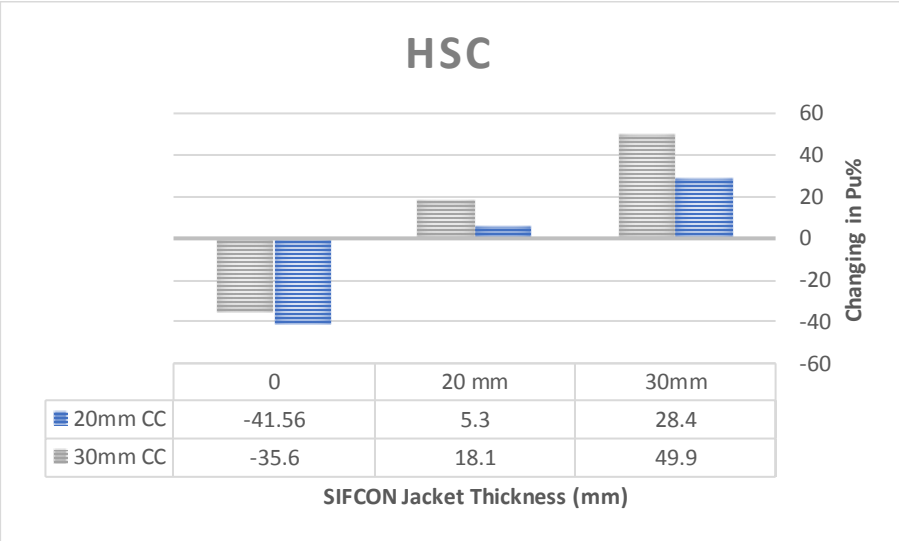

Figure 4-9: The percentage of change in load carrying capacity of the exposed HSC beam specimens at 600°C fire temperature.

4.5 Load-Displacement Relationships of NSC LWC Beam Specimens

All the curves showed elastic behavior before cracking and inelastic behavior after cracking. The results of the tests presented in Table (4-8) and Figure (4-10) showed that the ultimate load-carrying capacity of NSC LWC beams exposed to 60 min. is significantly reduced. The decay rate for the NSC beams of (20 and 30mm.) concrete cover were (24.4 and 20.5%) respectively.

The load displacement behavior after half and one hour burning reflected a noticeable degradation when compared with the reference specimen. Overall, NC1-01 has reflected a linear behavior till the failure load, with very slight hardening, while NC1-02 reflected higher ductility, but approximately was comparable to NC1-01 in term of load capacity. Also, NC1-01 was efficient to sustain maximum load for a considerable displacement, in contrary to the NC1-02. After strengthening of fire damaged specimens with half of an hour fire exposure, damaged specimens strengthened with 20 and 30 mm reflected higher load capacity, higher stiffnesses, approximately linear behavior till failure load, less ductility, and less absorption energies when compared with the un strengthened specimens. NC1-31 has reflected higher load capacity than NC1-21. For strengthened specimens subjected to 1-hour fire exposure (NC1-22 and NC1-32), strengthening with 30 mm SIFCON jacket reflected higher stiffness, higher load capacity, but comparable ductility. Moreover, the behavior was approximately linear till the failure load, and showed a sudden failure without sustaining the peak load for an adequate value of displacement.

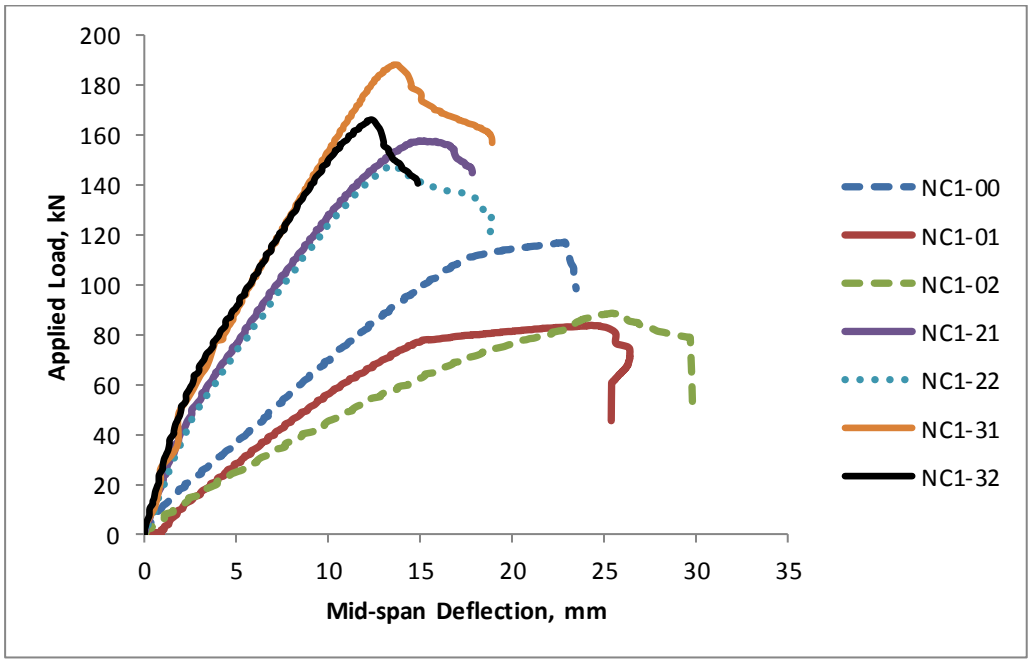

Figure 4-10: Load versus deflection at mid-span of NSC beam specimen with CC of 20mm before and after exposure to fire.

In the case of a 30 mm concrete cover, the reference model reflects a linear behavior at first, similar to the reference model for a 20 mm concrete cover, until a load of 95 kN is reached, and then tends to bend at a lower angle, resulting in a high deformation rate at a lower loading rate (meaning that the rate of Deformity occurs at a higher rate than the rate of load increasing). It is also noted that the models exposed to burning (damaged) models have a clear convergence with the reference model, but with lower loads value, where it shows greater displacement with a smaller increase in the load. As shown in Figure (4-11).

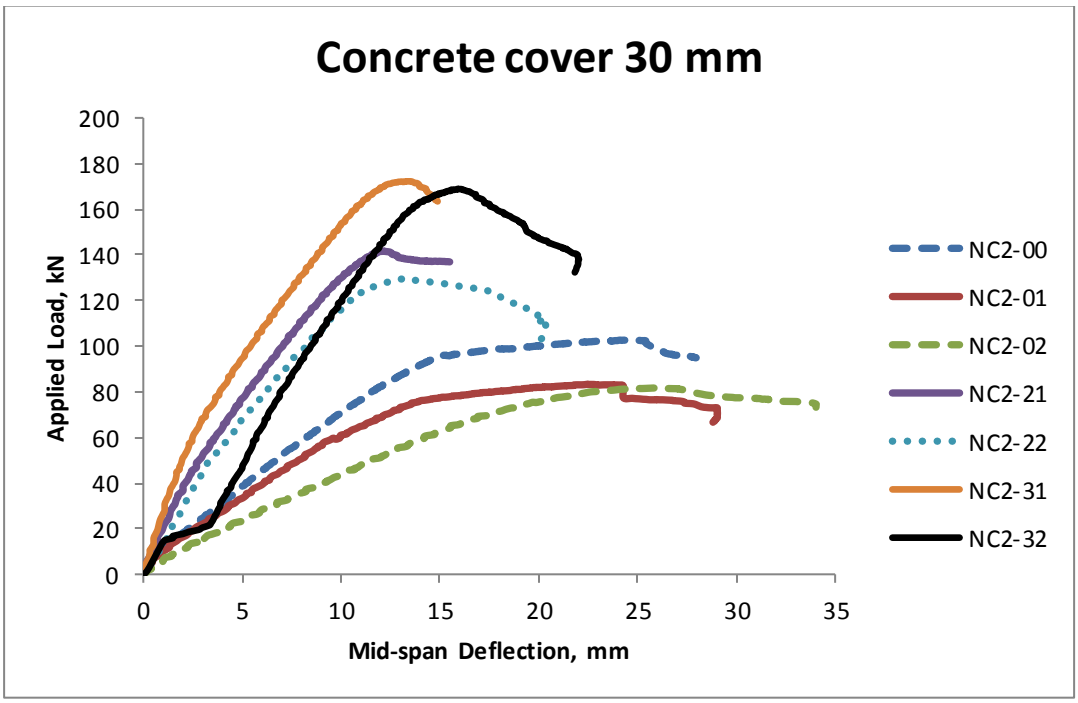

Figure 4-11: Load versus deflection at mid-span of NSC beam specimen with CC of 30mm before and after exposure to fire.

4.6 Load-Displacement Relationships of HSC LWC Beam Specimens

The application of a 20mm and 30mm SIFCON jacket on a high strength lightweight reinforced beam increases the ultimate load capacity by (53 to 83%) and (87 to 133%), respectively; referring to a fire damaged beam. These findings demonstrate the efficiency of the suggested strategy in enhancing bearing capacity in situations of strengthening. Figure (4-12) illustrates load displacement curves behavior of various reference un damaged, damaged after

half and one hour, and strengthened of damaged beams made of HSC mixture. All specimens in the previously mentioned figure have 20 mm concrete cover. Overall, from the same figure, it can be noticed that the strengthening of damaged specimens after ½ and 1 hr. with 20mm and 30 mm SIFCON jacket reflected highest initial and secant stiffness, highest load carrying capacity that the strengthened (damaged and undamaged) specimens. but still these specimens have an issue, where the ductility and absorption energy were lower the reference undamaged beams. Moreover, the linearity behavior of strengthened specimens with SIFCON jacket till the peak load can be considered as a disadvantage, since no yield loading can be observed till reaching failure loading. Additionally, the behavior of the degraded portion of the curves for the strengthened specimens was sharp, unlike the damaged specimens, which means that the specimens could not withstand the maximum load for acceptable limit (ductility issue). It is worth mentioning that, the strengthened specimens reflected no observable yield load, unlike the damaged specimens. generally speaking, the mid span displacement corresponded to the maximum load capacity of strengthened beams were lower than the values of damaged and undamaged beams.

The same explanation can be adopted for the specimens with 30 mm cover, as can be seen in Figure (4-13). The results of the tests presented in Table (4-8) and Figure (4-13) showed that the ultimate load-carrying capacity of HSC LWC beams exposed to 60 min. is significantly reduced. The decay rate for the HSC beams of (20 and 30 mm) concrete cover were (42 and 35.6%) respectively. The load displacement behavior after half and one hour burning reflected a noticeable degradation when compared with the reference specimen. Overall, HC1-02 has reflected higher ductility, while HC2-02, reflected a linear behavior till the failure load, with very slight hardening, but approximately was comparable to HC2-01 in term of load capacity. Also, HC1-01 was efficient to

sustain maximum load for a considerable displacement, in contrary to the HC1-02. After strengthening of fire damaged specimens with half of an hour fire exposure, damaged specimens strengthened with 20 and 30 mm reflected higher load capacity, higher stiffnesses, approximately linear behavior till failure load, less ductility, and less absorption energies when compared with the un strengthened specimens. HC1-31 has reflected higher load capacity than HC1-21.

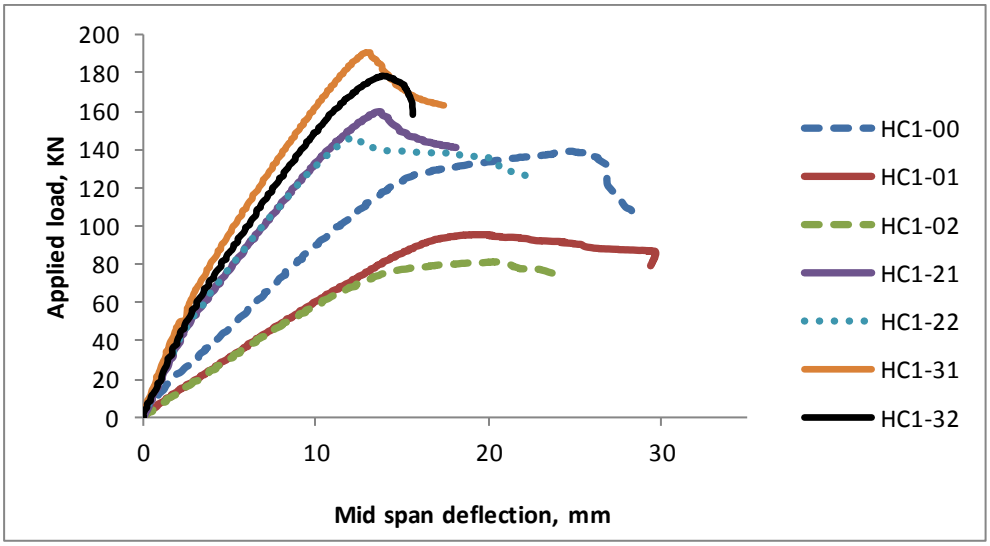

Figure 4-12: Load versus deflection curve at mid-span of HSC beam specimen with CC of 20mm before and after exposure to fire.

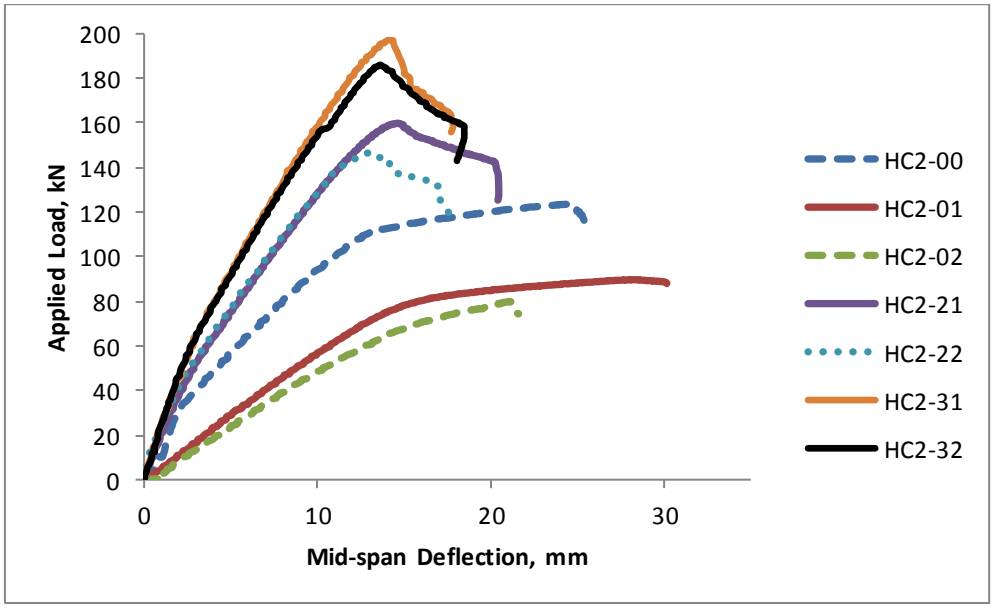

Figure 4-13: Load versus deflection curve at mid-span of HSC beam specimen with CC of 30mm before and after exposure to fire.

For strengthened specimens subjected to 1-hour fire exposure (HC1-22 and HC1-32), strengthening with 30 mm SIFCON jacket reflected higher stiffness, higher load capacity, but comparable ductility. Moreover, the behavior was approximately linear till the failure load, and showed a sudden failure without sustaining the peak load for an adequate value. In addition, the same linear behavior and steep slope when failure occurred was observed in the 30 mm thick concrete cover models, especially the part that is within the elastic range.

4.7 The Role of the Concrete Cover:

In general, from the test results of the reference beams, it can be seen that the concrete beam with higher concrete cover (C.C) has higher amount of displacement. For the both types of concrete cover (30 and 20 mm), it noted from Table (4-8) that the amount of load required for the first crack to occur is reduced after burning by (37 and 41%) of the load of the control specimen beam respectively. At the same time the percentage residual ultimate load decreased to amount between (75 and 79%) of the strength of control specimen with concrete cover (30 and 20 mm) respectively. It is also indicated from Figure (4-14), that the value of load carrying capacity of NSC beams increases with reducing the concrete cover, the reducing of the concrete cover (C.C) from (30 to 20 mm) for NSC LWC beams before and after burning gives an increasing in load carrying capacity of (14 and 8.5%) respectively. The reason for this is believed to be due to that reducing the concrete cover (C.C) for the same cross-section of the beam specimen will result in a larger confined concrete area and reflects the higher confinement efficiency. Figure (4-15) shows that the contribution of increasing concrete cover (C.C) in enhancing the fire resistance of HSC beams after burning at 600°C had important effect. On the contrary it had a slight effect on the reduction in load carrying capacity, as mentioned above according to experimental results listed in Table (4-8).

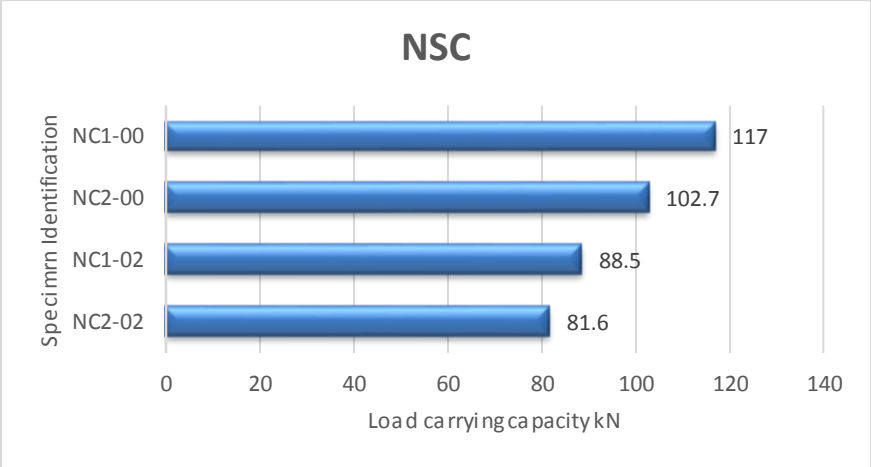

Figure 4-14: Effect of concrete cover on the load carrying capacity of NSC beams with different concrete cover before and after burning.

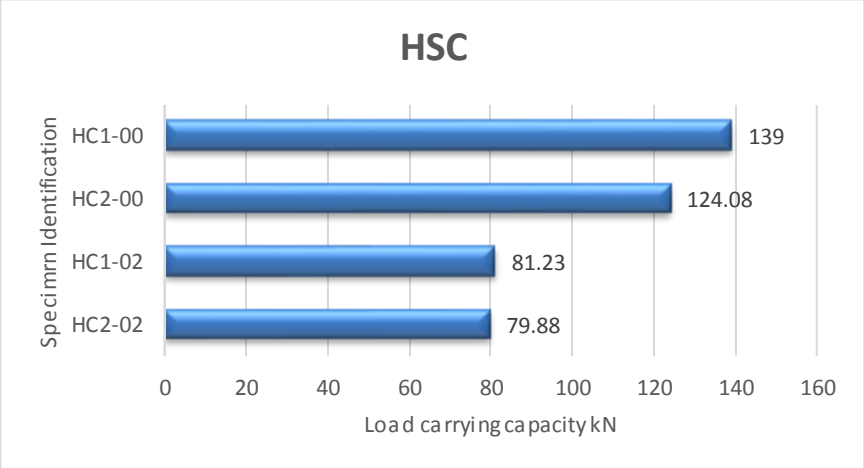

Figure 4-15: Effect of concrete cover on the load carrying capacity of HSC beams with different concrete cover before and after burning.

4.8 Moment-Curvature Relationship of NSC and HSC LWC Beam Specimens

The moment-curvature relationship of the tested specimens has gone through two stages. The curves initially remain straight until the first crack occurs, following which the slope of the curve changes. After the tension reinforcement yields, the curve remains almost flat. Figures (4-16) and (4-17) depicts the moment-curvature connection of the examined specimens. The first stage follows the occurrence of the first crack simultaneously with the initial loading rates, where the curve tends in a linear direction and at a nearly constant rate. Then, in conjunction with the increase in the moment resulting from the increase in the loading rate, the curvature angle (θ) increases, causing stresses

to develop on both sides of the cracks, to accommodate the increased stress, the cracks propagated and begin to extend and expand. Increasing the loading to higher rates leads to the transfer of stresses on both sides of the crack to the reinforcing steel, and thus the deformation moves to the (elastoplastic) stage. For references specimen of NSC the elastic stage ended when the moment reached value of 27.9 and 23.9 kN.m for 20mm and 30mm concrete cover respectively. While the highest value of moment capacity for reference model of 20mm and 30mm were 29.2 and 25.3 kN.m respectively.

In addition, the damaged model shows less capacity to sustain moment, from the figure, it was observed that both the damaged models of the normal concrete behave similarly, where the curve gradually increases slowly, but with much less slope than the reference model and the reinforced model in the initial phase, which reflects the low moment bearing capacity of the model. The maximum value of moment for the damaged model with 20mm and 30mm were 20.4 and 20.3 kN.m respectively, with reduction value of 30 and 19% respectively. In the other hand the strengthening models curve depicts before cracking straight section. Then at cracking; the curve slope beginning to descends downwards, reflecting a decrease in beam stiffness. The moment-curvature curve slope steadily decreases between cracking point and steel yielding, where at yielding stage a further decrease in the slope of the curve is noticed. The post-yielding region in the curve was showed a flat top section with so little strength development. Although there is an irregularity in the NC2-32 model in the first phase, the moment-curvature curves for strengthening concrete models are much steeper than those for non-strengthening concrete models during the pre-peak phase. As it can be observed, incorporating steel fibers boosts the moment bearing capacity of the beams.

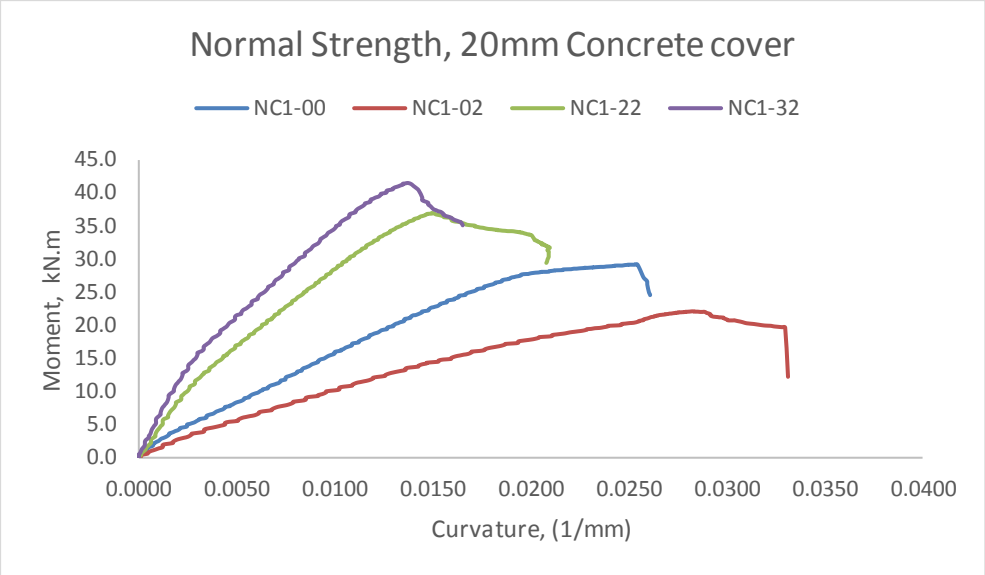

Figure 4-16: Moment-curvature relationship of NSC, with 20mm CC beam Specimens

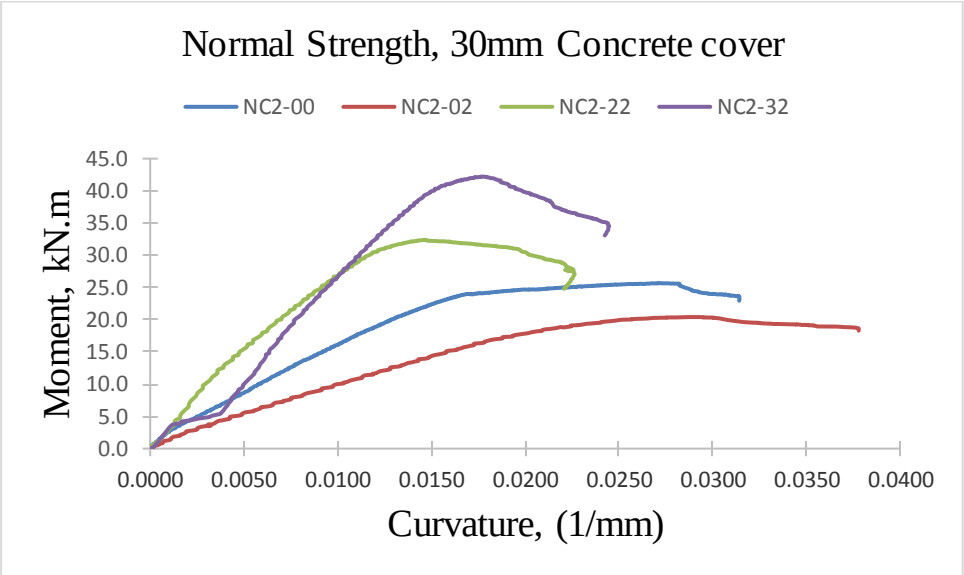

Figure 4-17: Moment-curvature relationship of NSC, with 30mm CC beam Specimens

The model with a higher concrete cover gives a higher moment capacity and this may be due to the fact that spalling occurred during burning in both models and thus the concrete cover lost its role in protecting the reinforcing steel, which led to it being affected in both models by exposure to burning, while the effective depth remained the dominant factor in bearing moments. Therefore, it noted from the Figures (4-18) and (4-19) that the moment values at the end of elastic phase for HSC damaged models with 20mm and 30mm

were 19.6 and 18.1 kN.m respectively. Moreover, the damaged models tend to show greater amount of curvature with lower moment values.

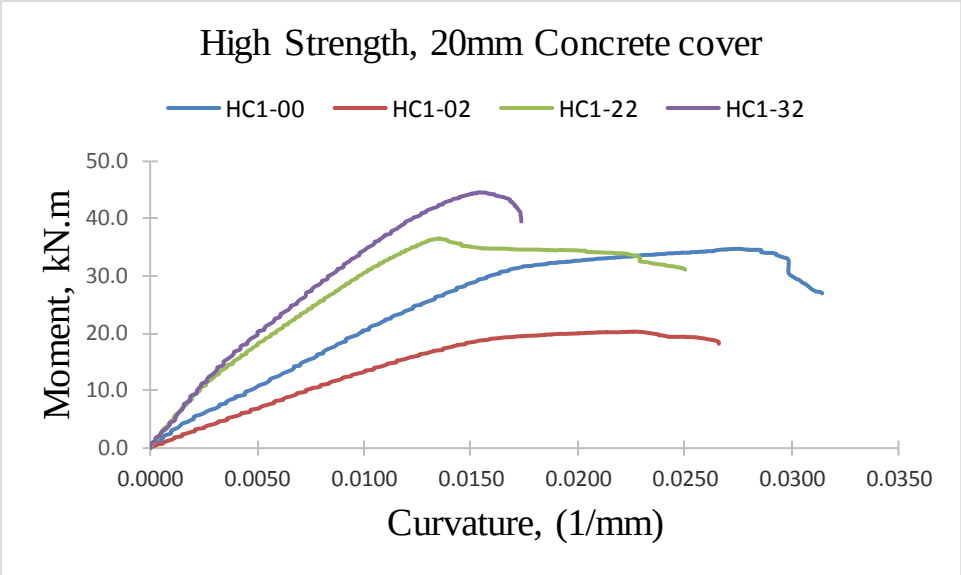

Figure 4-18: Moment-curvature relationship of HSC, with 20mm CC beam Specimens

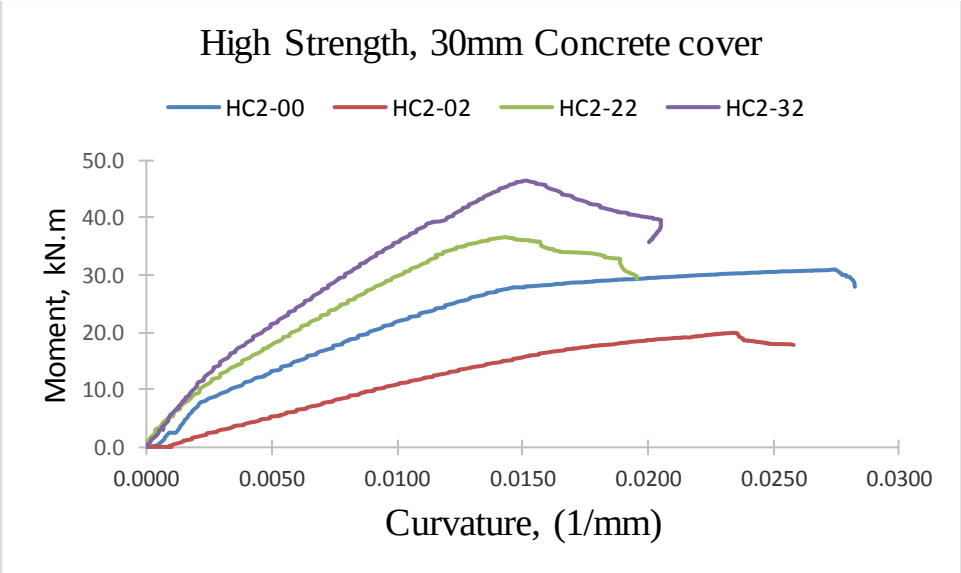

Figure 4-19: Moment-curvature relationship of HSC, with 30mm CC beam Specimens

4.9 Effectiveness of SIFCON Jackets

SIFCON in strengthening beams enhance the shear strength via four ways. They begin by supporting the longitudinal bars and stirrups and increasing their capacity. Second, the important role of the fibers to bridge and transport tensions stresses across both sides of diagonal crack to limits the propagation

of the diagonal cracks. Third, they improve crack resistance by delaying the beginning of first flexural and shear cracking, resulting in improved performance of reinforced concrete beams under service load levels and contributing to improvements in beam ultimate strength. Finally, shear failure is avoided and flexural failure is used in its place. In the present investigation, an attempt has been made to study the effect of SIFCON as a composite material in lightweight Concrete beams. The behavior of RC beams with SIFCON as external jacket along the bottom and both side of the beam was investigated under two-point loading system. The parameters like load carrying capacity, stiffness degradation, ductility and energy absorption capacity are investigated. The test results presented in Figures (4-20) and (4-21) clarify that using of SIFCON jacket increased the ultimate load carrying capacity of the beam specimens with different concrete cover.

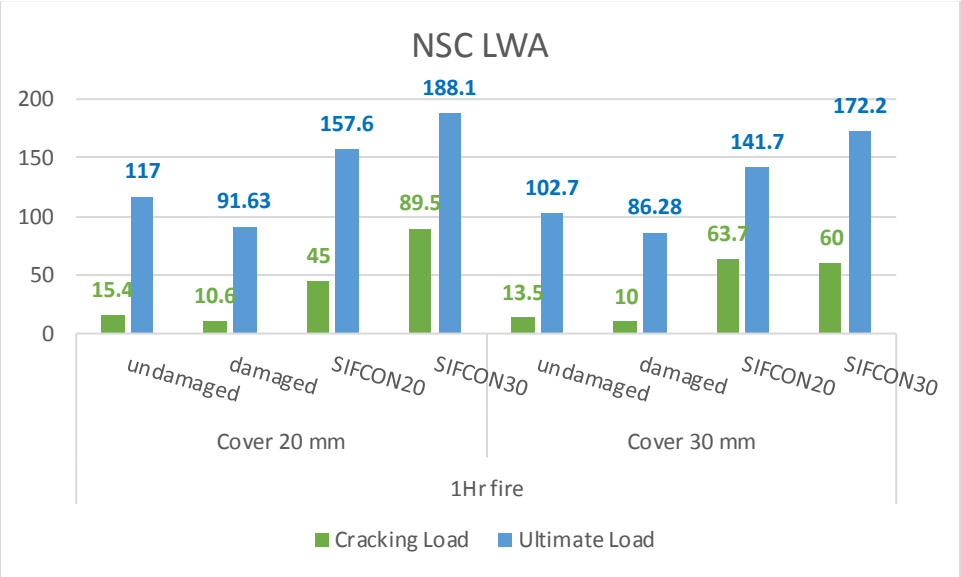

Figure 4-20: Effectiveness of SIFCON jacket on the load carrying capacity of NSC beams with different concrete cover before and after burning.

The effectiveness of using the SIFCON jacket in developing the load carrying capacity of the models can be discussed through two axes, the first is the general effect of the reinforcement: the results of the study showed that the use of the SIFCON jacket gave a significant increase in the load carrying

capacity of the models, ranging between (159% - 207%) and (180% - 220%) for normal and high strength concrete, respectively. The second is the effect of increasing the thickness of the SIFCON jacket: the results show a clear effect of increasing the thickness of the reinforcing layer on increasing the load capacity of the models, where the improvement rates ranged between (112% - 130%) and (102% - 122%) for NSC and HSC, respectively for all cases that have been studied.

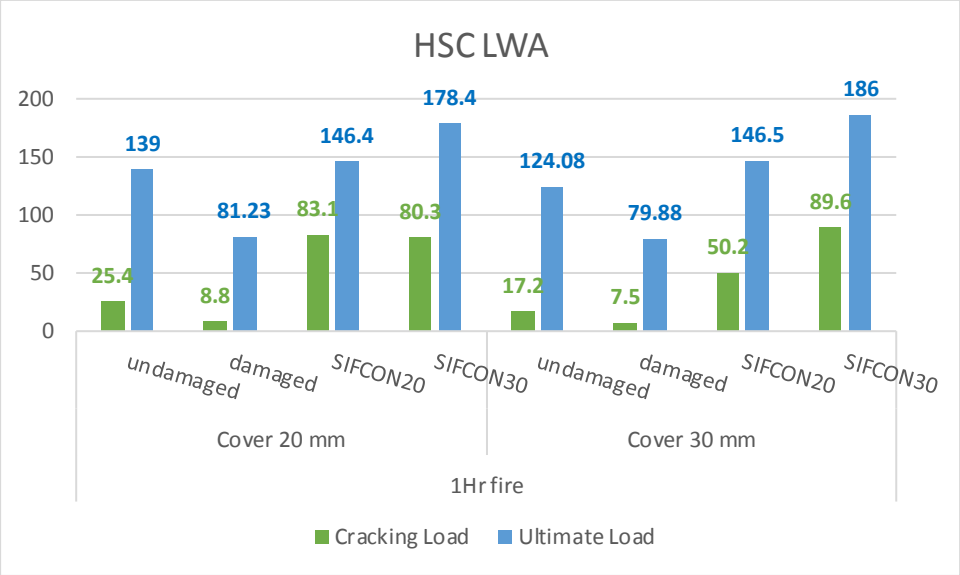

Figure 4-21: Effectiveness of SIFCON jacket on the load carrying capacity of HSC beams with different concrete cover before and after burning.

This is generally explained by steel fibers' efficacy in stopping the propagation and limiting the expansion of flexure and diagonal cracks within the beam when they cross them, and therefore steel fibers-maintained beam integrity throughout the post-cracking stages of behavior. As a result, the beam may sustain higher loads and deflections before failing. SIFCON is more cost-effective and operates in less time than conventional alternative concrete designs when used to repair a lightweight damaged concrete beam, where through the results SIFCON achieved a compressive strength of 48 MPa in just 3 days. In other word, the beam was brought back into service in a much shorter period of time than would be the case with conventional concrete repairs.

reduced the crack widths by at least one order of magnitude as shown in Figure. (4-22), decreased the need for stirrups, better controlling of cracks, and better constructability.

These factors, combined with a relatively simple construction process and the use of specialized and standard construction equipment, make SIFCON the ideal material for increasing shear strength.

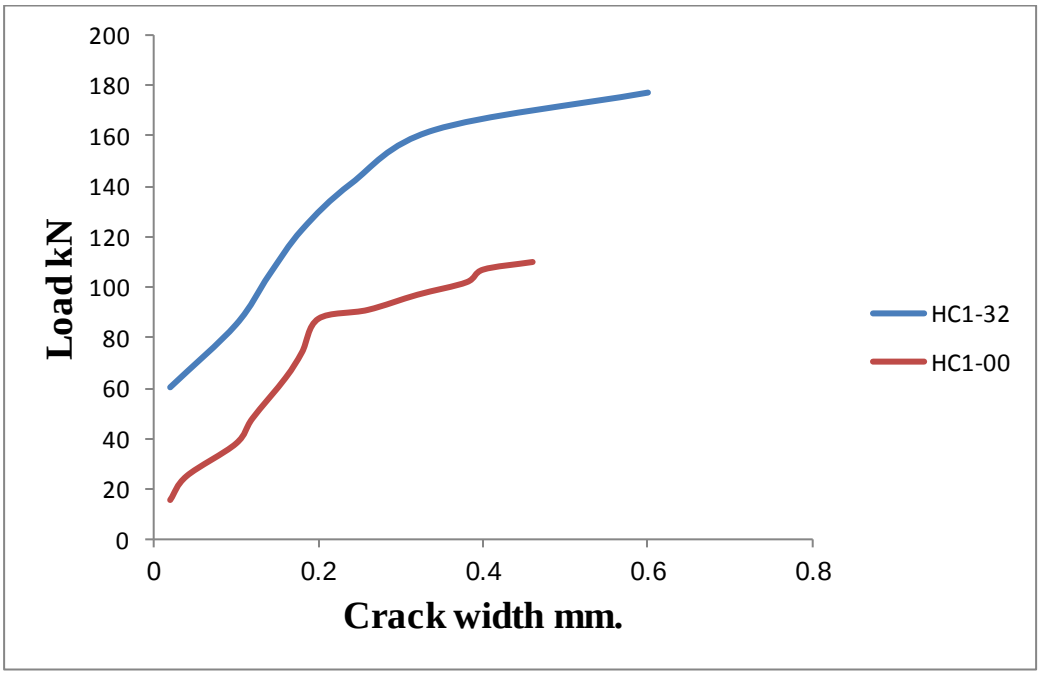

Figure 4-22:relation between applying load and crack width before and after using SIFCON jacket.

4.10 Ductility of NSC and HSC LWC Beam Specimens

The ability of a material or member to sustain deformation beyond the elastic limit while maintaining a decent load carrying capacity until total failure is defined as ductility. In this way, ductility reflects the total area ratio under the load-deflection curve to a portion area extended up to the service loads.

Deflection, which is tabulated in Table (4-9), can readily be used to calculate ductility.

Ductility may be computed using the formula:

$$\mu = \frac{\Delta u}{\Delta y} \qquad (4\text{-}2)$$

where,

μ: Ductility Index.

Δ_u: represents the maximal deformation at failure.

Δ_y: deformation as a result of material yielding.

Δ_y founded from the load- deflection curves through the intersection point of the curve tangent lines, where Δ_y represents the deflection opposite this point, **(Azizinamini et al.,1999)** as shown in Figure (4-23) and (4-24).

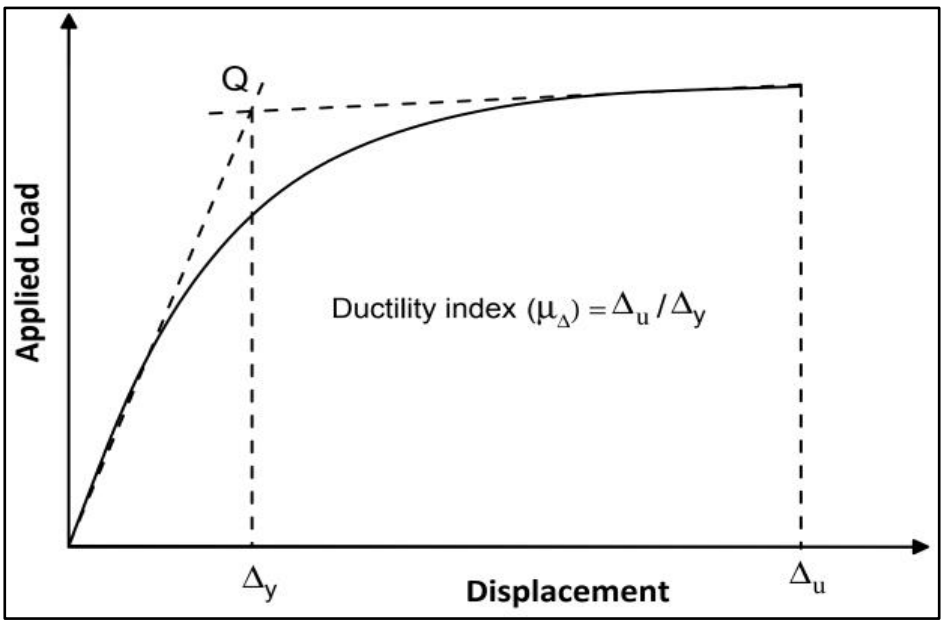

Figure 4-23: Finding the value of Δ_y through the load-deflection curve **(Azizinamini et al.,1999)**.

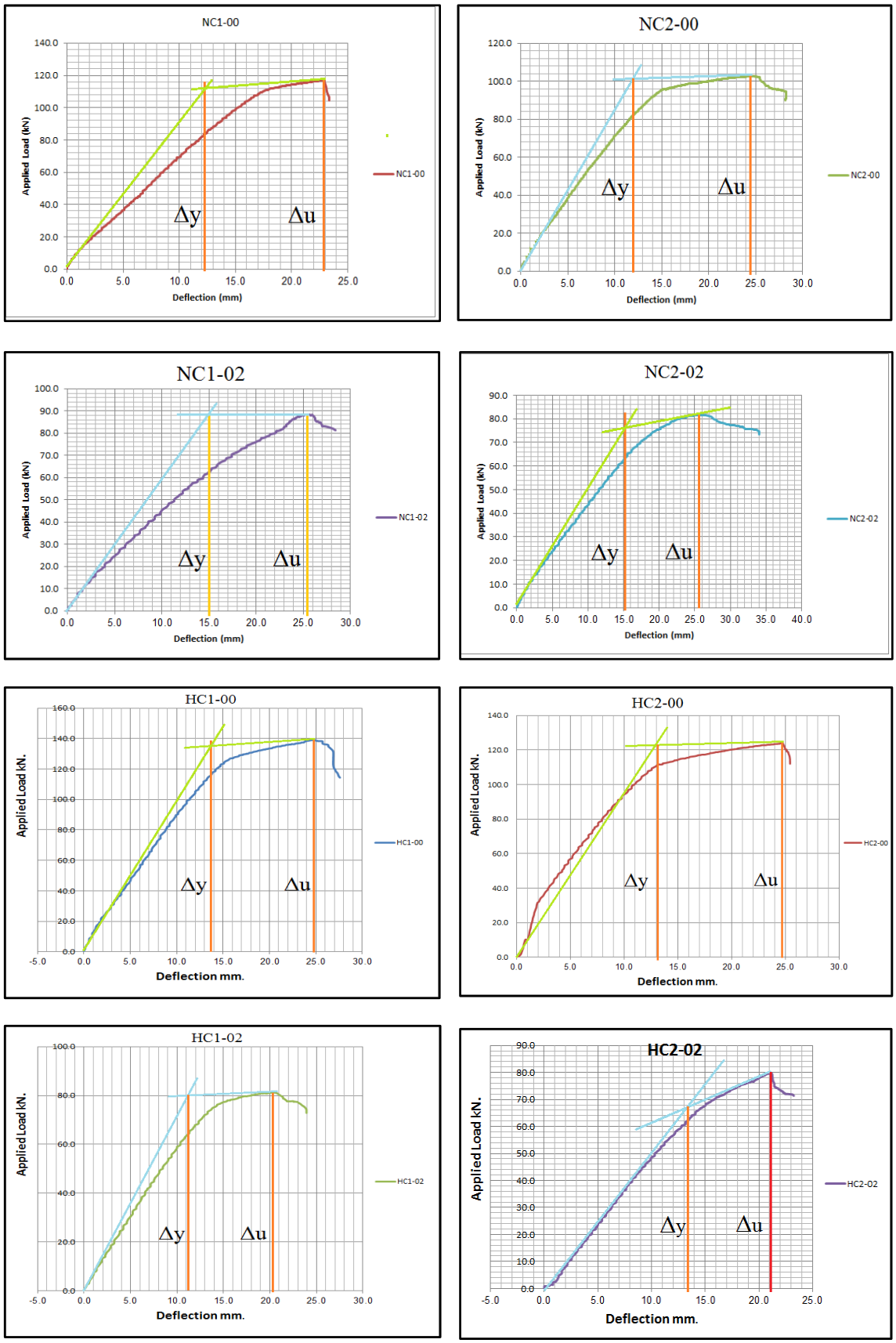

Figure 4-24: Calculating the yield displacement point on load –deflection curves.

Table 4-9: Ductility Index for NSC and HSC LWC beam specimens before and after exposed to fire flame.

Specimen Identification	Yield deflection Δy in mm	Ultimate deflection Δu in mm	Ductility Index $\mu = \frac{\Delta u}{\Delta y}$
NC1-00	11.9	22.85	1.920
NC1-01	13.4	24.31	1.814
NC1-02	14.8	25.41	1.717
NC1-21	7.0	14.94	2.134
NC1-22	7.0	13.46	1.922
NC1-31	6.2	13.55	2.185
NC1-32	6.0	12.32	2.053
NC2-00	12.0	24.41	2.034
NC2-01	12	22.47	1.872
NC2-02	14.5	25.64	1.773
NC2-21	6.3	12.15	1.928
NC2-22	7.0	13.24	1.891
NC2-31	5.8	13.25	2.284
NC2-32	8.7	15.91	1.828
HC1-00	13.8	24.87	1.802
HC1-01	10.4	19.09	1.835
HC1-02	11.1	20.31	1.830
HC1-21	7.1	13.69	1.928
HC1-22	6.4	12.19	1.905
HC1-31	6.5	12.93	1.989
HC1-32	7.6	13.84	1.941
HC2-00	13.1	24.73	1.888
HC2-01	14.8	28.04	1.895
HC2-02	11.4	21.04	1.847
HC2-21	7.7	14.63	1.900
HC2-22	6.2	12.83	2.069
HC2-31	7.3	14.07	1.927
HC2-32	6.4	13.59	2.123

According to the results of Table (4-9), the NSC shows ductility index less high than HSC for the control beam specimens, the increase was (6.2% and 7.2%) for beams with concrete cover (20 and 30mm) respectively. The ductility index for NSC beams was affected after fire exposure and got a small decrease, where for the exposed NSC beams of (0.5 hr.) with concrete cover (20 and 30

mm) the decrease was (5.5% and 7.97%) respectively. While the (1 hr.) exposed for same cover decreased larger for about (10.6% and 12.8%) respectively. This may attribute to that the calculation of ductility index depends only on displacement of the beams, NSC beams after exposed to fire exhibit a less steep and linear behavior in the ascending part of the load-displacement curve and then a quick descending portion prior to failure. Where the deflection value under 60kN was 8mm before burning and become 14mm after. This decrease in ductility can be due to deterioration of both concrete and steel mechanical properties. Furthermore, when temperature increased, the bonding strength between reinforcing bars and concrete decreased, indicating that reinforcing bars were unable to acquire adequate strength, as shown in Figure (4-25).

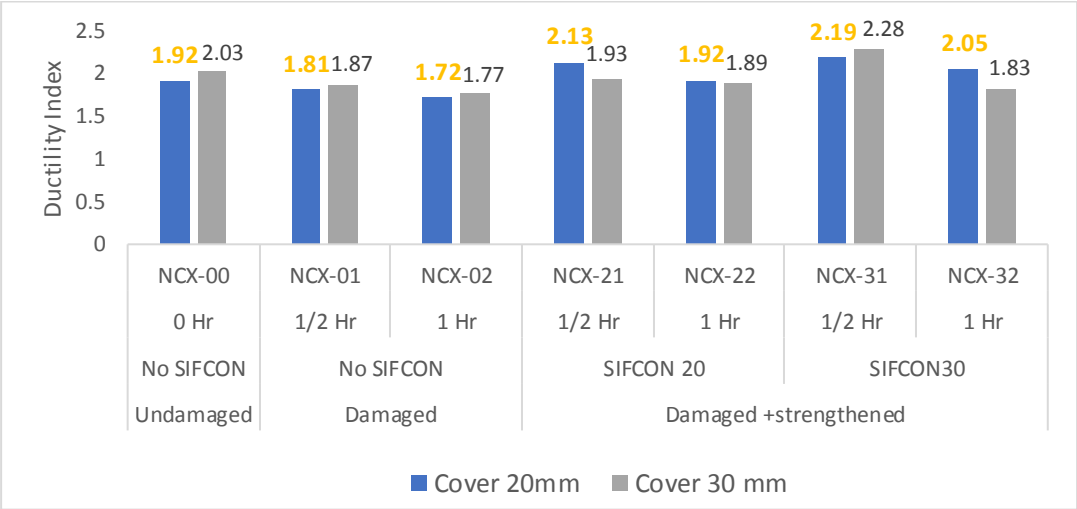

Figure 4-25: Ductility values of NSC with different fire exposure duration and concrete cover before and after burning

The results of HSC beams show that the ductility index not effected by burning. On the contrary, a slight increase was observed. Where for beams that exposed to (0.5 hr.) with concrete cover (20 and 30 mm) shows increase in ductility index of (1.8% and 0.37%) and increase (1.6%) for cover 20mm and decrease of (2.17%) after exposed to (1.0 hr.).

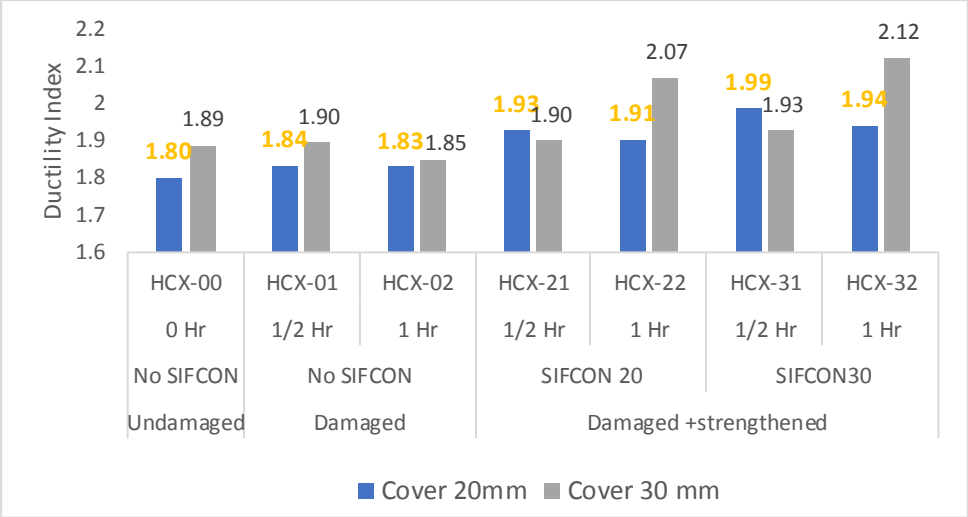

Figure 4-26: Ductility values of HSC with different fire exposure duration and concrete cover before and after burning.

The results of ductility index were between 1.717 and 2.284 for the tested beam specimens before and after burning. In general, a high ductility index indicates that a structural member can withstand considerable deformations before failing. For beams with ductility indexes ranging from 3 to 5, appropriate ductility is deemed essential, particularly in the fields of seismic design and moment redistribution **(Ashour, 2000; Kumar, 2008; Rashid & Mansur ,2005; Iffat et al., 2011)**. Beams having a ductility index of less than 1.99 lacked appropriate ductility and were unable to redistribute moment.

4.11 Stiffness of NSC and HSC LWC Beam Specimens.

The stiffness of a beam is defined as the load necessary to cause a unit deflection of the beam. As shown in Table (4-10), the secant and initial stiffness after burning at various exposure durations decreased dramatically with increasing fire temperature level, and the drop in stiffness is accompanied by a reduction in load carrying capacity. The secant stiffness of HSC beams dropped from 100% at room temperature to approximately (71 and 75%) after burning (1 hr.) at 600°C, with concrete cover (20 and 30 mm) respectively. While the secant stiffness of NSC beams reduced from 100% at room temperature to around (68 and 76%) after burning (1 hr.) at 600°C, for beams with concrete cover (20 and 30 mm) respectively. For the control specimen NSC of 20mm

concrete cover gives secant stiffness higher than NSC of 30mm cover as a normal behavior when taking in consideration the effect of the effective depth was larger in the first type and the same result noted in the case of HSC. After repairing with SIFCON jacket, the specimens with 30mm jacket shows stiffness value higher than cover 20mm in both cases (HSC and NSC). Also, the repairing specimens got stiffness value higher than control specimens in all cases as shown in the Table (4-10).

Table 4-10: Secant and initial stiffness test results of NSC and HSC LWC beam specimens before and after exposed to fire flame.

Group No.	Concrete grade	Specimen Identification	Secant Stiffness				Initial Stiffness			
			Pu	Δu	ks kN/mm	Residual Ks %	Pu	Δy	Kin kN/mm	Residual Kin%
Group One	NSC	NC1-00	117.00	22.85	5.12	----	117.00	11.9	9.83	----
		NC1-01	91.63	24.31	3.76	73.44	91.63	13.4	6.84	69.6
		NC1-02	88.5	25.41	3.48	67.96	88.5	14.8	5.98	60.8
		NC1-21	157.60	14.94	10.54	205.85	157.60	7.0	22.51	229.0
		NC1-22	147.90	13.46	10.98	214.45	147.90	7.0	21.13	214.9
		NC1-31	188.10	13.55	13.88	271.1	188.10	6.2	30.34	308.6
		NC1-32	166.10	12.32	13.48	263.28	166.10	6.0	27.68	281.6
		NC2-00	102.70	24.41	4.20	----	102.70	12.0	8.56	----
		NC2-01	86.28	22.47	3.83	91.19	86.28	12	7.19	84.0
		NC2-02	81.60	25.64	3.18	75.71	81.60	14.5	5.63	65.7
		NC2-21	141.70	12.15	11.66	277.61	141.70	6.3	22.49	262.8
		NC2-22	129.60	13.24	9.78	232.85	129.60	7.0	18.51	216.3
		NC2-31	172.20	13.25	12.99	309.28	172.20	5.8	29.69	346.8
		NC2-32	168.90	15.91	10.61	252.61	168.90	8.7	19.41	226.8
Group Two		HC1-00	139	24.87	5.58	----	139	13.8	10.07	----
		HC1-01	95.44	19.09	4.99	89.42	95.44	10.4	9.18	91.1
		HC1-02	81.23	20.31	3.99	71.50	81.23	11.1	7.32	72.7
		HC1-21	159.70	13.69	11.66	209.0	159.70	7.1	22.49	223.4
		HC1-22	146.40	12.19	12.00	215.1	146.40	6.4	22.88	227.2
		HC1-31	190.60	12.93	14.74	264.2	190.60	6.5	29.32	291.2
		HC1-32	178.40	13.84	12.89	231.0	178.40	7.6	23.47	233.1
		HC2-00	124.08	24.73	5.01	----	124.08	13.1	9.47	----
		HC2-01	89.70	28.04	3.19	63.67	89.70	14.8	6.06	64.0
		HC2-02	79.88	21.04	3.79	75.64	79.88	11.4	7.01	74.0
		HC2-21	159.90	14.63	10.92	217.96	159.90	7.7	20.77	219.3
		HC2-22	146.50	12.83	11.41	227.74	146.50	6.2	23.63	249.5
		HC2-31	197.20	14.07	14.01	279.64	197.20	7.3	27.01	285.3
		HC2-32	186.00	13.59	13.68	273.1	186.00	6.4	29.06	306.9

As mentioned in ductility the reduction in the load carrying capacity of the beam specimens after exposed to fire resulting by the deterioration of concrete and steel reinforcement in both chemical and mechanical properties, and led to reduce the difference between yielding point and failure point values and deteriorate the capacity of specimen to absorb applied loads with less deformation, and Figures (4-27) to (4-30) show the Stiffness of NSC and HSC LWC Beam Specimen.

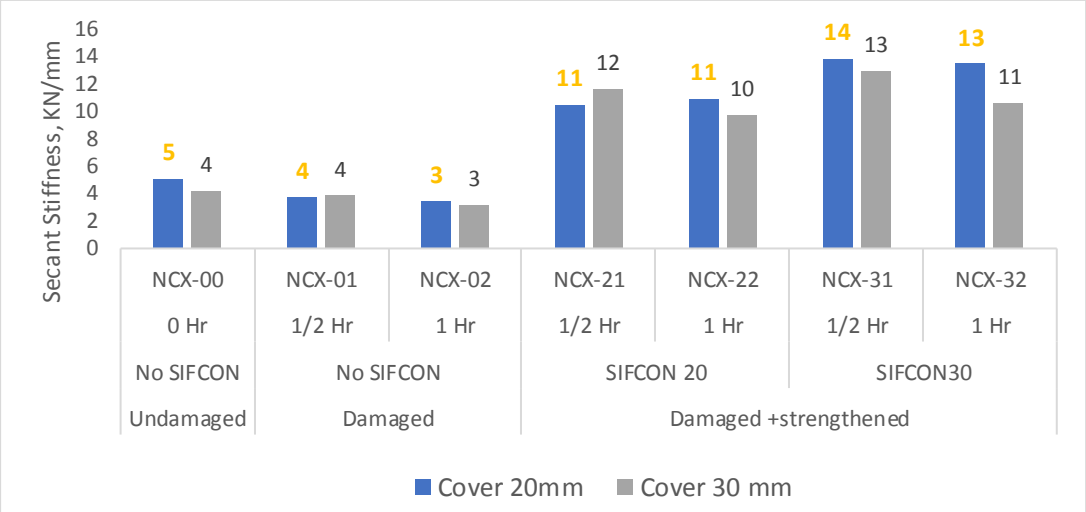

Figure 4-27: Secant Stiffness of NSC LWC Beam Specimen

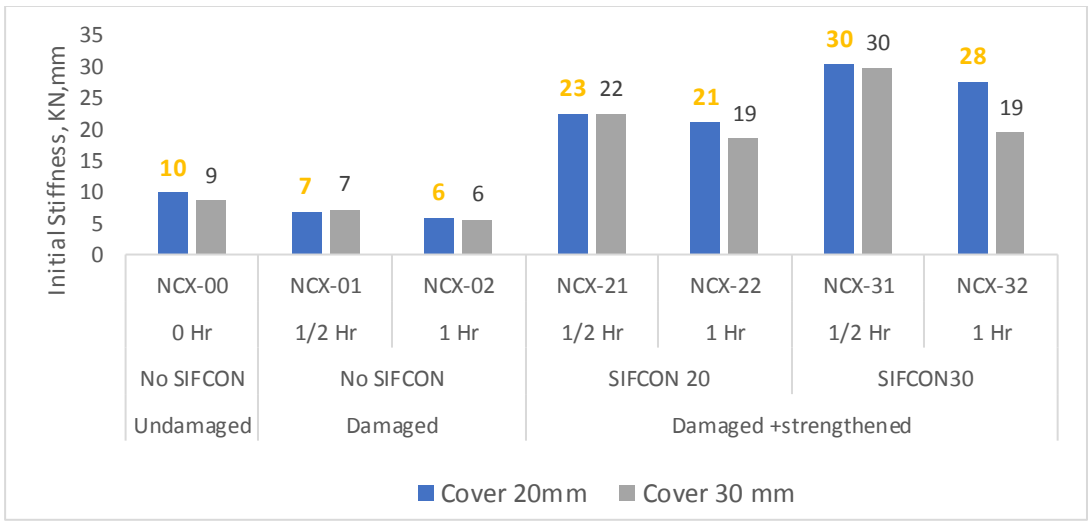

Figure 4-28: Initial Stiffness of NSC LWC Beam Specimen

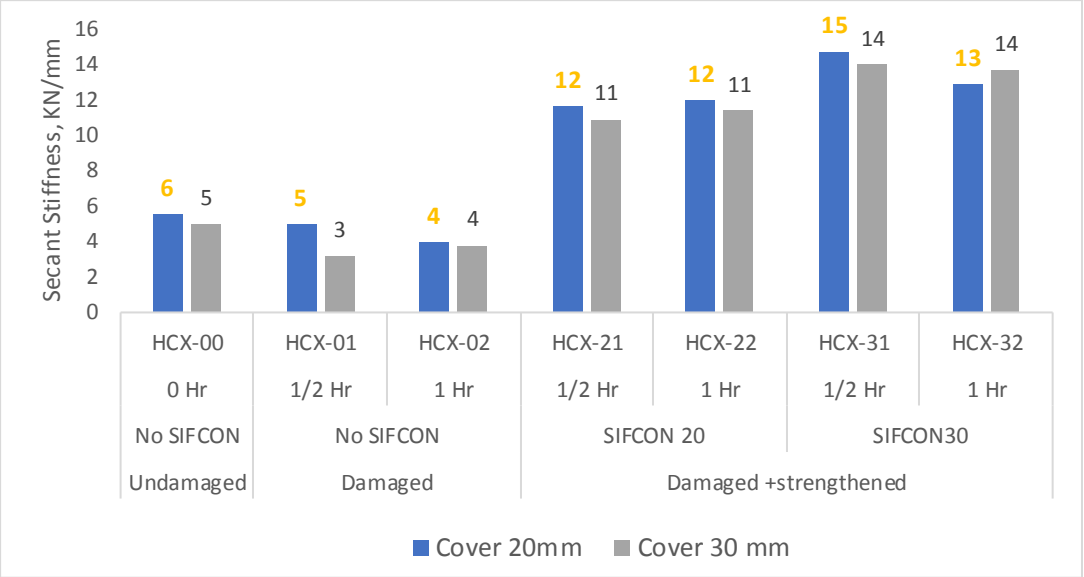

Figure 4-29: Secant Stiffness of HSC LWC Beam Specimen

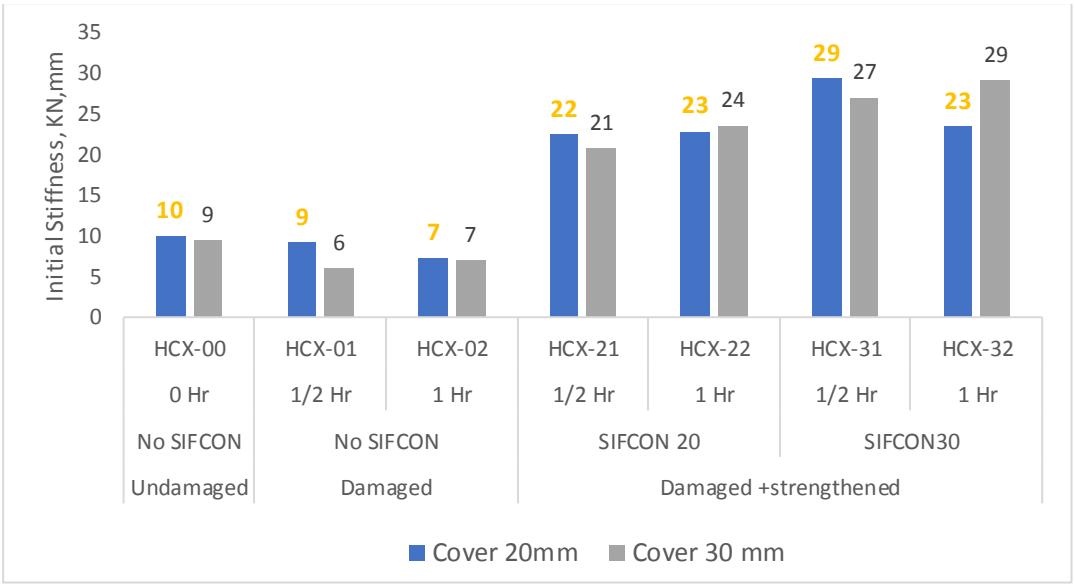

Figure 4-30:Initial Stiffness of HSC LWC Beam Specimen

4.12 Energy Absorption of NSC and HSC LWC Beam Specimens

The concrete beam's energy absorption capacity defined as the area contained by the load-displacement curve until the maximum load is attained, which shows the energy absorption of the concrete beam that might be sustained before exhibiting a significant decline in load carrying capacity. Since displacement ductility index depends only on the displacement values and does not differentiate the ductility between the beams with a low residual load resistance and those with a high load resistance, therefore the ductility index

method is not adequate in determining the ductility of the exposed beams. Accordingly, a better approach has been proposed to measure the ductility of those beams may be by using the energy absorption capacity which is based on estimating the area enclosed by the load-displacement curve for each beam, to take into account the reduction of load carrying capacity for these beams after fire exposure.

The energy absorption capacity is the most appropriate indicator of concrete structures not only for its structural response against earthquake motion, but also for concrete structures that must withstand fires and impact loads produced by events or terrorist attack. Table (4-11) shows the results of the energy absorption of HSC and NSC beams before and after fire exposure. According to these results, HSC shows higher energy absorption capacity compared to NSC for the control and exposed beam specimens, the energy absorption capacity of HSC beams with concrete covers of (20 and 30 mm) being higher than that of similar NSC beams at ambient temperature by (133.6 and 132.7) percent, respectively. Also, the values of energy absorption capacity decrease as the concrete cover increases for the two types of concrete (HSC and NSC).

It is also demonstrated that HSC severely affected after burning for (1 hr.) at 600 ºC, the residual energy absorption capacity of beams with concrete cover (20 and 30mm) were about (46% and 43.5%) respectively and even after strengthening with jacket the residual capacity were at range of (54 to 64%) and (61 to 67%) respectively, as shown in Figure (4-31).

At burning temperature of 600°C, for NSC beams with concrete cover of (20 and 30mm), the residual energy absorption capacity was (75.65 and 77.6%) respectively. While after strengthening, the residual energy absorption capacity was in the range of (68 to 72%) and (74 to 81%) respectively, as shown in Figure (4-32).

Table 4-11: The results of energy absorption capacity tests on HSC and NSC lightweight concrete beams before and after fire exposure.

Group No.	Temperature (ºC)	Specimen Identification	Energy Absorption Capacity (kN.mm)	Residual Energy Absorption Capacity%
Group One	**600**	**NC1-00**	**1739.0**	-----
		NC1-01	1378.3	79.26
		NC1-02	1315.7	75.65
		NC1-21	1476.6	84.91
		NC1-22	1188.1	68.32
		NC1-31	1509.8	86.82
		NC1-32	1259.9	72.45
		NC2-00	**1697.0**	-----
		NC2-01	1288.1	75.90
		NC2-02	1317.4	77.63
		NC2-21	1290.2	76.03
		NC2-22	1255.4	73.98
		NC2-31	1437.4	84.70
		NC2-32	1380.6	81.36
Group Two	**600**	**HC1-00**	**2323.0**	-----
		HC1-01	1921.91	82.73
		HC1-02	1073.7	46.22
		HC1-21	1308.0	56.31
		HC1-22	1265.6	54.48
		HC1-31	1473.4	63.43
		HC1-32	1486.5	63.99
		HC2-00	**2251.1**	-----
		HC2-01	1751.06	77.79
		HC2-02	980.50	43.55
		HC2-21	1417.60	62.97
		HC2-22	1369.70	60.84
		HC2-31	1628.60	72.34
		HC2-32	1509.70	67.06

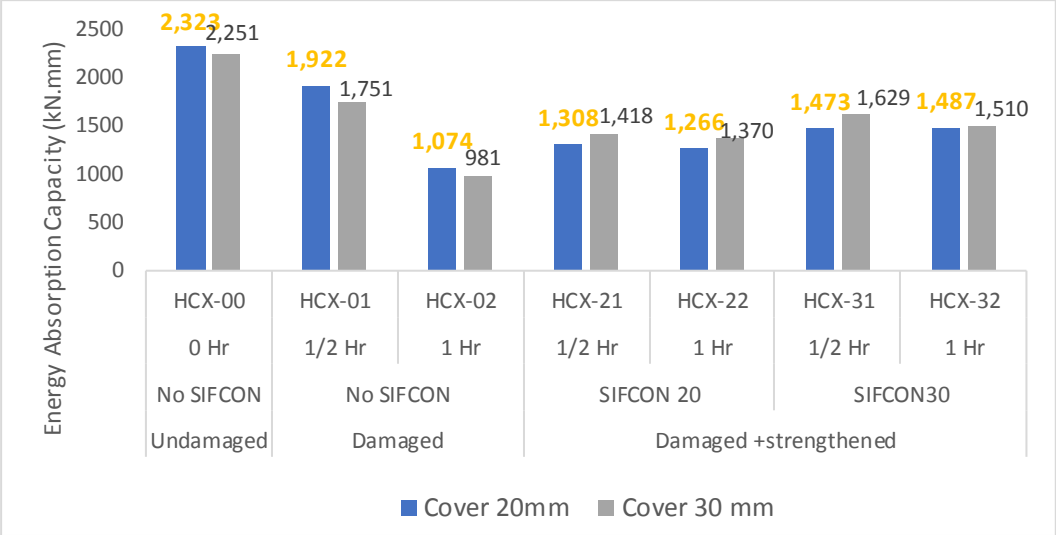

Figure 4-31: Values of energy absorption capacity for HSC before and after burning and strengthening with different concrete cover

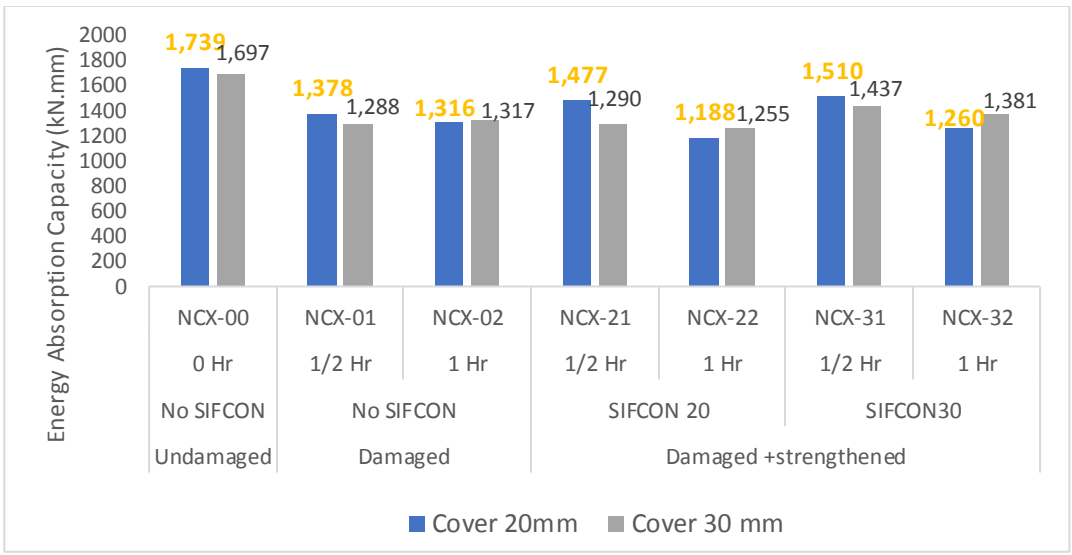

Figure 4-32: Values of energy absorption capacity for NSC before and after burning and strengthening with different concrete cover

4.13 Effect of Fire Exposure on Steel Reinforcement

The effect of high temperature on steel reinforcing bars is predicted to be minor if protected by the minimum cover prescribed by the code. Deformation owing to heat expansion and loss of bond between concrete and steel, on the other hand, may produce structural instability and compromise structural integrity. Steel reinforcement bars are typically thought to require to be protected against temperatures above 250-300°C, because steels with low carbon contents are known to exhibit blue brittleness between (200 and 300°C)

(Ünlüolu et al., 2007). Three groups of 12mm steel reinforcement bars were utilized to investigate the fire effect on steel reinforcement bars. Steel reinforcement samples were implanted in HSC and NSC beam specimens with a concrete cover of 30 mm in the first group (C.C). The samples in the second group were implanted in HSC and NSC beams with a 20mm concrete cover, while the samples in the third group were subjected to fire directly without any concrete cover. The steel reinforcement was retrieved from concrete and a yield stress test was performed after the three sets of samples were burned at 600°C for one hour. Tables (4–12) compare the yield stress test findings for reinforcement bars after 600°C exposure to those of the control sample.

Table 4-12:The effect of fire exposure on the yield stress of steel reinforcement.

Group No.		Temperature (°C)	Concrete Cover (mm)	Yield Stress f_y (MPa)	Reduction Ratio %
Control	Non exposed	25	-----	530.0	---
Group One	NSC	600	30	511.2	3.6
	HSC			494.3	6.8
Group Two	NSC	600	20	508.6	4.1
	HSC			491.0	7.4
Group Three	Unprotected	600	0	356.0	33

Table (4-12) show that increasing the concrete cover to the reinforcing steel bars has a favorable influence on the yield stress that the yield stress reduction for beams with a concrete cover of 30mm being (3.6 and 6.8%) for NSC and HSC, respectively. While for beams with a 20 mm concrete cover, the reductions were (4.1 and 7.4%) for NSC and HSC, respectively. The reduction was 33 percent for samples that were directly exposed to fire. It was also discovered that NSC provides better reinforcement bar protection when compared to HSC with the same cover, with the reduction in yield stress for NSC beams being (3.2 and 3.3%) lower than HSC beams with concrete cover (C.C) of (30 and 15 mm) respectively. The thickness of the concrete cover had almost a little effect on the decrease in strength properties when subjected to a

one-hour fire, indicating that cover thickness has no considerable effect on the strength of the embedded steel reinforcement. This is attributed to the reason that the thermal conductivity of lightweight concrete is relatively low up to 400ºC and increases insignificantly as the temperature rises to around 1000ºC. This supports the findings of **(Hu et al.,1993)**.

4.14 Appearance and Color Change of the Beam Specimens

The beams specimens after they have been exposed to fire. The color of the surfaces exposed to fire was light gray with some light reddish areas. On the exposed surfaces, tiny reticular cracks occurred., as shown in Plate (4-4). Random tiny cracks line of varying widths (0.04–0.18) mm were seen on surfaces after exposure to high temperatures up to 600 C for 1 hr. The most significant cracks were found near the primary and transverse reinforcing points on the concrete surface. These cracks could be caused by the RC element expanding, causing large tensile strains in the concrete, particularly at the reinforcing contact, and the cement matrix and aggregate responding differently to high temperatures.

Furthermore, concrete spalling occurred on the beam's corner without exposing any steel, with a maximum spalling depth of nearly 15 mm. However, no apparent beam curvature was detected.

(a) Specimen surface enlarged image**. (b)**Partial enlarge hairline cracks.
Plate (4-4): Speckle pattern of tested beam.

4.15 Discussions of Failure Process of NSC and HSC LWC Beam

The specimen beams without strengthening appeared an initial flexural crack at the midspan of the specimen and posterior flexural cracks away from that section. As the applied load was increased, some of the flexural cracks developed into a diagonal crack near of the hinge support, or a diagonal crack formed suddenly at the mid height of the specimen beam within the region of shear span.

The failure occurred as a result of splitting along the tension reinforcement after the formation of the diagonal crack ،as illustrated in Plate (4-5). Characteristic of higher a/d ratios more than 2.5 in which case the failure is caused by diagonal crack initiating near the tip of the flexural crack closest to the support. The failure mode was shear tension failure in the case of (HC1-02) specimen beam, where the crack resulting in loss of bonding, while it seems to be shear compression failure in the case of (HC2-00) specimen beam as a result of crushing of concrete at the loading point.

Plate (4-5): Failure of beam without strengthening of SIFCON jacket.

The specimen with SIFCON jacket shear reinforcement had a similar crack pattern as those specimens without diagonal cracking, but showed a higher load-carrying capacity after forming of diagonal cracking as illustrated in Plate (4-6). The ultimate failure mode was flexural failure in bending region near mid span point, formed as wide crack initiated on the bottom surface and head up to end close to the upper surface.

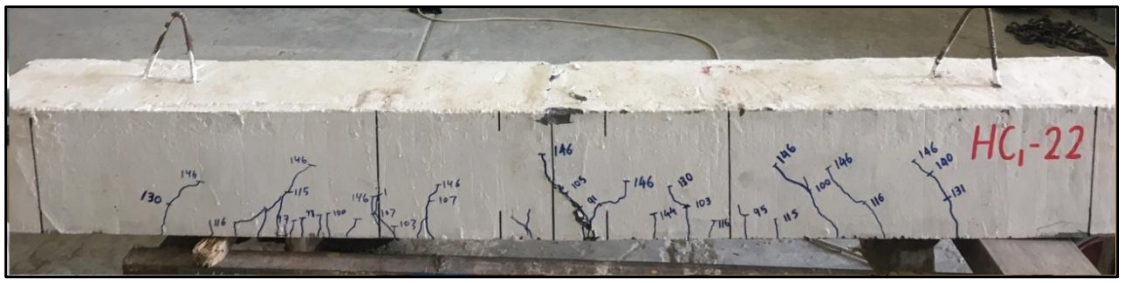

Plate (4-6): Failure of beam strengthening with SIFCON jacket.

4.16 Crack Width

The unpredictability of crack initiation and propagation in reinforced concrete structures can have a significant impact on structural stability and strength, and has consequently been the focus of numerous studies in recent years. Cracks usually begin as too narrow and elongated apertures with a width of less than 0.5 mm, and they are typically not visible to the human eye. Although design regulations impose fracture width limits based on empirical equations, cyclic/seismic stresses frequently cause uncertainty in crack width propagation. The infiltration of moisture, mist, saltwater, and chemical vapors into structural members can accelerate the corrosion of steel reinforcement, reducing the structure's service life. By assuming the distribution of bond stress while a member is subjected to tension with constant bending moment, the crack width initiation and propagation in reinforced concrete members could be approximated using classical theories.

The finite difference methodology was established by Base and Murray to estimate the crack response of concrete structures using numerical analysis on restrained elements. Gilbert also used basic equilibrium and compatibility principles to develop a set of formulas from computing the stresses in concrete and steel members, the number of cracks, and the average crack width. There are two factors may mainly affect the crack width such as the steel stress and concrete cover, and since steel reinforcement remained constant in all tested specimens in this study, the effect of the other factor was studied. Although the value of concrete cover is often regarded as the second most important

component influencing crack width, its effectiveness is evaluated differently in different building codes.

In this study increasing the concrete cover resulted in a (40 and 27%) before burning and a (30 and 28%) after burning for NSC and HSC LWC respectively rise in crack width, according to the results shown in Figure (4-33). It's also noticed that the crack width increased clearly after burning for the same value of applied load in both types of concrete (NSC and HSC), and significantly reduced after strengthening, which attributed to the effect of SIFCON jacket in controlling the crack width.

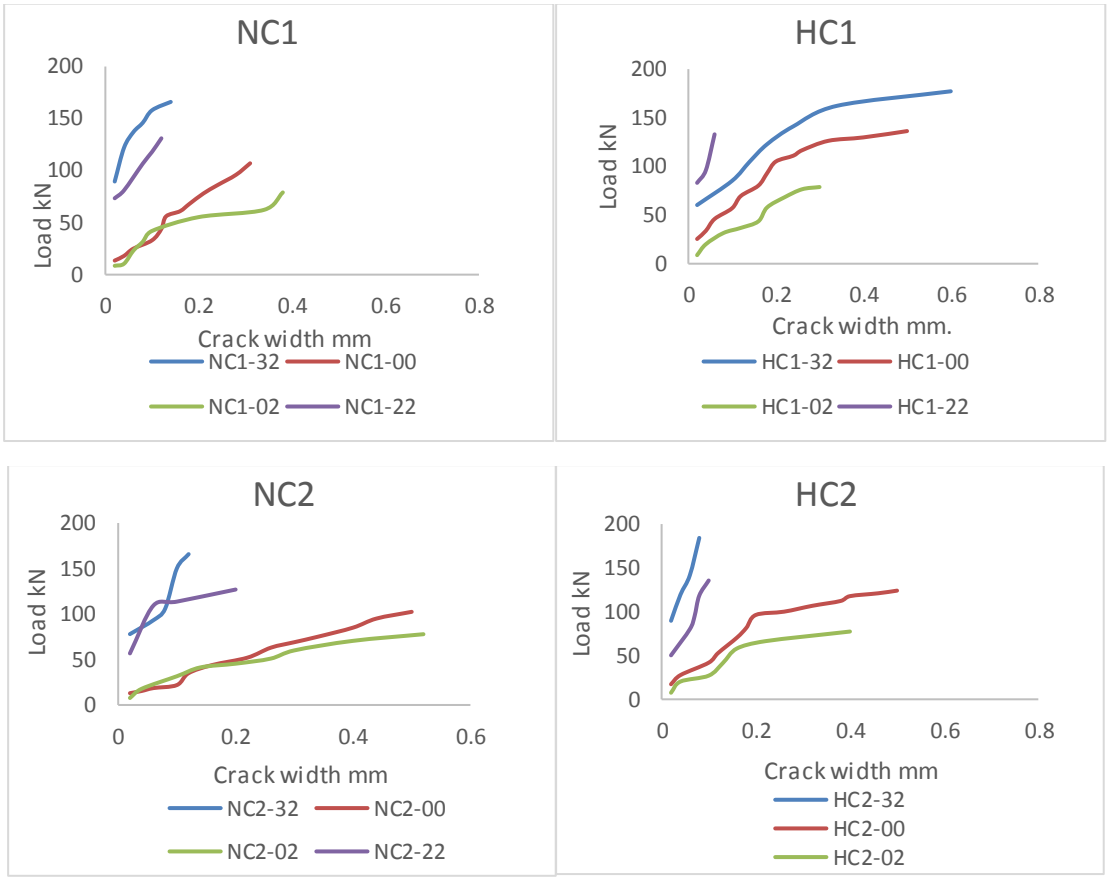

Figure 4-33: relation between applied load and crack width for NSC and HSC LWC before and after burning.

4.17 Surface Condition and Fire Endurance of Beam Specimens

Random severe hairline cracks of varying widths (0.04–0.18 mm) were seen on concrete surfaces after exposure to high temperatures up to 600 C for 1.0 h, as illustrated in Plate (4-4) (b). The most significant cracks were found

near the primary and transverse reinforcing points on the concrete surface. These cracks could be caused by (a) the RC element expanding, causing large tensile strains in the concrete, particularly at the reinforcing contact; and (b) the cement matrix and aggregate responding differently to high temperatures.

Furthermore, concrete spalling occurred on the beam's corner without exposing any steel, with a maximum spalling depth of nearly 15 mm. However, no apparent beam curvature was detected. Figure (4-34) depicts the relationship between beam temperature and fire exposure time.

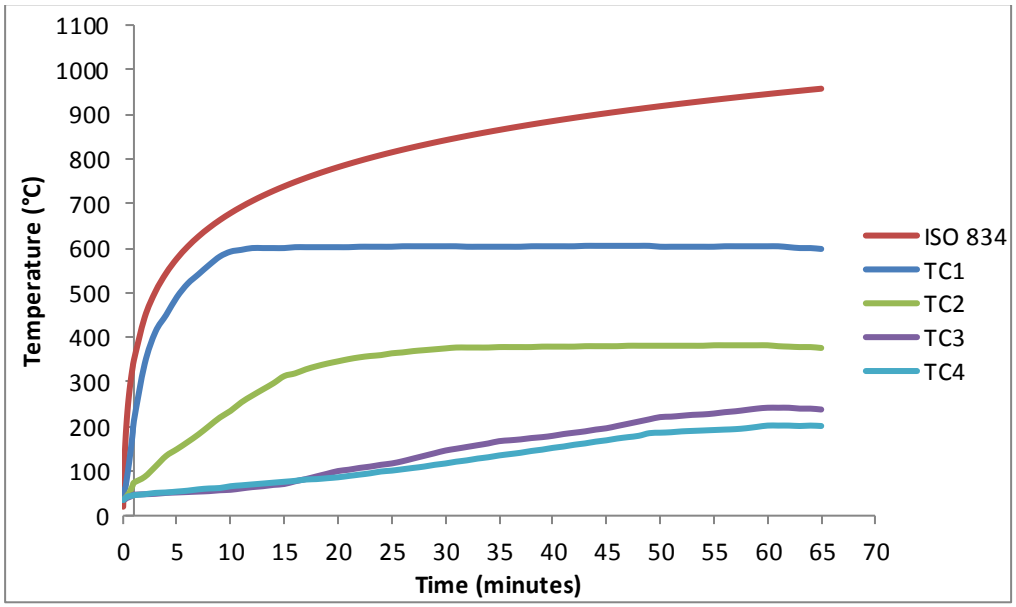

Figure 4-34: The relationship between measured temperatures and fire exposure time of beam.

The furnace temperature closely matched the ISO 834 heating curve with less than 10% variance till reach the target temperature(600°C). After this point, it is noticed that the values of curves diverge. Because the highest temperature of the beam bottom was 605°C, the compressive strength of the beam bottom concrete expected to reduce by amount more than deeper parts of beam specimen. Due to the fact that the recorded temperature of beam bottom TC1 was substantially greater than that of TC4, which is located 100 mm from the bottom, owing to concrete's limited thermal conduction Because of the evaporation of water in the concrete and the subsequent loss of heat, the

temperatures TC3 and TC4 at the middle depth of the beam were maintained at around 100 °C for 25 minutes. The temperatures dropped as you moved up the depth of the beam from bottom to top, suggesting a clear gradient. The highest temperatures of TC1 and TC2, which were higher than TC3, were 605 °C and 382 °C, respectively, and the strength of the concrete near TC3 and TC4 reduced little compared to normal temperature concrete. Table (4-13) shows the position and nomenclature of the thermocouples. In a nutshell, the temperatures of the fire-exposed areas exceeded 600°C, and the temperature dropped rapidly from the surface to the interior of the concrete. The temperature of the core concrete was between 200 and 240 degrees Celsius. As a result, the surface layer of concrete was significantly damaged and needed to be removed, while the interior concrete could be utilized.

A temperature of up to 400°C has a minor effect on the compressive strength of NSC concrete. NSC is typically porous, allowing water vapor to easily diffuse pore pressure. The use of various binders in HSC, on the other hand, creates a better and compact microstructure with less calcium hydroxide, resulting in a favorable compressive strength at room temperature. Binders like as slag and silica fume produce the best compressive strength at room temperature, owing to a dense microstructure.

Table 4-13: The position and naming of the thermocouples.

Thermocouple	**Type**	**Distance from exposed surface (mm)**	**Highest recorded temperature °C**
TC1	K	0	604
TC2	K	25	382
TC3	K	50	241
TC4	K	100	202

However, as previously stated, the compact microstructure is highly impermeable and becomes detrimental at high temperatures because it prevents

moisture from escaping, resulting in pore pressure build-up and rapid development of micro cracks in HSC, resulting in a faster deterioration of strength and occurrence of spalling. The presence of lightweight aggregates containing pores contributed to the absorption of pore pressure and to slow down the loss of strength at high temperatures.

4.18 Predicting the Shear Strength of RC LWC Beams Strengthened with SIFCON

According to **(Naaman, A. E.,2008),** the nominal shear strength of reinforced beams of critical section V_n was defined as follows:

$$Vn = Vc + Vs + Vsifcon \tag{4-3}$$

Where V_c is the shear strength of concrete (kN), V_s is the shear strength of stirrups, and V_{SIFCON} is the additional shear capacity supplied by SIFCON Jacket (kN), **(Lim TY, et al.,1987)**. Can be expressed as:

$$Vc = \frac{1}{6}\sqrt{f_C'}\, b_w d \tag{4-4}$$

$$Vs = \frac{d}{s}\, Avf_y \tag{4-5}$$

$$Vsifcon = 1.35\frac{d^2}{a}\cot\theta_C\, t_j \sum_{1}^{n}\frac{1}{n}(\sigma_{mu}(1 - v_f) + 2v_f a_r) \tag{4-6}$$

$$Vu = \emptyset(Vc + Vs + Vsifcon) \tag{4-7}$$

Table (4-14) compares the predicted shear strength from the abovementioned model to the achieved shear strength of the reinforced beams tested in this study. From the results, its noticed that the shear strength reduced after burning of NSLWC beams by (9.3 and 9.1%) for concrete cover 20mm and 30mm respectively. The same effect of burning noticed on the HSLWC beams, that the reduction was (13.9 and 13.6%) for concrete cover 20mm and 30mm respectively.

It is noticed from the results that the important values of shear strength come from the transverse reinforcement (stirrups), in which the effective depth (d) is the dominant factor. The effect of the concrete cover becomes slight as a result when comparing the total values of shear strength.

On the other hand, it is noted that the reinforcement with SIFCON jackets reflects a clear improvement in the shear strength of the beams affected by burning, with rates ranging between (48-50%) and (71-75%) for jacket with thickness of 20mm and 30mm respectively in NSC and between (45-48%) and (67.5-72%) in HSC. The data shown in Table (4-14) show that within the range of loads tested in this study, the variation between expected and obtained shear strength varied from 1 to 43%.

Table 4-14: A comparison between the expected and the achieved shear strength of strengthened beams with SIFCON Jacket.

Concrete cover	specimens	Expected				Achieved
		$V_{concrete}$	V_{steel}	V_{SIFCON}	V_u	V_u
20 mm	NC1-00	28.19	44.6	------	**54.59**	58.5
	NC1-02	23.33	42.7	------	49.50	44.25
	NC1-22	23.33	42.7	33.17	74.40	73.95
	NC1-32	23.33	42.7	49.76	86.84	83.05
30mm	NC2-00	26.57	42.0	------	**51.56**	51.35
	NC2-02	21.99	40.5	------	46.86	40.80
	NC2-22	21.99	40.5	29.47	68.97	64.80
	NC2-32	21.99	40.5	44.21	80.02	84.45
20mm	HC1-00	35.9	44.6	-------	**60.37**	69.50
	HC1-02	28.08	41.2	------	51.96	40.62
	HC1-22	28.08	41.2	33.17	76.83	73.20
	HC1-32	28.08	41.2	49.76	89.28	89.20
30mm	HC2-00	33.83	42.0	------	**56.87**	50.00
	HC2-02	26.47	39.0	-------	49.10	32.20
	HC2-22	26.47	39.0	29.47	71.20	59.05
	HC2-32	26.47	39.0	44.21	82.26	74.95

CHAPTER FIVE

Chapter 5. Finite Element Modelling and Simulation

5.1 Overview

This chapter presents and illustrates the adopted approaches to model and analyze the behavior of studied concrete beams under various conditions, as previously illustrated in the previous chapters. It has well known that the recent development of computer devices and its availability over the worldwide, had opened the door to create and develop the numerical solver software. one the most powerful software package that recently developed by Simulia company, is the Abaqus software. Abaqus can simulate various application numerically utilizing from the finite element method. Abaqus software is reinforced with different materials library for concrete, soil, metal, in addition to various failure theories which reflect materials response under different loading conditions (mechanical, thermal, coupled, …etc.).Most of researchers recommended to use such software for modelling and simulation, since it has been supported with powerful techniques that made it flexible platform.

This chapter will cover that adopted procedure for modelling and simulation the concrete beams that experimentally tested in the lab and ensure the accuracy of the results. Such approach, which is called numerical validation, are presented in next subsection. The results of the finite element simulation are also discussed along with the experimental one to illustrate the variations and point out some critical conclusions. Additionally, some the materials, those are unfortunately lacking to the full curve behaviors or under elevated temperature, shall be adopted according to the previous studies or standards. More comprehensive details regarding modelling and materials characterization are provided in next subsections.

5.2 Finite Element Modelling with Abaqus

In this section, the stage of samples' modelling and simulation stages shall be detailed and discussed. In general, the process includes three main phases, are:

- Phase A: modelling and simulating the reference samples (unfired beam, without enhancement)
- Phase B: modelling and simulating the concrete beam samples subjected to high temperatures, and without SFCON jacket enhancement.
- Phase C: modelling and simulating the fired concrete beam after enhancing with SFCON jacketing.

Generally, to simulate any process or behavior of concrete elements, some main process should pass through while suing Abaqus, as follows:

1- Parts modelling: in this step, the geometrical modelling of the part's simulation can be created.
2- Material property: in this step, the properties of the used concrete and steel parts are characterized and assigned.
3- Assembly: to assemble and collect all parts involved in the simulation process.
4- Step: to define type of analysis, duration of the simulation process, and solver configuration.
5- Constrain and interaction: to specify type and nature of the interacted surfaced, in addition to specifying the properties of the interface.
6- Loading and boundary conditions: to assign the type loading (mechanical, thermal, electrical …etc.), and boundary condition states of the samples.
7- Predefined field: to define the initial status of the assembly in terms of stress, temperature distribution, … etc.
8- Job: to perform and start simulation process.

The previous steps shall be detailed in next subsections. The simulation works shall be divided into three phases or stages, they are; Phase A for the reference undamaged models, Phase B for the fire damaged models, and finally Phase C for the strengthened models, as shall be presented in next subsections.

5.3 PHASE A: Modelling of Reference Concrete Beam Samples

5.3.1 Geometrical Modelling

Abaqus provide a flexible platform for modelling in addition to its ability to import parts from other software, such like AutoCAD, with suitable and various file extensions. Generally, the procedure followed for geometrical modelling was to create parts individually according to their types, 3D, 2D, or 1D part. Moreover, some of parts are deformable, some others are rigid parts according to the simulation status. Overall, there are four parts required for geometrical modelling, they are; concrete beam, streel reinforcement, loading and supporting plates, and finally steel fiber concrete jacket. It is worth mentioning the simulation process shall be in 3D space for all created parts.

Both concrete beam and jacket, 3D deformable parts were used using the extraction procedure, which in brief, the cross section of the beam or the jacket area drawn in XY plane, then a suitable extraction length are assigned to each part. This method is most common used for 3D part having straight longitudinal profile. On the other side, the modeling of steel reinforcement, which included longitudinal bars in addition to the ties, were modelled as one-dimensional parts, using 1D wire procedure. Although accurate simulation methodology requires identical modelling compared to the experimental program, some modifications were suggested by the previous authors which included to model steel bars as a wire element (1D part) for simplification and reduce required time to complete the analysis, and this considers as the most well-known procedure for steel bar modelling in concrete elements. Of course, some of application require to model steel bars as 3D element, such like when the steel-

concrete interaction is an issue to discuss. Figures (5-1) illustrates the adopted procedure for geometrical modeling of various parts.

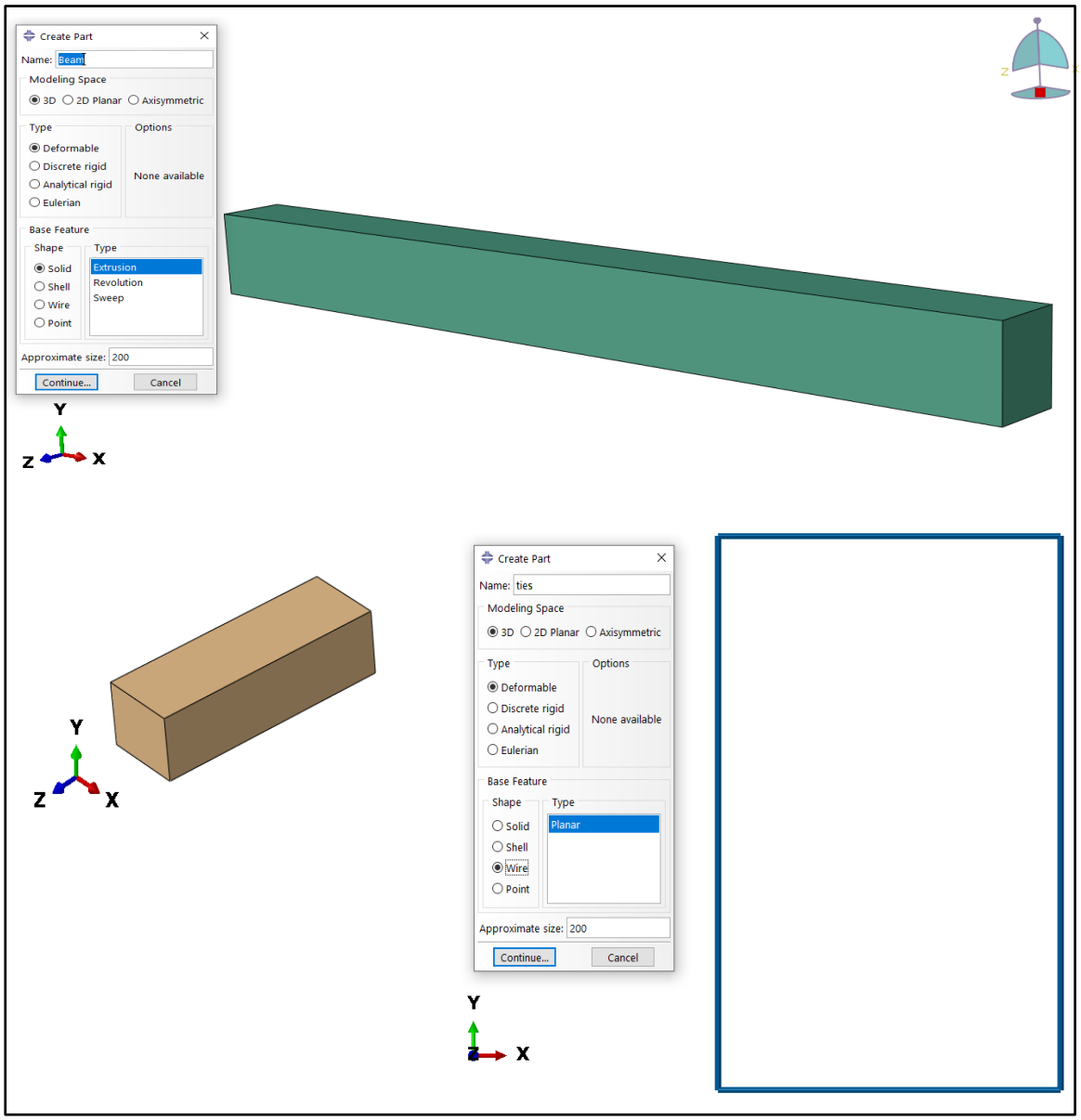

Figure 5-1: parts geometrical modelling

5.3.2 Materials Models and Assigned Section

Abaqus provide various materials properties that reflects their behavior under different simulation conditions. Moreover, different failure theories are provided for metals, soils, concrete, …etc. For simulate concrete elements, it is commonly used to define two phases are; elastic and plastic phases. The elastic phase for isotropic materials is commonly characterized by two parameters are; modulus of elasticity and Poisson's ratio. There are two models used

characterize concrete plastic phase are; concrete damaged plasticity model CDP, concrete smeared cracks model. Most of researchers recommended to use CDP model to characterize the plastic phase of quasi-brittle materials such like concrete because of its efficiency to predict concrete response under various conditions, such like monolithic and repeated loadings, plain and reinforced concrete, and application those depend on materials loading rate.

The most import aspect of such model is the ability to predict the isotropic elasticity and also the isotropic tensile and compressive damaged plasticity to represent the inelastic part. Below are the properties of each plastic phase model of concrete provided by Abaqus library:

A- The Concrete Damaged Plasticity Model Parameters in Abaqus

There are five main parameters required to be defined for The CDP model; they are, angle of dilation, eccentricity, surface plasticity flow number, viscosity, and ratio of biaxial compressive strength to the uniaxial compressive strength. These parameters are necessary to define failure surface envelope in three dimensions. Besides, the compressive (the inelastic compressive strength with plastic strain curve) and tensile behavior (inelastic stress with cracking strain curve, beyond the cracking strength) are required to be input, as can be seen in Figure (5-2). Table (5-1) illustrates the parameters of the CDP failure surface.

Table 5-1: selected CDP material parameter for unfired concrete

Parameter	Selected value
Material model	CDP model
E, MPa	Varied according to f'c
Possion's ratio	0.18
Dilation angel	35
*Ecc	0.1
*Fb0/fc0	1.16
*K	0.667
*Viscosity parameter	0.0001

*As recommended by Abaqus manual

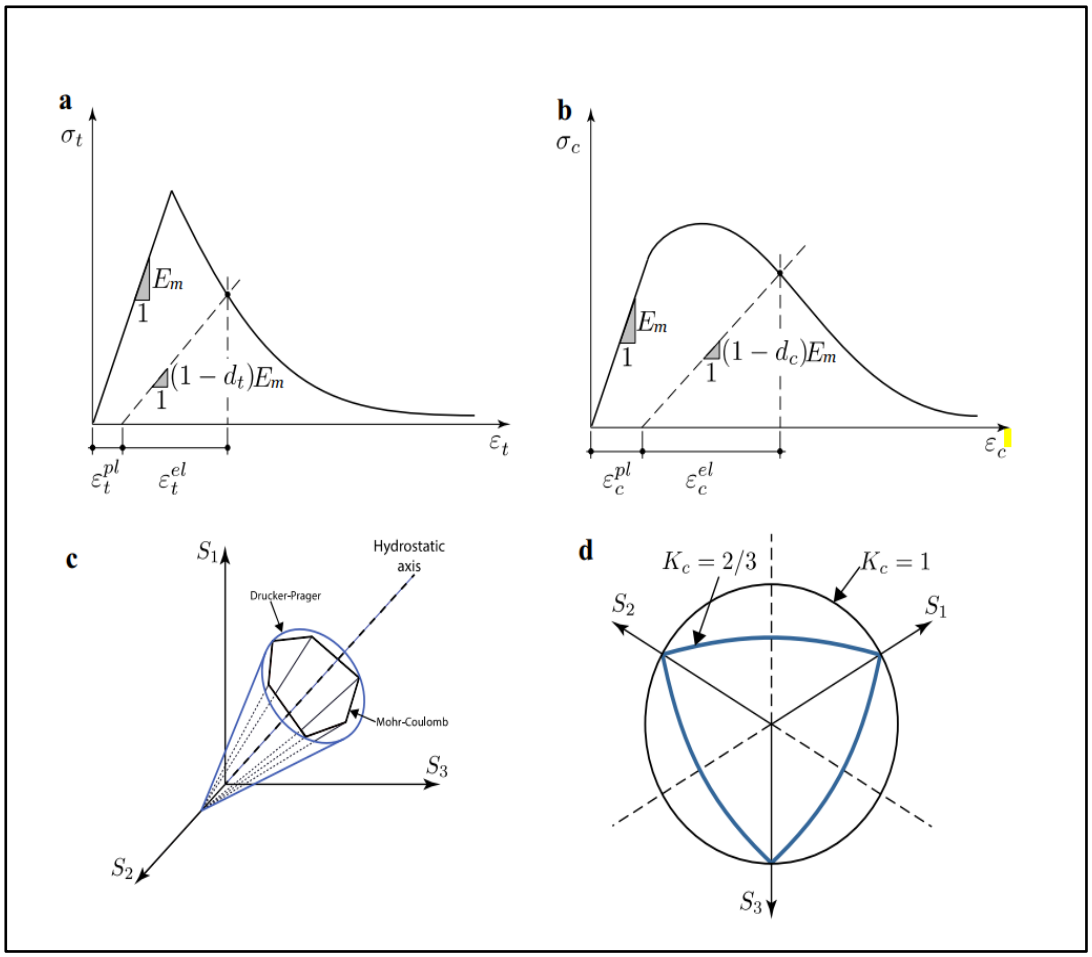

Figure 5-2: Tensile and compressive stress strain relation (a,b), failure surface criteria of CDP model in 3D space around the hydrostatic axis and in the deviatoric plane (c,d). **(Castellazzi, et al., 2018).**

Another two important curves required to be input to the CDP model are; the uniaxial unconfined stress-strain behavior under both compressive and tensile loading at ambient temperature (20C). These curves are segmented to elastic part, which is defined by the modulus of elasticity and possion's ratio, and the plastic part, which is defined the CDP model. The plastic phase is defined for both tensile and compressive behavior of concrete. The adopted curves are detailed in next subsections in the phase C.

B- Defining Steel Material Behavior

For steel material, generally, there are four stress strain models which are used to characterize its behavior are; engineering stress-strain, true or logarithmic stress-strain relation, elastic perfect plastic behavior, or the bilinear elasto-plastic with hardening. For steel reinforcement rebars, the elastic perfect

plastic behavior has been adopted herein this study. Such behavior requires to define the elastic and plastic model with a minimum one point at yielding, which corresponded to a zero-plastic strain. On the other side, the linear hardening of the plastic phase requires two point as a minimum, the yield point and the rapture point. Other mentioned relations require to define more than two points in the plastic behavior. Due to the lack of data availability for the plastic phase, the elastic perfect plastic behavior has been adopted herein this study.

Table 5-2: The elastic perfect plastic behavior model

parameter	Selected value
Model type	Idealized stress strain behavior
E, MPa	200000 (ambient temperature)
Possons ratio	0.3
Yield stress, Fy	Varies according to the bar type and temperature

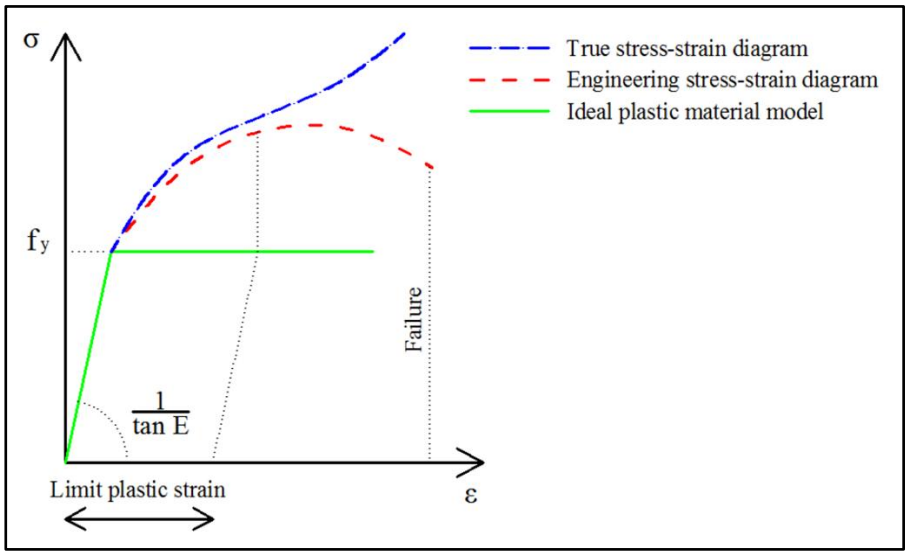

Figure 5-3: General types of steel stress strain representation and simplification. **(Standard, B. 2006)**.

As a general procedure in Abaqus, each material requires a section to be defined. For instance, concrete beam part should be defined as a solid homogenous one. On the other hand, steel reinforcement sections can be defined using both beam and truss section. Beam section commonly used for one dimensional element with have regular or irregular section and requires

section orientation. While truss section has equal stiffness in all direction (Circular cross section only), which is matches the steel reinforcement rebars. In this study, since there are three different bars diameter, three truss sections should be defined. Figure (5-4) illustrates the adopted procedure. Finally, after defining sections, each section must be assigned to tis specified part to complete materials characterization process.

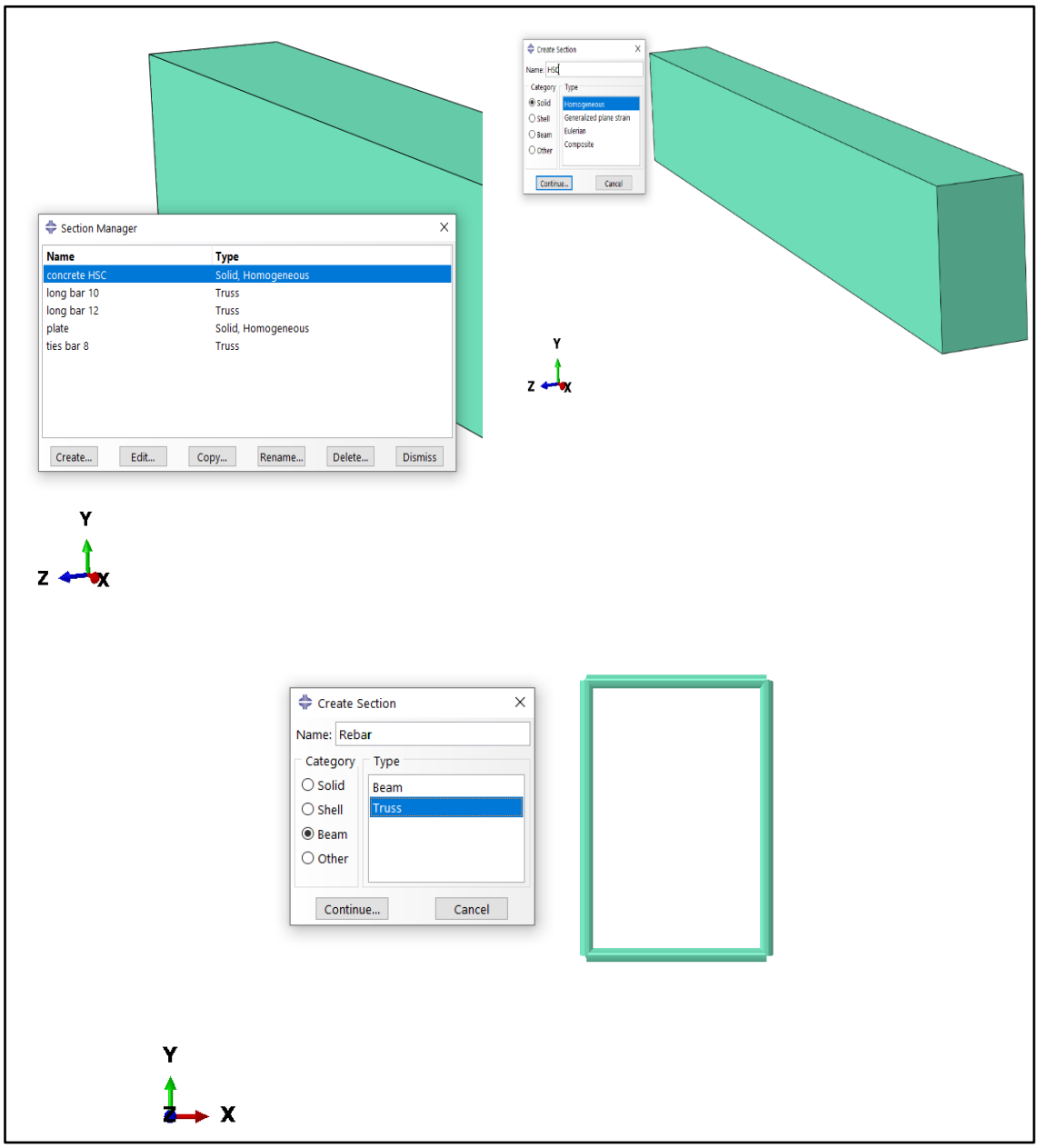

Figure 5-4:section assignment of concrete beams and steel bars

5.3.3 Materials Characterization and Response Modelling

5.3.3.1 Concrete Behavior Under Ambient and Elevated Temperatures

Various concrete compressive strength stress-strain behavior under elevated temperature were predicted, and for different types of concrete mixtures (NSC and HSC) and for normal and lightweight aggregate concrete. However, these statistical models are built according to the many parameters, such as, type of aggregate, type of additives, water- cement ratio, … etc. the most recent study which has been investigated by (**Dabbaghi et al.,2021a)** to predict the post fire behavior of LECA concrete. The predicted statistical model was for both normal and high strength concrete types, including lightweight clay aggregate, which is go accurately with the current study. The normalized compressive stress-strain relation under various temperature degrees are illustrated in Figure (5-5).

$$\sigma = f_{cT}\frac{\beta\left(\frac{\varepsilon}{\varepsilon_{cT}}\right)}{\beta - 1 + \left(\frac{\varepsilon}{\varepsilon_{cT}}\right)^{\beta}} \qquad (5\text{-}1)$$

Where:

f_{cT} is concrete compressive strength

σ stress at specified strain increment

ε strain increment

ε_{cT} strain correspond to the maximum concrete stress at temperature C

$$\frac{\varepsilon_{cT}}{\varepsilon_c} = 1 + \frac{2.82}{1 + (\frac{450}{T})^{2.22}}\, 25^{\circ}C \leqslant T \leqslant 750^{\circ}C \qquad (5\text{-}2)$$

β factor can be determined from the following formula:

$$\beta = 0.62 + f_{cT}^{0.46} + T^{5.56'} \quad (5\text{-}3)$$

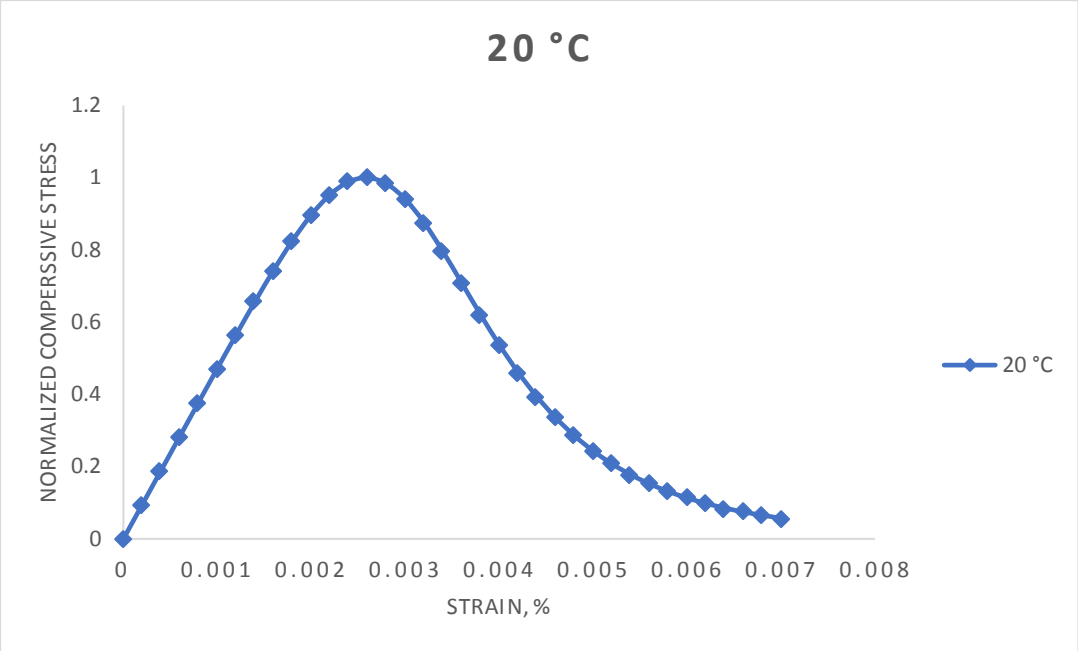

Figure 5-5: The adopted normalized stress-strain behavior of concrete under unconfined, uniaxial compressive loading **(Dabbaghi et al.,2021a)**.

5.3.4 Assembling Parts

Assembling means collecting the created parts into the simulation environment using assembly module. The inserted parts then called instances. In this module, instances are created, translated, rotated, or duplicated according to the required simulation. For example, after inserting the concrete beam, the long steel bars for top and bottom layers in addition to the stirrups are positioned and duplicated as can be seen in Figure (5-6). The stirrups are duplicated using the linear pattern tool. To clear some points, it is worth mentioning that Abaqus provide an extruded view for wire element for illustration only, and that what can be seen in the previously presented figures.

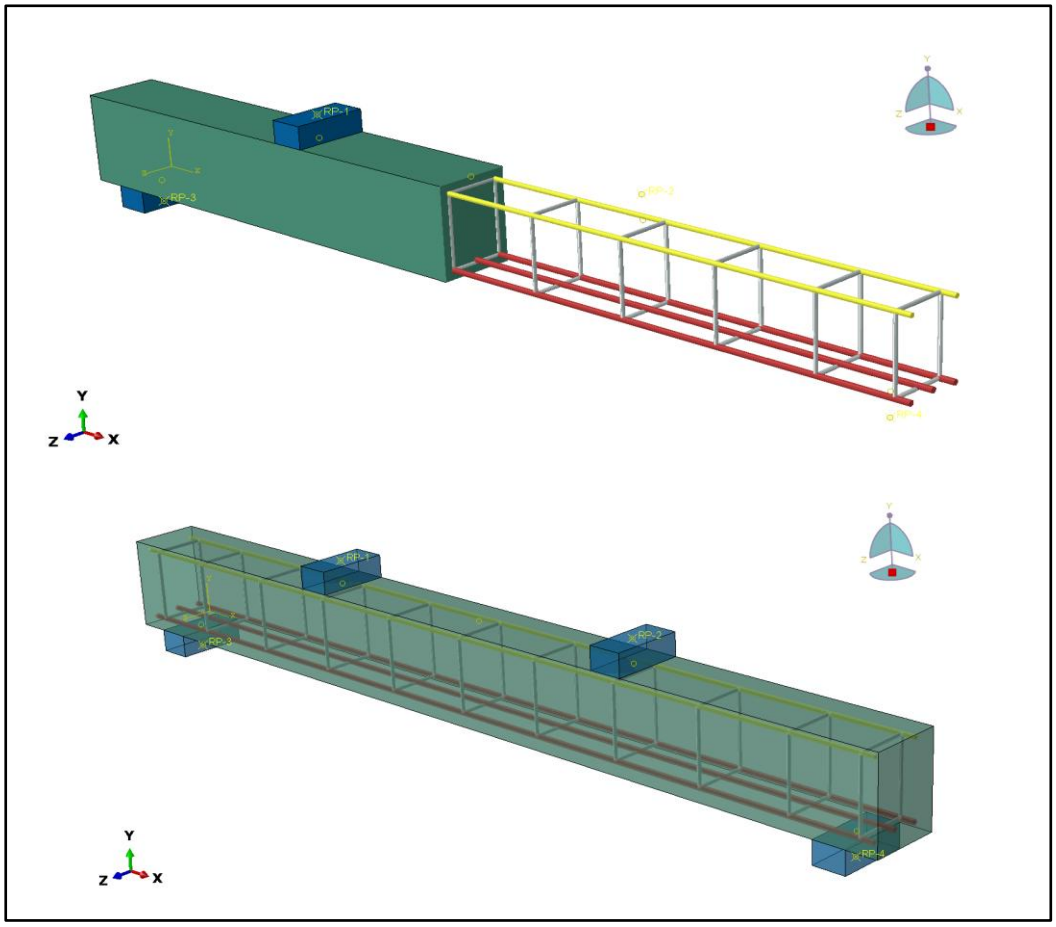

Figure 5-6: Part assembling of the concrete beam

5.3.5 Analysis Procedure

Abaqus provide various types of analysis suits for different engineering applications, they are called steps in Abaqus. The static step suits most of engineering applications where the loading frequency less than 1/3 the structure natural frequency, or when the kinetic energy is less than 5% of the internal energy. Beyond such limit, the quasi-static analysis is required to perform. The effect of Higher frequency rate of loading cannot be captured by such type of analysis. The dynamic procedure can be utilized for such purposes (impact, crashing, earthquake, …etc.). moreover, Abaqus library include heat transfer analysis procedure, and coupled thermal-displacement analysis to capture the coupled effect of mechanical and thermal loading on the structure. In this study, the static analysis procedure has been adopted to solve the concrete beam those are not subjected to fire. While to investigate the thermal distribution on the beam cross section, the heat transfer analysis procedure was used. Other

concrete beams those are tested after exposing them to fire and those are improved with concrete jacketing, are analyzed with the static analysis step.

5.3.6 Load and Boundary Condition

Abaqus environment have many various methods and capabilities to apply mechanical, thermal, or coupled of both of them. In general, the mechanical loading can be applied using either the load, or the boundary condition with specific downward displacement. The later called displacement control method, which most recommended and consumes lesser time while solving the problem. The former called load control method, which typically requires more time than the displacement control method to solve the problem. Most of static application procedure, both of the mentioned methods predict the same results.

5.3.7 Constrains and Interactions

Some useful tool was utilized within Abaqus working environment, they are constraining and interactions. One of the most useful constrain type that widely accepted by the structural researches, is the embedded region constrain. This type of constrains can be used to show that the steel reinforcement (the embedded regions) are fully interacted with the concrete beam (the host element). Which means, no slip is allowed for the long rebars or the stirrups, even with excessive applied loads. The second useful constrain type is the rigid body one. Such type was used for the loading and supporting plates, to that such parts are non-deformable parts, and the stress status, strains, or displacements are not a concern within this simulation process. To apply rigid body, constrain, a reference point is required to couple with the body required to be rigid.

For the mechanical interaction property was used to simulate the relation between the loading and supporting plates with the concrete beam. In general, any surfaces those are interacted physically must be defined, otherwise, the simulation process will not work correctly. The standard surface to surface contact was used in this study, with normal and tangential properties. The

normal (hard contact) means the first surface cannot penetrate the second one. The tangential behavior with penalty or friction coefficient of 0.4 as suggested for the static was assigned to simulate the friction between the concrete beam and the steel plates. The selected master surface type was the stiffer part, which were the steel plate, while the slave surface was the concrete beam. It's worth mentioning that no predefined field was assigned in this step, since the simulation was for mechanical loading only.

5.3.8 Meshing Properties

Meshing technique is the method of segmenting and converting the simulated parts into smaller using different shapes and division algorithms. The produced parts then called (elements). In general, different types of elements are provided in Abaqus library, as can be seen in Figure (5-7). Continuum solid element was used for 3D parts (plates, concrete beam, SFCON jacket), 3D stress family, brick (hexagonal) shape (C3D8R). while one dimensional element (truss) family was used for steel bar reinforcement (Type element solver for all parts was slandered solver, reduced integration, and linear geometric order). Structural mesh algorithm technique was used to generate mesh distribution. The dimension of concrete elements (brick, 8 nodes, reduced integration) was 20mmX20mmX20mm. The same length was used for steel reinforcement. Figure (5-8) illustrates the generated mesh for the concrete beam.

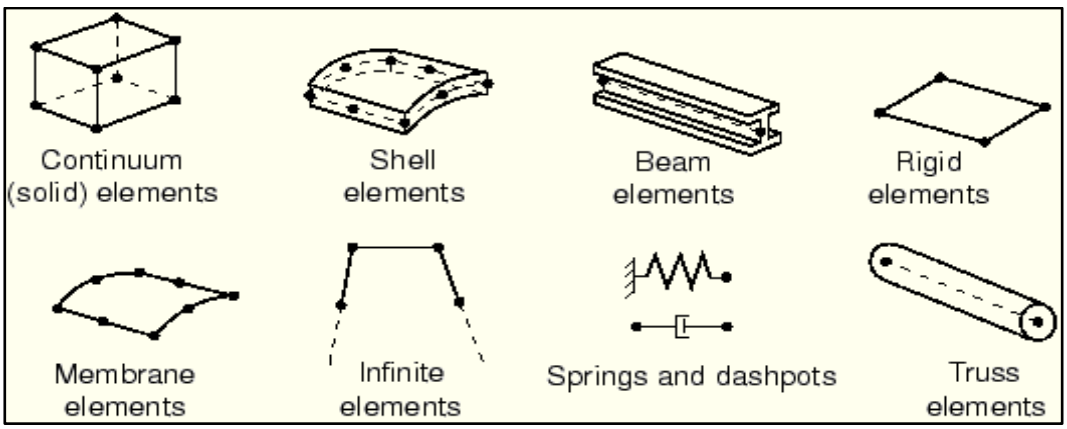

Figure 5-7: Element types library in Abaqus

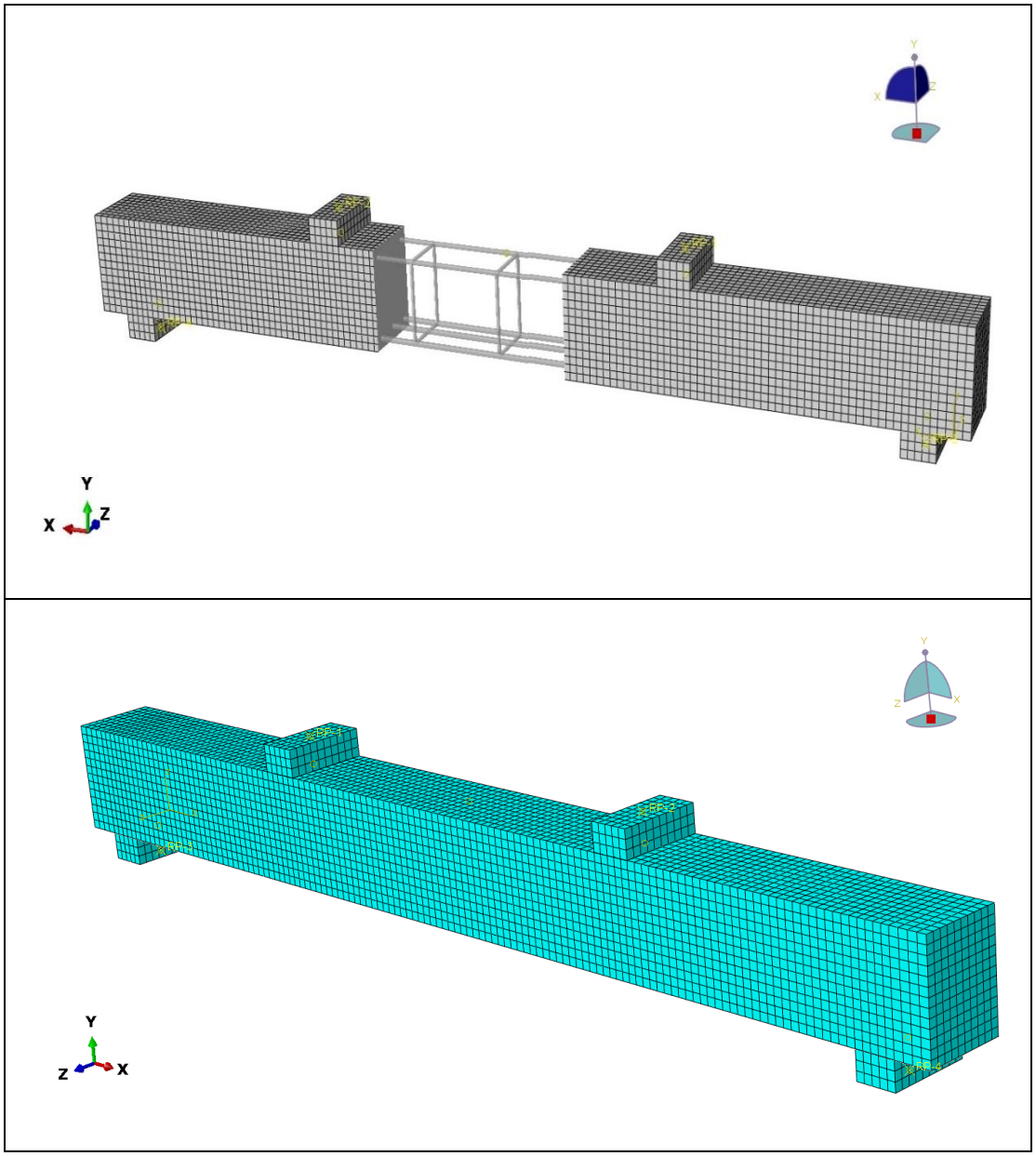

Figure 5-8: Meshing of the concrete beam using structural mesh algorithm techniques.

5.4 Phase B: Modelling the Thermal Distribution on Concrete Samples

5.4.1 Geometrical Modelling and Assembling:

Same techniques and dimensions used in phase A, used herein this stage.

5.4.2 Material Properties

Like other materials, when concrete subjected to fire of high temperatures, the strength of the material starts to degrade proportionally due to its nature. The chemical bonding of cement mortar in addition to the expansion of the components. Therefore, it is necessary to characterize the thermal properties of

such concrete type since they are required as input data Abaqus for heat transfer analysis. Generally, it is necessary to define concrete thermal properties such as thermal connectivity, density, and specific heat. LECA concrete

Overall thermal is transferred through three methods are, conduction, convection, and radiation. Conduction means that heat is transferred by means of direct contact of bodies. While convection mean the surface file condition used to simulate the interaction between the model and the surrounding media. While the emissivity used to define the ability to radiate heat to the surrounding.

5.4.3 Type of Analysis (Step)

Thermal analysis procedure has been utilized in this phase to simulate heat distribution on the fired beam.

5.4.4 Constrains, Interactions Properties, and Predefined Field

To simulate heat convection between the ambient air temperature and concrete beam, a surface film condition option was assigned to the concrete sides and the bottom edges. The sink temperature was set to 20C to simulate the initial air temperature. Heat amplitude of TC1 was assigned to represent the raising in the surrounding temperature due to firing.

While for thermal analysis, conductivity, concrete surface film condition, the conductivity used to simulate how heat is transferred from an object to another on (steel and concrete), while the surface file condition used to simulate the interaction between the model and the surrounding media. As recommended by Fib modal code, the recommended surface film condition value for surfaced subjected to fire is 25, while for the unfired surface is 9.

Thermal analysis requires to define the initial temperature state of the assembly as a whole. Accordingly, a referenced temperature value of 20 C has been assigned as an initial condition to the whole model.

5.4.5 Meshing Techniques and Type Element Solver Library

Same mesh techniques, element shape and size used in phase A for concrete and steel element, used herein this phase. Except element solver library (element degree of freedom). The selected element solver family was heat transfer for both concrete elements and steel bar reinforcement, which has only the thermal degree of freedom. Concrete and steel reinforcement elements code is (DC3D8: An 8-node linear heat transfer brick).

5.4.6 Boundary Condition and Loading

No mechanical loading has been assigned in this phase, only temperature boundary to the bottom and side surfaces with amplitude of TC1 obtained from the experimental work.

5.5 Phase C: Modelling of Fired Samples Subjected to Mechanical Loading

5.5.1 Part Modelling and Assembling

Same techniques and dimensions used in phase A, used herein this stage.

5.5.2 Materials' Characterization

The postfire concrete stress strain behavior subjected to a uniaxial unconfined compressive loading under various temperatures are presented in Figure (5-10). It's clear that the high exposed temperature to the concrete have not only a significant reduction on the compressive strength, but also on the overall behavior such as strain corresponding to peak stress and secant modulus of elasticity. Also, it can be observed that, the degradation phase of the material behavior becomes steeper at higher temperatures, which means, in other words, the material brittleness started to decrease gradually and becomes more ductile at elevated temperatures.

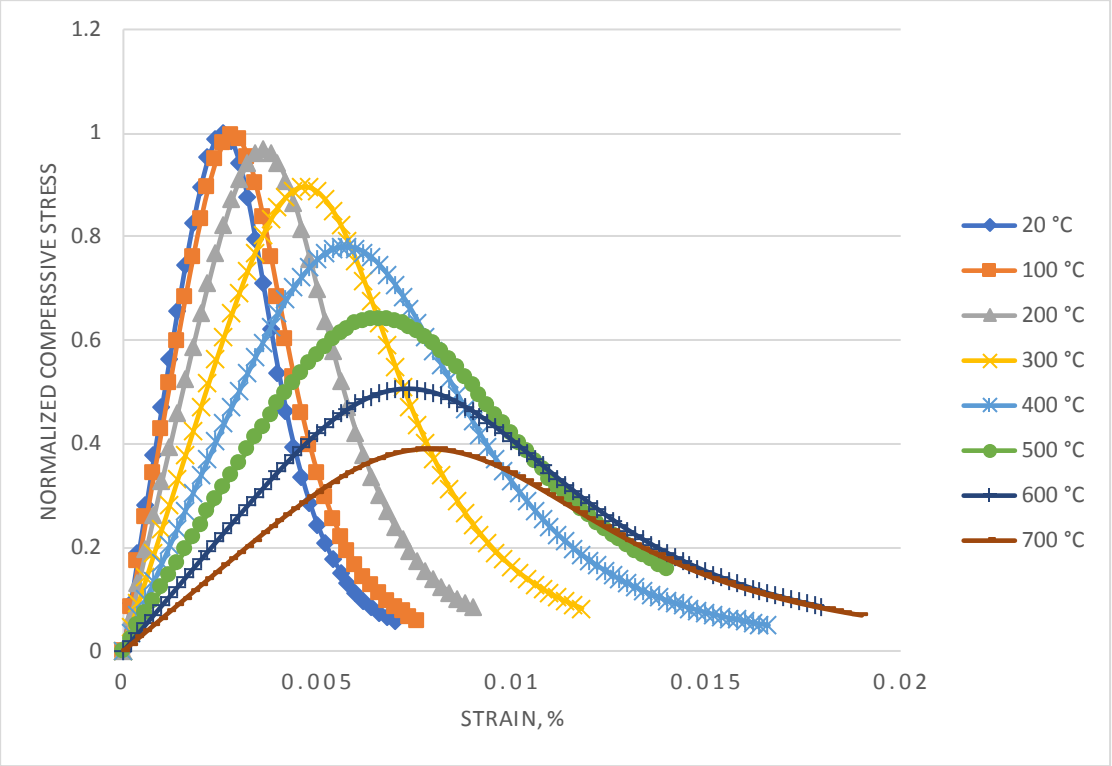

Figure 5-9: Concrete stress – strain behaviour under elevated tempertures.

Accordingly, the normalized residual compressive strength and elastic modulus of light weight concrete are illustrated in Figure (5-11). Form the presented figure, it is clear that, a slight reduction can be observed in the f'c and Ec values for temperatures below 150 C. Moreover, the concrete start losing 10% and 28% of the total compressive strength and the elastic modulus values at 300 C, respectively reaching to 600 C, the residual *f*'c and Ec values are 22% and 50%, respectively.

From the other side, the normalized concrete strain at peak stress are presented in Figure (5-12). Till the 150 C, only 10% increase in the strain can be observed, after such limit, the rate of strain increase is increase dramatically reaching to 81% increase in strain at 300°C, while about 181% increase in the same value at 600C.

$$\frac{f_{cT}}{f_c} = \frac{1}{1+(\frac{T}{605})^{3.07}} \quad 25^{\circ}\mathrm{C} \leqslant T \leqslant 750^{\circ}\mathrm{C} \tag{5-4}$$

$$\frac{E_{cT}}{E_c} = \frac{1}{1+(\frac{T}{408})^{3.14}} \quad 25^{\circ}\mathrm{C} \leqslant T \leqslant 750^{\circ}\mathrm{C} \tag{5-5}$$

$$E_c = 0.043\gamma^{1.5}\sqrt{f_c} \tag{5-6}$$

$$\frac{\varepsilon_{cT}}{\varepsilon_c} = 1 + \frac{2.82}{1+(\frac{450}{T})^{2.22}} \quad 25^{\circ}\mathrm{C} \leqslant T \leqslant 750^{\circ}\mathrm{C} \tag{5-7}$$

Where;

$$\varepsilon_c = 3.496 \times 10^{-5} \times f_c' + 0.001 \tag{5-8}$$

It is worth mentioning that (**Dabbaghi et al.,2021b)** has covered in his research, concrete behavior till temperature 750C. Where, at such point, the residual *f'*c and Ec values are approximately 12.8% and 34%, respectively. while to strain corresponding to the peak stress is increased about 3 times the value at ambient temperatures.

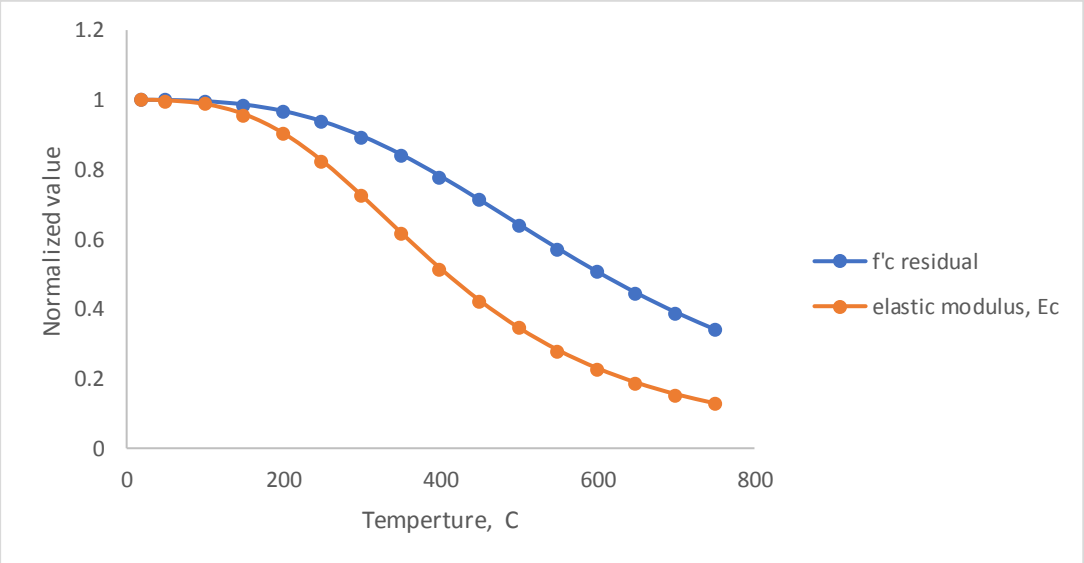

Figure 5-10: Normalized values of the residual f'c and Ec for concrete subjected to high temperatures. **(Dabbaghi et al.,2021b)**.

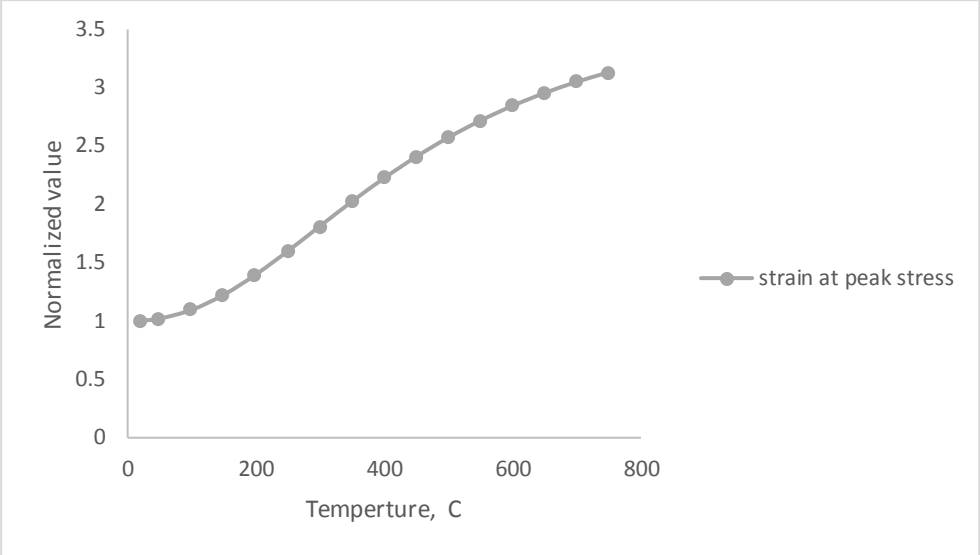

Figure 5-11: Normalized value of the concrete strain corresponded to the $f'c$. **(Dabbaghi et al.,2021b)**.

Heating and exposing duration have an adverse effect on the overall concrete performance. Numerous researchers had been worked out that significant concrete degradation was observed in the compressive strength at elevated temperatures. Figure (5-13) illustrates the concrete residual compressive strength at elevated temperatures. Form the pervious figure, it can be noticed that, most of research works regards concrete residual strength are varied slightly till temperature 300C. After such limit, a significant variation in the concrete residual strength were observed ranged from 43% to 70%. Moreover, **(Hertz, 2005;Bastami et al.,2010;Huang et al.,2017;Dabbaghi et al.,2021b)** research works are approximately the same till temperature 600C.

The tensile strength behavior of concrete exposed to high temperatures had been predicted extensively by many researchers, as illustrated in Figure (5-14). It can be observed that, at 250 C, most of researchers predicted formula are the same, in which the residual tensile strength is about 80%. After this point, Chang et.al and Li and Guo formulas predicted the same value of the residual tensile strength of about 40%. On the other hand, the suggested formula by **(EN 2:part1-2,1992)** is the most conservative among other mentioned models, and the residual tensile strength is about 0% at 600C.

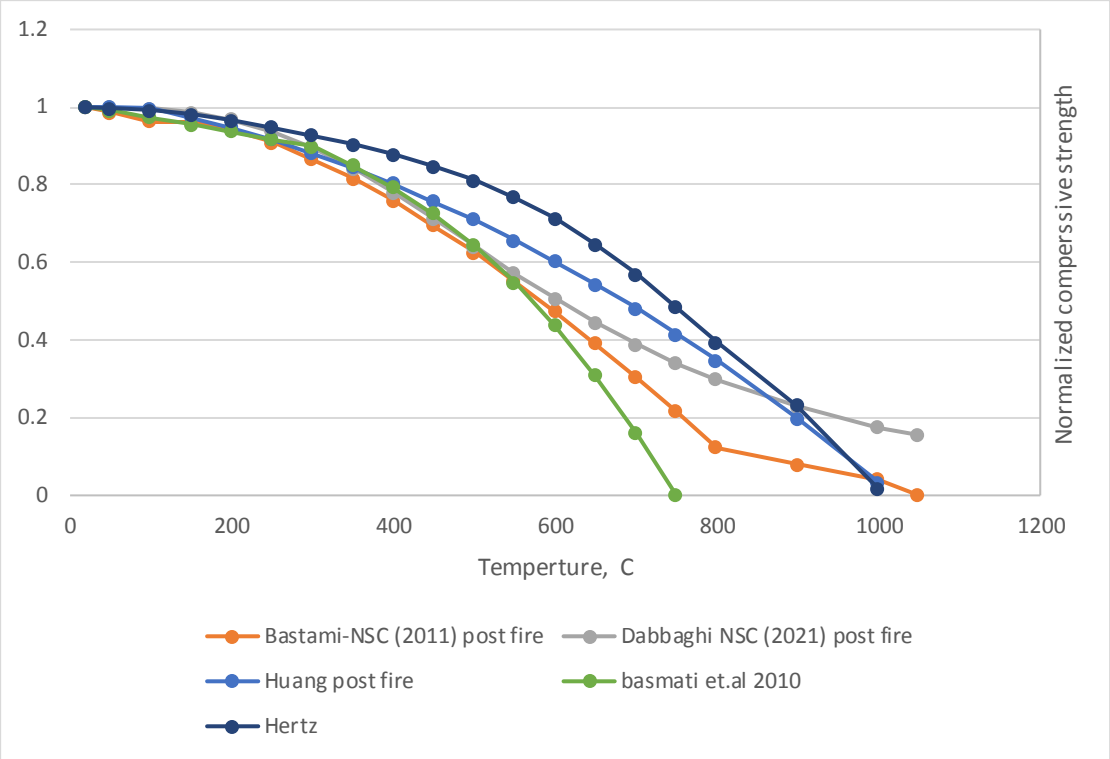

Figure 5-12: Normalized concrete compressive strength at high temperatures **(Hertz, 2005;Bastami et al.,2010; Huang et al.,2017; Dabbaghi et al.,2021b)**

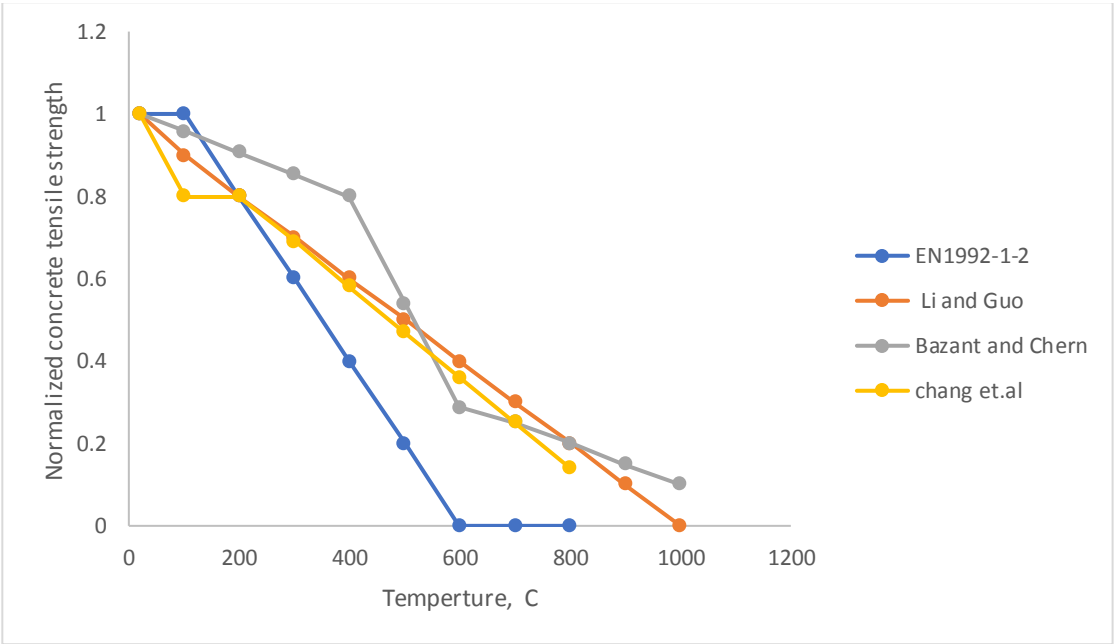

Figure 5-13: Normalized concrete tensile strength at high temperatures **(Bažant&Chern, 1987;Guo& Shi,2003;Chang et al.,2006;Li et al.,2007)**

It is worth mentioning that the suggested model by **(Guo& Shi,2003; Li et al.,2007)** was adopted herein this study to assign maximum tensile strength corresponded to the cracking strain. Also, to simplify the simulation process,

the bi linear behavior of concrete tensile stress strain has been assigned to Abaqus.

5.5.2.1 Steel Reinforcement Behavior at Ambient and Elevated Temperatures

After validating the experimental results numerically, it can be said that, the most critical case, when concrete cover was about 20mm, the temperature of steel reinforcement was about 394 C. Most of codes and previous researches had pointed out that when steel is heated to 400 C, no observable reduction was noticed in the yield stress point. In the contrary to the elastic modulus, where noticeable change can be observed at such temperatures.

In general, the stress-strain relation of steel bars can be attributed using the following formula:

As clarified in Figure (5-15), The residual elastic and yield strength of steel bar reinforcement is adopted as suggested by Lie, which is adopted herein this study. as illustrated, the residual normalized yield strength and initial elastic modulus of steel bar are about 76% and 91%, respectively at temperature 300C. while at 600C, the same values are about 33% and 72%, respectively. The rate of strength reduction is higher than what has been observed for the elastic modulus. Moreover, it can be noticed that exposing steel reinforcement to temperatures near 500 C would reduce the elastic modulus of about 19%, while about 50% reduction in the yield strength.

(Lie, 1992)

$$f_{yT} = \begin{cases} [1 + \dfrac{T}{900 \times \ln(T/1750)}] \times f_y & 0 < T \leq 600^{\circ}\text{C} \\ [\dfrac{340 - 0.34 \times T}{T - 240}] \times f_y & 600 < T \leq 1000\ \text{C} \end{cases} \quad (5\text{-}9)$$

(Lie& Stanzak,1974)

$$f_{yT} = f_y(1 - 0.78 \cdot T^* - 1.89 \cdot T^{*4}) \quad (5\text{-}10)$$

$$E_T/E = 1.02 - 0.035e^{T/280} 20°C \leq T \leq 800°C \quad (5\text{-}11)$$

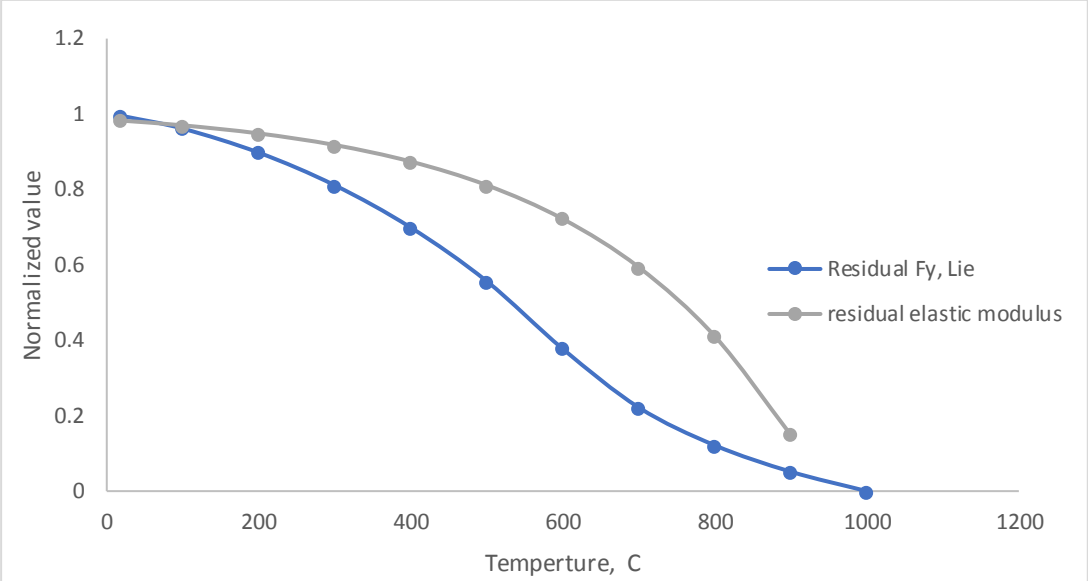

Figure 5-14: Normalized values of the residual Fy and E values for steel bars subjected to high temperatures**(Lie, 1972)**

5.5.2.2 Concrete Possion's ratio at elevated temperatures

Most of previous research works revealed that when concrete specimens exposed to high temperatures, a noticeable reduction in the possion's ratio value was observed. **(Bahr et al., 2012)** experimented the effect of high temperatures on concrete behavior. He stated that possion's ratio was reducing at elevated temperatures as can be seen in Figure (5-16) and suggest a statistical model to predict it. The suggested formula was adopted herein this study to assign Possion's ratio at elevated temperatures, as expressed in Equation (12).

$$\mu_\theta = a \cdot e^{-b \cdot \theta} = 0.204 \cdot e^{-0.002 \cdot \theta} \quad \text{with} 20°C \leqslant \theta \leqslant 500°C \quad (5\text{-}12)$$

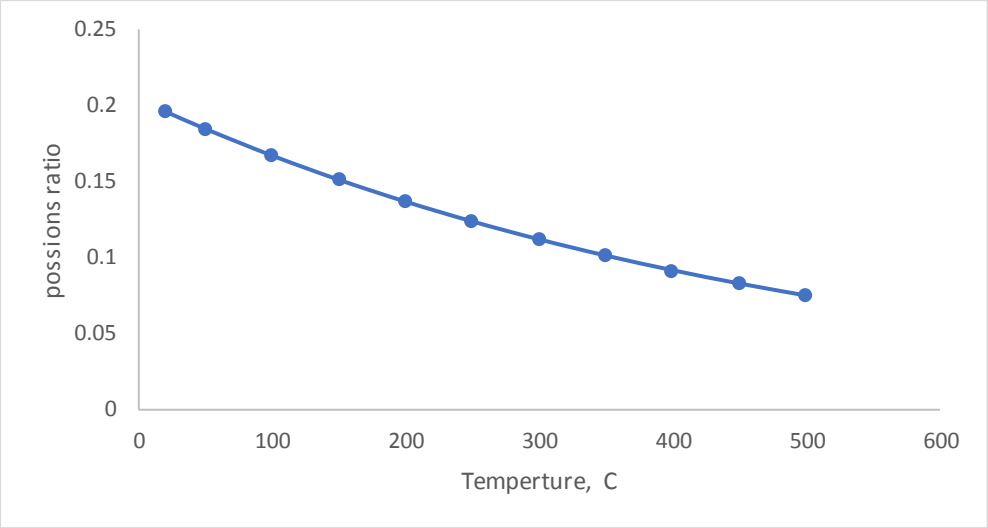

Figure 5-15: Concrete possions ratio changes at high temperatures **(Bahr et al., 2012)**.

5.5.3 Step (Type of Analysis)

In this stage of simulation, the transient coupled temperature-displacement analysis was used to simulate to coupled effect of thermal and mechanical loading. It is worth mentioning that, the maximum allowable temperature per increment was set to 20C, to avoids excessive change and disseverance issues during performing the simulation.

5.5.4 Interactions and Constrains

Only the mechanical interactions listed in phase A, was adopted herein this phase.

5.5.5 Meshing Techniques and Element Type

Same element shape and meshing distribution algorithm technique used in stage A, was used herein this stage of modelling, except element type (solver). To solve and account both mechanical and thermal loading, For both concrete and steel reinforcement, the types of element ware C3D8T and T3D2T, respectively.

5.5.6 Predefined Fields

To include the effect of firing on the concrete beam, the predefined option used herein this model. The initial state option to assign the initial temperature

distribution on the fired samples. This will facilitate to redistribute concrete strength characteristics according to the temperature profile. The fired model output results files (ODB) obtained from phase B, have been recalled in this step for phase D.

5.6 Phase D: Modelling of The Improvement of Concrete Beams Using SFCON Jacketing

5.6.1 Geometrical Modelling and Assembling

For geometrical modelling, the same dimension for the beam and steel reinforcement was used, except the jacketing. A 3D deformable solid part, with two different thickness of 20 and 30 mm were modeled using the extraction method, with the same length of concrete beam, as illustrated in Figure (5-17). Moreover, it is worth mentioning that the lengths of the supporting and loading plates were increased to match the new concrete beam's width. The final assembly of the improved models is presented in Figure (5-18).

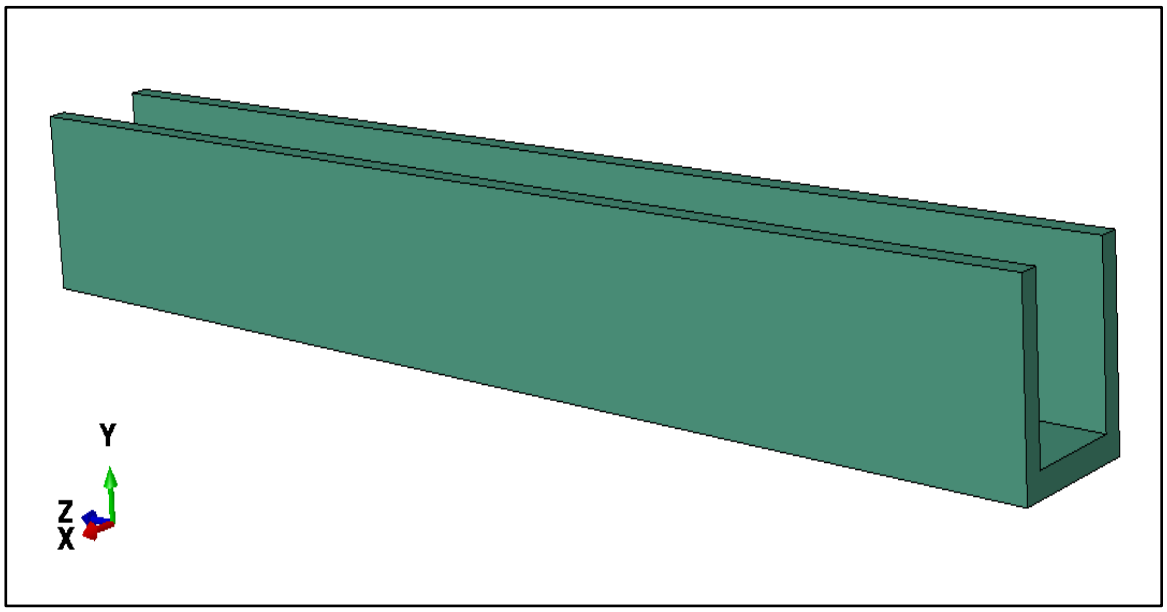

Figure 5-16:SIFCON jacket layer part along the three faces of the concrete

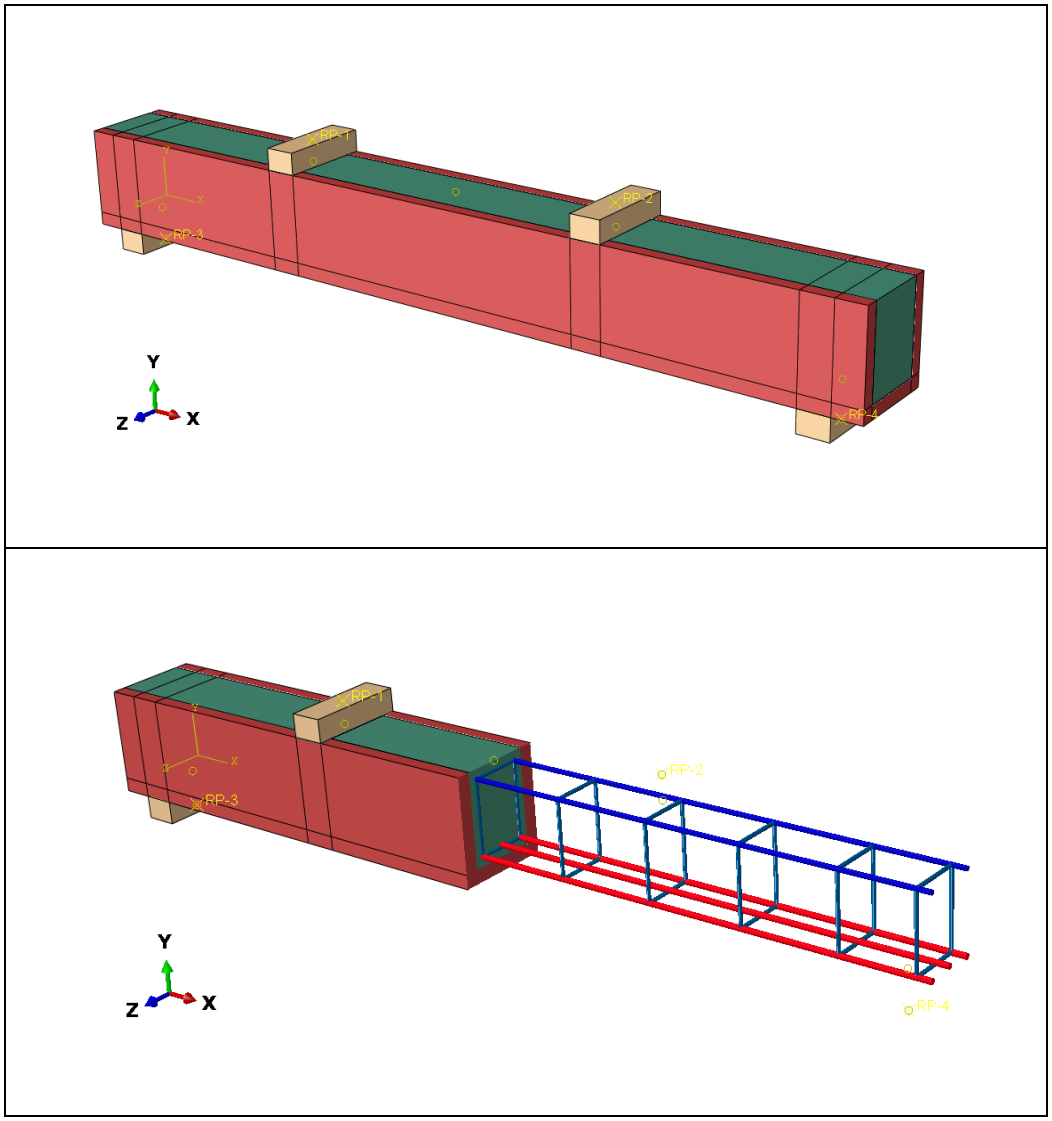

Figure 5-17: Part assembling of the strengthened models with SICON jacket

5.6.2 Material's Characterization: Stress Strain Relations of SFCON Material

It is well known that the behavior of high strength concrete has some differences when compared with the normal concrete behavior, especially when the mixture includes micro steel fibers. Figure (5-19) illustrates the stress strain behavior of SFCON mixture when subjected to monolithic, uniaxial compressive and tensile stress. It can be noted that, the high percentage of steel fiber resulted a mixture with high ductility and higher sustain to resist loading, and the strain corresponded to the maximum stress approaches 0.02. It is worth

mentioning that maximum compressive and tensile strength were about 94.5 MPa and 13.75 MPa, respectively.

In Abaqus, the stress strain data was refined and the elastic phase was separated from each other. The elastic modulus defined as elastic isotropic model, while for the plastic phase behavior, the same model previously used in concrete characterization (concrete damaged plasticity) had adopted. The material property then assigned to the 3D solid jacket. Other parts like the concrete beam and the streel reinforcement are fixed as they mentioned previously in phase C.

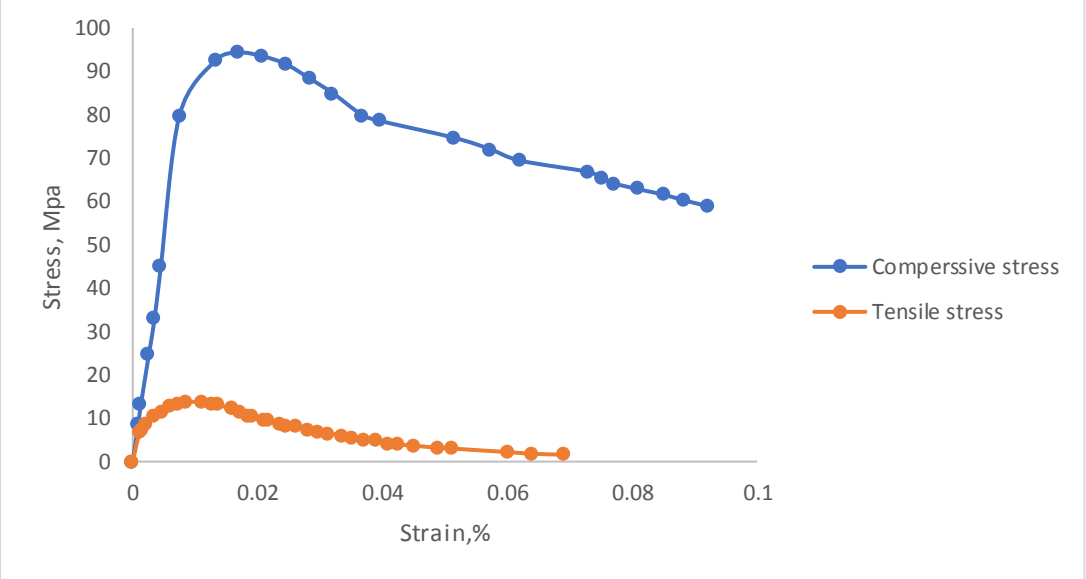

Figure 5-18:SICON stress- strain behavior under unconfined, uniaxial loading

5.6.3 Constrains and Interactions

For the strengthened models, the same interaction used between the loading and supporting plates was used herein this model. Where, in brief, the general surface to surface contact was assigned with two mechanical interactional properties are; normal behavior (hard contact), and tangential behavior (penalty) with 0.3 fraction factor. In addition, to model the full interaction behavior between the interface between the concrete beam faces and

the interior jacket faces, tie constrain was assigned for such purpose to prevent bonding slippage.

5.6.4 Step (Type of Analysis)

In this stage of simulation, same as type of analysis for phase C, the transient coupled temperature-displacement analysis was used to capture to coupled effect of thermal and mechanical loading.

5.6.5 Meshing

The same meshing techniques, element shape, size, and type used in modelling phase C, used herein this phase for the enhanced models. Except the element size in the direction of the jacket thickness. The assigned elements dimension was 4 mm in such direction to get higher results accuracy, as illustrated in Figure (5-20).

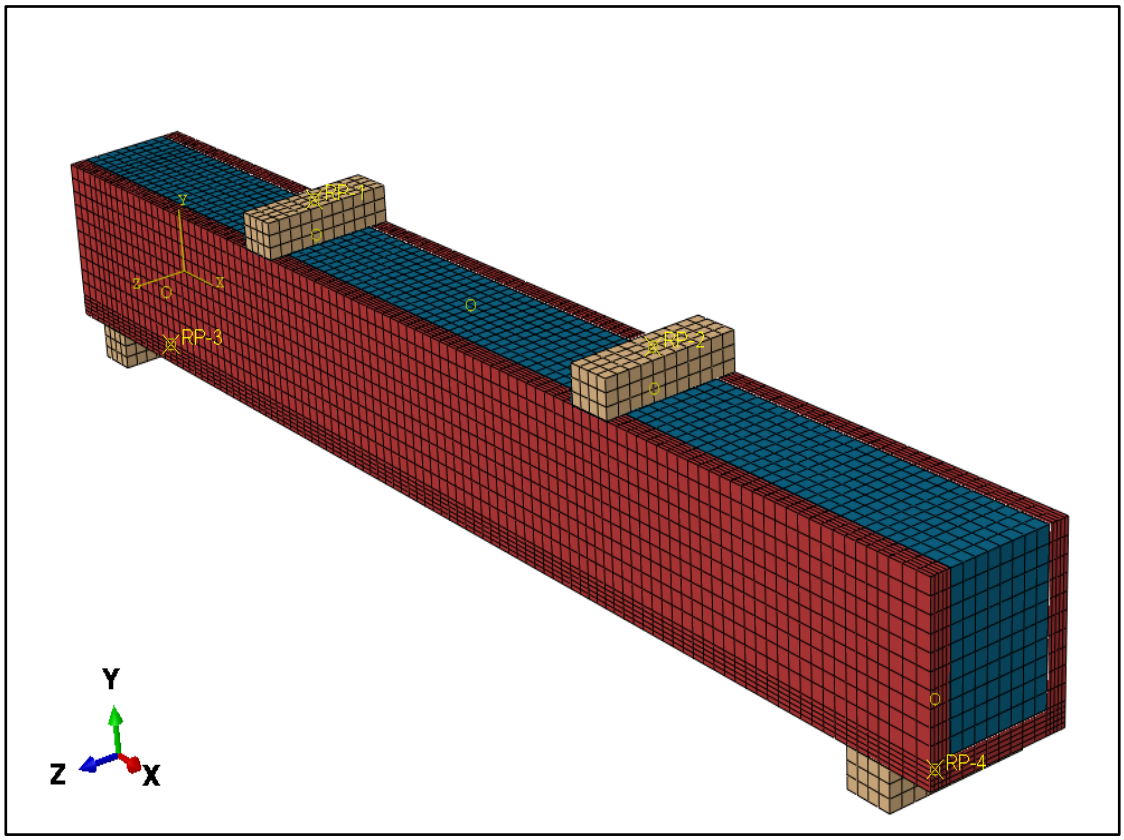

Figure 5-19: Meshing of the strengthened models with SIFCON jacket

5.6.6 Predefined Fields

Same as phase C, the thermal distribution of the fired model output results files (ODB) that obtained from phase B, have been recalled in this step for phase D as temperature initial condition.

5.7 FEM Results

5.7.1 Phase A: Validation Results of NSC and HSC at Ambient Temperatures (20C)

Simulation results of the normal and high strength concrete specimens before firing are presented herein this subsection. As can be seen in Figure (5-21, 23, 25, and 27), the load-displacement curves of the experimental and numerical approaches are close to each other for normal concrete specimen. The FEM result curve possessed higher initial stiffness than the experimental results. Also, the FEM result reflected higher load carrying capacity than the experimental results by about 7%, and corresponded displacement difference of about 1.7%. Such difference can be accepted and the adopted parameters can be said to be accurate herein this study. The von mises stress distribution for the concrete beam body and steel reinforcement, in addition to the true strain are illustrated in Figures (5-22,5-24,5-26 and 5-28).

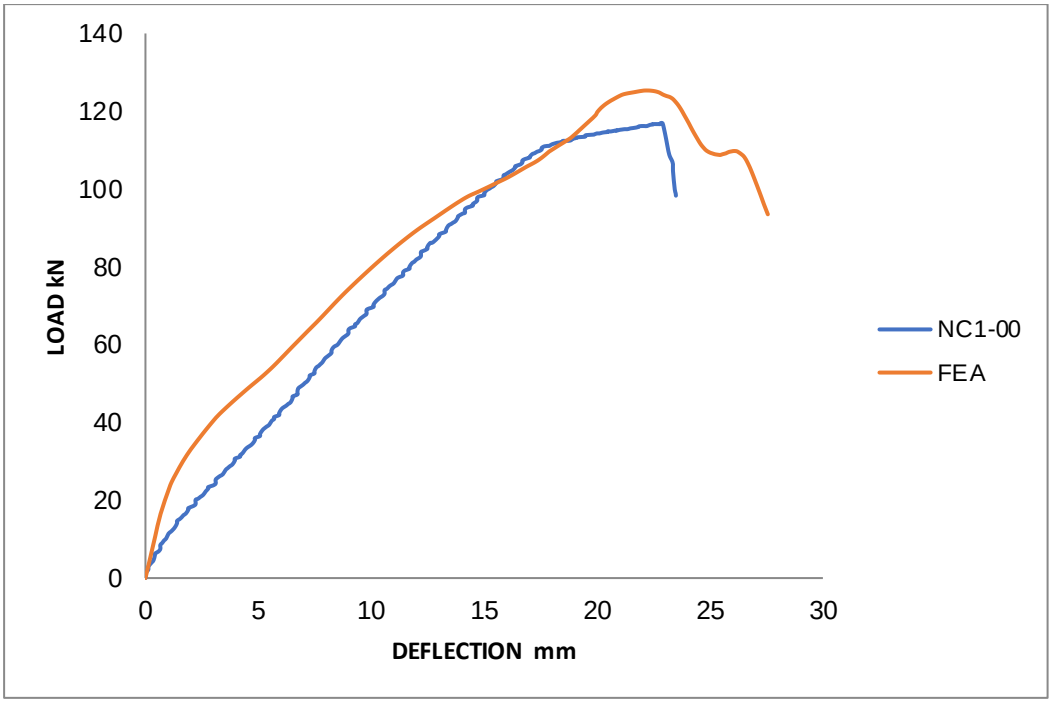

Figure 5-20: Load-displacement curves' comparison between the FEM and the experimental work results for NC1-00

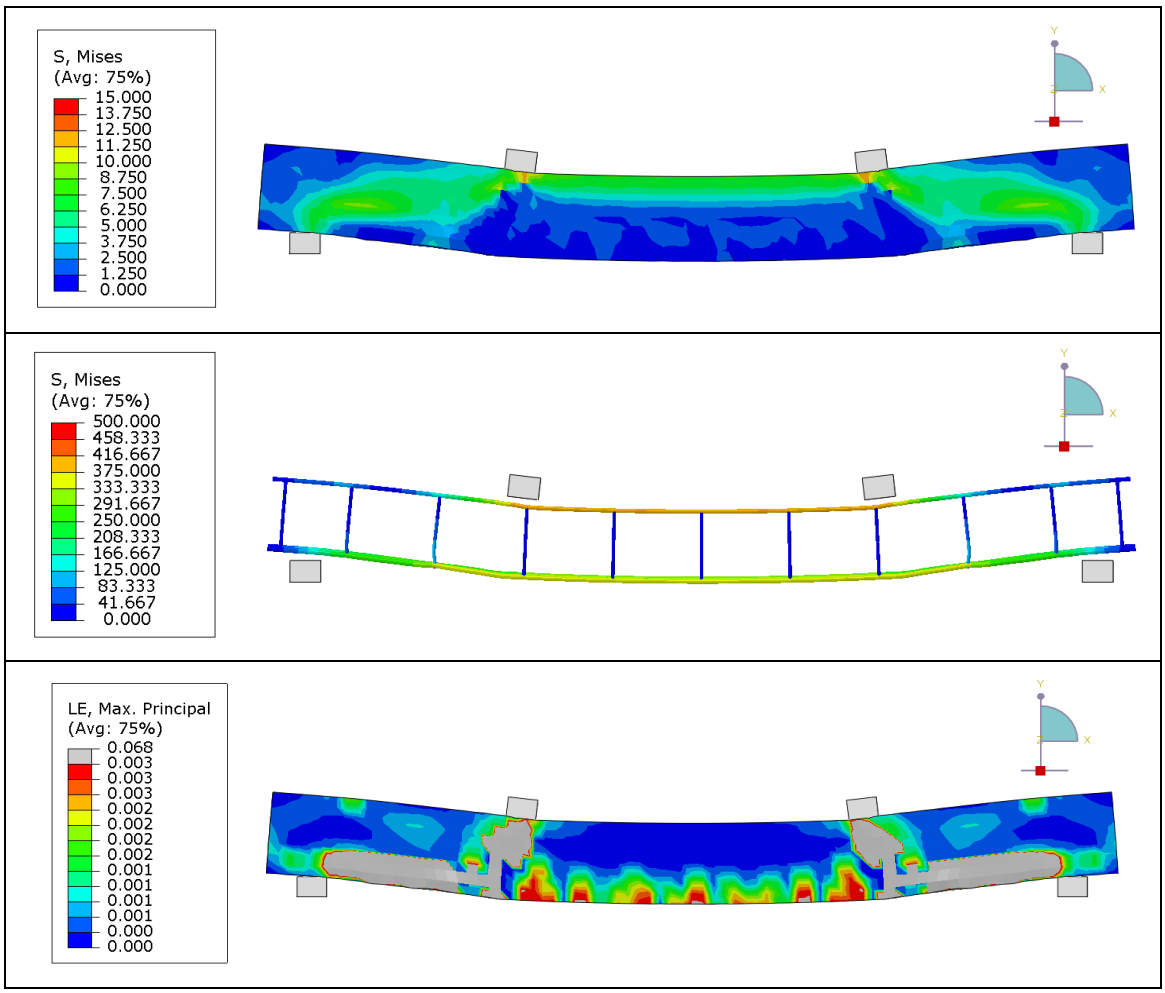

Figure 5-21: Von Mises stress distribution for concrete beam and steel reinforcement, in addition to the max. principal true strain of the beam (from top to bottom), NC1-00.

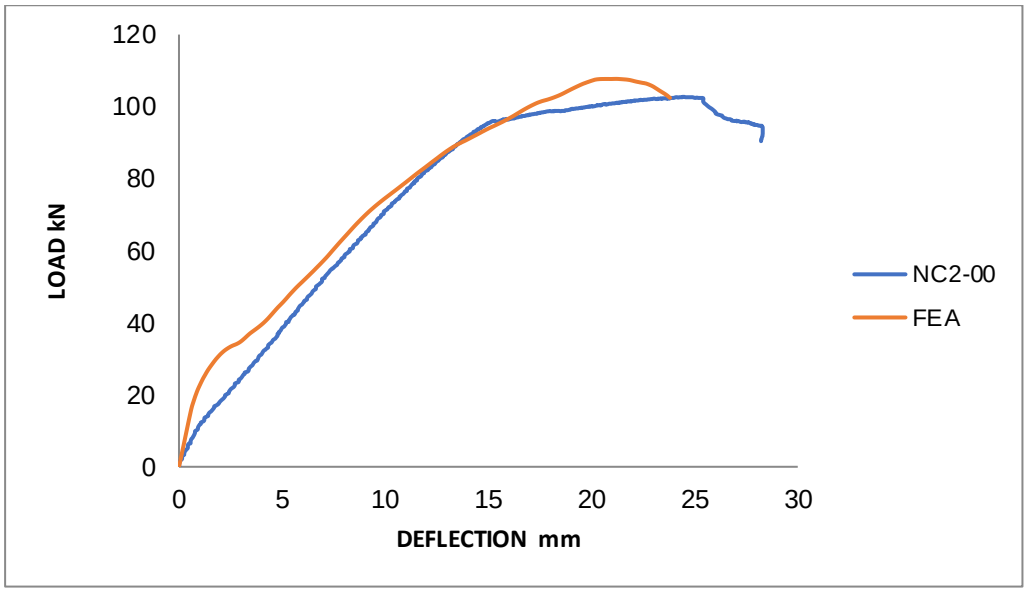

Figure 5-22: Load-displacement curves' comparison between the FEM and the experimental work results for NC2-00

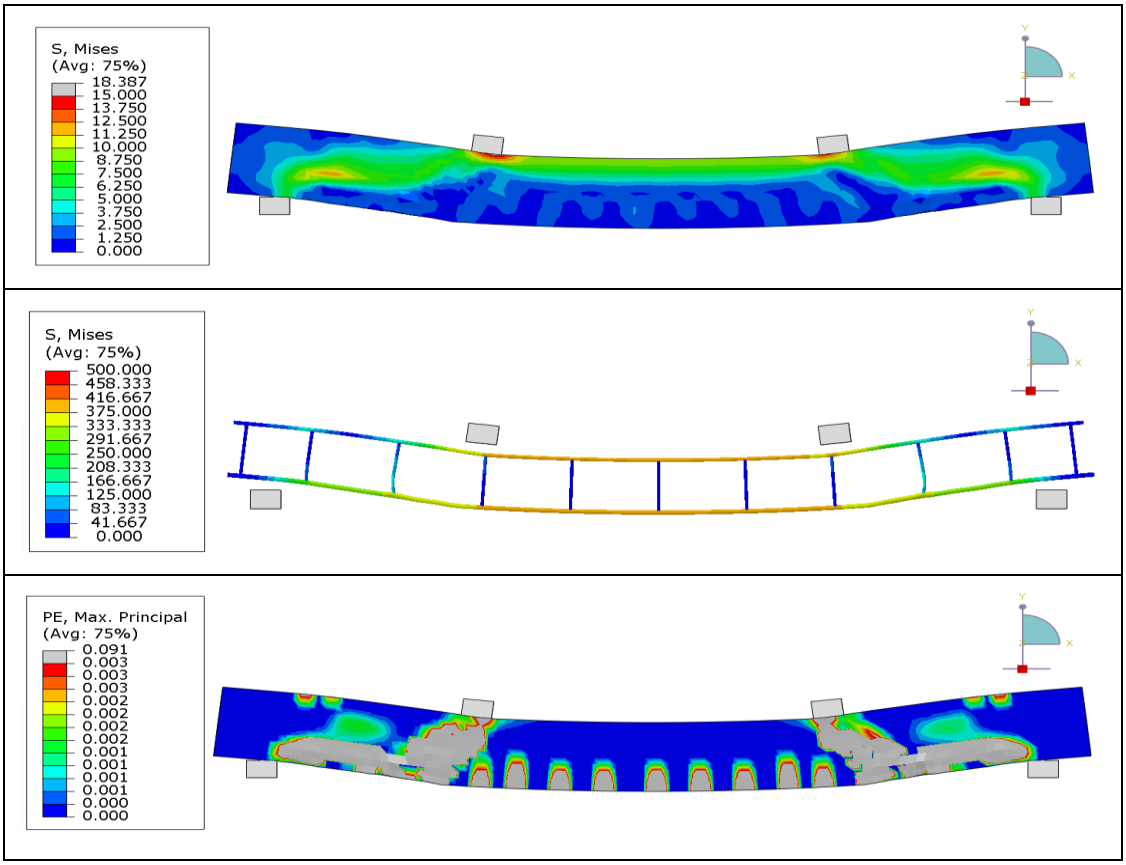

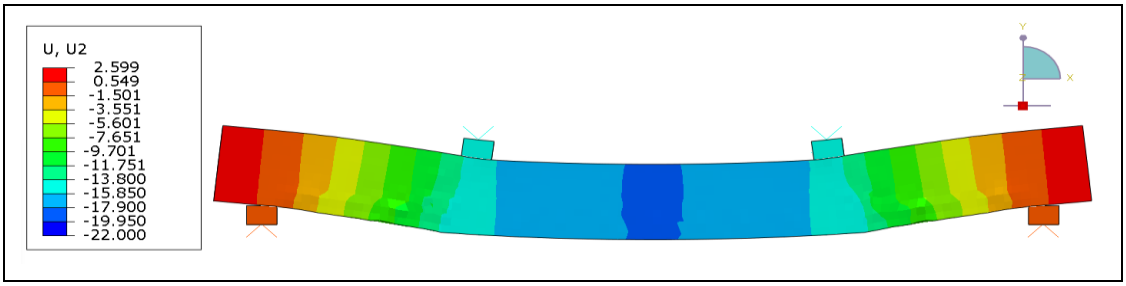

Figure 5-23: Von mises stress for the beam and steel reinforcement, plastic strain and deflection of NC2-00

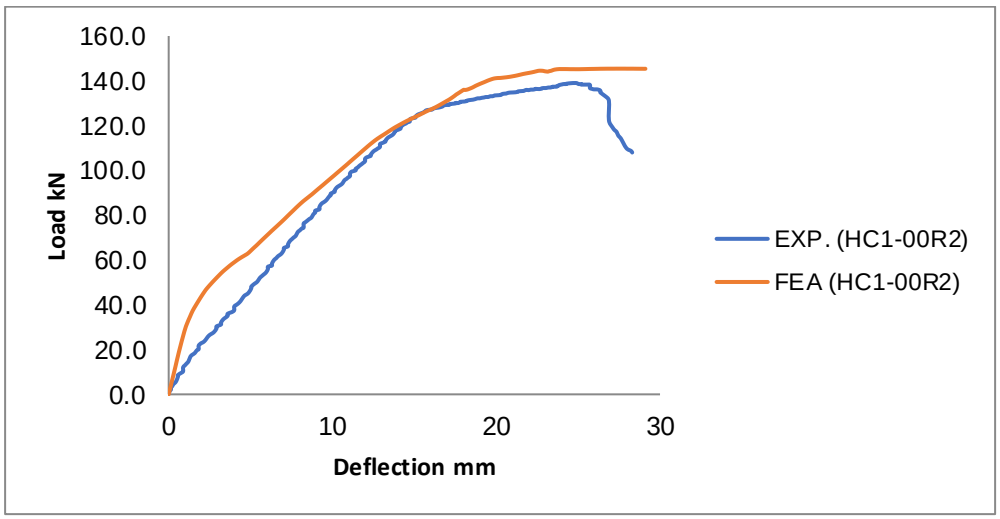

Figure 5-24: Load-displacement curves' comparison between the FEM and the experimental work results for HC1-00

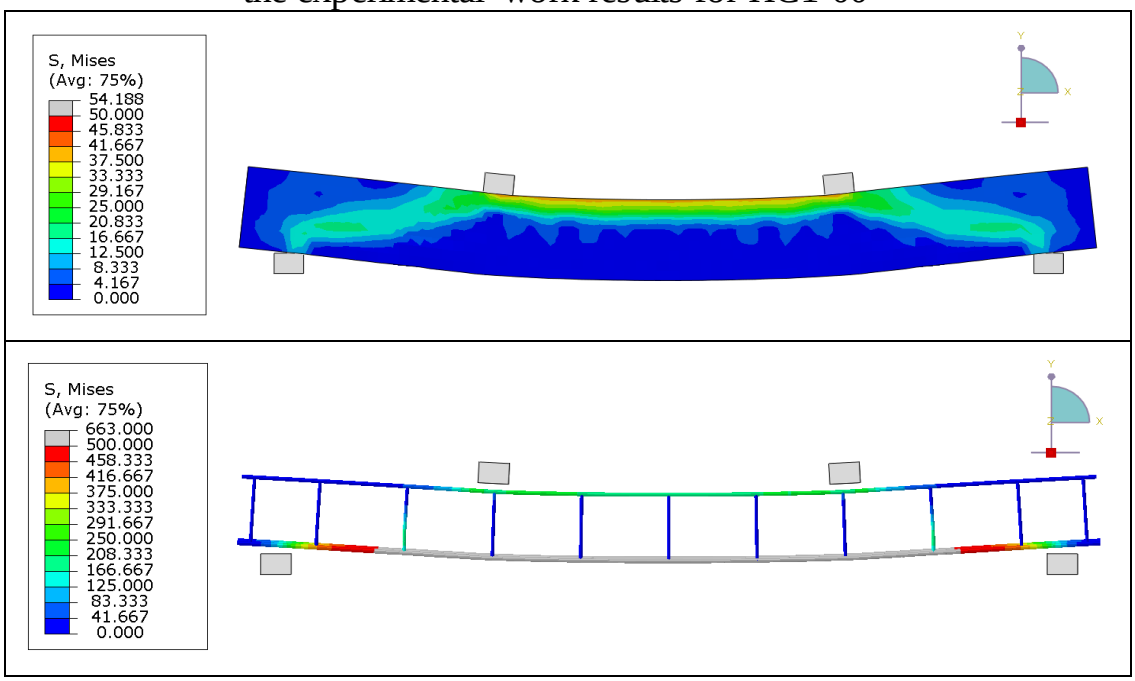

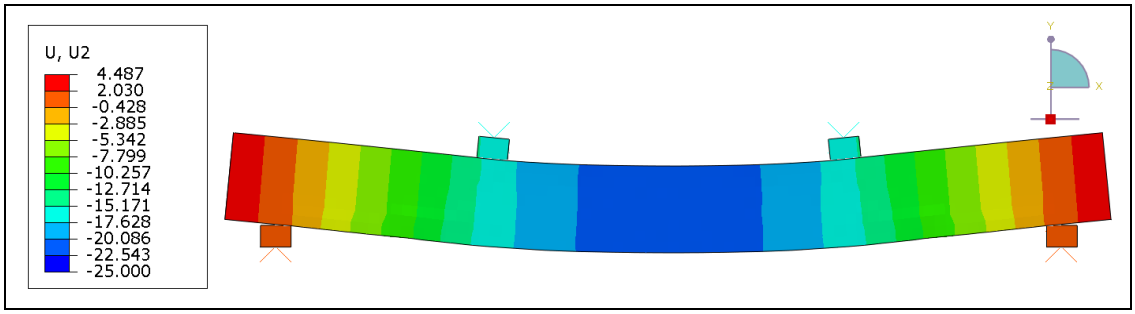

Figure 5-25: Von mises stress for the beam and steel reinforcement, and deflection of HC1-00

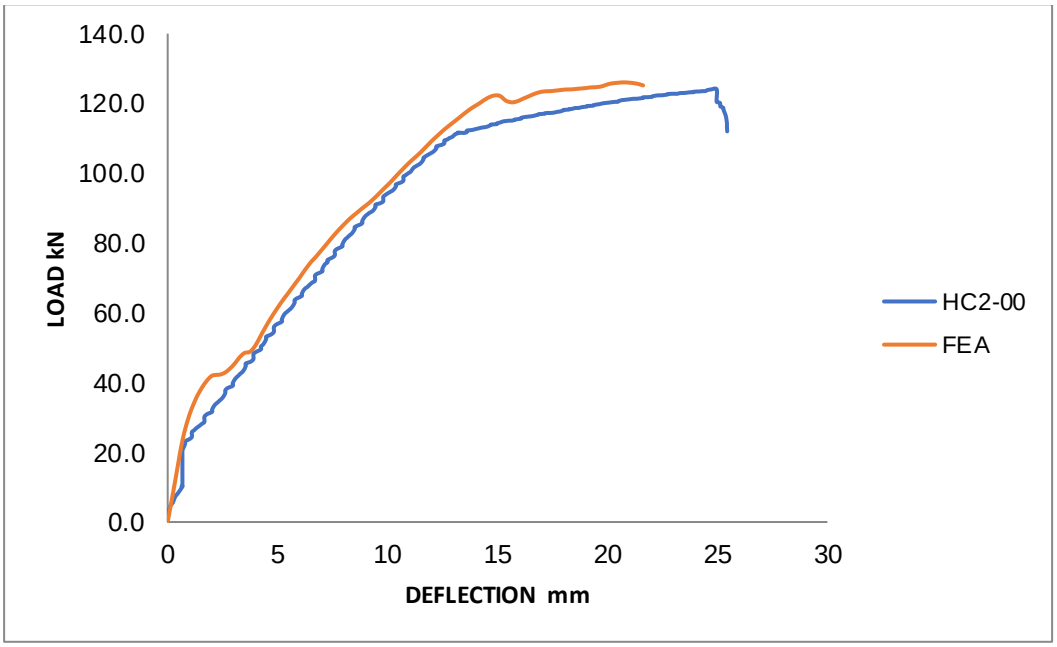

Figure 5-26: Load-displacement curves' comparison between the FEM and the experimental work results for HC2-00

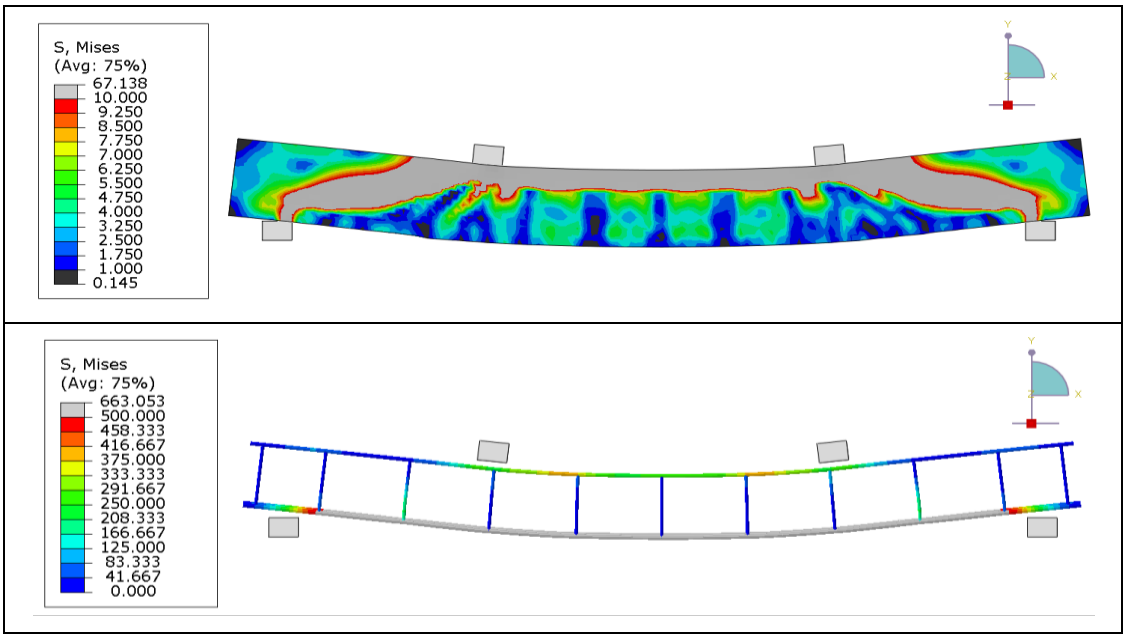

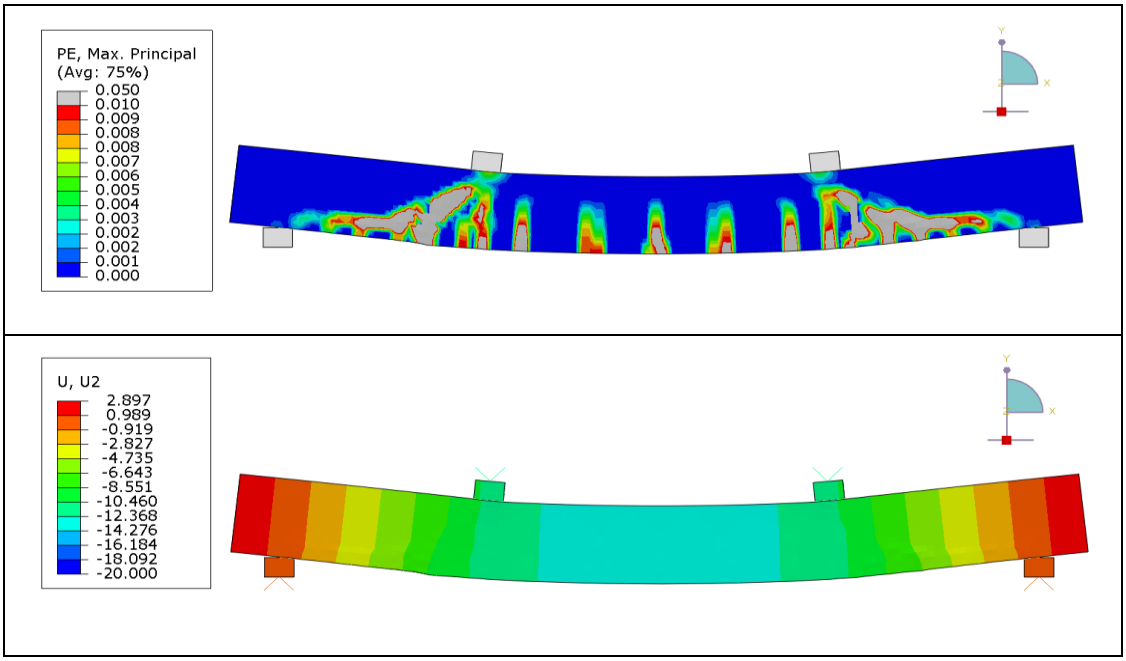

Figure 5-27: Von mises stress for the beam and steel reinforcement, plastic strain and deflection of HC2-00 at the maximum load capacity.

5.7.2 Stage B: Validation Results of Time- Temperature Distribution Along the Beam Cross Section and Simulation Results

The heat transfer analysis of a LECA beam sample have shown very close results to those data extracted from the experimental work. As can be seen in Figure (5-29), and after applying TC1 amplitude curve as heating boundary to the beam surfaces, the nodal temperature parameter at the bottom steel position have shown very close result after 1 hour of heating compared to the experimental data (at TC2 location), which was approximately about 2%. While a small vibration was observed after half of an hour heating for the same location, which was about less than 10%. Moreover, there was an observable gap between the experimental and the numerical curves ranged from 10 min to 30 min, after 30 min of heating, the curves are gradually become very close to each other. In the contrary to the temperature curve at the mid of the concrete beam location (TC3), where, approximately the numerical behavior matches the experimental one most of heating time.

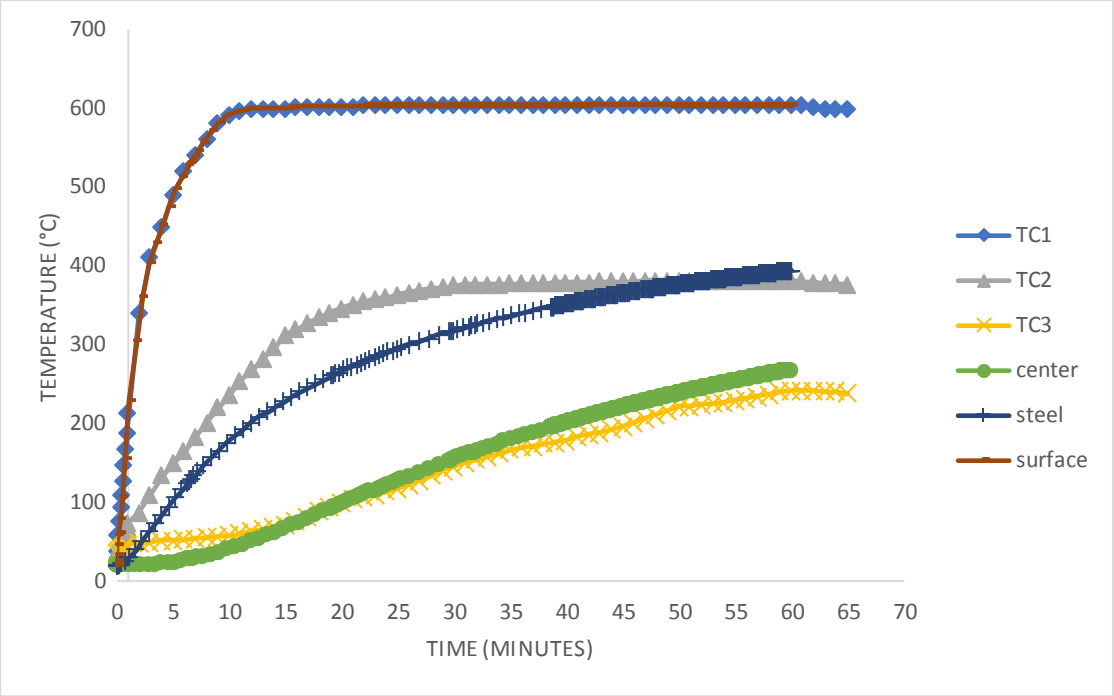
700
600
500
400
300
200
100
0
TEMPERATURE (°C)
0 5 10 15 20 25 30 35 40 45 50 55 60 65 70
TIME (MINUTES)
TC1
TC2
TC3
center
steel
surface

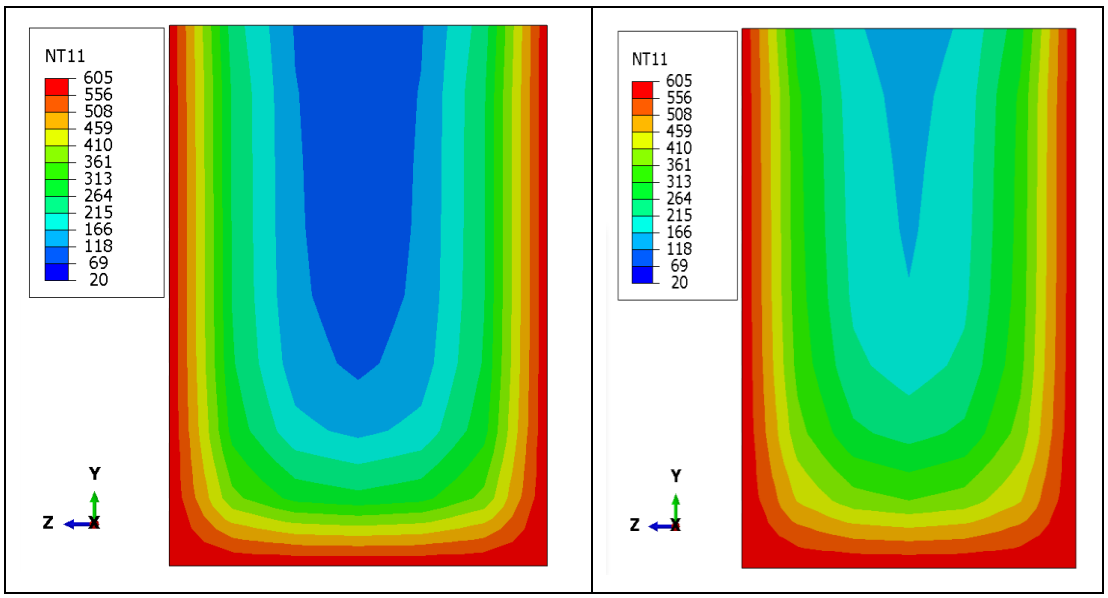
NT11
605
556
508
459
410
361
313
264
215
166
118
69
20
Y
Z
X
NT11
605
556
508
459
410
361
313
264
215
166
118
69
20
Y
Z
X

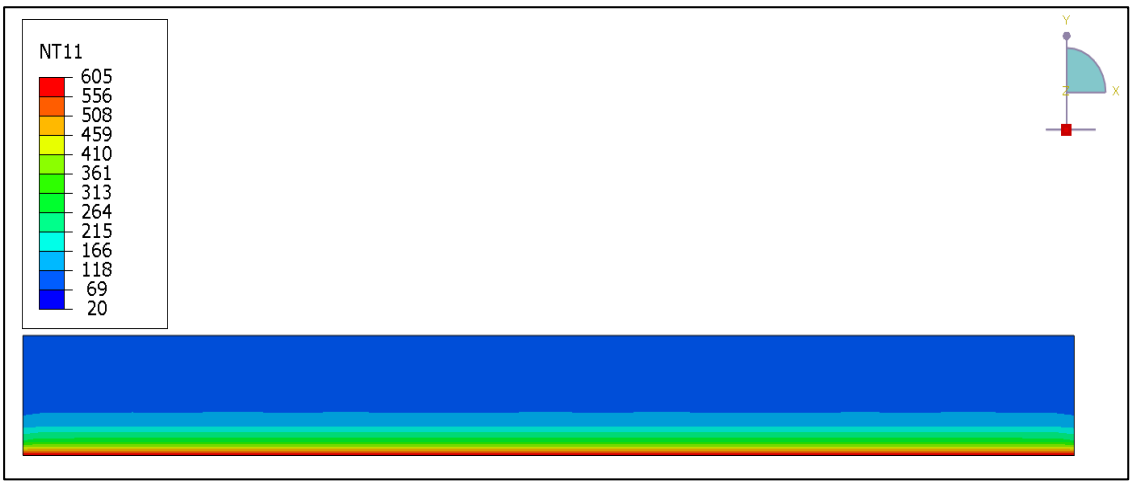
NT11
605
556
508
459
410
361
313
264
215
166
118
69
20

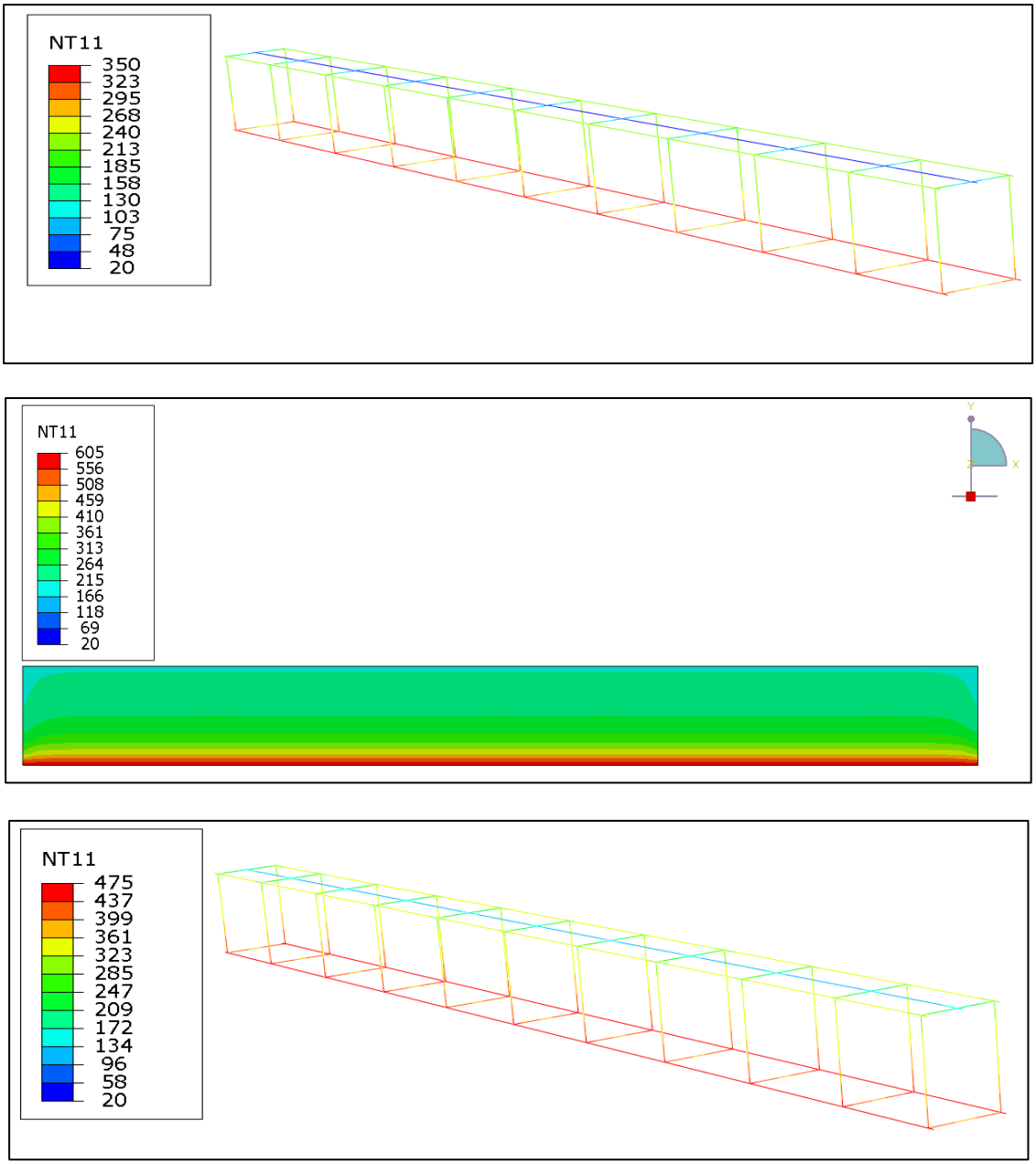

Figure 5-28: Time- temperature distribution along the beam cross section

5.7.3 FEA Results of NSC Beams at Elevated Temperatures

Figure (5-30) illustrates the measured Load carrying capacity verses the midspan deflection of NC1-02 specimen based on the numerical and the experimental results. Form the Figure, it can be observed a good agreement have noticed when compared the both mentioned curves results. The elastic stage of the FEA result was perfectly fitted the experimental curve. While slight variations the inelastic phase have been observed after 30 KN of loading. In addition, it is clear the midspan displacement corresponded the maximum load

capacity was approximately the same. Furthermore, a noticeable variation in the degradation phase was observed. Overall, the percentage of error between the experimental and numerical results for the load capacity and midspan displacement were about 7.05% and 1.65%, respectively. Figure (5-31) illustrate von mises distribution contour map stress, plastic strain, von mises of steel bars, and downward displacement distribution contour maps.

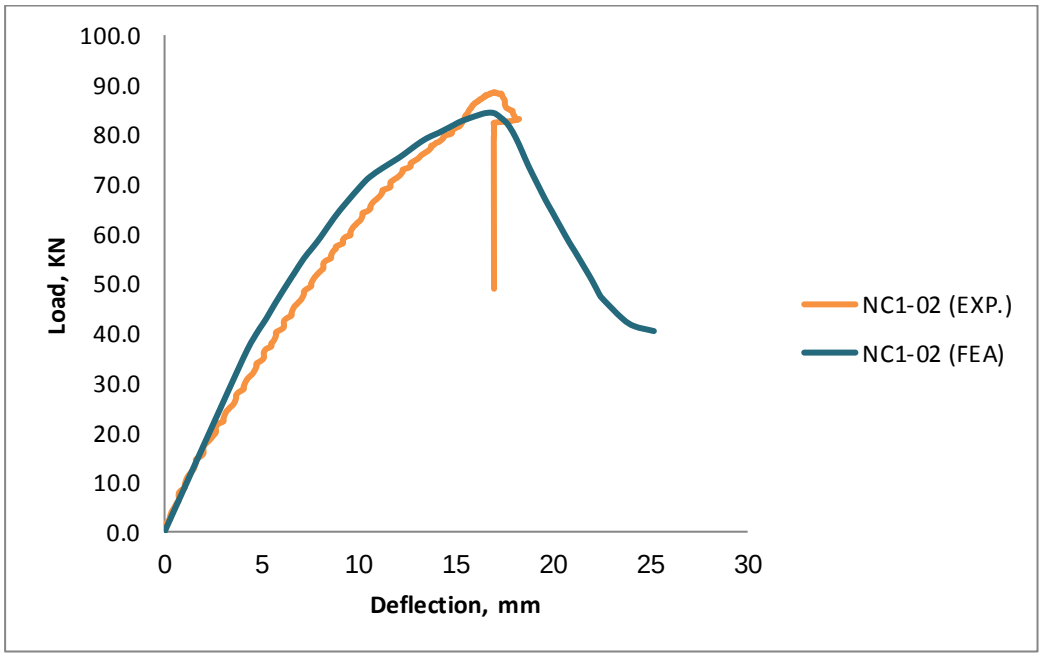

Figure 5-29: Comparison between load-mid span deflection curves of the FEM and the experimental work for NC1-02

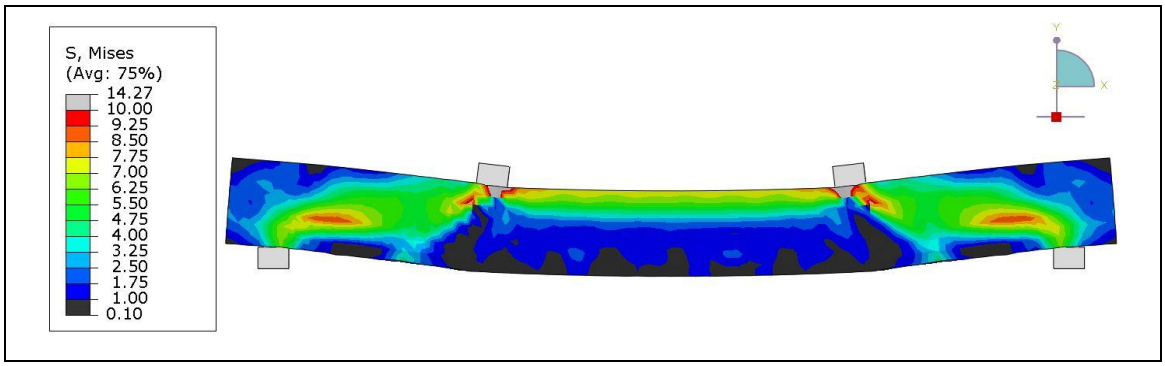

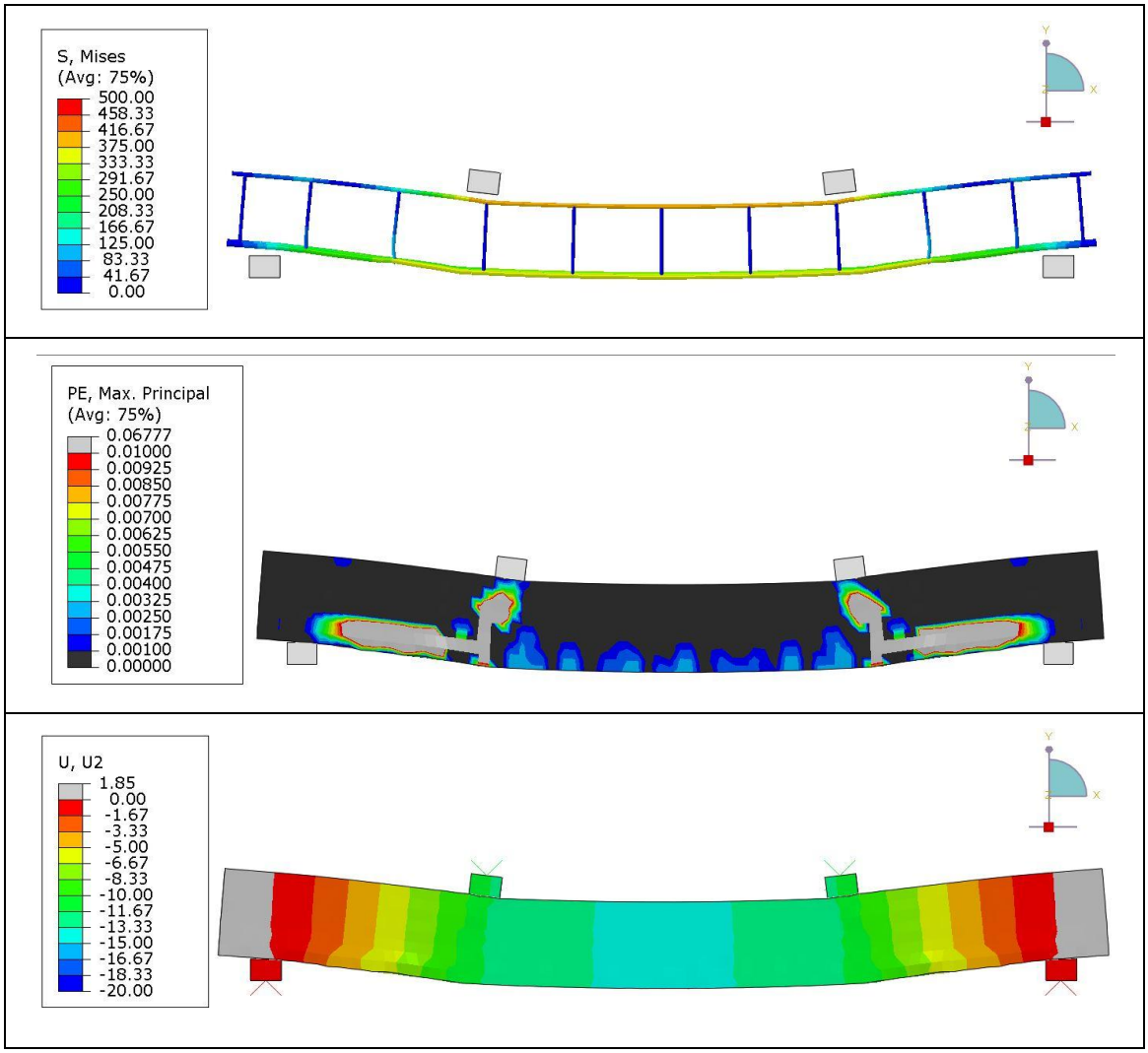

Figure 5-30: Von mises stress for the beam and steel reinforcement, plastic strain and deflection of NC1-02 at the maximum load capacity.

5.7.3.1 Normal Cover 30 mm- 1 Hour Fire

Figure (5-32) illustrates the measured Load carrying capacity verses the midspan deflection of NC1-02 specimen based on the numerical and the experimental results. Form the previous Figure, it can be observed a good agreement have noticed when compared the both mentioned curves results. The elastic stage of the FEA result was perfectly fitted the experimental curve. While slight variations the inelastic phase have been observed after 35 KN of loading. In addition, it is clear the midspan displacement corresponded the maximum load capacity was approximately the same.

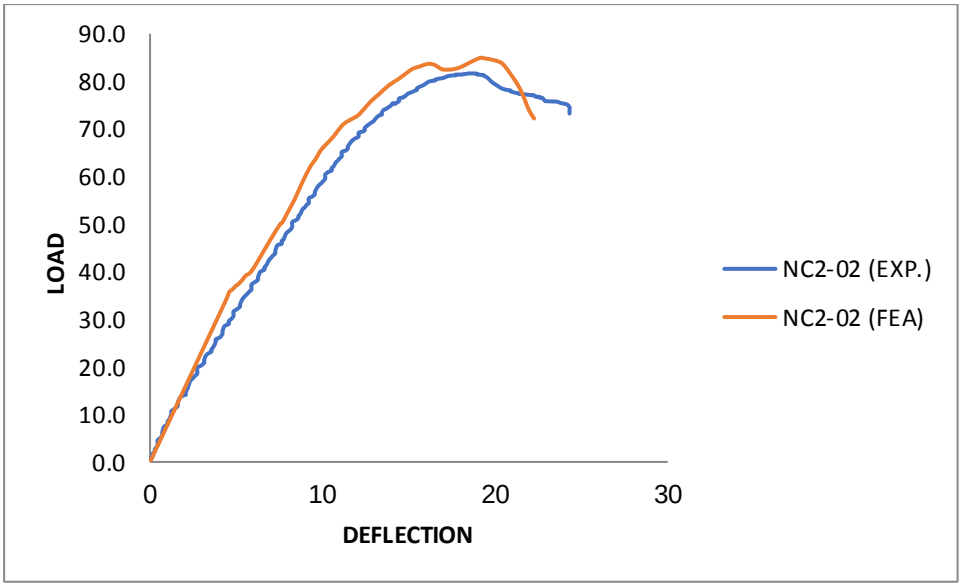

Figure 5-31: Comparison between load-mid span deflection curves of the FEM and the experimental work for NC2-02

Furthermore, a noticeable variation in the degradation phase was observed. Overall, the percentage of error between the experimental and numerical results for the load capacity and midspan displacement were about 4.1% and 4.3%, respectively. Figures (5-33) illustrate von mises distribution contour map stress, plastic strain, von mises of steel bars, and downward displacement distribution contour maps.

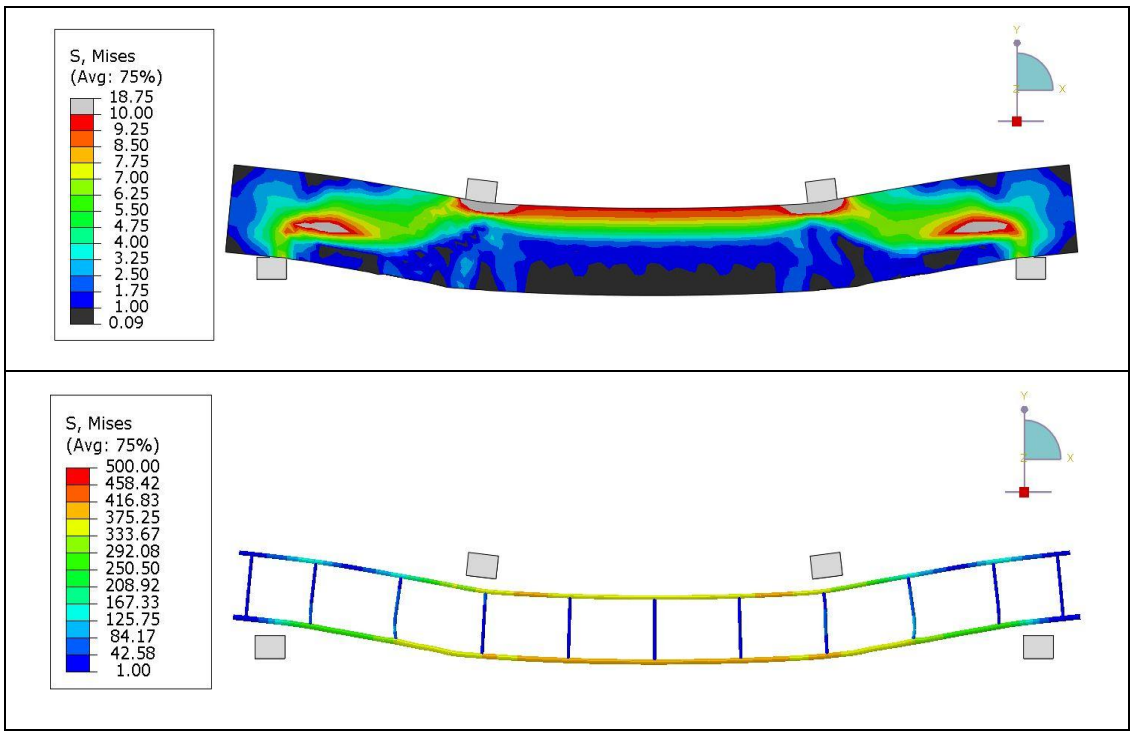

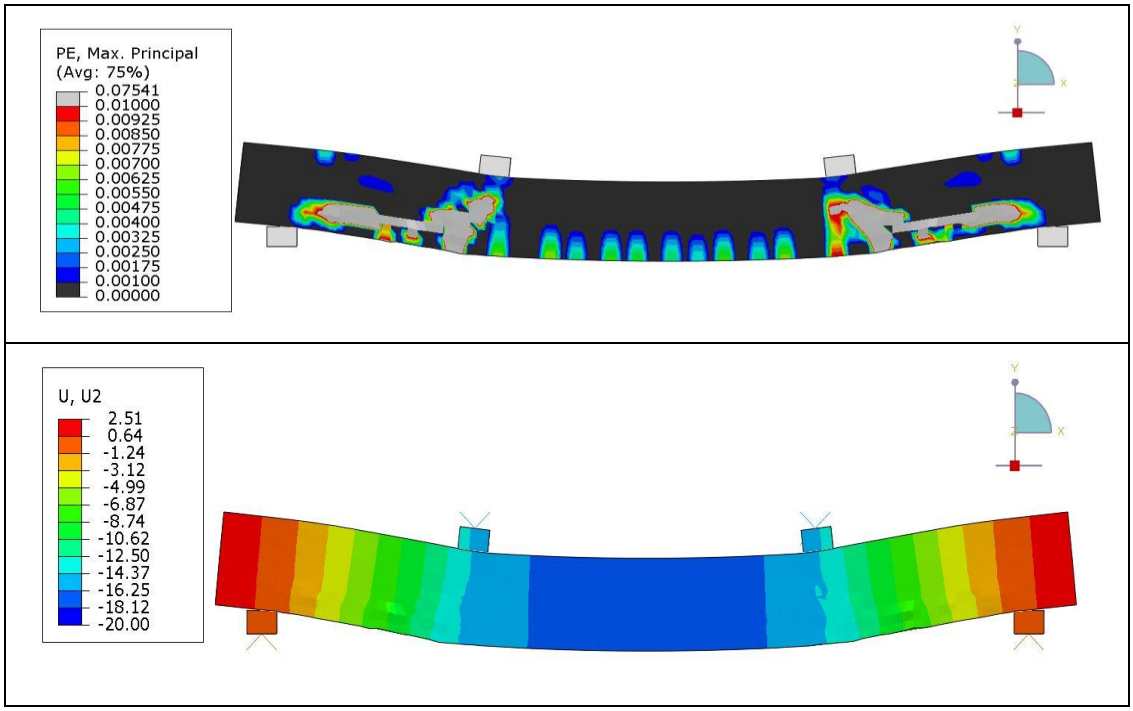

Figure 5-32: Von mises stress for the beam and steel reinforcement, plastic strain and deflection of NC2-02 at the maximum load capacity.

5.7.4 FEA Results of HSC Beams at Elevated Temperatures

5.7.4.1 High Strength Concrete Cover 30 mm- 1 Hour Fire

Load- displacement curves results for both experimental and numerical processes for HC1-02 specimens are shown in Figure (5-34). The percentage of error between the FEM and the experimental results for the peak load and corresponded downward displacement were about 6.78% and 10.97%, respectively. In addition, it can be observed that both curves were matched to each other till 15 mm displacement. Moreover, the degradation phase of the FEM process was higher than of the experimental result's curve. Figures (5-35) illustrate von mises distribution contour map stress, plastic strain, von mises of steel bars, and downward displacement distribution contour maps.

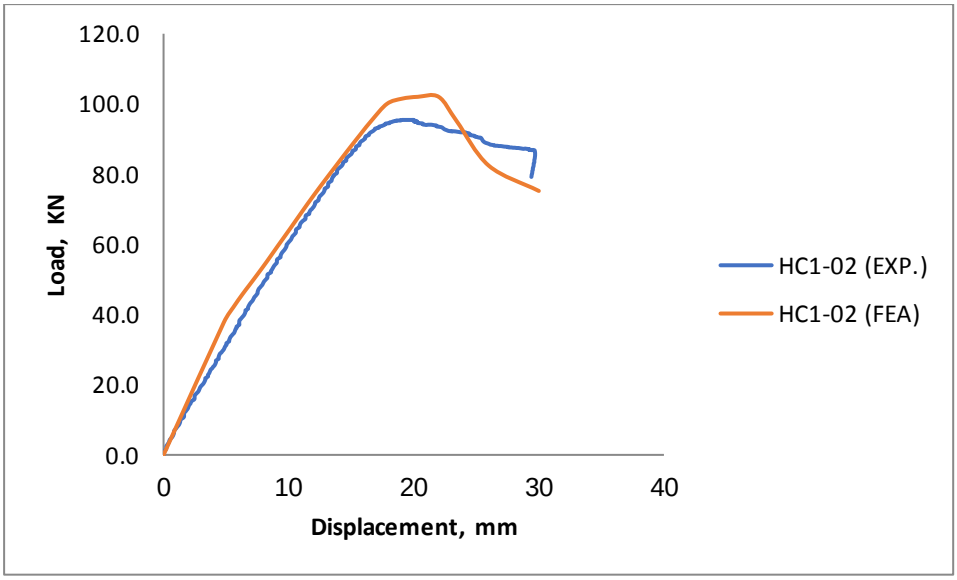

Figure 5-33: Comparison between load-mid span deflection curves of the FEM and the experimental work for HC1-02

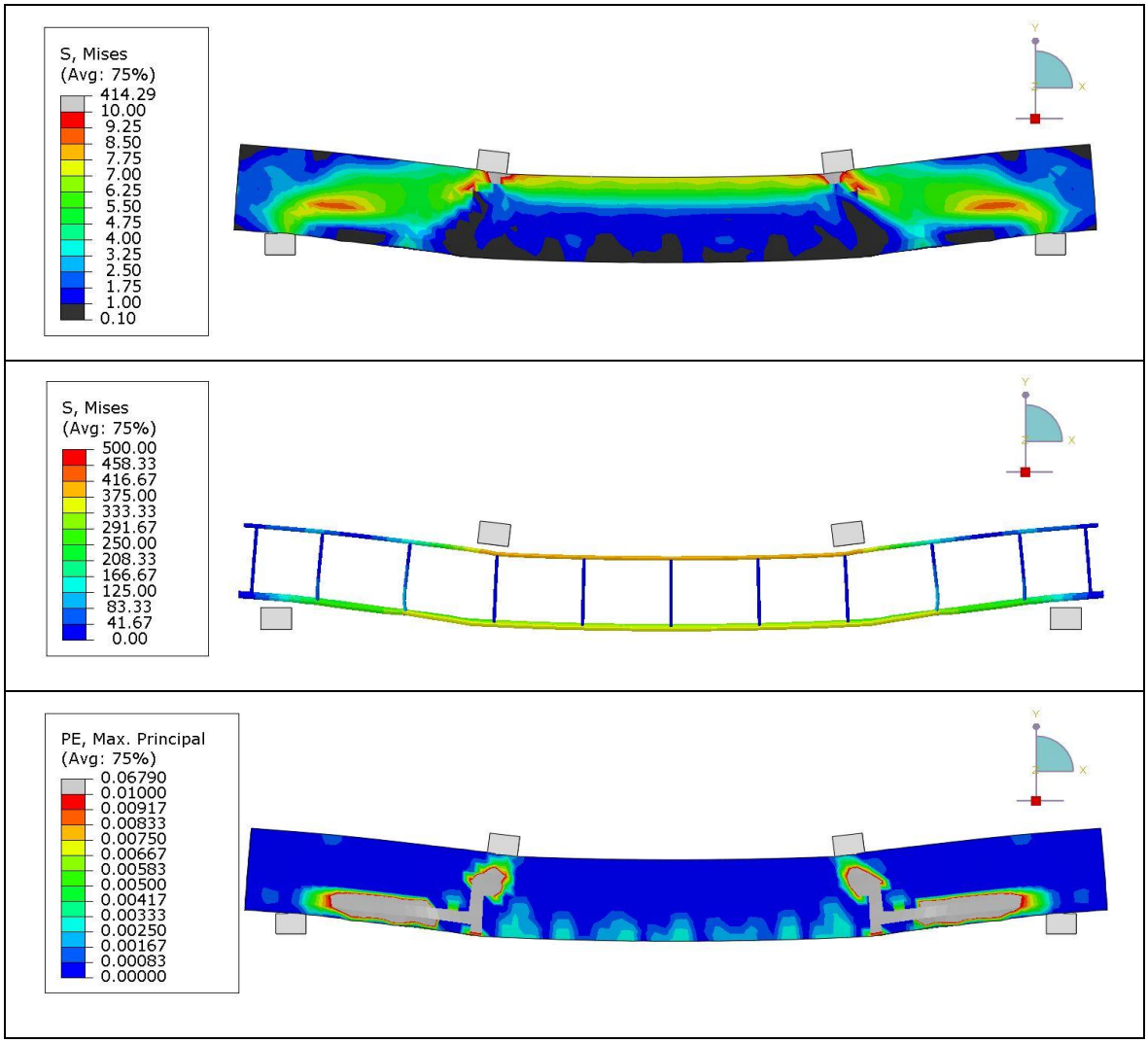

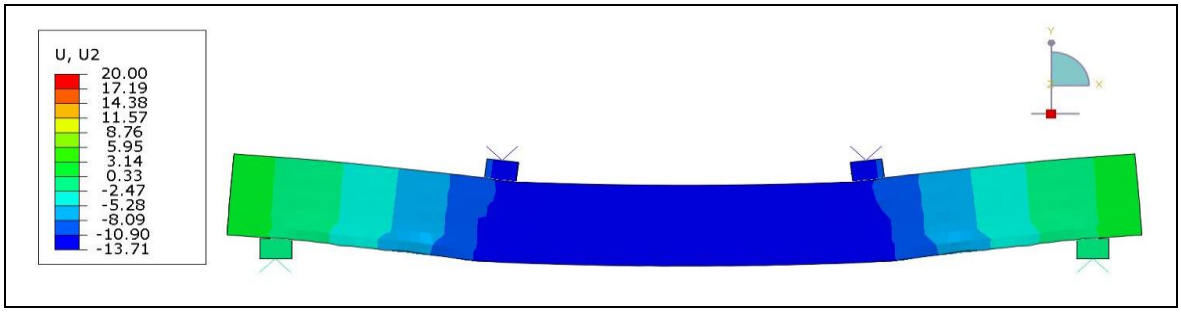

Figure 5-34: Von mises stress for the beam and steel reinforcement, plastic strain and deflection of HC1-02 at the maximum load capacity.

Figure (5-36) illustrates the measured Load carrying capacity verses the midspan deflection of HC2-02 specimen based on the numerical and the experimental results. Form the mentioned Figure, it can be observed a good agreement have noticed when compared the both mentioned curves results. The elastic stage of the FEA result was approximately matching the experimental curve in the first phase. While a smooth transition in FEM curve was observed in the contrary to the experimental one. This is because of tension stiffening parameter. In addition, it is clear the midspan displacement corresponded the maximum load capacity was somewhat varied. Overall, the percentage of error between the experimental and numerical results for the load capacity and midspan displacement were about 1.85% and 9.41%, respectively. Figure (5-37) illustrates von mises distribution contour map stress, plastic strain, von mises of steel bars, and downward displacement distribution contour maps.

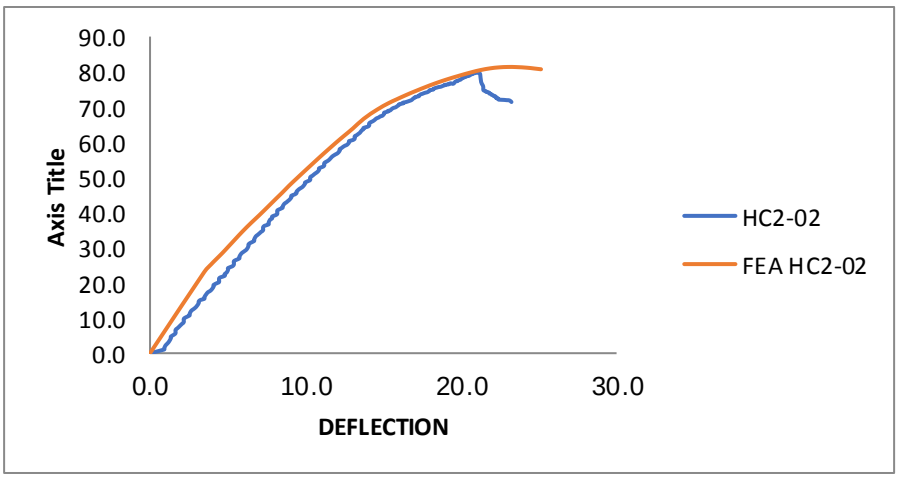

Figure 5-35: Comparison between load-mid span deflection curves of the FEM and the experimental work for HC2-02

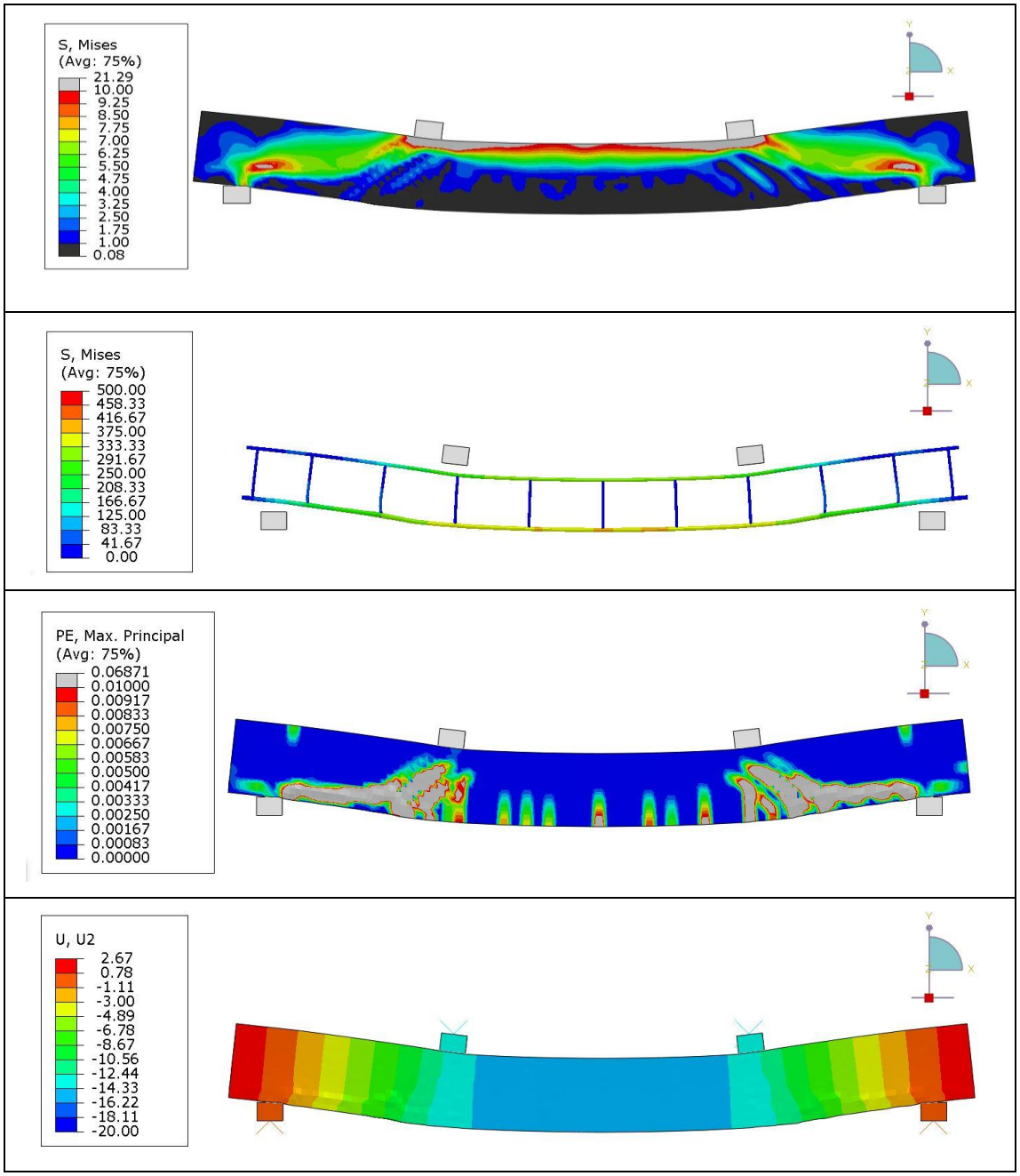

Figure 5-36: Von mises stress for the beam and steel reinforcement, plastic strain and deflection of HC2-02 at the maximum load capacity.

5.7.5 Stage C: Validation Results of Postfire Treated NSC And HSC Beams with SIFCON Jacket

5.7.5.1 Normal Strength Concrete Specimens

Figure (5-38) illustrates the measured Load carrying capacity verses the midspan deflection of NC1-22 specimen based on the numerical and the experimental results. The first phase matches the experimental results up to 3.7 mm displacement. After such limit, the FEM curve load was noticeably higher

the load values of the experimental result. Up to the maximum load carrying capacity, a slight difference between the experimental and FEM result of the load and corresponded displacement of about 3.88% and 0.96%, respectively. followed that point, the FEM degradation behavior curve style matches the experimental curve behavior. Figures (5-39) illustrate von mises distribution contour map stress, plastic strain, von mises of steel bars, and downward displacement distribution contour maps.

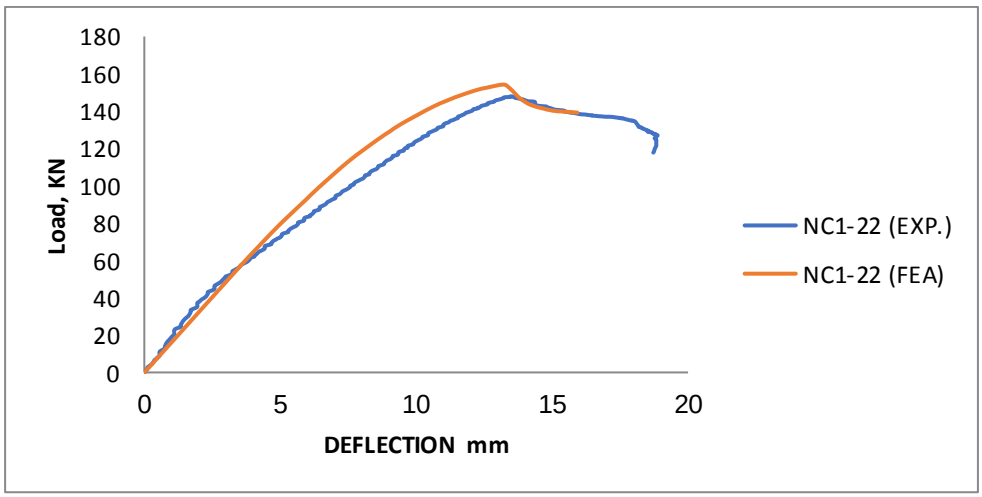

Figure 5-37: Comparison between load-mid span deflection curves relation of the FEM and the experimental work for NC1-22

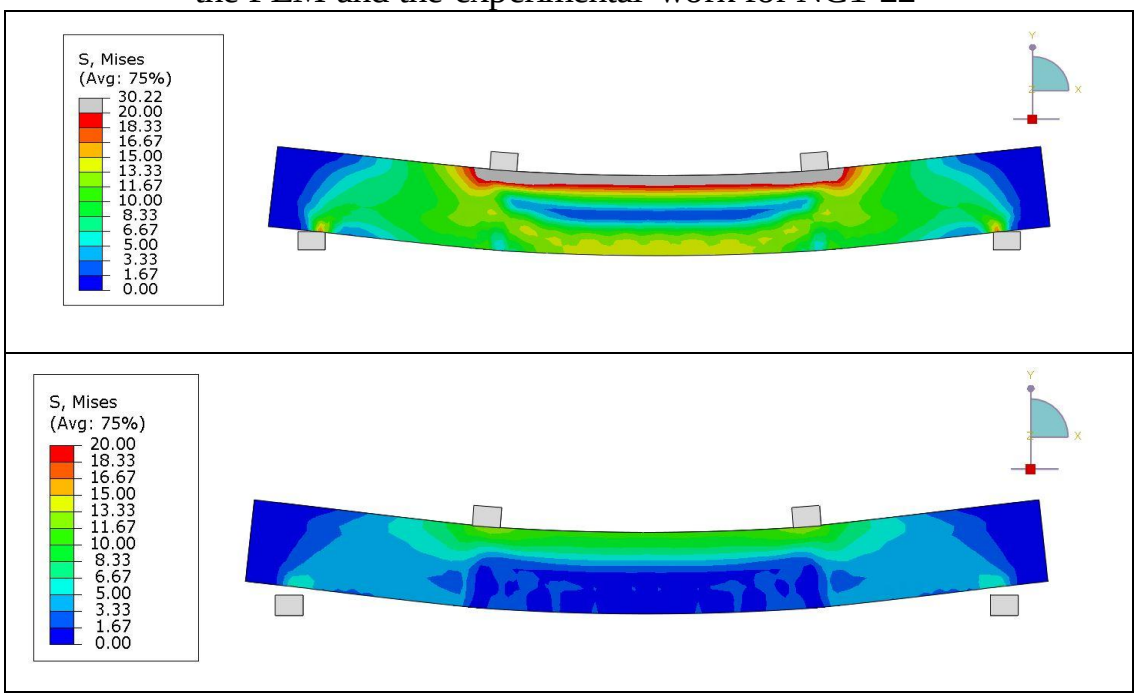

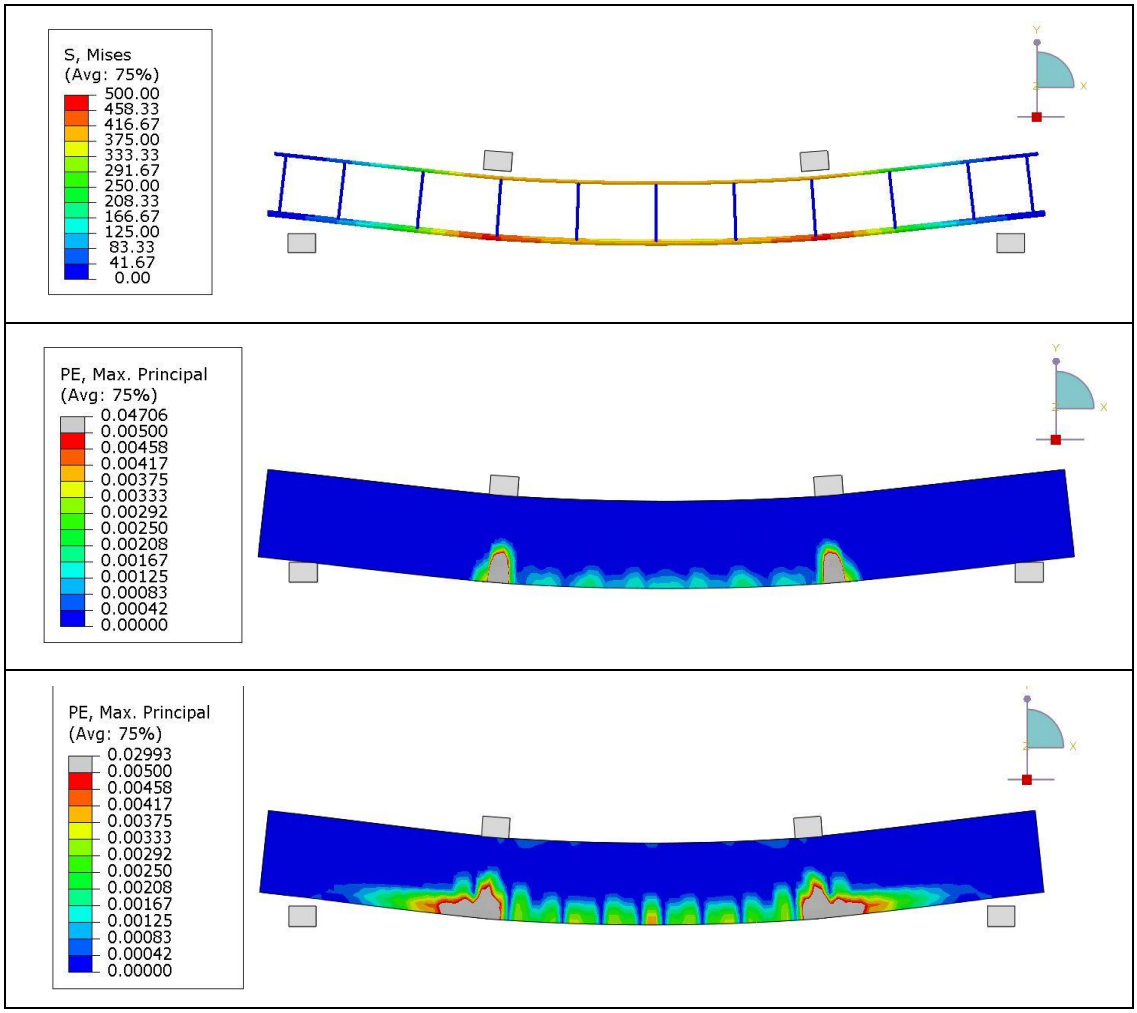

Figure 5-38: Von mises stress for the beam with and without SIFCON, Von mises stress of steel reinforcement, plastic strain for the beam for SIFCON and the beam NC1-22 at the maximum load capacity.

Figure (5-40) illustrates the measured Load carrying capacity verses the midspan deflection of NC1-32 specimen based on the numerical and the experimental results. The first phase matches the experimental results up to 4.1 mm displacement. After such limit, the FEM curve load was noticeably higher the load values of the experimental result. Up to the maximum load carrying capacity, a slight difference between the experimental and FEM result of the load and corresponded displacement of about 9.29% and 0.73%, respectively. Followed that point, the FEM degradation behavior curve style matches the experimental curve behavior. Figure (5-41) illustrates von mises distribution contour map stress, plastic strain, von mises of steel bars, and downward displacement distribution contour maps.

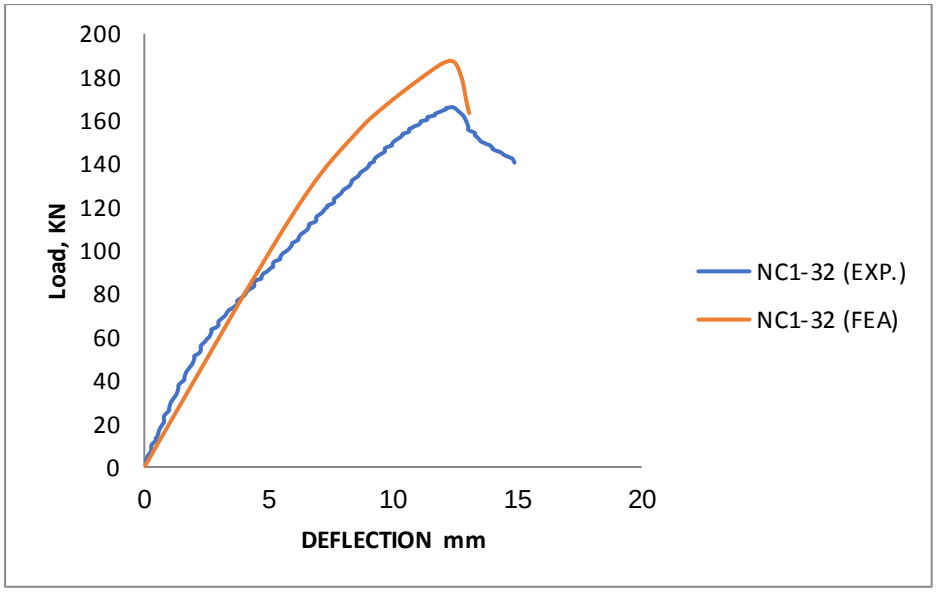

Figure 5-39: Comparison between load-mid span deflection curves of the FEM and the experimental work for NC1-32

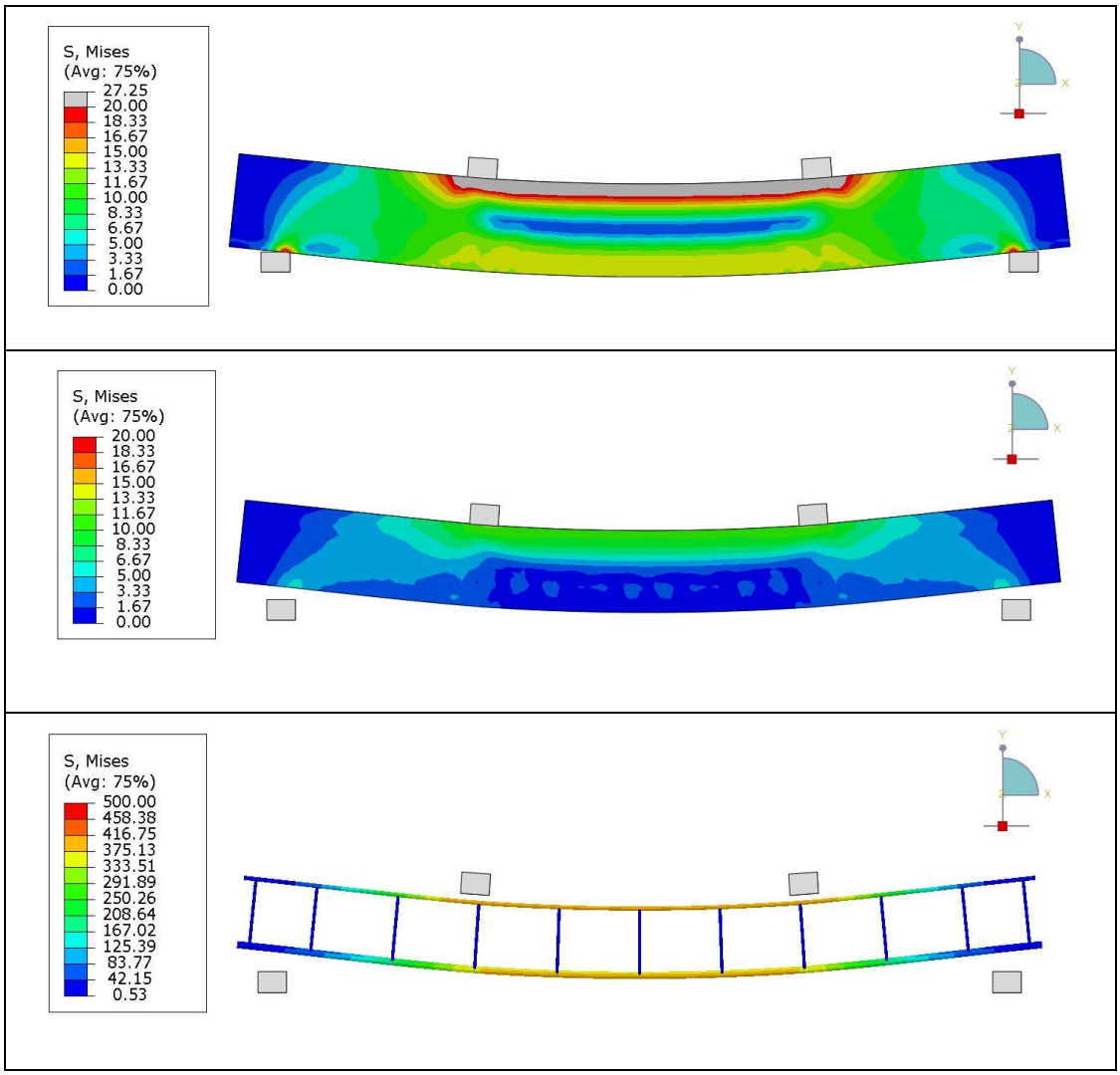

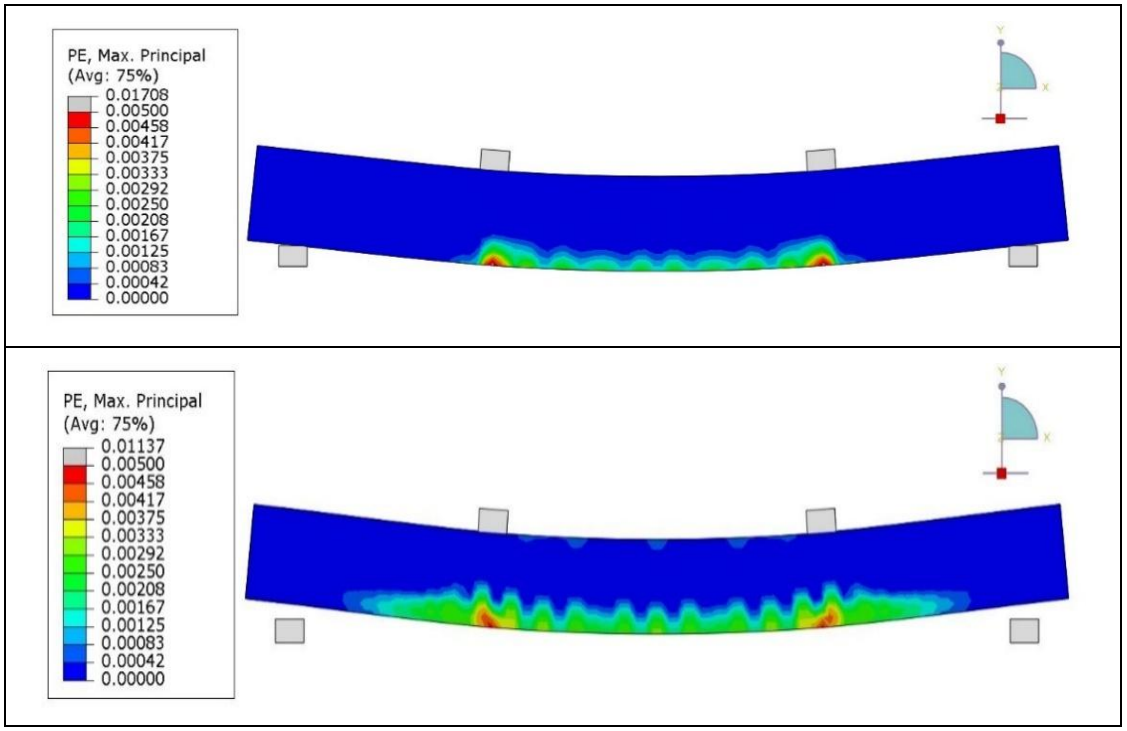

Figure 5-40: Von mises stress for the beam with and without SIFCON, Von mises stress of steel reinforcement, plastic strain for the beam for SIFCON and the beam NC1-32 at the maximum load capacity.

Figure (5-42) illustrates the measured Load carrying capacity verses the midspan deflection of NC2-22 specimen based on the numerical and the experimental results. Form the Figure, it can be noticed a big difference when comparing the both mentioned curves results. The elastic stage of the FEA result was perfectly fitted the experimental curve. While a noticeable variation the inelastic phase has been observed after 73 KN of loading. Furthermore, a slight variation in the degradation phase was observed. Overall, the percentage of error between the experimental and numerical results for the maximum load capacity and the corresponded midspan displacement were about 15.61% and 8.82%, respectively. Figure (5-43) illustrates von mises distribution contour map stress, plastic strain, von mises of steel bars, and downward displacement distribution contour maps.

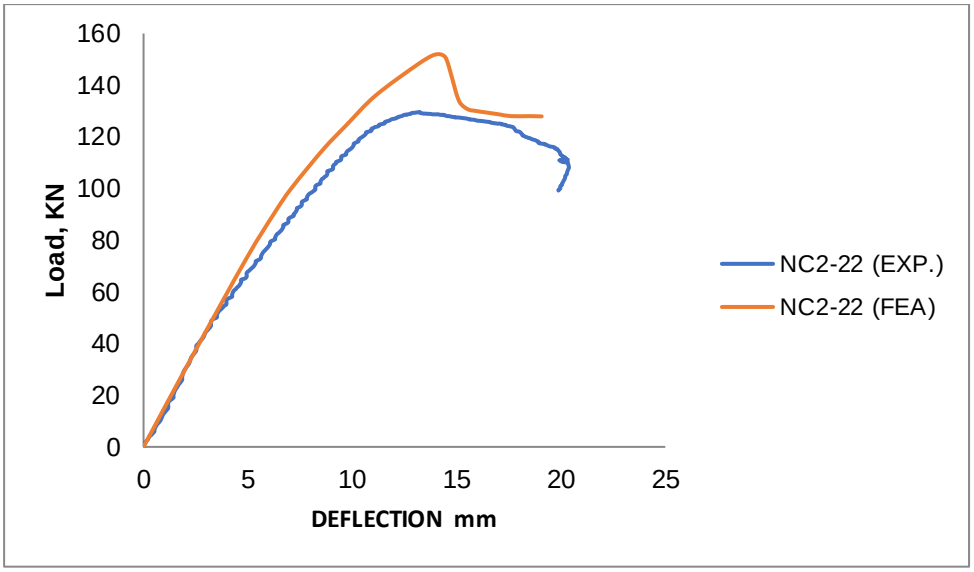

Figure 5-41: Comparison between load-mid span deflection curves of the FEM and the experimental work for NC2-22

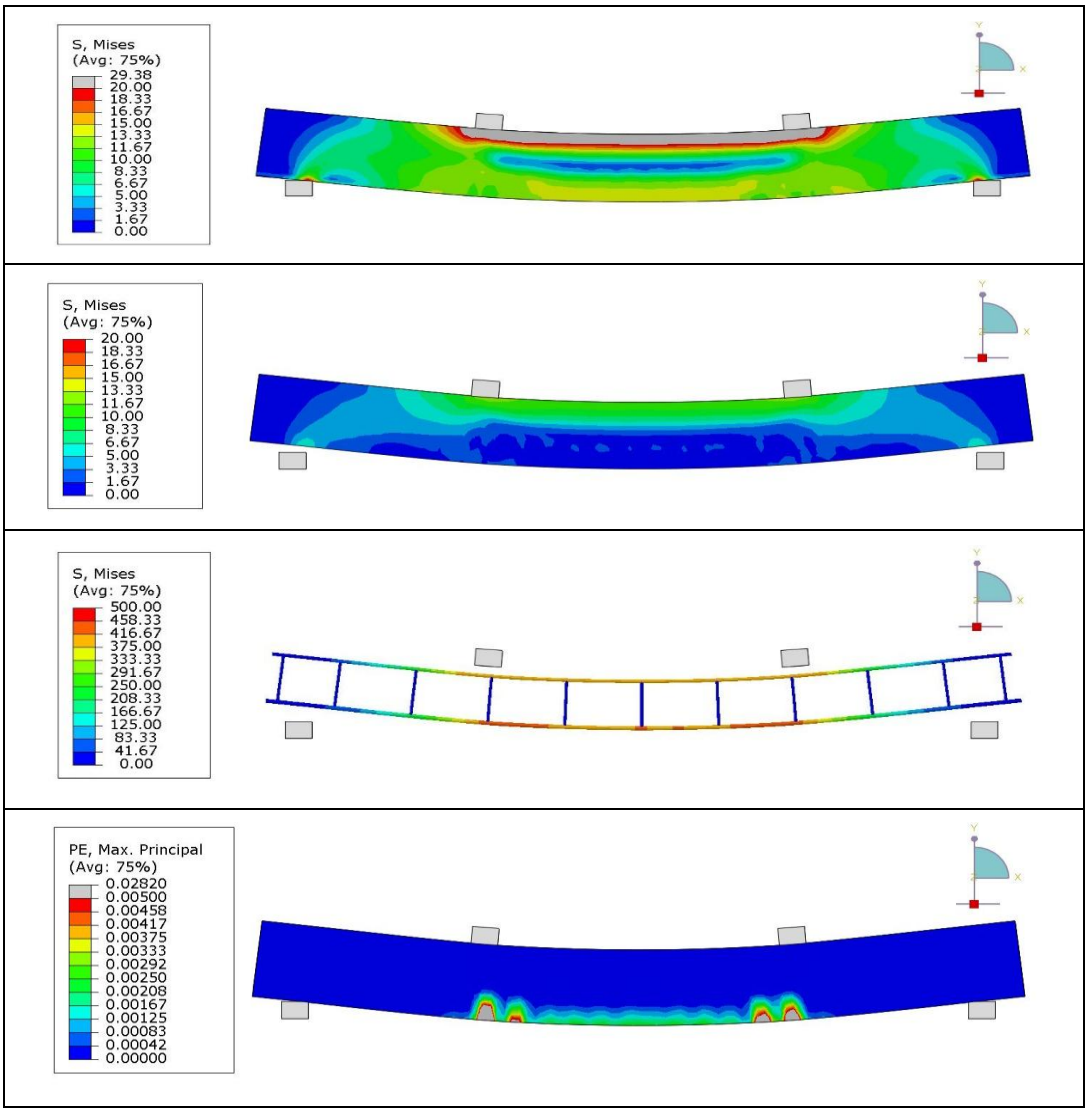

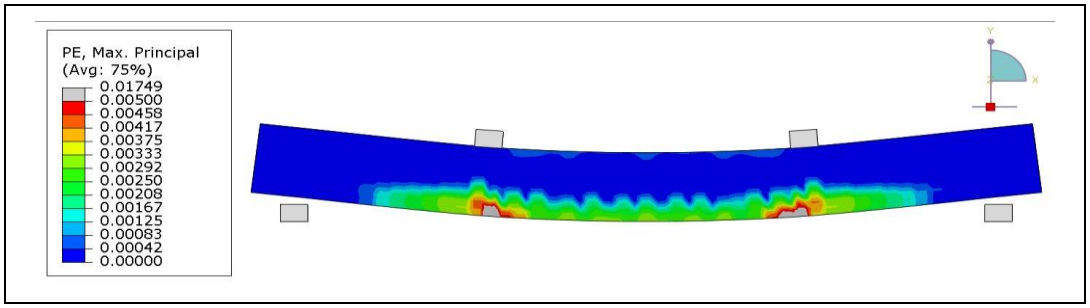

Figure 5-42: Von mises stress for the beam with and without SIFCON, Von mises stress of steel reinforcement, plastic strain for the beam for SIFCON and the beam NC2-22 at the maximum load capacity.

The measured Load carrying capacity verses the midspan deflection of NC2-32 specimen based on the numerical and the experimental results are presented in Figure (5-44). The first phase matches the experimental results up to 10.83 mm displacement. After such limit, the FEM curve load was noticeably higher than the experimental result value. Up to the maximum load carrying capacity, a slight difference between the experimental and FEM result of the load and corresponded displacement of about 5.06% and 6.67%, respectively. followed that point, the FEM degradation behavior curve style was sharp and unmatched the experimental curve behavior. Figure (5-45) illustrates von mises distribution contour map stress, plastic strain, von mises of steel bars, and downward displacement distribution contour maps.

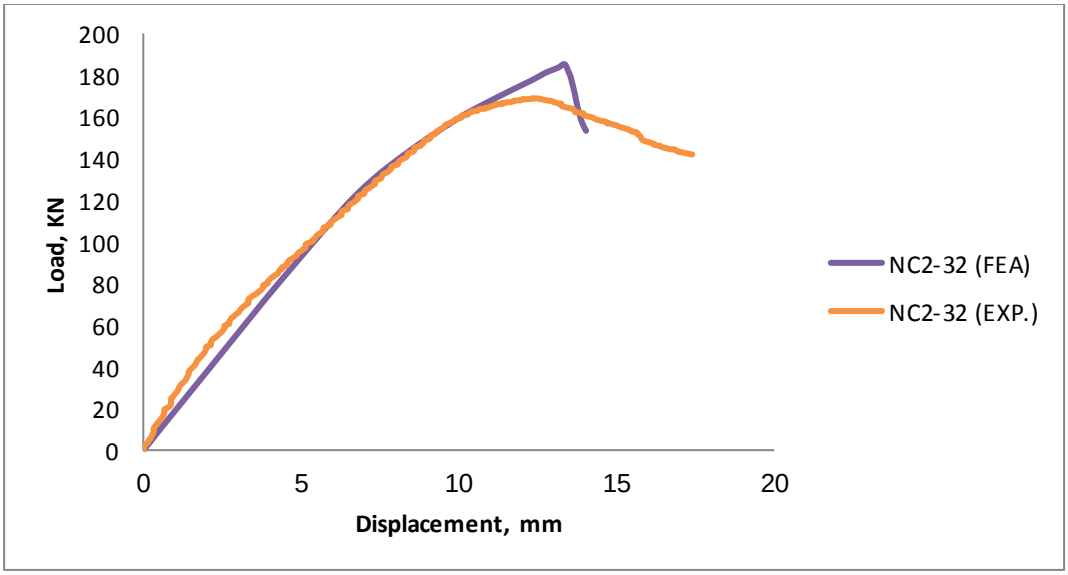

Figure 5-43: Comparison between load-mid span deflection curves of the FEM and the experimental work for NC2-32

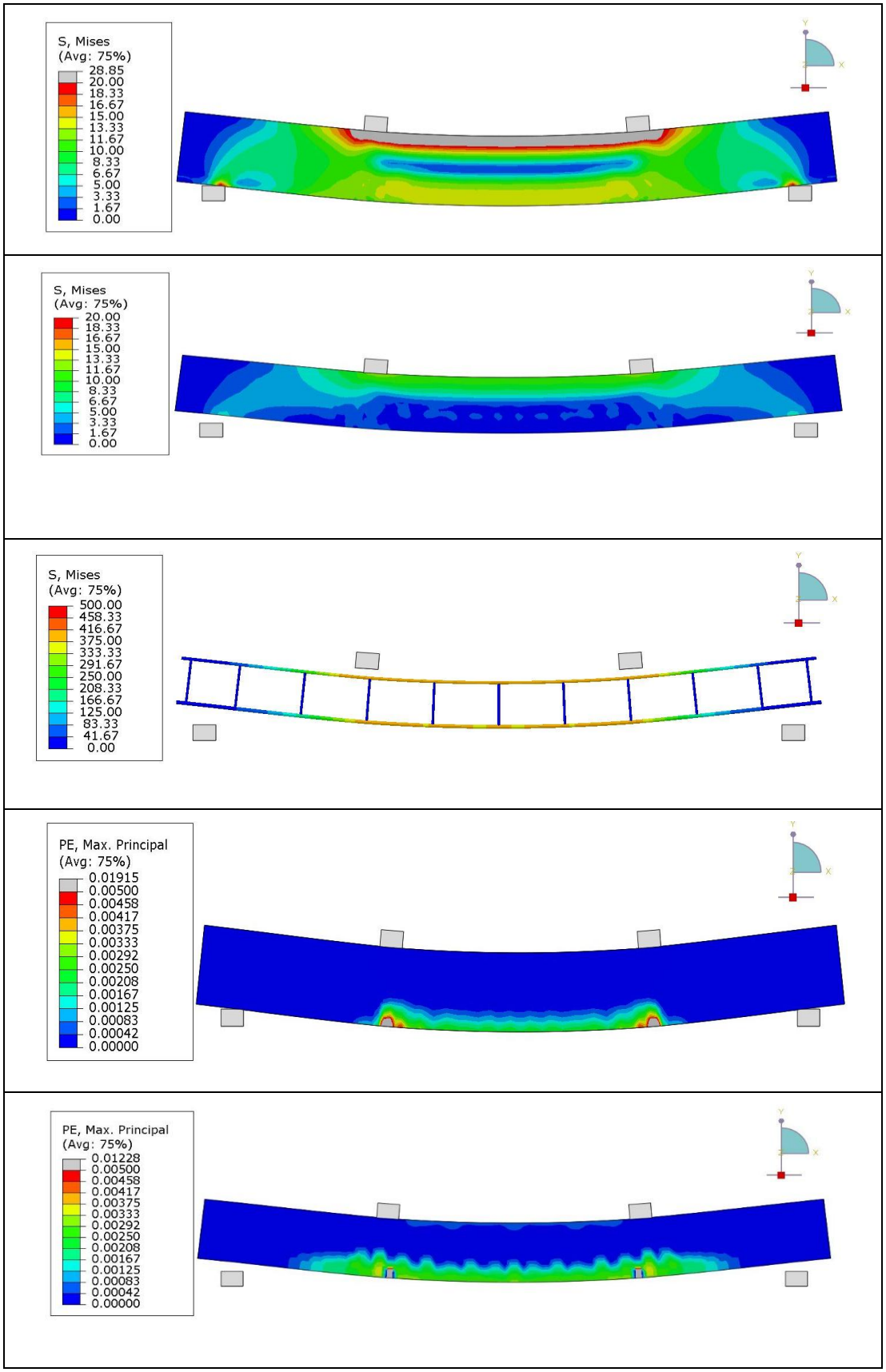

Figure 5-44: Von mises stress for the beam and SIFCON, Von mises stress of steel reinforcement, plastic strain for the beam for SIFCON and the beam NC2-32 at the maximum load capacity.

5.7.5.2 Validation Results of Postfire Treated HSC Beams with SFCON Jacket

Figure (5-46) illustrates the measured Load carrying capacity verses the midspan deflection of HC1-22 specimen based on the numerical and the experimental results. The first phase matches the experimental results up to 4.1 mm displacement. after such limit, the FEM curve load was noticeably higher the load values of the experimental result. Up to the maximum load carrying capacity, a slight difference between the experimental and FEM result of the load and corresponded displacement of about 5.06% and 6.76%, respectively. Followed that point, the FEM degradation behavior curve style matches the experimental curve behavior. Figure (5-47) illustrates von mises distribution contour map stress, plastic strain, von mises of steel bars, and downward displacement distribution contour maps.

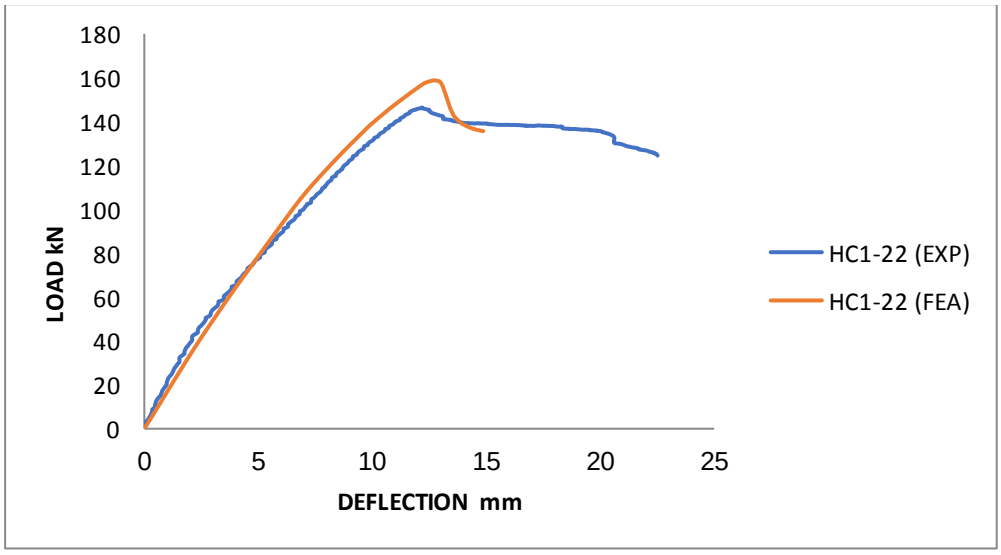

Figure 5-45: Comparison between load-mid span deflection curves of the FEM and the experimental work for HC1-22

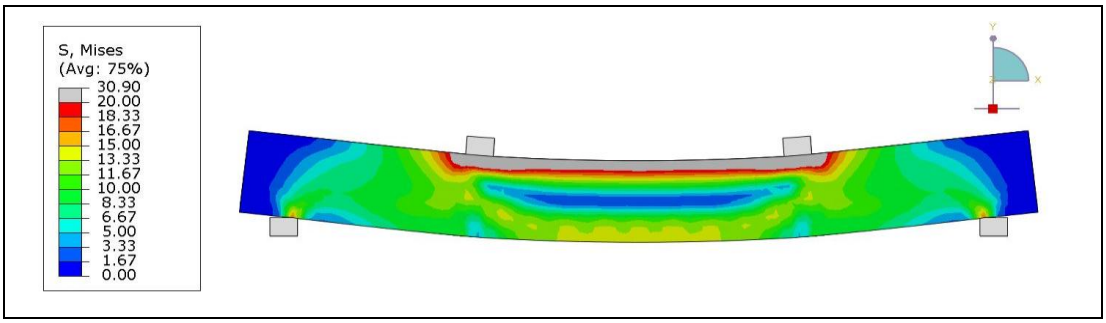

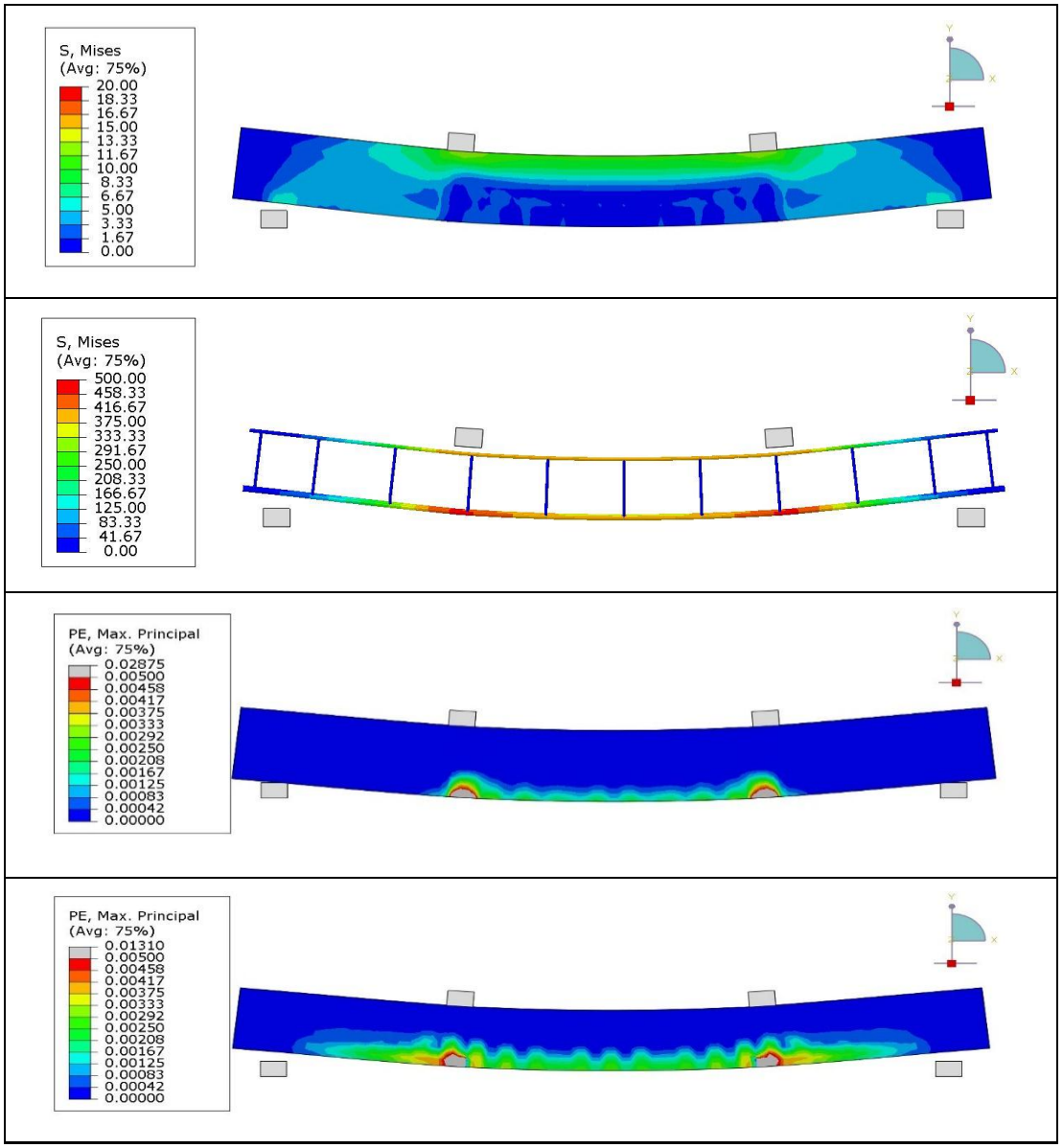

Figure 5-46: Von mises stress for the beam and SIFCON, Von mises stress of steel reinforcement, plastic strain for the beam for SIFCON and the beam HC1-22 at the maximum load capacity.

Figure (5-48) clarifies an overall comparison between the experimental and numerical results of HC1-32 beam. Both of them were matched from the start up to 3 mm displacement. after such limit the FEA curve showed higher load resistance when compared with the experimental curve. While the displacement corresponded to the maximum load capacity of the FEM was lower than the value of the experimental results. Overall, percentage of difference between the maximum load capacity and corresponded midspan downward displacement were about 13.87% and 11.37%, respectively.

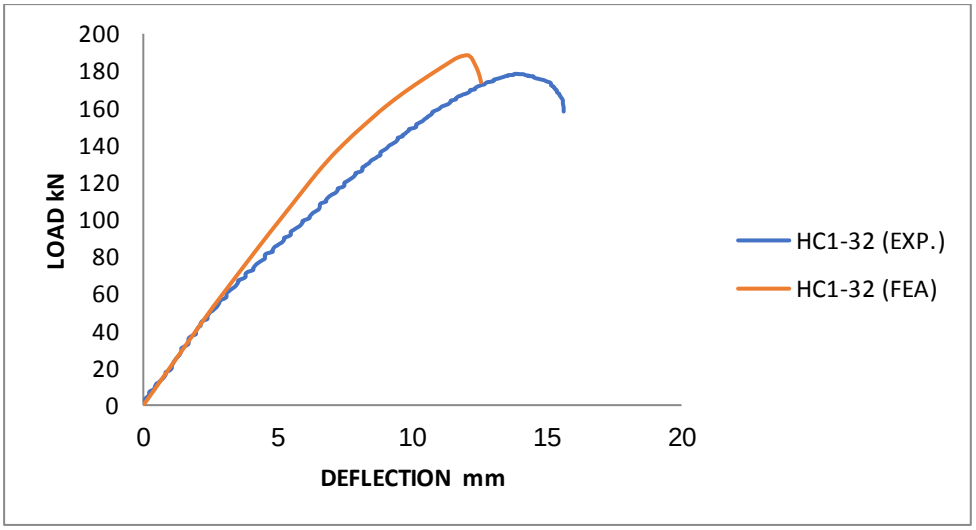

Figure 5-47: Comparison between load-mid span deflection curves of the FEM and the experimental work for HC1-32

Figure (5-49) illustrates von mises distribution contour map stress, plastic strain, von mises of steel bars, and downward displacement distribution contour maps.

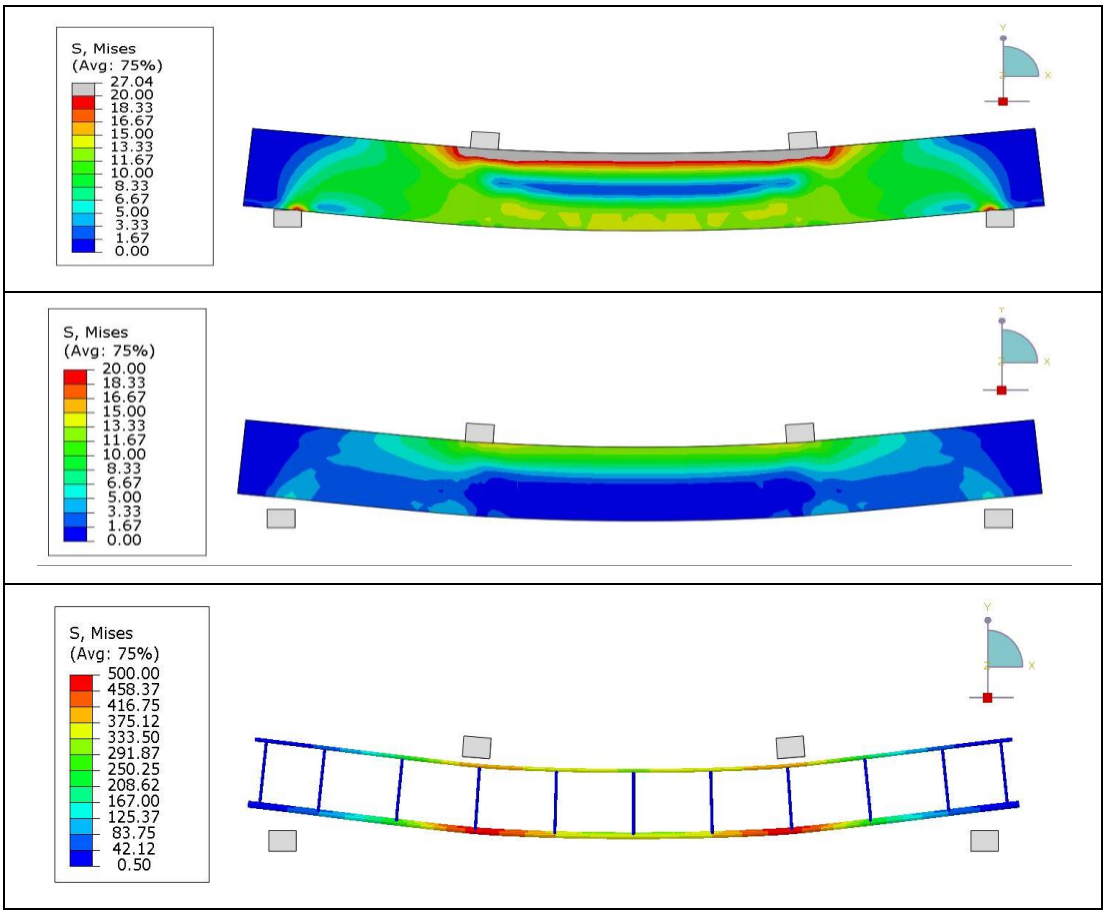

Figure 5-48: Von mises stress for the beam and SIFCON, Von mises stress of steel reinforcement of HC1-32 at the maximum load capacity.

Figure (5-50) illustrates the measured Load carrying capacity verses the midspan deflection of HC2-22 specimen based on the numerical and the experimental results. The first phase matches the experimental results up to 12 mm displacement, or at the maximum load capacity. after such limit, the FEM curve load was noticeably higher than the load value of the experimental result. A slight difference between the experimental and FEM result of the load and corresponded displacement of about 4.83% and 6.07%, respectively. Followed that point, the FEM degradation behavior curve mode dropped suddenly, unmatching the experimental curve behavior, which have noticed a smooth transition between the two phases. Figure (5-51) illustrates von mises distribution contour map stress, plastic strain, von mises of steel bars, and downward displacement distribution contour maps.

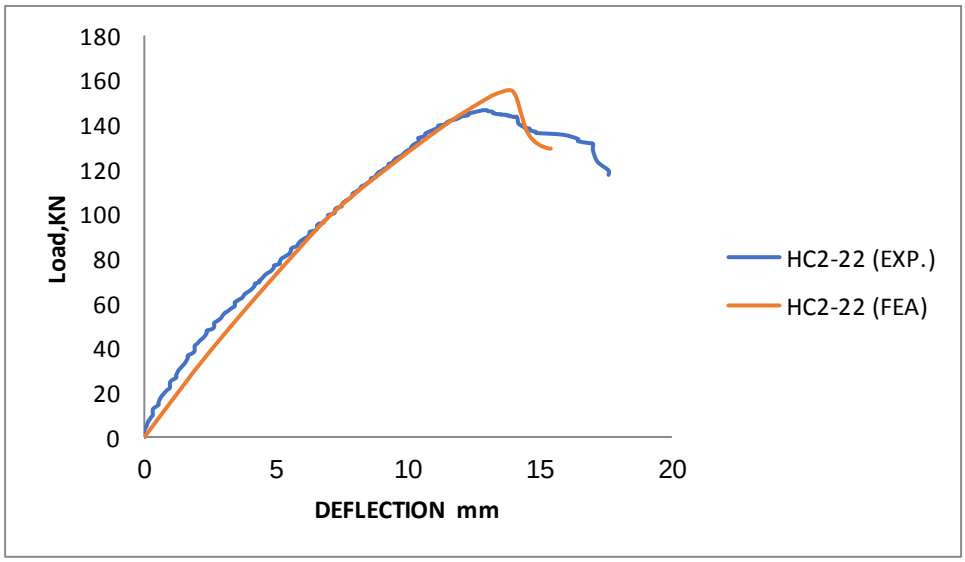

Figure 5-49: Comparison between load-mid span deflection curves of the FEM and the experimental work for NC2-22

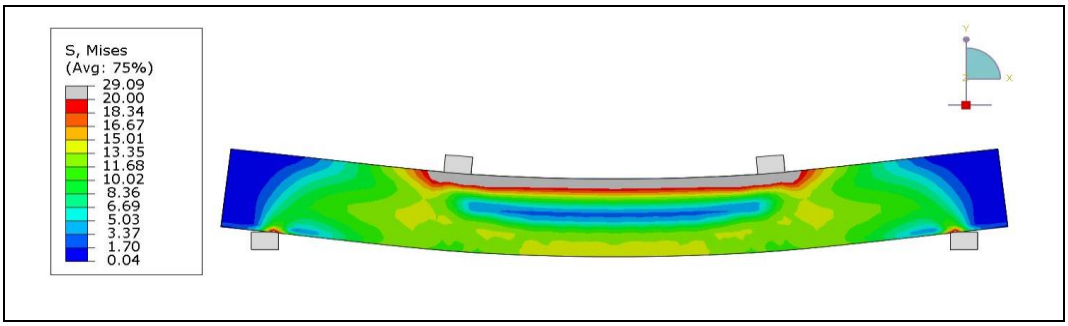

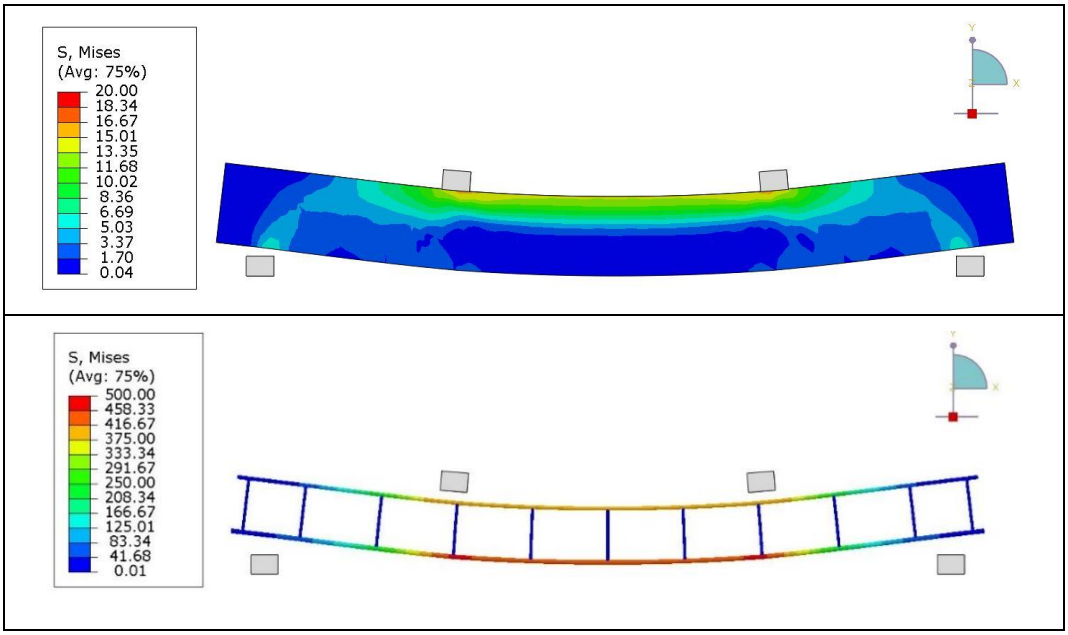

Figure 5-50: Von mises stress for the beam and SIFCON, Von mises stress of steel reinforcement of HC2-22 at the maximum load capacity.

Figure (5-52) illustrates the measured Load carrying capacity verses the midspan deflection of HC2-32 specimen based on the numerical and the experimental results. The first phase matches the experimental results up to the maximum load capacity. A negligible difference between the experimental and FEM result of the load and corresponded downward midspan displacement was observed estimated of about 0.52% and 0.42%, respectively.

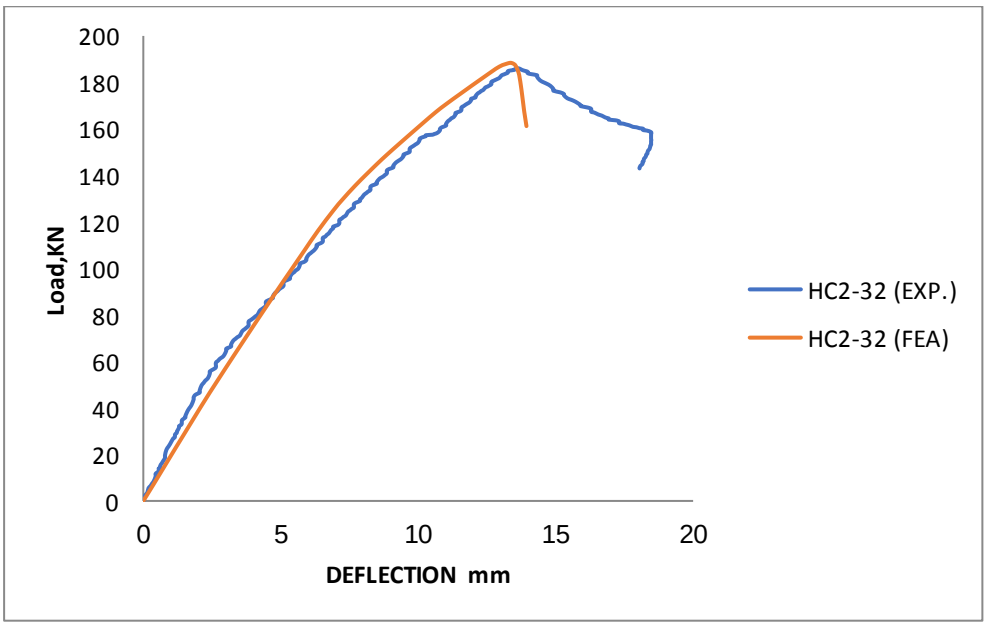

Figure 5-51: Comparison between load-mid span deflection curves of the FEM and the experimental work for NC2-32.

Followed that point, the FEM degradation behavior curve mode dropped suddenly, unmatching the experimental curve behavior. Also, Figure (5-53) illustrates von mises distribution contour map stress, plastic strain, von mises of steel bars, and downward displacement distribution contour maps.

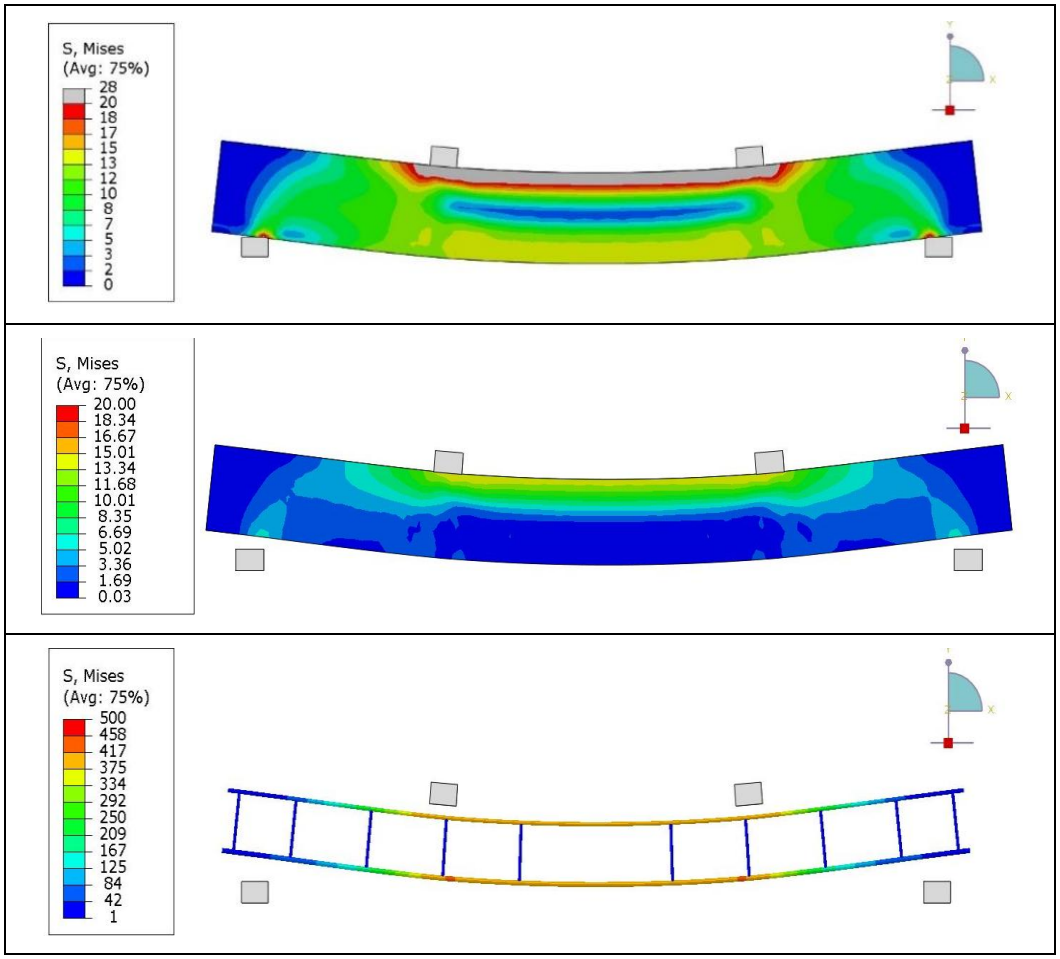

Figure 5-52: Von mises stress for the beam and SIFCON, Von mises stress of steel reinforcement of HC2-32 at the maximum load capacity.

5.8 Chapter Summery

This chapter presented the possibility of simulating the performed experimental work through investigating the behavior of various specimens' types in different conditions using the finite element modelling with Abaqus software. Specimens with normal and high strength types, before and after firing, in addition to the improvement with SIFCON jacketing technique, were simulated and compared with the experimental results. The absolute error was determined between the experimental and numerical results, for both of the displacement

at mid span and the maximum load carrying capacity of the specimens. The summery of the results is clarified in Table (5-3).

Table 5-3: Summery of the results

Group No.	Specimen Identification	Ultimate Load (kN) EXP.	Ultimate Load (kN) FEA	Max Deflection at Mid-span (mm), EXP.	Max Deflection at Mid-span (mm), FEA	Difference in load, %	Difference in disp., %
Group One	**NC1-00**	**117.00**	**125.30**	**22.85**	**22.471**	**7.09**	-1.65
	NC1-01	91.63		24.32			
	NC1-02	88.5	84.87	16.94	16.21	-4.101	-4.30
	NC1-21	157.60		14.94			
	NC1-22	147.90	153.64	13.46	13.33	3.88	-0.96
	NC1-31	188.10		13.55			
	NC1-32	166.10	181.54	12.32	12.41	9.29	0.73
	NC2-00	**102.70**	98.31	**24.41**	21.871	**-4.27**	**-10.40**
	NC2-01	**86.28**		**22.47**			
	NC2-02	81.60	84.047	18.32	**19.841**	2.99	**8.3**
	NC2-21	**141.70**		**12.15**			
	NC2-22	129.60	149.84	13.24	**14.409**	15.61	**8.829**
	NC2-31	172.20		13.25			
	NC2-32	168.90	177.45	12.59	**13.43**	5.06	**6.67**
Group Two	**HC1-00**	**139**	**145.17**	**24.87**	**23.56**	**4.43**	**-5.26**
	HC1-01	95.44		19.09			
	HC1-02	95.52	102	19.95	22.14	6.78	10.97
	HC1-21	159.70		13.69			
	HC1-22	146.40	153.81	12.19	13.015	5.06	6.76
	HC1-31	190.60		12.93			
	HC1-32	178.40	185.31	13.84	12.266	13.87	-11.37
	HC2-00	**124.08**	**125.22**	**24.73**	**22.93**	**0.918**	**-7.27**
	HC2-01	89.70		28.04			
	HC2-02	79.88	81.36	21.04	23.02	1.85	9.41
	HC2-21	159.90		14.63			
	HC2-22	146.50	153.59	12.83	13.61	4.83	6.079
	HC2-31	197.20		14.67			
	HC2-32	186.00	186.97	13.59	13.648	0.521	0.42

From the presented table, it can be seen that the minimum and maximum determined absolute error for specimens' load carrying capacity was about 0.521% and 15.61%, respectively.

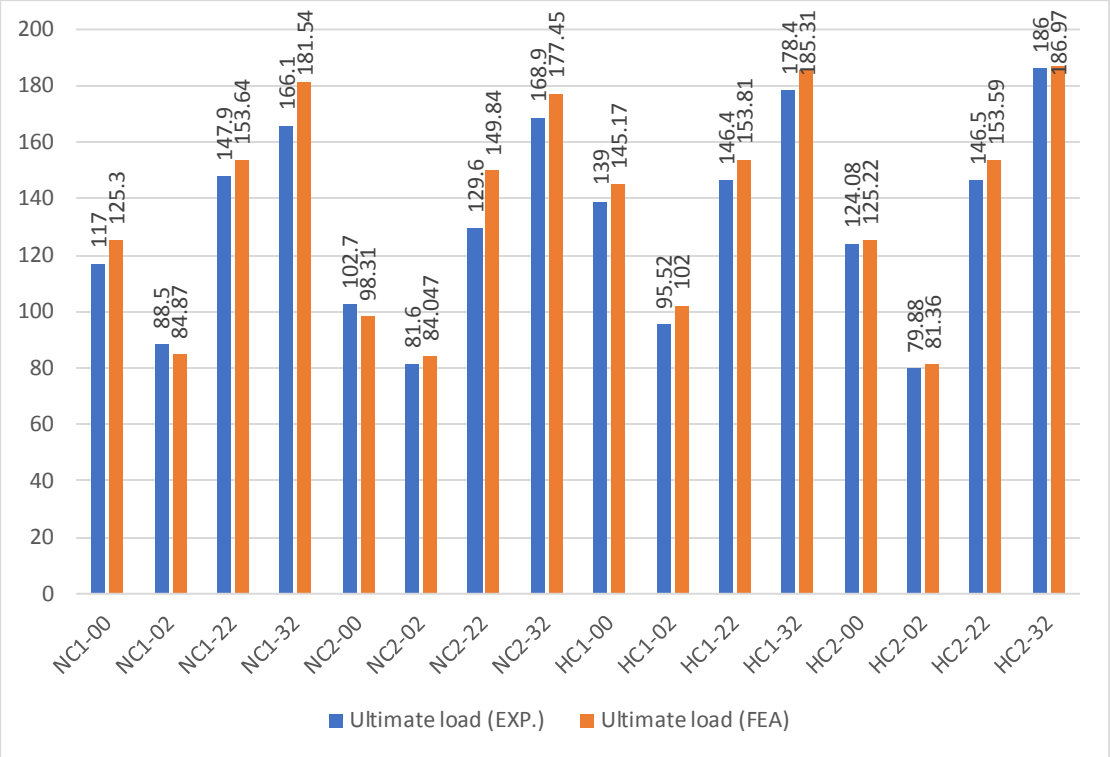

Figure 5-53: Comparison between the experimental and numerical results of NSC and HSC beams ultimate load.

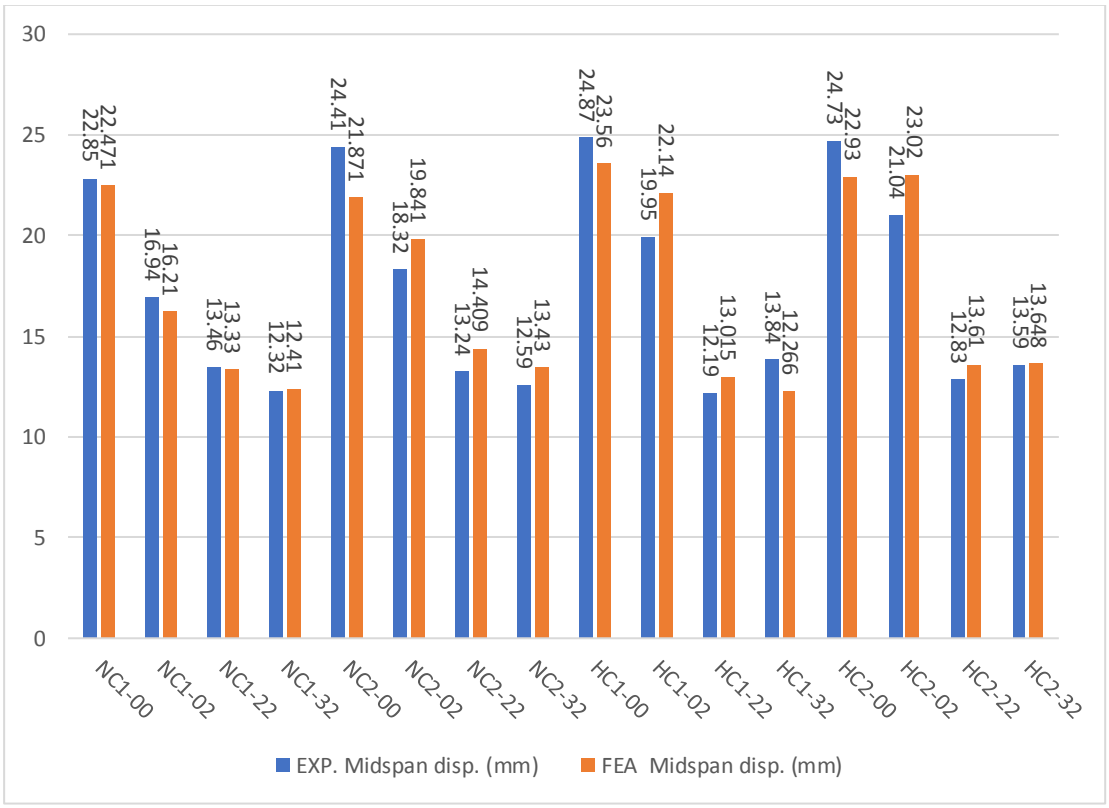

Figure 5-54: Comparison between the experimental and numerical results of NSC and HSC beams mid-span displacement.

On the other side, minimum and maximum determined absolute error for specimens' displacement corresponded to the max load were 0.42% and 11.42%, respectively. Accordingly, and since the estimated errors less than 15%, it can be said that the performed simulation process was accurate and successful when compared with other researchers' studies.

CHAPTER SIX

Chapter 6. Conclusions and Recommendations

6.1 Conclusions

This study investigates the level of enhancement of fire damaged LECA light weight high strength concrete beams using three sided SIFCON jacketing layer. Fire duration exposure concrete cover, in addition to the SIFCON layer thickness were the main parameters of this study. Accordingly, the following conclusions were drawn:

1- Very Limited past laboratory researches or on the other words (no previous studies) has been conducted to study the effects of externally applied SIFCON (slurry infiltrated fiber concrete) jackets on the structural behavior of normal and high strength lightweight reinforced concrete (LWRC) beams after exposed to realistic fire flame.

2- It has observed that the temperature was varied slightly between the mid and the quarter distances of beam cross section, which was about 16%. While the temperature reduction between the concrete mid core and the steel bar location was about 89%. Overall, temperature gradient reduction between the outer beam surface and the mid core was about 66%.

3- Concrete spalling occurred on the beam's corner without exposing any steel, with a maximum spalling depth of nearly 15 mm. However, no apparent beam curvature was detected.

4- Results have shown that subjecting the concrete beams to a 1-hour firing, resulted in reducing cracking load (service loading) by a range of 57%-65%, when compared with the reference beam.

5- Strengthening of fire damaged beams with SIFCON jacket resulted in a superior improvement ranged between 3.16-3.27 times reference beam and 2.86-5.12 times for 20mm and 30 mm jacket thickness respectively.

6- Crack opening of strengthened fire damaged beams, was improved by about 2.25 and 1.54 times the undamaged concrete beam value, respectively at earlier and final loading stages.

7- In terms of shear load capacity, the one-hour fire damaged beams compared with the undamaged beam, have reflected a noticeable reduction of about 41.5% and 35%, respectively for beams with 20 mm and 30 mm concrete cover. While the strengthening with 20mm and 30mm thickness SIFCON jackets reflects a good improvement in the shear strength of the beams affected by burning, with rates ranging between (45-48%) and (67.5-72%) respectively.

8- It was not observed during the test of the strengthened models that there was any crack or separation in the contact area between the model body and the strengthening layer, which concludes with the success of the methodology used in the study, so that both components acted as one part to bear the applied stresses, that positively reflects on the accuracy of the results obtained.

9- Beams' strengthening with SIFCON jacket layer of thickness 20 mm and 30 mm resulted in an improvement in shear load capacity of about 80% and 119% for 20 mm concrete cover, and 83% and 133% for 30 mm concrete cover, respectively compared with the fire damaged beams.

10- It is worth mentioning that the strengthened beams reflected comparable shear load capacity values to the undamaged beam (reference) value, which were found to be 5.3% and 28.3% for jacket layer thicknesses of 20 mm and 30 mm respectively for 20 mm concrete cover. while for the same degree of comparison, the level of enhancement was about 18% and 50% for jacket layer thicknesses of 20 mm and 30 mm, respectively for 30 mm concrete cover.

11- The thickness of the concrete cover seems to have effect in short fire exposing time (less or equal to 1 hr.), and not very high temperature (not exceed 600ºC), but it has no influence on the decrease in strength properties when exposed to a 2 hour fire, meaning that cover thickness has no major effect on the strength of the embedded steel reinforcement.

12- The presence of absorbed water within the lightweight aggregate concrete resulting temperature rises in a non-constant rate. The temperature of the concrete rises to 100 °C and continues to rise with a very slow rate until all of the water is evaporated. The moisture content and permeability of concrete affect the heat transfer phenomena. During the heating process, an endothermic reaction occurs due to the evaporation of free water. This dehydration process requires a certain amount of energy, which slows down the heating process.

13-The evaporation process in LWC is significantly slower than that in NC. This is due to the LWC's greater permeability and the porosity of the expanded clay, both of which enhance the moisture content. As a result, during fire situations, LWC exposed surface temperature and heat transfer are lesser than that for NC.

14- With regard to the damaged beams that were strengthened with SIFCON, the results showed a clear effect of increasing the thickness of the concrete cover, as increasing the thickness of the cover from 20 mm to 30 mm led to an improvement in the carrying capacity by (53% and 76%) for the normal and high strength beams respectively.

15- The Experimental results have cleared that a 1 hour fire damage has a negligible effect on the ductility index, for both concrete covers. While strengthening of damaged beam resulted in improving the ductility index by about 5% and 14% for beam with 20 mm and 30 mm concrete cover, respectively compared with the unstrengthen members.

16- On the other hand, the ductility index was enhanced by about 14% and 11% for 20- and 30-mm concrete cover, respectively when comparing the strengthened beams with the undamaged (reference) beam.

17- The absorption energy of damaged concrete beams, after 1-hour duration exposure to fire, was reduced by about 54% and 56%, respectively for beams with cover 20mm and 30 mm, when compared with the undamaged beam.

18- Strengthening of damaged beams with 20 mm and 30 mm SFICON jacket thickness resulted in an improvement of the energy absorption by about 17.9% and 38.4% for concrete cover of 20 mm, and by about 40% and 54% for 30 mm concrete cover, respectively compared with the damaged beams.

19- Tests results have cleared that when firing samples to 1 hour, the initial stiffness values have reduced by about 26% for both 20 mm and 30 mm cover thickness. On the other hand, the strengthened members have reflected a superior stiffness estimated approximately by about 3 times and 3.5 times the initial stiffness of the damaged members, and about 2.25 and times the undamaged (reference beam) value, respectively for 20 mm and 30 mm concrete cover.

20- The numerical validation of the obtained experimental data of load carrying capacity of the reference, fire damaged beam, and detailed temperature distribution using the ABAQUS program demonstrated a high degree of simulation process accuracy.

21- Through using of the finite element modelling with Abaqus software, the absolute error was determined between the experimental and numerical results, the results showed that the minimum and maximum determined absolute error for specimens' load carrying capacity was about 0.521% and 15.61%, respectively. on the other side, minimum and maximum

determined absolute error for specimens' displacement corresponded to the max load were 0.42% and 11.42%, respectively. accordingly, and since the estimated errors less than 15%, it can be said that the performed simulation process was accurate and successful when compared with other researchers' studies.

22- The suggested strengthening method provides a good structural improvement at the serviceability limit phase; the mid-span deflection significantly decreased due to the significantly increased beam stiffness under service load. Where the reduction for 20mm and 30mm jacket thickness were about 39% and 36% respectively; comparing with fire damaged model.

6.2 Recommendations:

1- It is highly recommended to utilize from SIFCON technology as a jacket layer to rehabilitate the fire damaged concrete members, since it approved its efficacy to recover fill strength.

2- The SIFCON layer thickness affects the overall performance of the strengthened beams, hence, it is highly recommended to select an appropriate thickness that overcome the economic aspects in addition to the strength and serviceability aspects.

3- For above purposes 25 mm is considered an ideal thickness as it meets the requirements of strengthening, economy and methodology of practical application (in terms of fibre alignment, direction and distribution).

4- The adopted strengthening approach is effective when the exposure duration equal or less than one hour to ensure that concrete strength capacity not deteriorate to sever rate.

5- The experimental program and the adopted methodology of strengthening can be adopted and recommended as a general guide for

strengthen fire damaged beam, since it approved its efficiency and applicability.

6- Studying the effect of the concrete cover on the strength resistance of the beam exposed to burning with the stability of the effective depth to give a better possibility of comparison on the basis of one starting line for both models and eliminating the role of effective depth as a controlling factor on the resistance values of the beam before and after burning.

REFERENCES

REFERENCES:

- Abdollahi, B., Bakhshi, M., Mirzaee, Z., Shekarchi, M., & Motavalli, M. (2012). SIFCON strengthening of concrete cylinders in comparison with conventional GFRP confinement method. Construction and Building Materials, 36, 765-778.
- Abeles, P. W., & Bardhan-Roy, B. K. (2014). Prestressed concrete designer's handbook. CRC Press.
- ACI 211.2.(1998). Standard Practice for Selecting Proportions for Structural Lightweight Concrete.
- ACI 213R. (2014). Guide for Structural Lightweight-Aggregate Concrete; American Concrete Institute: Farmington Hills, MI, USA,p. 53.
- ACI 234R. (2006). Guide for the Use of Silica Fume in Concrete.
- ACI Committee. (2014). Building Code Requirements for Structure Concrete and Commentary ACI 318M. American Concrete Institute, Michigan.
- Adhikary, B. B., & Mutsuyoshi, H. (2006). Shear strengthening of RC beams with web-bonded continuous steel plates. Construction and Building Materials, 20(5), 296-307.
- Alarcon-Ruiz, L., Platret, G., Massieu, E., & Ehrlacher, A. (2005). The use of thermal analysis in assessing the effect of temperature on a cement paste. Cement and Concrete research, 35(3), 609-613.
- Ali, M. A. (2018). Properties of slurry infiltrated fiber concrete (SIFCON). PhD diss., Ph. D Thesis, civil engineering dep., UOT, Iraq.

- Aljaafreh, T. (2016). Strengthening of lightweight reinforced concrete beams using carbon fiber reinforced polymers (CFRP) (Doctoral dissertation).
- Al-Jabiri, Z. S. (2015). Effect of Burning by Fire Flame on Mechanical Properties of Reactive Powder Concrete. Master thesis, Civil Engineering dep., University of Babylon, Iraq.
- Al-Nasra, M., & Wang, L. R. (1994). Parametric study of slab-on-grade problems due to initial warping and point loads. structural Journal, 91(2), 198-210.
- Amin, M. G. (2014). Selection of Materials and processes. Properties of Engineering Materials.
- Arafa, A. I., & Ali, H. O. S. M. A. (2017). Effect of fire on structural behavior of Normal and High Strength Concrete beams. International Journal of Structural and Construction Engineering, 10(9), 1245-1248.
- Ashour, A. F., El-Refaie, S. A., & Garrity, S. W. (2004). Flexural strengthening of RC continuous beams using CFRP laminates. Cement and concrete composites, 26(7), 765-775.
- ASTM C 1240. (2015). Standard Specification for Silica Fume Used in Cementitious Mixtures. ASTM International, West Conshohocken, PA.
- ASTM C 109. (2009). Standard test method for compressive strength of hydrulic cement using 50mm cube specimens. American Society for Testing and Materials International, West Conshohocken, Pennsylvania.
- ASTM C 143. (2008). Test Method for Slump or Hydraulic Cement Concrete.

- ASTM C 494. (2017). Standard specification for chemical admixtures for concrete. American Society for Testing and Materials (ASTM) International, West Conshohocken, Pennsylvania.
- ASTM C 494. (2017). Standard specification for chemical admixtures for concrete. American Society for Testing and Materials (ASTM) International, West Conshohocken, Pennsylvania.
- ASTM C 597. (2002). Standard test method for pulse velocity through concrete. American Society for Testing and Materials (ASTM) International, West Conshohocken, Pennsylvania.
- ASTM C330. (2006). Standard specification for lightweight aggregates for structural concrete. Annual Book of ASTM Standard, ASTM, West Conshohocken, PA.
- ASTM C330. (2017). Standard Specification for Lightweight Aggregates for Structural Concrete, American Society for Testing and Materials.
- ASTM C331. (2010). Standard Specification for Lightweight Aggregates for Concrete Masonry Units.
- ASTM C332. (2017). Standard Specification for Lightweight Aggregates for Insulating Concrete; ASTM International: West Conshohocken, PA, USA.
- ASTM C39. (2016). Standard Test Method for Compressive Strength of Cylindrical Concrete Specimens; ASTM International: West Conshohocken, PA, USA.
- ASTM C469. (2014). Standard Test Method for Static Modulus of Elasticity and Poisson's Ratio of Concrete in Compression.ASTM International, West Conshohocken, PA.

- ASTM C78. (2016). Standard Test Method for Flexural Strength of Concrete (Using Simple Beam with Third-Point Loading). ASTM International, West Conshohocken, PA.
- ASTM C496. (2017a). Standard Test Method for Splitting Tensile Strength of Cylindrical Concrete Specimens. ASTM International, West Conshohocken, PA.
- B.S 1881: Part 116. (1983). Method for Determination of Compressive Strength of Concrete Cubes. British Standards Institution.
- Babu, K. G., & Babu, D. S. (2003). Behaviour of lightweight expanded polystyrene concrete containing silica fume. Cement and Concrete Research, 33(5), 755-762.
- Balaguru, P., & Kendzulak, J. (1987). Mechanical properties of slurry infiltrated fiber concrete (SIFCON). Special Publication, 105, 247-268.
- Bashandy, A. A. (2013). Influence of elevated temperatures on the behavior of economical reactive powder concrete. Journal of civil engineering research, 3(3), 89-97.
- Bastami, M., Aslani, F., & ESMAEILNIA, O. M. (2010). High-temperature mechanical properties of concrete. International Journal of Civil Engineerng,8(4),337-351.
- Bažant, Z. P., & Chern, J. C. (1987). Stress-induced thermal and shrinkage strains in concrete. Journal of engineering mechanics, 113(10), 1493-1511.
- Behbahani, H. P., Nematollahi, B., Sam, A. R. M., & Lai, F. C. (2012). Flexural behavior of steel-fiber-added-RC (SFARC) beams with C30 and C50 classes of concrete. International Journal of Sustainable Construction Engineering and Technology, 3(1), 54-64.

- Bernhart, D. (2004). The effect of support conditions on the fire resistance of a reinforced concrete beam. Diploma report,Civil Engineering, University of Canterbury ,New Zealand
- Bobrowski, J. (1982). Origins of safety in concrete structures. University of Surrey, United Kingdom.
- BS 1881: Part 202. (1986). Testing Concrete: Recommendations for Surface Hardness Testing by Rebound Hammer. London, British Standards Institution.
- BS EN 197-1. (2011). Cement, Composition, Specifications and Conformity Criteria for Common Cements. British Standard Institution.
- Castellazzi, G., D'Altri, A. M., de Miranda, S., Chiozzi, A., & Tralli, A. (2018). Numerical insights on the seismic behavior of a non-isolated historical masonry tower. Bulletin of Earthquake Engineering, 16(2), 933-961.
- Chandra, S., & Berntsson, L. (2002). Lightweight aggregate concrete. Elsevier, 450.
- Chang, Y. F., Chen, Y. H., Sheu, M. S., & Yao, G. C. (2006). Residual stress–strain relationship for concrete after exposure to high temperatures. Cement and concrete research, 36(10), 1999-2005.
- Choi, E. G., & Shin, Y. S. (2011). The structural behaviour and simplified thermal analysis of normal-strength and high-strength concrete beams under fire. Engineering Structures, 33(4), 1123-1132.
- Choi, W. C., Kim, S. W., Jang, S. J., & Yun, H. D. (2017). Research trends and design guidelines for fire resistance of structural concrete in South Korea. Magazine of Concrete Research, 69(7), 347-364.

- Clarke, J. L. (1993). Structural lightweight aggregate concrete. CRC Press.
- Clarke, J. L. (2002). Structural lightweight aggregate concrete. CRC Press, 161.
- Concrete Society. (1990). Assessment and repair of fire-damaged concrete structures. Technical Report 33, The Concrete Society, Camberley.
- Cook, C. R. (1983). FIP manual of lightweight aggregate concrete: Published by The Surrey University Press, Bishopriggs, Glasgow G64 2NZ, Scotland, 1983 ISBN 0 903384 43 4, 259 pp.
- Core, B., & Long, M. (2004). Analysis of Rotational Column with Plastic Hinge. Rice University and Bates College.
- Dabbaghi, F., Dehestani, M., & Yousefpour, H. (2021a). Residual mechanical properties of concrete containing lightweight expanded clay aggregate (LECA) after exposure to elevated temperatures. Structural Concrete.
- Dabbaghi, F., Dehestani, M., Yousefpour, H., Rasekh, H., & Navaratnam, S. (2021b). Residual compressive stress–strain relationship of lightweight aggregate concrete after exposure to elevated temperatures. Construction and Building Materials, 298, 123890.
- Dagar, K. (2012). Slurry infiltrated fibrous concrete (SIFCON). International Journal of Applied Engineering and Technology, 2(2), 99–100.
- Dagar, K. (2012). Slurry infiltrated fibrous concrete (SIFCON). International journal of Applied engineering and technology, 2(2), 99-100.

- De Lange, G. (1980). Structural repair of fire damaged concrete. Concrete International, 2(9), 27-29.
- Deepesh, P., & Jayant, K. (2016). Study of mechanical and durability properties of SIFCON by partial replacement of cement with fly ash as defined by an experimental based approach. International Journal for Innovative Research in Science & Technology, 5(5), 8568-8574.
- del Coz-Díaz, J. J., Martínez-Martínez, J. E., Alonso-Martínez, M., & Rabanal, F. P. Á. (2020). Comparative study of Lightweight and Normal Concrete composite slabs behaviour under fire conditions. Engineering Structures, 207, 110196.
- Du Béton, F. I. (2001). Externally bonded FRP reinforcement for RC structures. Bulletin, 14, 138.
- Dwaikat, M. B., & Kodur, V. K. R. (2009). Hydrothermal model for predicting fire-induced spalling in concrete structural systems. Fire safety journal, 44(3), 425-434.
- Dwaikat, M. B., & Kodur, V. K. R. (2009). Hydrothermal model for predicting fire-induced spalling in concrete structural systems. Fire safety journal, 44(3), 425-434.
- E. N. (2004). 2: Design of Concrete Structures—Part 1–2: General Rules—Structural Fire Design. European Standard: London, UK.
- EC2. (1995). Design of Concrete Structures. ENV 1992: Part1-2: General Rules -Structural Fire Design. European Committee for Standardization, Brussels.
- Elavarasi, M. (2016). KSR, Performance of Slurry Infiltrated Fibrous Concrete (Sifcon) with Silica Fume. International Journal of Chemical Sciences, 14(4), 2710-2722.

- Elnono, M. A., Salem, H. M., Farahat, A. M., & Elzanaty, A. H. (2009). Use of slurry infiltrated fiber concrete in reinforced concrete corner connections subjected to opening moments. Journal of Advanced Concrete Technology, 7(1), 51-59.
- EN 13055. (2016). Leichte Gesteinskörnungen (Lightweight Aggregates).
- EN 13055. (2016). Lightweight aggregates. London,UK
- Falkner, H., Henke, V., & Hinke, U. (1997). Steel fibre concrete for deep building pits in ground-water. Bauingenieur, 72(1), 47-52.
- Fares, H., Toutanji, H., Pierce, K., & Noumowé, A. (2015). Lightweight self-consolidating concrete exposed to elevated temperatures. Journal of Materials in Civil Engineering, 27(12), 04015039.
- Farnam, Y., Moosavi, M., Shekarchi, M., Babanajad, S., & Bagherzadeh, A. (2010). Behaviour of slurry infiltrated fibre concrete (SIFCON) under triaxial compression. Cement and concrete research, 40(11), 1571- 1581.
- Fib Bulletin. (2010). Model code 2010. First complete draft,1,318.
- Gao, W. Y., Dai, J. G., & Teng, J. G. (2017). Fire resistance of RC beams under design fire exposure. Magazine of Concrete Research, 69(8), 402-423.
- Gilani, A. M. (2007). Various durability aspects of slurry infiltrated fiber concrete. Ph. D Dissertation in Middle East Technical University.
- Giridhar, R., Rama, P., & Rao, M. (2015). Determination of mechanical properties of slurry infiltrated concrete (SIFCON). International Journal for Technological Research in Engineering, 2(7), 1366-1368.

- Guo, Z. H., & Shi, X. D. (2003). Behaviour of reinforced concrete at elevated temperature and its calculation. Tinghua university press, 19(15), 55-61.
- Haddad, R. H., & Shannis, L. G. (2004). Post-fire behavior of bond between high strength pozzolanic concrete and reinforcing steel. Construction and Building Materials, 18(6), 425-435.
- Hertz, K. D. (2005). Concrete strength for fire safety design. Magazine of concrete research, 57(8), 445-453.
- Holm, T. A., & Ries, J. P. (2007). Reference manual for the properties and applications of expanded shale, clay and slate lightweight aggregate. Prepared by Expanded Shale Clay and Slate Institute.
- Hu, X. F., Lie, T. T., Polomark, G. M., & MacLaurin, J. W. (1993). Thermal properties of building materials at elevated temperatures. Internal report/National Research Council of Canada, Institute for Research in Construction; no. 643.
- Huang, Z., Liew, J. R., & Li, W. (2017). Evaluation of compressive behavior of ultra-lightweight cement composite after elevated temperature exposure. Construction and Building Materials, 148, 579-589.
- Ibrahim & Jannoulakis. (1994). The effectiveness of steel fiber reinforcement in composite slabs. International conference on Modern concrete, 3(4), 243-250.
- Ipek, M., Aksu, M., Yilmaz, K., & Uysal, M. (2014). The effect of presetting pressure on the flexural strength and fracture toughness of SIFCON during the setting phase. Construction and Building Materials, 66, 515-521.

- IQS 45. (1984). Aggregates. Central Agency for Standardization and Quality Control.
- ISO 834–1. (1999). Fire resistance tests-elements of building construction. Part 1: General requirements. Geneva, Switzerland.
- Jiang, Y. C., Huo, D., Teng, H. W., & Qiao, Y. (2013). Study on performance of shale ceramsite concrete after exposure to high temperature. J. Build. Mater, 16, 888-893.
- Kadhum, M. (2015). Prediction of mechanical properties of reactive powder concrete by using artificial neural network and regression technique after the exposure to fire flame. Jordan Journal of Civil Engineering, 9(3).
- Kadhum, M. M. (2011). Effect of burning by fire flame on the behavior of reinforced concrete beam models. Journal of Babylon University, 21(5).
- Kani, M. A. (2016). Investigation on Strength and Durability of Slurry Infiltrated Fibrous Concrete. International Journal of Emerging Technologies in Engineering Research (IJETER),4(5).
- Khalifa, A., & Nanni, A. (2002). Rehabilitation of rectangular simply supported RC beams with shear deficiencies using CFRP composites. Construction and building materials, 16(3), 135-146.
- Kigha, F., Sadeeq, J. A., & Abejide, O. S. (2015). Effects of temperature levels and concrete cover thickness on residual strength characteristics of fire exposed reinforced concrete beams. Nigerian Journal of Technology, 34(3), 429-437.

- Kılıç, A., Atiş, C. D., Yaşar, E., & Özcan, F. (2003). High-strength lightweight concrete made with scoria aggregate containing mineral admixtures. Cement and Concrete Research, 33(10), 1595-1599.
- Kim, S.-K., & Choi, J.-H. (2006). Compressive and Tensile Strength Properties of Slurry Infiltrated Fiber Concrete. Journal of the Korea Concrete Institute, 18(5), 703-708.
- Kodur, V. (2014). Properties of concrete at elevated temperatures. International Scholarly Research Notices.
- Kodur, V. K. R., & Dwaikat, M. B. (2008). Effect of fire induced spalling on the response of reinforced concrete beams. International journal of concrete structures and materials, 2(2), 71-81.
- Kodur, V. K. R., & Phan, L. (2007). Critical factors governing the fire performance of high strength concrete systems. Fire safety journal, 42(6-7), 482-488.
- Kodur, V. R., & Raut, N. (2010). Performance of concrete structures under fire hazard: emerging trends. The Indian Concrete Journal, 84(2), 23-31.
- Kotsovos, M. D. (1982). A fundamental explanation of the behaviour of reinforced concrete beams in flexure based on the properties of concrete under multiaxial stress. Materiaux et constructions, 15(6), 529-537.
- Kotsovos, M. D. (1983). Mechanisms of 'shear' failure. Magazine of Concrete Research, 35(123), 99-106.
- Krstulovic-Opara, N., & Al-Shannag, M. J. (1999). Slurry infiltrated mat concrete (SIMCON)-based shear retrofit of reinforced concrete members. Structural Journal, 96(1), 105-114.

- Kumar, A. R., & Prakash, P. (2015). Mechanical properties of structural light weight concrete by blending cinder and LECA. International Advanced Research Journal in Science, Engineering Technology, 2(10), 64-67.
- Kunieda, M., Hussein, M., Ueda, N., & Nakamura, H. (2010). Enhancement of crack distribution of UHP-SHCC under axial tension using steel reinforcement. Journal of Advanced Concrete Technology, 8(1), 49-57.
- Lamprecht, H. O. (1996). Opus caementitium: Bautechnik der Römer. Beton-Verlag.
- Lankard, D. R. (1984). Slurry infiltrated fiber concrete (SIFCON): properties and applications. MRS Online Proceedings Library Archive, 42.
- Li, G., Wang, P., & Shouchao, J. (2007). Non-linear finite element analysis of axially restrained steel beams at elevated temperatures in a fire. Journal of Constructional Steel Research, 63(9), 1175-1183.
- Li, V. C. (1993). From Micromechanics to Structural Engineering the Design of Cementitious Composites for Civil Engineering Applications. Doboku Gakkai Ronbunshu, 1993(471), 1-12.
- Libre, N. A., Shekarchi, M., Mahoutian, M., & Soroushian, P. (2011). Mechanical properties of hybrid fiber reinforced lightweight aggregate concrete made with natural pumice. Construction and Building Materials, 25(5), 2458-2464.
- Lie, T. T. (1992). ASCE manuals and reports on engineering practice No. 78, structural fire protection. New York: American Society of Civil Engineers (ASCE).

- Lie, T. T., & Stanzak, W. W. (1974). Empirical method for calculating fire resistance of protected steel columns. Division of Building Research, National Research Council.
- Lim TY, Lee SL. (1987). Shear and moment capacity of reinforced steel-fiber-concrete beams. Magazine of Concrete Research, 39(1),148–60.
- Lin, C. H., Chen, S. T., & Yang, C. A. (1995). Repair of fire-damaged reinforced concrete columns. Structural Journal, 92(4), 406-411.
- Lindgard, J., & Hammer, T. A. (1998). Fire resistance of structural lightweight aggregate concrete a literature survey with focus on spalling. Nordic Concrete Research-Publications, 21, 64-77.
- Lydon, F. D. (1982). Concrete mix design. London.
- Lytag, UK. (2011). Introduction to Lytag Lightweight Aggregate. Technical Manual –Section 1. Lytag Ltd, London, UK.
- Malhotra, V. M., & Carino, N. J. (2003). Handbook on nondestructive testing of concrete. CRC press.
- Marini, A., & Meda, A. (2009). Retrofitting of R/C shear walls by means of high-performance jackets. Engineering Structures, 31(12), 3059-3064.
- Martinola, G., Meda, A., Plizzari, G. A., & Rinaldi, Z. (2010). Strengthening and repair of RC beams with fiber reinforced concrete. Cement and concrete composites, 32(9), 731-739.
- Minelli, F., Cominoli, L., Meda, A., Plizzari, G. A., & Riva, P. (2006). Full Scale Tests on HPSFRC Prestressed Roof Elements Subjected to Longitudinal Flexure. RILEM-PRO 49 International RilemWorkshop on High Performance Fiber Reinforced Cementitious Composites (HPFRCC).

- Naaman, A. E. (1992). SIFCON: Tailored properties for structural performance. In High Performance Fiber Reinforced Cement Composites (Vol. 18). Chapman & Hall/E&FN Spon, London/New York.
- Naaman, A. E. (2003). Engineered steel fibers with optimal properties for reinforcement of cement composites. Journal of advanced concrete technology, 1(3), 241-252.
- Naaman, A. E., Otter, D., & Najm, H. (1992). Elastic modulus of SIFCON in tension and compression. Materials Journal, 88(6), 603-613.
- Naaman, A. E. (2008). High performance fiber reinforced cement composites. Naaman AE. High-performance construction materials: science and applications. Singapore: World Scientific Publishing, 91-153.
- Naaman, A. E., Wight, J. K., & Abdou, H. (1987). SIFCON connections for seismic resistant frames. Concrete International, 9(11), 34-39.
- Newman, J. B. (1993). 2Properties of structural lightweight aggregate. Structural lightweight aggregate concrete, 19.
- Newman, J., & Choo, B. S. (Eds.). (2003). *Advanced concrete technology set*. Elsevier.
- Newman, J., & Owens, P. (2003). Properties of lightweight concrete. Advanced concrete technology, 3, 1-29.
- Ng, C. K., & Tan, K. H. (2006). Flexural behaviour of externally prestressed beams. Part I: Analytical model. Engineering Structures, 28(4), 609-621.

- Oluokun, A. F., & Haghayeghi, A. R. (1998). Flexural behavior of reinforced concrete beams retrofitted or repaired with slurry infiltrated mat concrete. Structural Journal, 95(6), 654-664.
- Ozawa, M., Uchida, S., Kamada, T., & Morimoto, H. (2012). Study of mechanisms of explosive spalling in high-strength concrete at high temperatures using acoustic emission. Construction and Building Materials, 37, 621-628.

- Ozawa, M., Uchida, S., Kamada, T., & Morimoto, H. (2012). Study of mechanisms of explosive spalling in high-strength concrete at high temperatures using acoustic emission. Construction and Building Materials, 37, 621-628.

- Parameswaran, V., Krishnamoorthy, T., Balasubramanian, K., & Gangadar, S. (1993). Studies on Slurry-Infiltrated Fibrous Concrete (SIFCON). The National Academies of Sciences, Engineering, and Medicine (1382), 57-63.
- Prasad, D. M. S. P., Kumar, V., Sharma, U. K., & Bhargava, P. (2010). Moment curvature relationships for fire damaged reinforced concrete sections. In Structures in Fire: Proceedings of the Sixth International Conference, 247.
- Raithby, K. D., & Lydon, F. D. (1981). Lightweight concrete in highway bridges. International Journal of Cement Composites and Lightweight Concrete, 3(2), 133-146.
- Ramezanianpour, A. A., Ghiasvand, E., Nickseresht, I., Mahdikhani, M., & Moodi, F. (2009). Influence of various amounts of limestone powder on performance of Portland limestone cement concretes. Cement and Concrete Composites, 31(10), 715-720.

- Rossi, P., & Chanvillard, G. (Eds.). (2000). PRO 15: 5th RILEM Symposium on Fibre-Reinforced Concretes (FRC)-BEFIB'2000 (Vol. 15). RILEM Publications.
- Ryu, E. M., An, A. Y., Kang, J. Y., Shin, Y. S., & Kim, H. S. (2015). Investigation of rehabilitation effects on fire damaged high strength concrete beams. International Journal of Architectural and Environmental Engineering, 9(7), 898-904.
- Sancak, E., Sari, Y. D., & Simsek, O. (2008). Effects of elevated temperature on compressive strength and weight loss of the light-weight concrete with silica fume and superplasticizer. Cement and Concrete Composites, 30(8), 715-721.
- Sánchez-Fajardo, V. M., Torres, M. E., & Moreno, A. J. (2014). Study of the pore structure of the lightweight concrete block with lapilli as an aggregate to predict the liquid permeability by dielectric spectroscopy. Construction and Building Materials, 53, 225-234.

- Sánchez-Fajardo, V. M., Torres, M. E., & Moreno, A. J. (2014). Study of the pore structure of the lightweight concrete block with lapilli as an aggregate to predict the liquid permeability by dielectric spectroscopy. Construction and Building Materials, 53, 225-234.

- Shannag, M. J., & Al-Rousan, R. (2004). Shear strengthening of high-strength reinforced concrete beams using fibrous composites. Magazine of Concrete Research, 56(7), 419-428.
- Sharif, A., Al-Sulaimani, G. J., Basunbul, I. A., Baluch, M. H., & Ghaleb, B. N. (1994). Strengthening of initially loaded reinforced concrete beams using FRP plates. Structural Journal, 91(2), 160-168.
- Smart, S. (1999). Concrete: The burning issue. Concrete, 33(7), 30-34.

- Sonebi, M., Svermova, L., & Bartos, P. (2005). Statistical modelling of cement slurries for self-compacting SIFCON containing silica fume. Materials and structures, 38(1), 79-86.
- Sonebi, Svermova, L., & Bartos, P. J. (2004). Factorial design of cement slurries containing limestone powder for self-consolidating slurry infiltrated fiber concrete. Materials Journal, 101(2), 136-145.
- Standard, B. (2006). Eurocode 3—Design of steel structures—. BS EN 1993-1, 1, 2005.
- Šušteršič, J., & Zajc, A. (2012). SIFCON with Latex Modified Cement Slurry Used for a Thin Overlay of a Bridge Deck. Restoration of Buildings and Monuments, 18(3-4), 195-202.
- Swamy, R. N., & Bahia, H. M. (1979, February). Influence of fiber reinforcement on the dowel resistance to shear. In *Journal Proceedings* (Vol. 76, No. 2, pp. 327-356).
- Tai, Y. S., Pan, H. H., & Kung, Y. N. (2011). Mechanical properties of steel fiber reinforced reactive powder concrete following exposure to high temperature reaching 800 C. Nuclear Engineering and Design, 241(7), 2416-2424.
- Tanyildizi, H., & Coskun, A. (2008). Performance of lightweight concrete with silica fume after high temperature. Construction and Building Materials, 22(10), 2124-2129.
- Thomas, M., & Bremner, T. (2012). Performance of lightweight aggregate concrete containing slag after 25 years in a harsh marine environment. Cement and concrete research, 42(2), 358-364.

- Topçu, İ. B., & Uygunoğlu, T. (2007). Properties of autoclaved lightweight aggregate concrete. Building and Environment, 42(12), 4108-4116.
- Türkmen, İ., & Fındık, S. B. (2013). Several properties of mineral admixtured lightweight mortars at elevated temperatures. Fire and materials, 37(5), 337-349.
- Ünlüoğlu, E., Topçu, İ. B., & Yalaman, B. (2007). Concrete cover effect on reinforced concrete bars exposed to high temperatures. Construction and Building Materials, 21(6), 1155-1160.
- Van Mier, J. G. M. (2004). Cementitious composites with high tensile strength and ductility through hybrid fibres. In 6th International RILEM Symposium on Fibre Reinforced Concretes ,219-236.
- Vijayakumar, M., & Kumar, P. D. (2017). Study on Strength Properties of SIFCON. International Research Journal of Engineering and Technology (IRJET), 4(1).
- Vijayakumar, M., & Kumar, P. D. (2017). Study on Strength Properties of SIFCON. International Research Journal of Engineering and Technology (IRJET), 4(1), 235-238.
- Wang, M. L., & Maji, A. K. (1994). Shear properties of slurry-infiltrated fibre concrete (SIFCON). Construction and Building Materials, 8(3), 161-168.
- Yazıcı, H., Yiğiter, H., Aydın, S., & Baradan, B. (2006). Autoclaved SIFCON with high volume Class C fly ash binder phase. Cement and concrete research, 36(3), 481-486.

- Yoon, M., Kim, G., Choe, G. C., Lee, Y., & Lee, T. (2015). Effect of coarse aggregate type and loading level on the high temperature properties of concrete. Construction and Building Materials, 78, 26-33.
- Yu, X. M., Zha, X. X., & Huang, Z. H. (2011). The influence of spalling on the fire resistance of RC structures. In Advanced Materials Research, 255,519-523.
- Zareef, M. A. M. E. (2010). Conceptual and structural design of buildings made of lightweight and infra-lightweight concrete.

الخلاصة

تناقش هذه الدراسة استخدام الخرسانة المتخللة بالالياف (SIFCON) كمواد تقوية القص لأعتاب الخرسانة المسلحة خفيفة الوزن العادية وعالية المقاومة من خلال استخدام الركام المتمدد خفيف الوزن (LECA) كركام خشن في الخلطة المرجعية للاعتاب. الهدف من الدراسة هو توفير مواد بناء فعالة عالية الأداء تستخدم في عملية تقوية اعتاب الخرسانة خفيفة الوزن المتضررة من الحريق.

مرت التجارب العملية في هذه الدراسة خلال ثلاث مراحل رئيسية. تضمنت المرحلة الأولى دراسة سلوك الأعتاب الخرسانية العادية والعالية المقاومة (LWA) بعد تعرضها لدرجة حرارة عالية (600 درجة مئوية). لهذا الغرض استخدمت 28 عينة بأبعاد (2000mm ×200mm × 150mm). تضمنت المرحلة الثانية تحسين مقاومة الأعتاب المتضررة بسبب الحرق بأستخدام سترات تقوية بطبقة من ال SIFCON. بصرف النظر عن العينات المرجعية ، تم فحص العديد من المتغيرات والظروف للأعتاب الخرسانية ، بما في ذلك مدة التعرض للحريق ، والغطاء الخرساني ، وسماكة سترة SIFCON. كانت المعاملات الاساسية في هذا الاختبار تتمثل بغطاءين خرسانيين 20 مم و 30 مم ، ومدة تعرض للحريق نصف ساعة وساعة ، وسمكين لسترات ال SIFCON بسماكة 20 مم و 30 مم. تم قياس التدرج الحراري عبر المقطع العرضي للعتب الخرساني عن طريق تضمين المستشعرات الحرارية المزدوجة في مواقع مختلفة داخل العتب، و اختبار الخواص الفيزيائية والكيميائية لجميع المواد المستخدمة في هذه الدراسة. بشكل عام ، حيث تم اختبار ثمانية وعشرين عينة عتب خرساني لجميع المراحل الثلاث (المرجعية HSC وNSC، والعينات المتضررة من الحريق ، ونماذج ما بعد التقوية باستخدام سترة SIFCON). تم تركيز مستوى المقارنة لعينات الاختبار على معايير مختلفة ، بما في ذلك سعة التحمل القصوى والهطول المقابل ، ومؤشر السحبية او المطولية ، وحمل التشقق ، والصلابة (الأولية والقاطع) ، وامتصاص الطاقة.

كشفت نتائج الاختبار التجريبي التي تم الحصول عليها كجزء من هذه الدراسة عن تحسن كبير في الأعتاب المقواة مقارنة بالعينات المتضررة. علاوة على ذلك ، أوضحت النتائج أنه ، باستثناء امتصاص الطاقة ، استعادت الأعتاب المقواة قابلياتها بمقدار مماثل أو أكثر من الأعتاب غير المتضررة (الأعتاب المرجعية) من حيث المعاملات المشار إليها.

وفقًا لنتائج الاختبار ، فإن جميع الأعتاب المقواة بسترات SIFCON تتمتع بقدرة جيدة على تحمل الأحمال. بعد الاحتراق ، انخفضت قيم تحمل الأعتاب المتضررة. بلغ معدل التراجع لأعتاب NSC و HSC للغطاء الخرساني (20 و 30) مم (24.4 و 20.5) % و (41.56 و 35.6) %على التوالي. أما بالنسبة للأعتاب المقواة فقد ازدادت سعة التحمل بشكل ملحوظ ، حيث بالنسبة لأعتاب NSC فكانت الزيادة بين (159 و 207) % و لأعتاب HSC بين (180 و 220) %. علاوة على ذلك ، فإن سترات SIFCON المستخدمة كتقوية خارجية منعت حصول فشل القص الهش وزادت من قوة القص النهائية للعينات المعززة.

أخيرًا ، تم إجراء محاكاة التعبير النظري من خلال بناء نموذج العناصر المحدودة (FEM) ، ونمذجة ومحاكاة الأعتاب الخرسانية التي تم اختبارها تجريبيًا في المختبر والتأكد من دقة النتائج. يسمى هذا الأسلوب بالتحقق العددي باستخدام برنامج ABAQUS مع خطأ مطلق مقبول أقل من 15٪.

جمهوريـــــــــة العـــــــــراق
وزارة التعليم العالي والبحث العلمي
جامـــعة بابـــــــــــــــل
كلية الهندسة
قسم الهندسة المدنية

إصلاح وتقوية القص لعوارض الخرسانة المسلحة خفيفة الوزن العادية وعالية المقاومة المتضررة من الحريق باستخدام ملاط الخرسانة المتخللة للألياف

رسالة

مقدمه إلى كلية الهندسة / جامعة بابل

كجزء من متطلبات نيل درجة ماجستير في الهندسة / الهندسة المدنية / مواد انشائية

من قبل
احمد حبيب عبدالحسين يوسف

بأشراف
أ.د.محمد منصور كاظم

1443 A.H. 2022 A.D.